UNIVERSIDADE DO ALGARVE

FACULDADE DE CIÊNCIAS DO MAR E AMBIENTE

Tectono-Magmatic Processes At The Azores Triple Junction

(Tese provisória para a obtenção do grau de doutor no ramo de Ciências do Mar, especialidade de Geologia Marinha)

João Nuno Vilhena de Sousa Lourenço

FARO
(2007)

UNIVERSIDADE DO ALGARVE

FACULDADE DE CIÊNCIAS DO MAR E AMBIENTE

Tectono-Magmatic Processes At The Azores Triple Junction

(Tese provisória para a obtenção do grau de doutor no ramo de Ciências do Mar, especialidade de Geologia Marinha)

João Nuno Vilhena de Sousa Lourenço

FARO
(2007)

Prologue

During the last decade a large effort has been developed by the scientific community to map, study and understand tectonic and magmatic processes taking place in the Azores Triple Junction Area. The move between small and localized observations centred on a few Islands to a general plan to study the whole triple junction area required a multitude of means, a multidisciplinary approach and a significant level of logistics.

One piece of the global effort was organized in Portugal through the research project STAMINA. Even if the two cruises planned in the scoope of this project, were never completed, it gathered a variety of geophysical, geochemical, geodetic and tectonic teams that organized their effort in the same scientific problem. It also allowed the means to coordinate the national participation in a series of research operations led by the international community where we had the opportunity to act as active partners and benefit from their much better technical means.

In what concerns this work, those cruise limitations were important in the amount of new swath bathymetry data acquired (6.5 hours of high quality EM300 swath bathymetry data collected as piggy back to the main SIRENA I cruise; PI J. Jean Goslin); several hours more of magnetic data collected over the Serreta eruption site west of Terceira Island again marginally to the SIRENA II cruise. Such a data scarcity led to the broadening of the thesis objectives thematically although centred in the Azores, still the core of this work. The scientific objectives remained under the umbrella of "the volcano-tectonic interactions" but with a broader spatial and temporal scale to allow integration of other research topics

To improve efficiency of research and overcome data availability limitations, we developed a set of collaborations with foreign partners in complementary lines of research, (Peter Cobbold; Jean Goslin) and a stronger focus on the cooperation with the remaining STAMINA colleagues: Fernando Ornelas Marques (Tectonics, University of Lisbon); Rui Fernandes (Geodesy, University of Beira Interior), João Catalão (Geodesy, University of Lisbon), All these collaborations resulted in a number of publications, currently in preparation, submitted or already published. The current manuscript is constructed with a large amount of this material collated into a single volume. Some original texts have been enhanced whereas others have been edited, reduced or focused on specific topics related with the manuscript theme.

NOME: João Nuno Vilhena de Sousa Lourenço
FACULDADE: Faculdade de Ciências do Mar e Ambiente
ORIENTADORES: Jorge Miguel Alberto Miranda
António Augusto Ramos Ribeiro
DATA: 22 de Janeiro de 2007
TÍTULO DA TESE: Processos tectono-magmáticos na Junção Tripla dos Açores

Resumo

Apresentam-se resultados de estudos multi-disciplinares, centrados na interacção espacio-temporal entre o Ponto Quente dos Açores (PQA) e a Junção Tripla dos Açores (JTA) no decurso da evolução geodinâmica da plataforma vulcânica dos Açores e sintetiza-se um modelo tectono-magmático para a JTA na actualidade.

Desde os 33.4 Ma o regime tectónico prevalecente é trans-tractivo com rotação progressiva das direcções de abertura Eurásia-Africa de ca. N-S para ca. ENE-WSW. Desde aquela idade os Açores apresentam um comportamento cinemático independente e possivelmente dominado por deformação distribuída.

A máxima interacção entre o PQA e a JTA ocorre entre os 20 Ma e os 10 Ma. Consequentemente entre os 33.4 e os 20Ma os Açores terão resultado de um controlo tectónico proeminente e reduzida influência do PQA.

O desenvolvimento das cristas vulcânicas lineares (CVL) é associado à progressiva migração para NW do JTA de um contexto intra-transformante desde os ca. 15 Ma. No presente considera-se que persiste a propagação das CVL para WNW.

A modelação de dados GPS, permite definir na actualidade a fronteira de placas Euro-asiatica e Núbia no Eixo da Terceira e no alinhamento Faial-Pico. Propõe-se que a zona inter-placa entre estes dois eixos principais activos corresponde a um domínio de deformação distribuída não coaxial em regime de trans-tracção. Nesta zona ocorre partição entre processos de *rifting* (dominados por magmatismo) em tracção pura normal às CVL, processos de cisalhamento com desligamentos esquerdos (NNW-SSE) e zonas de acomodação (WSW-ENE). Contrastando, o padrão de falhamento no sector imediatamente a Leste da ilha Terceira, é interpretado como resultado de um regime de alastramento oblíquo focalizado no eixo da terceira, com deformação co-axial, e um campo de tensões com compressão máxima vertical e compressão mínima sub-paralela às direcções de abertura previstas pelos modelos cinemáticos NUVEL-1A ou baseados em GPS (e.g. REVEL ou DEOS2K).

Palavras Chave: Ponto Triplo Açores; Ponto quente Açores; cristas vulcânicas; sismo-tectónica; modelação elástica; deformação distribuida.

Tectono-magmatic processes in the Azores Triple Junction

Abstract

Multi-disciplinary results on the spatio-temporal interaction between the Azores hot-spot (AHS) and the Azores Triple Junction (ATJ) during the Azores plateau evolution, are presented. In addition a tectono-magmatic model of the ATJ for the present day is summarized.

Since 33.4 Ma, the dominant tectonic regime is transtensional with progressive rotation of the Eurasia-Africa opening directions from ca. N-S to ca. ENE-WSW. Since that early age, the Azores present a kinematic behavior which is independent from that of the larger plates and possibly dominated by distributed deformation.

The maximum interaction between the AHS and the ATJ occurs between the 20 and 10 Ma. Consequently, between 33.4 and 20 Ma the evolution of the Azores has been prominently a result of tectonic controls and had little influence of the AHS.

The growth of the linear volcanic ridges (LVR) is interpreted as the result of the progressive migration of the ATJ, since ca. 15 Ma, from an intra-transform context, towards NW. Their propagation subsists in the present day, now towards WNW.

The modeling of GPS data has allowed to constrain in the present day, the Eurasia-Nubia plate boundary along the Terceira axis and in the Pico-Faial alignment. It is suggested that the inter-plate zone adjoining this two active axis, corresponds to a domain of non-coaxial distributed deformation dominated by transtension. In this zone there is a partition between rifting processes (dominated by magmatism) in pure tension, normal to the LVR axis, and shear processes characterized by left lateral strike slips (along NNW-SSE) and relay zones (along WSW-ENE). Contrastingly, the faulting pattern, east of Terceira Island suggests prevalence of co-axial oblique extension, focalized within the Terceira axis, and a stress field with maximum compressive axis vertical, and minimum compressive axis sub-parallel to the opening directions predicted by NUVEL-1A or GPS based (e.g REVEL, DEOS2K) kinematic models.

Keywords: Azores Triple Junction; Azores Hot-Spot; Sismo-tectonics; elastic modeling; linear volcanic ridges; distributed deformation.

Acknowledgments

Miguel Miranda was my compellingly enthusiastic supervisor and PI of STAMINA, under which most of the recent data sets used in this PhD project, were acquired. Miguel has always stroke me with his capacity of finding some shed of bright light in a sometimes all black scenario, for example, when all the cruises scheduled for the Azores "sank". I acknowledge him, the countless discussions we had about different Azores and other topics, his critical review of this manuscript, and above all for making me face new challenges and pushing me forward in what concerns scientific research. STAMINA project from FCT sponsored all the Azores field work and my visits to Rennes University.

António Ribeiro was my co-supervisor on this thesis from the beginning. I thank him the thoughtful review of this manuscript and his sharing of views and opinions both in the field when discussing Terceira Island tectonics in the Azores and at the office, in a great variety of issues His constant availability during this work is greatly appreciated by me.

The work with Fernando Ornelas Marques, within STAMINA project, particularly during several field campaigns in the Azores for tectonic mapping and field observations, gave me the opportunity to have new insights in the analysis of geological processes. I am also indebt to Fernando for his availability and for introducing me to analogue modelling techniques. Although some of the work of this manuscript is the direct result of this collaboration, it does not make justice to the overall benefices of my learning process from Fernando.

I thank Joaquim Luís, for continuously providing me copies of his software, which I used intensively during the course of this work. Additionally, Joaquim has always been a source of fruitful discussions on the many different questions regarding the Azores and Geophysics.

João Alveirinho Dias, was my coordinator at the University Algarve and gave me the opportunity to realize this extensive research program. These acknowledgments are extensible to my collegues in the Algarve University: Oscar Ferreira, Ana Barbosa, Cristina Pires, Delminda Moura and Tomasz Boski, for their friendship and support.

During this work time span I had the privilege to meet Jean Goslin, a skilled senior researcher from UBO (Université de Bretagne Occidental) which became a very good friend. With Jean Goslin, we sailed two missions (SIRENA I and II). The SIRENA I with heavy roll and pitch during most of the sailing will never be forgotten.

I benefited also from a 3 month scholarship sponsored by IFREMER-ICCTI protocol in the framework of French-Portuguese bilateral agreements, which enabled me to participate in the SIRENA data processing and analysis at IUEM – Brest, along with Dr. Robert Dziak from NOAA, which provided numerous and valuable insights on the strategy for the data processing and analysis. This stay was the natural prolongation of the good time spent at sea. I am indebt to Jean Goslin and his family, Julie Perrot, Christophe Martin, J. Y. Royer from the SIRENA team and remaining staff of IUEM with whom I contacted during my stay, for this profitable and enjoyable visit. "Merci a tous pour votre super accueil à Brest".

I thank Peter Cobbold for sharing with me new ideas on the role of fluids in deformation and for the level of exigence and rigor he imposes in the research work. This led to the improvement in the quality of my own work. I acknowledge also the help of my colleagues particularly: Nuno Rodrigues, Regis Morgues, J J Kemarrec and Xavier Le Fort during my stay in Geoscience Rennes in the Analogue modeling lab.

I thank the researchers of CGUL with whom I worked for a long time: Maria Ana Baptista, Luis Matias, Fernando Santos and Pedro Soares. Pedro Silva has been my close "compagnon de route" for most of this work and helped forming a united front to survive Miguel's barbarian provocations when our soccer club was in disgrace! Nuno Dias, also a PhD student in seismology of the Azores assured a fruitful cooperation and information exchange which benefited this (and hopefully his) work.

Pedro Madureira (from U. Évora) also a PhD student in geochemistry and petrology of the Azores, is first of all a very close friend, and secondly a colleague with whom I had enormous discussions about the Azores and the interpretation of our data. Pedro has showed me quite clearly that I ceased to be a full bodied geologist, but I am still not a geophysicist. Thank you Pedro for the proof of my precarious position!

A large amount of this manuscript was written while I was at the EMEPC. I am deeply thankful to the head of this organization, Manuel Pinto de Abreu, its Technical Coordinator, Fernando Maia Pimentel and remaining EMEPC colleagues for their support.

My Family is grand. Mother: thank you for having revised the manuscript. Father: thanks for pointing me, at times, the north, and remembering me (in those times) that serenity is not just a word.

To my wife Raquel, no written acknowledgement makes justice to what she had to put up with me. I guess a thank you with the size of the Azores Plateau, for your patience, support and help is in order and says it all. This manuscript final stages (or at least my strength to accomplish it) also largely benefited from the smiles and laughs of my daughters Rita and Maria.

While the work benefited from many discussions and collaborations with the above stated colleagues, all misconceptions or errors present in this manuscript are my full responsibility.

Contents

List of Figures

Chapter IV

Chapter V

Chapter VII

Chapter VIII

Chapter IX

List of Tables

Chapter I - Introduction

The Azores Archipelago consists of nine Islands. The Western group (two Islands) is located in the stable North America plate, whilst the Central (five Islands) and the Eastern (two Islands) groups lie in the Eurasian (EU)-Nubian (NUB) plate boundary area. The Azores Islands, themselves, represent a small emerged area of a vast submarine volcanic platform. This platform, roughly defined by the 2000 m isobath, is relatable to an excess in volcanism/magmatism. It presents a triangular shape, whose western side is located west of the Mid-Atlantic Ridge. It is limited to the south by the East Azores Fracture Zone and to the northwest by the Terceira axis (Machado, 1957).

Within the Azores plateau a large V-shaped volcanic feature roughly bisected by the MAR, designated hereafter as Faial ridge and Flores ridge (after Vogt 1976) is probably a result of a major thermal or magmatic event under the Mid-Atlantic Ridge at 10 Ma, reflecting the interaction between the so-called Azores hot spot and the Mid-Atlantic ridge (Cannat *et al.,* 1999; Escartin *et al.,* 2001, Gente *et al.,* 2003).

The precise location of the MAR (Figure I.1), which forms the boundary between the North American and Eurasian/Nubian plates is well known, particular after the efforts developed in recent years to map the ridge system in the Azores area; in contrast, the

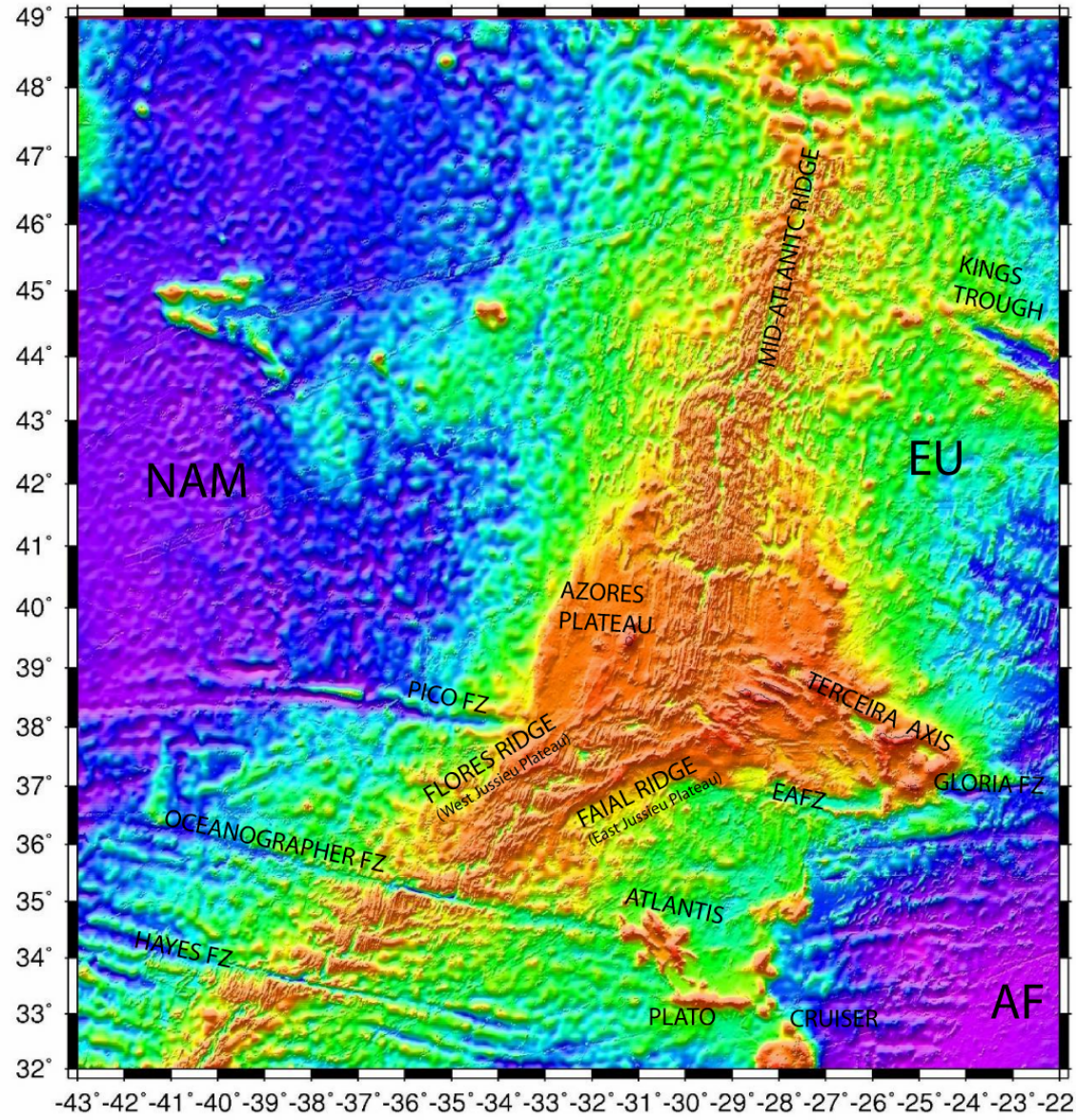

Figure I.1 - Regional bathymetry of the Azores Plateau with main morphological features discussed in the text (Gente, 2003).

exact details and nature of the boundary between the Eurasian and Nubian plates, its location and segmentation pattern , the evolution of this triple junction and the way in which tectonic and volcanic processes interact, within the plate boundary zone, remain unclear, and has been elusive to geophysical and geological studies, in spite of the efforts developed.

The plate boundary between Eurasia and Africa is generally characterized in its westernmost part by transtension in a complex area striking WNW-ESE, the Terceira Axis, linking the Mid-Atlantic Ridge to the Gloria fault. The spreading rates across the plate boundary in the Terceira axis, between Eurasia and African plates amount to 4 mm/yr in an average N75°E direction (Euler rotation pole located at 19.5°N, 23.7°W, Demets *et al.,* 1994). The direction of motion predicted by the global kinematic model does not account for all structure orientations and their variations from south to north (Lourenço *et al.,* 1998).

The internal structure of the plateau (Figure I.2) displays a coherent structure of linear volcanic ridges developed along fissure systems roughly aligned sub-parallel to the Terceira Axis (Lourenço *et al.,* 1998). This axis presents a marked clockwise rotation from N110-120º near its intersection with the MAR and which mostly characterizes the central Islands (Pico, São Jorge, Terceira); to directions closer to N140º-150º at its intersection with the GLORIA fault. These directions appear to characterize the tectonic pattern on the Islands and in the extensional basins between them, as well as some elongated, volcanic ridges. Guest *et al*. (1999) suggested that the conical volcanic edifices are emplaced at the intersection of tectonic structures with both directions. In particular, the Furnas volcano on São Miguel Island, displays such a tectonic setting.

The seismic activity that constitutes the best tool to trace plate boundaries and interplate deformation processes, is characterized by earthquakes with focal mechanisms compatible with right-lateral strike-slip faults or normal faults, oriented N120°E to N150°E (Grimison and Chen, 1986; Buforn *et al.,* 1988). A strong earthquake (M=7.2), however, occurred in 1980, probably on a left-lateral strike-slip fault oriented N150°E, according to its focal mechanism and the aftershock distribution (Hirn *et al.,* 1980),

implying that the kinematics is not simple in the area. The focal mechanism for the 1998 Faial earthquake showed also a complex fracture pattern (Fernandes *et al.*, 2002).

The volcanic activity is distributed over all the Central and Eastern Azores Islands, and all record historical activity. The most recent volcanic activity occurred on the Serreta ridge (Luis *et al.*, 1999), northwest of Terceira Island. The WNW-ESE-trending zone of volcanic and tectonic activity, which also marks the northeast boundary of the Azores plateau, is a rift zone, with a significant part of transtensional motion (leaky transform).

The ages of the Azores Plateau, the Terceira axis, and the linear volcanic ridge structures within the plateau are still unclear. Little constraint is provided by magnetic anomalies in what concerns islands evolution, and isotopic age determinations only provide an upper bound for the age of these structures. Little is also known about the thermal structure (or lithospheric structure) of the Terceira axis and the partition, style and dynamics between magmatic and tectonic processes which have shaped the plate boundary and the Azores plateau.

An analysis based on an aeromagnetic survey and the compilation of ship born magnetic data of the plateau showed that only the Brunhes and possibly Matuyama magnetic epochs can be identified in the rift area, even though the magnetic anomalies generated along the mid-Atlantic ridge are disrupted on the plateau (Miranda *et al.*, 1991, Luis *et al.*, 1994). The lack of older magnetic lineations on either side of the Terceira rift suggests that the relative motion between Africa and Eurasia in the westernmost part of the plate boundary was accommodated by extension distributed across the plateau rather than by accretion focused along the rift. Major questions on the kinematics and the dynamics of the area are therefore still unresolved:

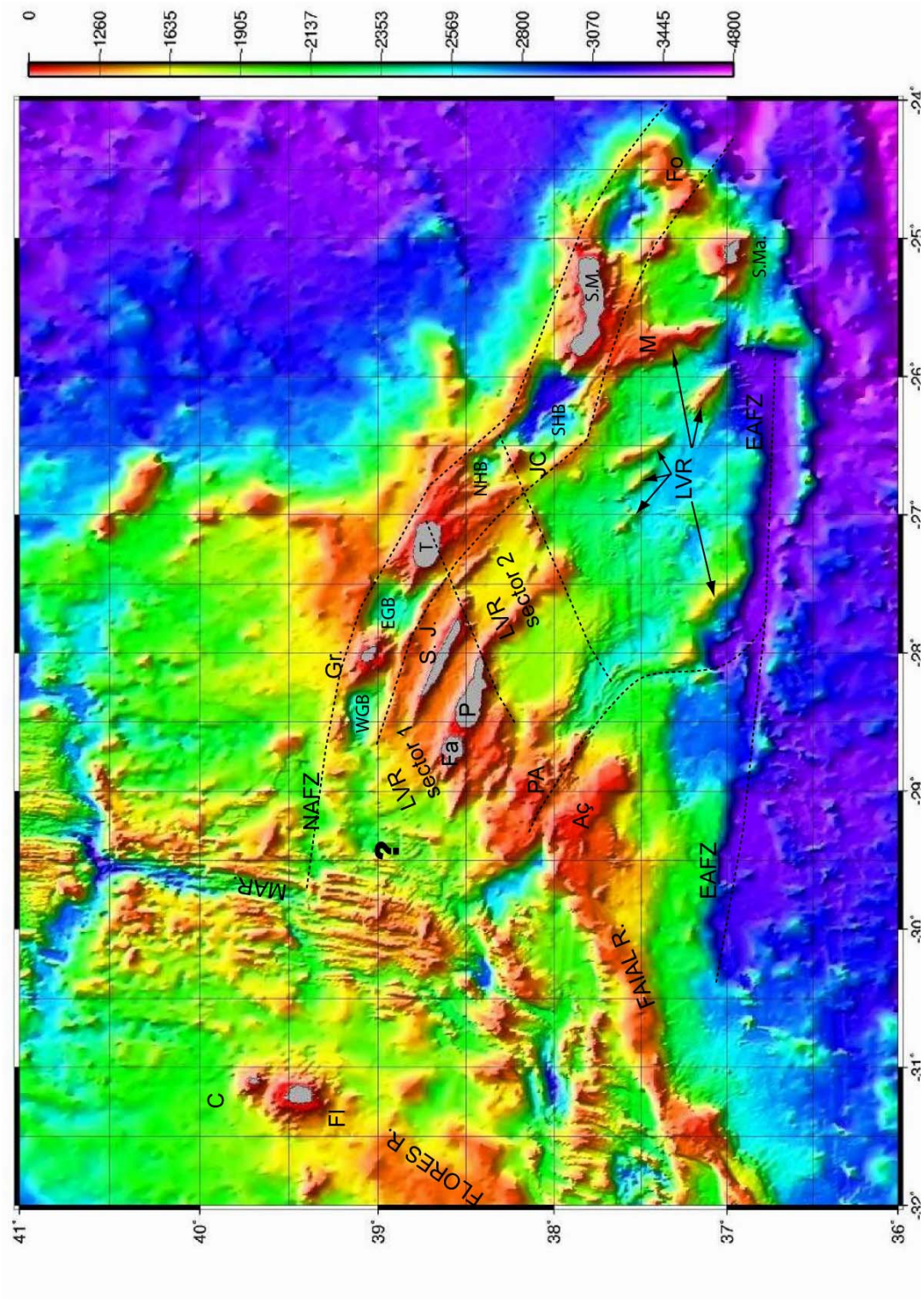

Figure I.2 - Detailed bathymetry of the Azores plateau from Lourenço *et al.,* (1998). Islands: C. – Corvo, Fl. – Flores (Western Group); Gr – Graciosa, T –Terceira, Fa – Faial, P- Pico (Central Group); SM – São Miguel, S.Ma - Santa Maria (Eastern Group). Basins: WGB - West Graciosa Basin, EGB – East Graciosa Basin; NHB – North Hirondelle Basin, SHB – South Hirondelle Basin. Banks: JC – João de Castro, Aç- Açor, Pa - Princesa Alice, Fo – Formigas Islets. NAFZ – North Azores Fracture Zone, EAFZ - East Azores Fracture Zone. MAR – Mid-Atlantic Ridge. Stippled lines: significant morpho-tectonic limits discussed in this manuscript.

Has the kinematic setting of the plate boundary and of the triple junction changed with time, and how?

Is the North America-Africa-Eurasia Triple junction clearly a ridge-ridge-ridge junction? Can we describe the area bounded by two branches of the Eurasia-Africa plate boundary as a microplate? Is the triple junction a discrete feature or a complex zone?

How is the relative motion between Africa and Eurasia accommodated in the westernmost part of the plate boundary? Is the motion distributed across the Azores plateau? Or does the Terceira rift account for all the relative motion?

In the following chapters, we will address some of this questions and present results from studies in which the author has been involved between 1999 and 2006. The Azores plateau is a particularly suitable area to study tectono-magmatic interactions in space and time and at different scales. It comprises the existence of a disputed plume or at least a significant upper mantle anomaly, hereafter refered as the Azores Hot-Spot (AHS) which is considered the main intervining factor for the formation of the Azores volcanic plateau. The internal structure of this plateau can be explained by interaction along time of the AHS with both the Mid-Atlantic Ridge (MAR) and the Azores Triple Junction (ATJ. Significant consequences of this interaction are: the position, kinematic and related tectonic response of the ATJ, the distribution of magmatic contribution for lithospheric structure and thermal structure of the Azores plateau and on the geophysical, geological and biological segmentation pattern of the MAR through time.

To understand the plateau inner structure and the consequences of AHS-ATJ-MAR interaction it is crucial that plate kinematic constraints are provided. Several kinematic interpretations have been provided in the past, but all of them fail to integrate a

significant portion of currently available multi-disciplinary data on the Azores plateau. In Chapter II, we review critically kinematic models described in the literature; discuss the interactions with the AHS they propose. We use morpho-structural and marine magnetic data on the Azores and we analyse the consequence of assuming different positions in time for the ATJ (i.e. the EU/NUB plate boundary), and test plate tectonic reconstructions using Euler stage poles from existing kinematic models. The main objective is to evaluate relative ages for the generation of first order bathymetric features within the plateau and try to constrain the expectable tectonic response within the plateau at each considered geodynamic time interval.

One of the strategies designed to identify the effects of the present day AHS influence is the mapping of seismicity resulting from volcanic and tectonic activity along the MAR. This can be done very efficiently with the use of hydrophone arrays, a technique developed for submarine acoustic surveying that is now available for scientific use. This is discussed in Chapter III.

The spreading velocities deduced from global models like NUVEL 1A (DeMets *et al.,* 1994) or based exclusively on GPS-derived models like REVEL (Sella *et al.,* 2002) or DEOS2K (Fernandes *et al.,* 2004) yield reduced full spreading velocities, varying from 3 to 4 mm per year (ultra-slow spreading ridges are classified as such for full spreading velocities below 1 cm/yr) for the EU/NUB plate boundary in the Azores. This allows the classification of this ridge as one of the slowest of the ridge global system (or hyper-slow, following Vogt and Jung (2003). The spatial distribution of the geodetically retrieved deformation field starts now to be understood. This is discussed in Chapter IV.

The short time span of geodetic observations only provides a snapshot of present day kinematic context, which relevance from the tectonic point of view is at least partially unknown. In Chapter V, we present and discuss complementary kinematic and tectonic markers of active processes that can be identified from the morphotectonic analysis of high resolution TOBI sonar.

This type of approach can be made systematically in the Terceira Island and neighbouring areas, where we tentatively infer how tectonics and volcanism do distribute and relate to each other. This is the aim of chapter VI. Here we will describe in detail the morphology and main geophysical characteristics of an area comprising Terceira Island and its neighbouring basins along the Terceira axis. The way volcanic and tectonic structures condition each other is analysed by integrating high resolution bathymetry and sonar on submerged areas where some new swath and sonar data have been collected with high resolution digital elevation models of the Terceira Island and meso-scale tectonic observations. A regional tectonic map is assembled and analysed. Directional data are compared with expected EU/NUB differential motion and consequently an assessement of fault kinematics and the role they play in magmatic accretion in that domain of Terceira axis is performed.

The smallest spatio-temporal scale is approached in this manuscript considering the sequence of tectono-magmatic events that took place in the 1957 and 1958 Capelinhos eruption in Faial. In Chapter VII we discuss and interpret the sequence of events which resulted on the Surtseyan eruption type (despite that the Faial eruption was prior to the 1963-1966 Surtsey Island eruption in Iceland) and triggered two strong tectonic shocks in faults neighbouring the volcanic fissural system, that links the Island main caldera and the eruption site in its western tip. Geodetic and GPS data for 60 years are

compared with 2D crustal dislocations models, resultant from fault slip data inversion. A geological interpretation is then performed, about the eruption driving mechanism, the earthquakes triggering mechanism and the style of accretion in this linear volcanic systems which constitute a significant part of the Azores plateau.

In Chapter VIII we use analogue modelling techniques to analyse the effect of ridge push in ridge extension and transform fault generation, and in particular the case for active transform faults which, contrary to what is expectable from fault mechanics, lie normal to the ridge axis. Despite approaching normal seafloor spreading ridge sections, this topic is relevant within the context of the EU-NUB plate boundary, as in the later there are evidences from earthquake activity and fault mapping that similar orthogonal geometries exist within the Azores.

Finally Chapter IX we perform the discussion of the data presented in this manuscript and integrate them into a coherent tectonic model for the ruling kinematics conditions at the EU-NUB plate boundary and ATJ at the present day. Topics for future researches in this complex geodynamical framework are also underlined.

Chapter II - Review of the kinematic Models for the ATJ and AHS

II.1 Overview

The evolution and shaping of the Azores Plateau is usually considered as the result of the interaction between two key processes: the ATJ instability and the Azores Hot Spot (AHS) position in the course of time. Past interpretative models, addressing their roles, put little emphasis on their interactions and consequent implications to the birth and evolution of the Azores plateau, and thus tend to treat each process as acting stand alone.

Two types of interpretative models have been presented: those which are based on constraints provided by kinematic models thus providing plate tectonic reconstructions of the previous geometries of the triple junction (Krause and Watkins, 1970; McKenzie, 1972; Searle, 1980; Luis *et al.,* 1994) and those that address particular aspects of the Azores tectonics, based on morpho-tectonic analysis (Machado *et al.,* 1957; Madeira and Ribeiro, 1990; Lourenço *et al.,* 1998; Vogt and Jung, 2003), isotopic dating (Féraud, 1980), focal mechanisms and earthquake epicenter distributions (Miranda *et al.,* 1998) and GPS observations (Fernandes *et al.,* 2004, 2006). Analyses of the present-day context of the ATJ will be dealt with later on.

Here, we present a summary of presented models which are sustained by kinematic interpretations; we test their underlying assumptions in respect of available geo-

information. Kinematic models are also confronted with models for the evolution of the AHS, notably those of Cannat *et al*., (1999) and Gente *et al.,* (2003) to try to identify the strong links and/or contradictions between both geodynamic histories across time.

II.2 ATJ Models based on plate kinematic reconstructions

II.2.1 The ATJ prior to 20 Ma: from Kings through to Gloria Fault

Regional studies comprising the kinematic evolution of the Atlantic basin, namely the evolution of the Gloria fault, always met problems when incorporating the complex behaviour of the Iberian microplate, described at times as attached to the Eurasian plate, or others attached to the African plate (Bonnin, 1978, Olivet, 1984; Klitgord and Schouten, 1986). Some models also consider that during different time intervals, Iberia has moved independently from the two larger plates (Galdeano *et al.,* 1989, Srivastava *et al.,* 1990a, 1990b and Roest and Srivastava, 1991).

The analysis of the kinematic behaviour of the Iberian micro-plate is limited by the lack of prevalent magnetic lineations, and the difficulties in tracing the homologues of Fracture Zone's traces between the North American Plate (NAM) and Iberian (Canpam, 1995). A thorough analysis of the evolution of the Iberian micro-plate during the opening of the Northern Atlantic basin is out of scope of this work.

Here we consider just a short summary of the main kinematic events and onset of resulting morpho-tectonic features during the course of this evolution since anomaly M0, as proposed by Srivastava *et al*. (1990a) and depicted in Figure II.1.

After mid-Cretaceous (since anomaly M0, 118 Ma), a triple junction developed at the Gulf of Biscay while Iberia is supposed to have shared a common kinematic history with Africa. This Triple junction will constitute the main plate boundary during most of

the Atlantic evolution and its trace is defined along the Gulf of Biscay towards a region north of the Kings trough. Its behaviour is mainly extensional between anomalies 33 and 31, and becomes dominantly right lateral strike slip until anomaly 21 times.

The unstable configuration of the triple junction led to its southward migration and the opening of the Kings trough at anomaly 17 times (ca. 37 Ma). The plate boundary then becomes defined by the Kings Trough, Azores-Biscay ridge and the Pyrenees chain.

After anomaly 19 (41.4 Ma) Iberia detached progressively from the African plate, with the development of a southern Iberian plate boundary defined by the Gloria fault. The northern boundary gradually losses significance and differential motion between Eurasia and Iberia plate nearly cease at anomaly 10.

At anomaly 6c (23.4 Ma) activity on the Kings trough ceases completely and Iberia becomes attached to the Eurasian plate. Only one triple junction becomes active at the Azores level and the plate boundary is solely located along the Gloria fault.

This model is disputed as it presents several inconsistencies with inland geology, namely with regard to the Pyrenees tectonic history, where major wrench events are documented prior to 37.5 Ma. Other difficulties result from the assumption of coupled movement between Iberia and Northern Africa as both Atlas, the Rif and the Betics were onset prior to anomaly 17 (Canpam, 1995 and references therein).

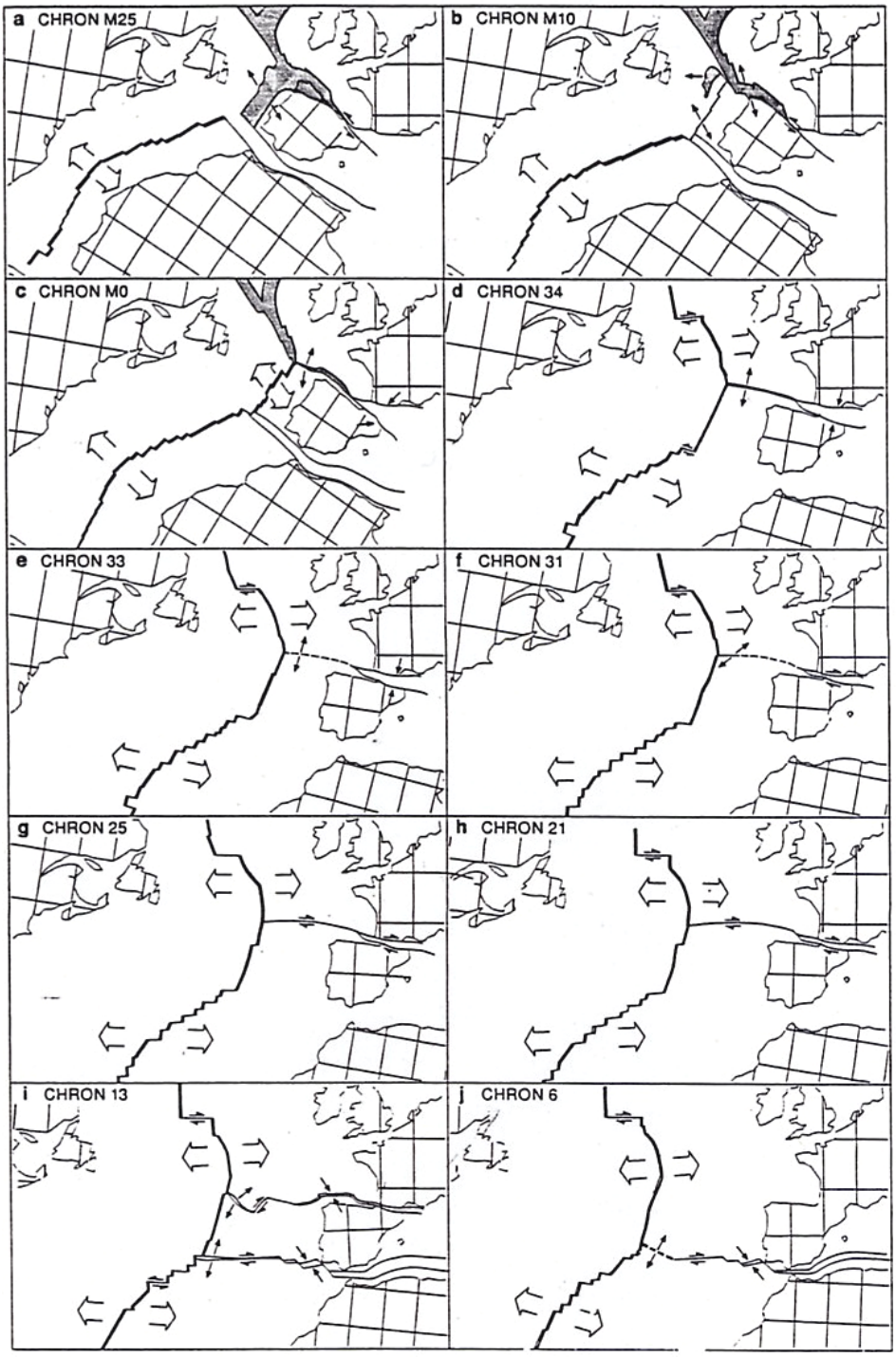

Figure II.1 - Evolution of the Iberian Microplate since anomaly M25 to anomaly C6. Note the definition according to this model of an independent Iberia since anomaly 19 (41.4 Ma) and the definition of two triple junctions, one at the north in Kings trough and the southern one defined at the Gloria fault. (Srivastava *et al.,* 1990a).

Other authors simplify this history and only consider one triple junction active at each time thus precluding an independent Iberia. The transfer of Iberia Lithosphere from African plate to the Eurasian plate is signed at anomaly 13 (33.4 Ma) by Ollivet (1984), during anomaly 10 (28.3 Ma) by Klitgord and Schouten (1986) or at 25 Ma following collision between EU and AF in southern Iberia (Silver *et al.,* 1998).

As we shall see below, regardless of the preferred model, when one considers plate reconstructions confined to a more local scale (the scale of the Azores) it will cause significant difficulties and caveats. Moreover, the Azores block presents the same degree of obscurity in kinematic terms as the Iberian plate. Its evolution seems to have been marked by transference from African to Eurasian megaplates behaving sometimes as an independent block. Understanding the behaviour of its northern (Terceira axis) and southern (EAFZ) limits is therefore crucial for tracing its evolution. Below, we review critically the attempts performed by different authors to constrain it

II.2.2 The ATJ prior to 20 Ma: from Gloria fault to Terceira axis or to EAFZ?

Early studies, centred on the characterization of the Azores Triple Junction and the EU-AF plate boundary, were based on sparse ship-borne bathymetric and magnetic profiles. Calculated global or regional Euler poles suffered from similar limitations.

A first attempt was made by Krause and Watkins (1970) based on the first surface magnetic compilation. They considered a RRR (Ridge-Ridge-Ridge) triple junction type, with oblique spreading on the Eurasia-African plate boundary. According to these authors, such a configuration would have evolved from a RFF triple junction with migration of the MAR westwards, south of the EAFZ and change in the spreading direction from E-W to ESE-WNW. This re-orientation of the spreading direction would

additionally result in the creation of a Leaky transform in the ATJ third arm, which would ultimately facilitate the formation of the Terceira axis as a secondary spreading center. These authors make no assumptions regarding the stability of the proposed configuration but attribute an age of at least 45 Ma for the beginning of the Terceira axis leaky transform (Figure II.2).

McKenzie (1972) reviewed critically this first model and discussed for the first time the stability of the ATJ. His model is very similar to that of Krause and Watkins as it considers an evolution of the ATJ from an initial RFF configuration originated at the junction of the MAR with the EAFZ. Northward migration along the MAR of this triple junction would result in the formation of two oblique spreading centers and a RRR type triple junction (Figure II.3a). He considered that the Triple Junction is stable through time provided that all three branches would spread obliquely. Contrary to the previous one, this model precludes change in the spreading direction but as noted by McKenzie (1972), it would imply a tendency for the ATJ to migrate northward.

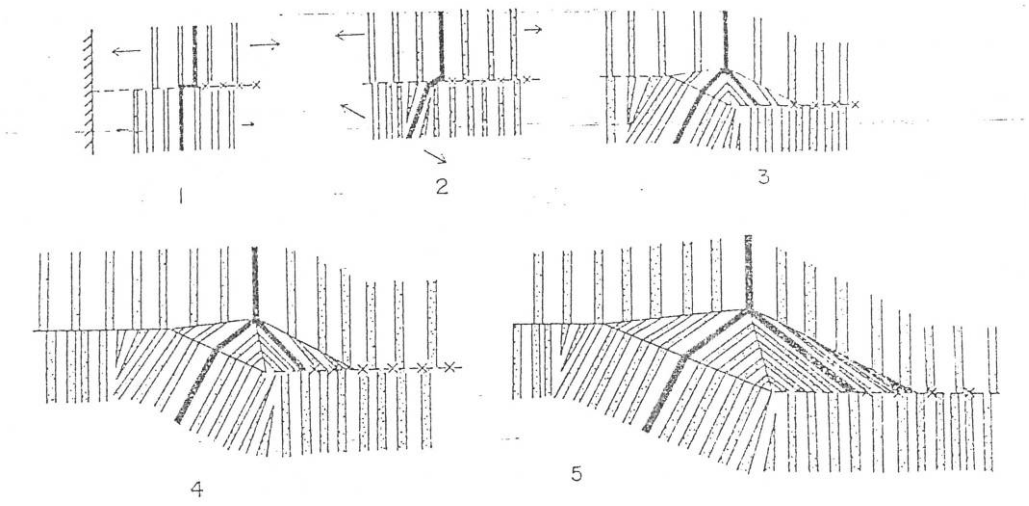

Figure II.2 – Sketch depicting the evolution of the Azores Triple Junction proposed by Krause and Watkins (1970). Arrows indicate plate spreading directions.

Both models imply the existence of a triangular domain of Azores topography with apex on the triple Junction, bisected by the Terceira axis. The present knowledge of the Azores plateau as we shall discuss in up-coming sections, its morpho-structural and the magnetic anomalies patterns and the kinematic conditions which subsisted through time allow us to refute this models as un-realistic

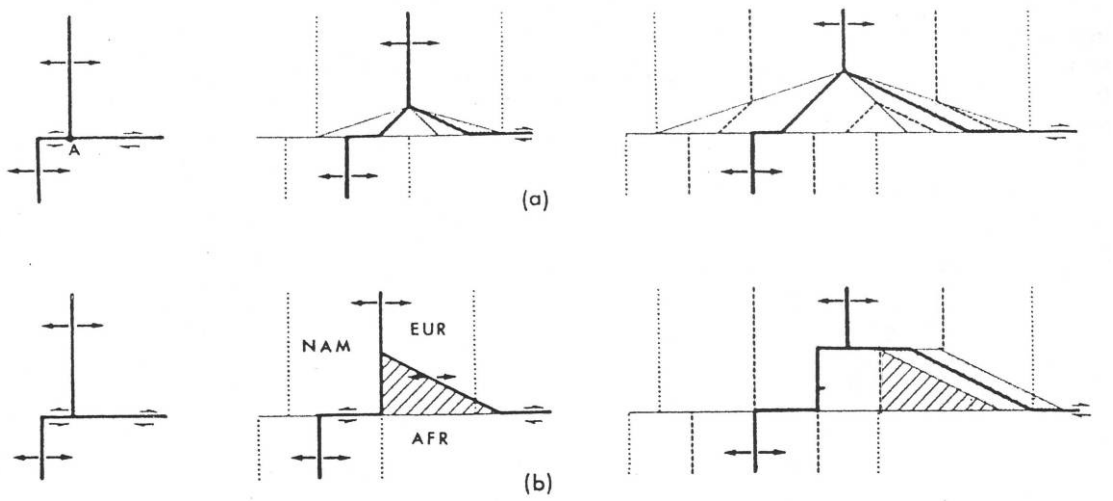

Figure II.3 - Evolution of the Azores Triple Junction according to: a) Mckenzie (1972). b) Searle (1980), pattern expresses lithosphere sections transferred from the Eurasian to the African plate due to onset of the Terceira axis (From Searle, 1980).

The first strongly documented work on the Azores was produced by Searle (1980), using ship-borne magnetic and Gloria lateral sonar mosaics. Searle re-evaluated the previous interpretations and defined a first overall segmentation pattern in the Terceira axis. In his interpretation (Figure II.3b), the Azores Triple Junction evolves, again from the EAFZ intersection with the MAR, as a RFF (Ridge-Fault-Fault) configuration, to a position defined at the intersection between the Terceira axis and the MAR at the North Azores Fracture Zone, due to a sudden northward jump of the triple junction. A

triangular section of previous Eurasian generated lithosphere would than be truncated by Terceira axis generation and transferred to the African plate..

Searle (1980) was however renitent in assuming the present ATJ position on the NAFZ, on grounds of the orientation of this Fracture zone with respect to predicted directions of opening between Eurasian and African plates (closer to ca. N58º), and does not exclude, considering the tectonic fabric interpreted from the sonar images and the recent volcanic activity, that the Triple Junction could be located further south around 38º 40' N in the region west of Faial. He further considered the Terceira axis as a spreading center but does not exclude the possibility, given the numerous linear ridges running sub-parallel to the Terceira axis, that true seafloor spreading generating Azores crust could be limited and the Azores would therefore represent a rift zone with a high complex architecture resulting from a mélange of crust generated previously at the MAR predated by Azores generated crust possibly along pre-existing tectonic structures.

Finally, an assumption is made by this author concerning the age of the Triple junction migration and beginning of the Terceira axis. By extrapolating the calculated spreading of ca 3 $mmyr^{-1}$ to the width of the spreading center (along the spreading direction), he reaches an age of 55 Myr as an upper bound, although he assumes 36 Myr as more realistic age for the generation of the Terceira axis, as a result of changes between the African and Eurasian plates relative movement (Figure II.4).

II.2.3 The ATJ in the last 10 Ma: fine scale evolution of Triple Junction

Luís *et al*. (1994) and Luis (1996) presented a new Azores plateau aeromagnetic chart with a much higher level of definition than previous ones (cf. Figure II.5). This new

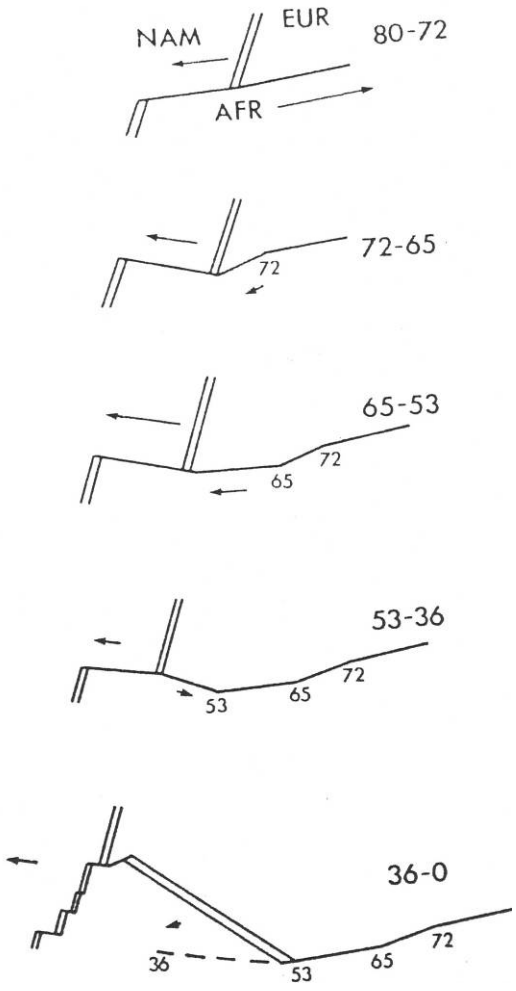

Figure II.4 - Kinematic model of the ATJ evolution according to Searle (1980).

magnetic anomaly map allowed them to perform a highly detailed kinematic analysis of the ATJ confined to the last 10 Ma. It revealed the recent evolution of the segmentation pattern of the MAR and in particular several northward migrations of the Eurasia-African-North America triple junction, from a past location near 37° N up to its present location interpreted to lay on Pico-Faial alignment with the Mid-Atlantic ridge. Their proposed evolution comprises: from Chron 5 to Chron 3 (~10-3.85 Ma) existence of an independently moving Azores block detached from both Eurasian and African plate.

During this time span two triple junctions were active at the northern and southern boundaries of the block. They could only constrain the position of the southern one initially at 38º00'N, 38º50'W and gradually jumping north to 38º20'N, 30º15' W between C4 and C3A. At C2A (2.45 Ma), ATJ reaches its present position at 38º55'N, 30º00'W. From that time on, they consider that the Azores block moves attached to the Eurasian plate.

This analysis was however based on plate tectonic reconstructions with regards to the MAR, and little can be inferred about the tectonic implications of their proposed ATJ evolution within the plateau. For example, the northward migration of the southern ATJ implicitly implies that some amount of internal deformation should exist within the Azores block, and also that sections of Azores block lithosphere have possibly been transferred to the African plate, as also suggested by Searle (1980). Lack of constraints on the kinematic behavior and position of the northern ATJ from the past until anomaly 2A, limits the ability to understand the Azores Plateau evolution through time.

II.3 Testing two kinematic models for the evolution of the ATJ

Triple junctions are intrinsically unstable features (Cronin, 1992) and several authors (e.g. Bird *et al.,* 1998 and 1999; Rusby and Searle, 1995; Mitchell and Livermore, 1998) have suggested that the approach to be followed when performing plate tectonic reconstructions in these domains should account for tectonic explanations rather than performing strict kinematic reconstructions. The problem of using a purely kinematic approach has been addressed by Cox and Heart (1986) as "The three plate problem", where in a triple junction defined by three plates A, B and C, if one rotates plates A and B relative to the C, about fixed Euler poles than relative movement between plates A and B cannot be described by a fixed Euler pole through time.

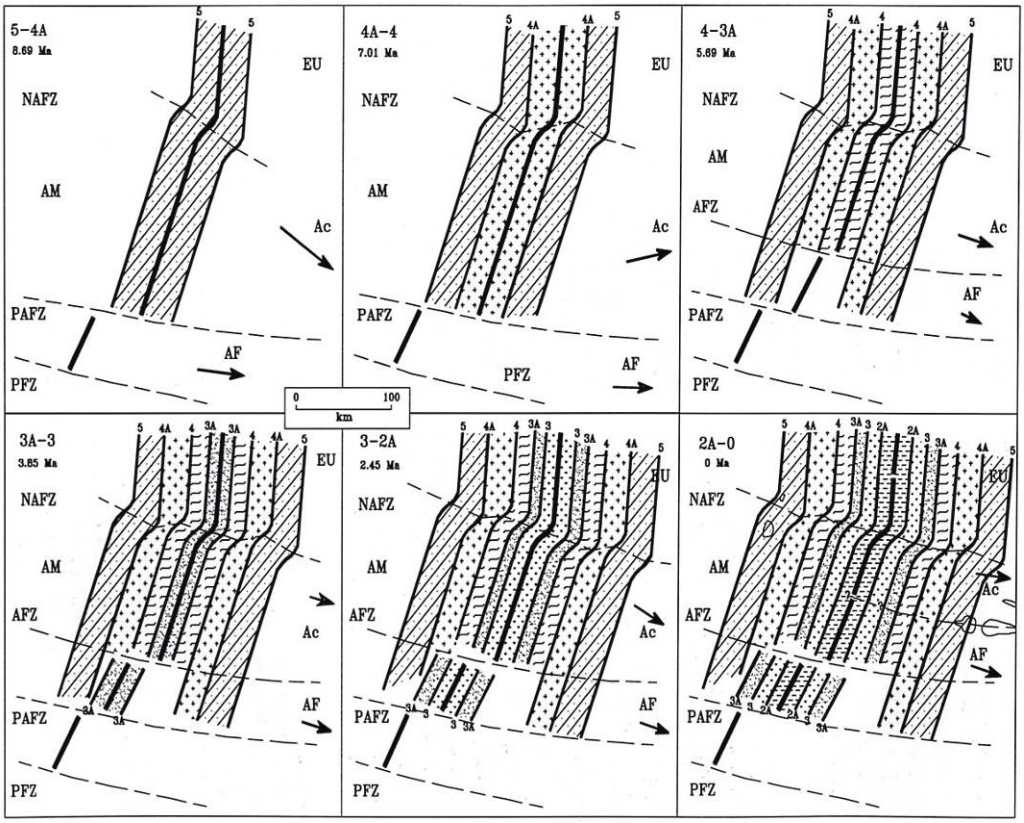

Figure II.5 - Schematic model of the Azores Triple Junction according to Luis *et al.,* (1994) from anomaly 5 to the present. The axis is marked by the heavy line. The arrows represent the velocity of the Azores and Africa relative to North American Plate. AF-Africa; Ac – Azores; AM – America; EU – Eurasia; EAFZ – East Azores Fracture Zone, PFZ – Pico Fracture Zone; PAFZ – Princess Alice Fracture Zone; AFZ – Açor Fracture Zone; FFZ – Faial Fracture Zone; NAFZ – North Azores fracture Zone.

The attempt to resolve the different positions of the ATJ and the configuration of the EU/AF plate boundary through time in the Azores using kinematic models has two additional obstacles linked with the intrinsic nature of the plateau and provided by the unstable triple junction configuration of this domain:

1. The EU/AF (or EU/NUB) plate boundary, with some exceptions around Terceira axis, does not provide a coherent pattern of seafloor magnetic anomalies, thus not providing consistent isochrones for plate tectonic reconstructions;

2. There are no clear transform faults across the Azores plateau that can provide plate spreading direction constraints through time.

Here, we use the isochrons from Luis *et al*. (1996) and Canpam (1995) to check the consistency of plate reconstructions and the validity of kinematic models presented in section II.2.2. We consider specifically their underlying hypothesis that Pico is the N. American plate structural analogue of the EAFZ, which, as presented previously, is generally assumed as the plate boundary between EU and AF from times prior to at least anomaly 6 in those models.

Anomaly picks from these authors complement each other. Canpam (1995) picked anomalies covering a wider region from the Northern and Central Atlantic, whereas Luis *et al.,* (1994) and Luis (1996) chrons were retrieved from a denser aero-magnetic map centred on the Azores region and therefore allowing a more detailed analysis of this region. Magnetic anomalies selected for this approach are C13 (33.4 Ma), C6 (20.1 Ma), C5 (9.8 Ma) on all three plates. The magnetic time scale is from Cande and Kent (1995). Their anomalies are displayed in Figure II.6.

The figure reveals that magnetic anomaly picks display a rather close pattern with the exception of anomaly C13. Due to higher resolution of the aero-magnetic chart in the Azores area, Luis was able to trace within the plateau, a trail of points for anomalies C5 and C6. Canpam does not consider any anomalies within the plateau and only traces them to the intersection with the Terceira axis to the north and with the EAFZ to the south. The definition of anomalies south of the Pico F.Z and in the African plate is sparse due to very poor quality of existing magnetic data and the fit between both authors is poor probably due to the magnetic time scale choosen.

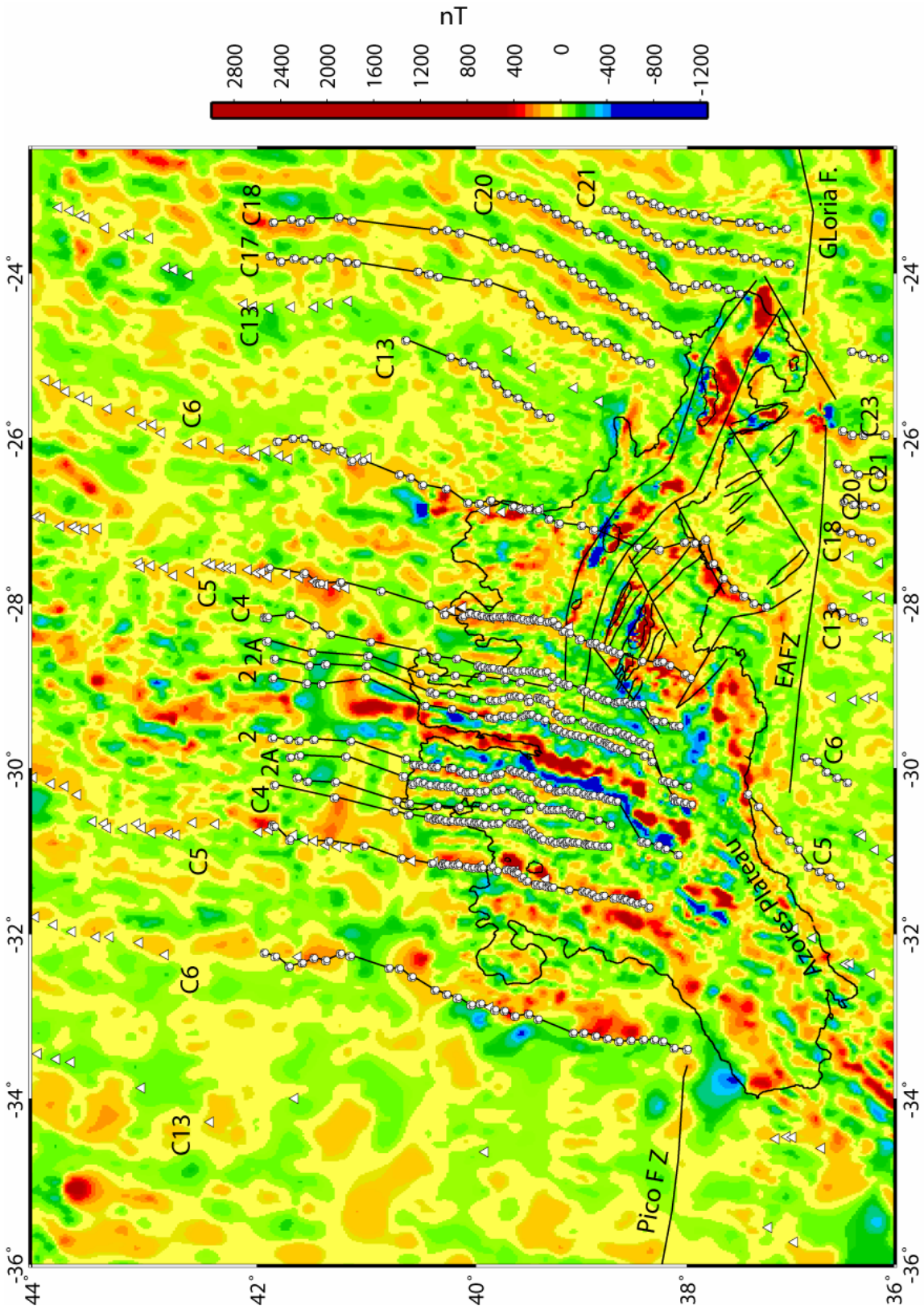

Figure II.6 - Magnetic anomaly map of Luis *et al.* (1996). Magnetic anomalies from Luis *et al.*, 1994 are represented by circles, and those of Canpam *et al.*, (1995) by triangles. The Azores Plateau 2500 m bathymetric contour and the outline of main morpho-tectonic features are also presented for reference as solid black lines.

To perform our kinematic analysis, we consider two sets of poles, presented in Table II.1 for the NAM/AF and the EU/AF and NAM/IB. Apart from the poles presented in Table II.1 there are a considerable amount of poles calculated for these plate pairs. Analysing them is out of the scope of this work. For the interested reader, an exhaustive list of finite rotation poles describing the relative movement of EU and AF with regard to NAM can be accessed through Mirone (Luis, *in press*), a software which, amongst other tasks, allows finite rotations of graphic elements in a geographical space[1].

Table II.1 – Finite poles describing the relative motion between Eurasia (EU) - North America (NAM) and NAM –Africa (AF) plates for Chrons: 13, 6 and 5. These are grouped in two pole series.

Anomaly	Longitude	Latitude	Angle	Age	Reference
Poles series 1					
EU(IB)-NAM					
C5	133.84	64.57	-2.39	9.8	Klitgord & Schouten (1986)
C6	138.2	68	-4.75	19.7	Srivastava *et al.* (1990)
C13	143.5	48.06	-7.2	33.2	Srivastava & Tapscott (1986)
NAM-AF					
C5	77.95	79.08	2.41	9.8	Klitgord & Schouten (1986)
C6	37.84	79.57	5.29	19.7	Klitgord & Schouten (1986)
C13	2.22	76.28	9.96	33.2	Srivastava *et al.* (1990a)
Poles series 2					
EU(IB)-NAM					
C5	137.59	63.92	-2.4	9.8	Canpam (1995)
C6	136.05	66.48	4.83	20.7	Canpam (1995)
C13 *	143.47	54.14	-7.33	33.4	Canpam (1995)
NAM-AF					
C5	21.9	80.31	2.48	9.8	Campan (1995)
C6	23.66	80.84	5.25	20.7	Canpam (1995)
C13	5.96	76.04	9.77	33.4	Canpam (1995)

* Considering and independent Iberian plate, see section II.2.1

[1] Mirone can be downloaded from http://w3.ualg.pt/~jluis/mirone.

II.3.1 Constraints provided by stage pole rotations

The method of describing the relative motion between Eurasian and Nubia plates consists on the estimation of rotation parameters between these two plate pairs, by studying their relative movement to the NAM plate. Finite rotation poles between African (AF) and Eurasia (EU) can therefore be calculated by:

$$_{AF}ROT_{EU}(t) = {}_{AF}ROT_{NA}(t) + {}_{NA}ROT_{EU}(t) \quad \text{(II.1)}$$

Where $_{A}ROT_{B}(t)$ is the rotational parameters (latitude, longitude and angle) of the finite rotation of plate A relative to plate B for a given time (t).

Stage poles (describing plates relative movement between time intervals), can, on the other hand, be calculated by finite rotations as below.

$$_{EU}ROT_{AF}(C6\text{-}0) + {}_{EU}ROT_{AFR}(0\text{-}C5) = {}_{EU}ROT_{AF}(C6\text{-}C5) \quad \text{(II.2)}$$

Stage poles are here used to provide an assessment of the tectonic regimes acting on the Azores plateau during discrete time intervals. This is achieved by rotating a set of elements from their expected initial locations at the oldest time considered and trace their circuit from that initial time to the present. One should bear in mind that the vector for each time interval only provides an integral measurement of the total displacement and not the incremental path within the time interval under consideration.

To perform this analysis we calculated the stage poles using equations (1) and (2) for set of poles 1 and we also used stage poles calculated by Canpam (1995) from her finite rotations poles. The resulting stage poles are presented in Table II.2.

Table II.2 – List of stage poles between EU (IB) - AF tested in this study

Anomaly interval	Longitude	Latitude	Angle	Age Interval (Ma)	Reference
EU(IB)-AF					
Pole series 1					
C13-C6	-22.053	36.1816	-6.4315	13.5	This study (Pole series 1)
C6-C5	-10.0129	23.6348	-1.4405	9.9	This study (Pole series 1)
C5-0	-18.8309	13.3936	-0.8828	9.8	This study (Pole series 1)
Pole series 2					
C13-C6	-15.12	35.17	-4.77	12.7	Campan (1995)
C6-C5	-20.46	22.39	-1.17	10.9	Canpam (1995)
C5-0	-24.28	12.59	-1.32	9.8	Canpam (1995)

Figure II.7 and Table II.3, display the results of the rotation using the calculated stage poles, for a set of points distributed along the East Azores Fracture Zone and Gloria fault. Rotations are performed assuming points belong to Eurasian plate at the time of anomaly C13 and considering a fixed African plate. Their circuit comprises therefore three stages from C13 to C6 (20 Ma), from C6 to C5 (10 Ma), and from C5 to the present.

We verify that, regardless of the poles series chosen, the bulk tectonic regime during the growth and evolution of the Azores was transtensional with a variable component of right lateral shear. The initial rotation between C13 and C6 is characterized by a transtensional regime dominated by extension in a N10º to a N13º direction between AF and EU plates. In this instance, rotations with the two pole series differ drastically in spreading velocities.

The spreading directions between both time series vary more significantly between C6 and C0. During this time span both are characterized by an increase in the lateral shear component of transtension. In Pole series 1, the bulk extensional direction changes to

approximately SW-NE between C6 and C5, and then to WSW-ENE from C5 to the present. These later spreading directions are very similar to that retrievable form NUVEL1A for AF/EU, which vary between N65º to N70º from West to East across the plateau (DeMets *et al.,* 1994). Pole series 2 rotates from WSW-ENE to a nearly E-W spreading direction therefore suggesting a more oblique spreading with respect to the strike of the main plateau morphological features. The spreading direction predicted by the stage poles series 2 between C5 and C0 is very similar to the present day spreading direction retrieved from global and regional geodetic models based solely on GPS observations like the Revel2000 (Sella *et al.,* 2002) and Deos2K (Fernandes *et al.,* 2006, see also chapter IV).

Considering the orientation of small wavelength relief generation like the linear volcanic ridges and assuming that they were formed in a context of pure traction, then the possible timings for their generation can be constrained by kinematic scenarios outlined in Figure II.7 and Table II.3.

From C13 and C6, considering Pole Series 1, the optimally oriented structures for pure shear extension within the Azores domain are the EAFZ and some significant linear features such as the linear volcanic ridge trending E-W between 25º30'W and 26º30'W at the latitude of Terceira Island and the E-W elongated plateau which culminates in the S. Miguel Island (Figure II.7). The orientation of these structures supports the consideration that their growth is controlled by pré-existing FZ (Guest *et al.*, 1999). Their favorable orientation with respect to direction of extension during that time span, could have promoted FZ reactivation and extension. Other E-W south facing morphological steps between flat horizontal, probably highly sedimented terraces at ca. 38ºN between 26ºW and 27º30'W, might have been favored in the same time interval.

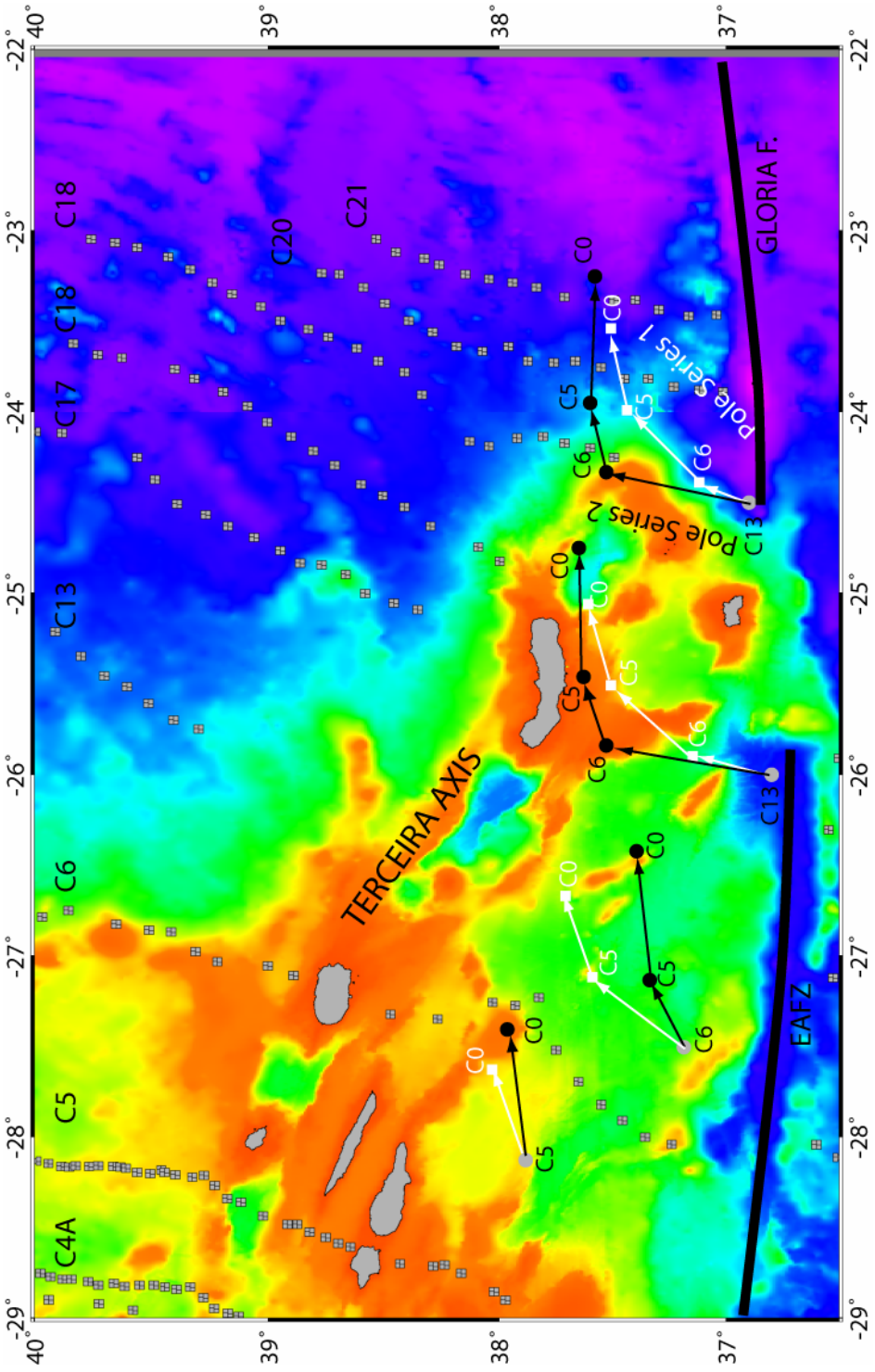

Figure II.7 - Rotation of point elements using stage poles calculated in Table II.2. Points are considered to be in Eurasia plate at an initial C13 time and rotated afterwards considering a fixed AF plate. The relation between vector direction in each time interval and reloief orientation, provide a possible age constraint to relief formation. White squares and arrows: pole series 1. Black circles and arrows: pole series 2.

Table II.3 - Numerical results from the stage pole rotations presented in Figure II.7.

Pole Series 1													
Initial Position (C13)		**at C6**		**Distance**	**Azimuth**	**at C5**		**Distance**	**Azimuth**	**at present**		**Distance**	**Azimuth**
Lon	**Lat**	**Lon**	**Lat**	**(km)**	**Cw from N**	**Lon**	**Lat**	**(km)**	**cw from N**	**Lon**	**Lat**	**(km)**	**cw from N**
-23.13	36.8	-23.04	36.89	13.0103	N39°	-22.65	37.18	47.3186	N48°	-22.2	37.23	40.9292	N81°
-26.6	36.7	-26.51	37.11	47.15192	N10°	-26.12	37.48	54.0784	N40°	-25.67	37.59	41.2996	N72°
-28.6	36.9	-	-	-	-	-28.09	37.9	56.6712	N36°	-27.63	38.03	42.596	N70°
Pole Series 2													
-23.13	36.8	-22.96	37.33	64.2644	N13°	-22.58	37.37	33.336	N83.5°	-21.89	37.32	61.8568	N95°
-26.6	36.7	-26.46	37.47	87.044	N08°	-26.08	37.58	35.96584	N70°	-25.38	37.61	61.4864	N87°
-28.6	36.9	-	-	-	-	-28.06	37.95	38.3364	N63°	-27.34	38.03	63.3384	N81°
Pole Series 1													
Initial Position (C13)		**at C6**		**Distance**	**Azimuth**	**at C5**		**Distance**	**Azimuth**	**at present**		**Distance**	**Azimuth**
Lon	**Lat**	**Lon**	**Lat**	**(km)**	**Cw from N**	**Lon**	**Lat**	**(km)**	**cw from N**	**Lon**	**Lat**	**(km)**	**cw from N**
-23.13	36.8	-23.04	36.89	13.0103	N39°	-22.65	37.18	47.3186	N48°	-22.2	37.23	40.9292	N81°
-26.6	36.7	-26.51	37.11	47.15192	N10°	-26.12	37.48	54.0784	N40°	-25.67	37.59	41.2996	N72°
-28.6	36.9	-	-	-	-	-28.09	37.9	56.6712	N36°	-27.63	38.03	42.596	N70°
Pole Series 2													
-23.13	36.8	-22.96	37.33	64.2644	N13°	-22.58	37.37	33.336	N83.5°	-21.89	37.32	61.8568	N95°
-26.6	36.7	-26.46	37.47	87.044	N08°	-26.08	37.58	35.96584	N70°	-25.38	37.61	61.4864	N87°
-28.6	36.9	-	-	-	-	-28.06	37.95	38.3364	N63°	-27.34	38.03	63.3384	N81°

The remaining orientations of the linear volcanic ridges in the central sector of the Plateau do not fit this pattern of fracture zone reactivation and their generation can be linked to the migration northwards of the Triple junction as discussed. Stage poles from both time series and corresponding extension directions favor their generation at a time younger than 20 Ma.

The linear volcanic ridges in the plateau western sector (corresponding to the Central group Islands of Pico-Faial and S. Jorge), considering their orientations, may again result from reactivation of some Fracture Zone sections, their growth as magmatic systems is favoured between anomaly 6 and 5, taking Poles Series 1 or in right lateral transtensional considering Poles series 2. As we shall see later on (in chapter VII), to some extent, magmatic growth of these structures can be considered irrespective of far-field stresses, and more conditioned by local circumstances such as internal magma pressure, and magma migration mechanisms.

II.3.2 Is the Pico FZ the structural homologue of the EAFZ?

The approach from previous section does not allow constraining the position of the ATJ for a given time, as the chosen points used for rotation with the stage poles have arbitrary positions with respect to the plate boundary for that time. They only provide a measure of expectable plate boundary tectonic behavior. To constraint the position of the ATJ at specific time intervals, we performed finite rotations between morpho-tectonic elements and isochrones using the two poles series presented in table II.1. Plate tectonic reconstructions were performed aiming at verification of the hypothesis that Pico and EAFZ are structurally homologue structures.

If one considers that the ATJ was located at the EAFZ-Pico FZ at the times C13 (33 Ma) and C6 (20 Ma), and that depart of the ATJ from this position has started in a younger age, than the finite rotation of the points marking the intersection of each chron with the Pico F.Z from the American plate with NAM-EU and NAM-AF finite poles should plot over the position (in present coordinates) of the EAFZ. The results of this approach are presented in Figures II.8 and II.9.

These reveal a large misfit and a poor closure of the ATJ at each time interval considered. For example at C13 time (33.4 Ma), the misfit in the position between stable EU/NAM and stable AF/NAM finite rotations of the equivalent point in the N. American Plate is of ca. 87 km using poles from series 1. Considering poles from series 2 the misfit is larger, ca. 146 km. Even if we consider the mismatch in the overlap between Canpam magnetic anomaly picks of C13NAM with respect to C13EU after finite rotation (about 73 km), the resulting misfit in Pico F.Z with respect to EAFZ would still be in the order of 73 km.

These misfits between the Pico FZ and the EAFZ in present day coordinates observed in both Figures II.8 and II.9, regardless of the kinematic model chosen as a reference; imply that, no simple kinematic closure of the three plates at the ATJ can be achieved.

Poles in series 1 and 2, perform relatively well in fitting the Pico FZ to the EAFZ after rotation, when using NAM/AF poles. Therefore, EAFZ migth have acted as a plate boundary fault between the northern limit of stable AF and the Azores domain. We shall refer to this limit from now on as the SATJ (Southern Azores Triple Junction).

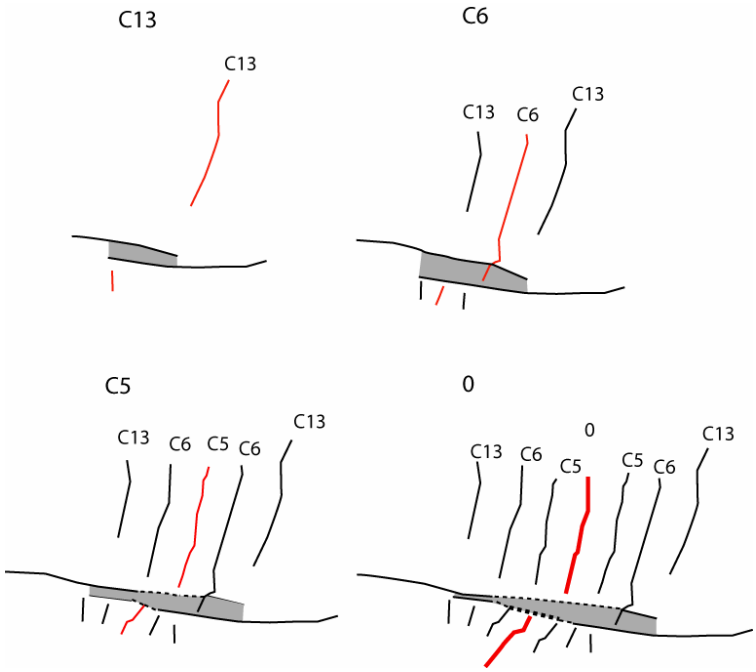

Figure II.8 - Schematic representation of Pico Fz rotations using Pole series 1 as kinematical constraint. Gray polygon provides a measure of mismatch between Pico FZ and EAFZ after finite rotation and constitutes a bulk measure of Azores related extension at each time considered.

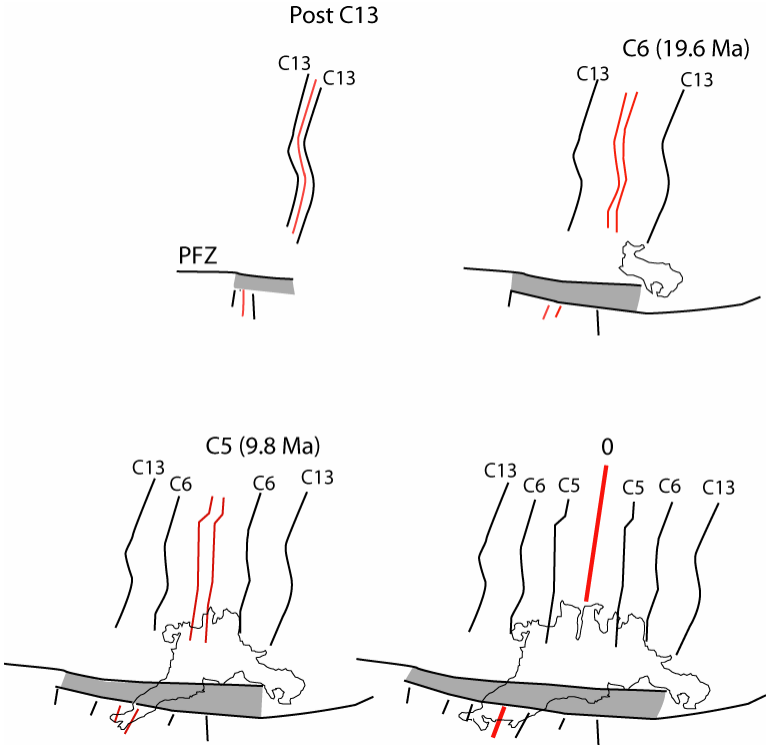

Figure II.9 - Schematic representation of Pico Fz rotations using Pole series 2 as kinematical constraint. Gray polygon provides a measure of mismatch between Pico FZ and EAFZ after finite rotation and constitutes a bulk measure of Azores related extension at each time considered.

Between C13 and C6, if the SATJ was located at the EAFZ, then this structure should have been subject to a significant component of pure traction, as already suggested in the previous section. When considering the width of the Fracture Zone, we verify that in its eastern section, between 26º42'W and 27º54'W, the fracture zone valley is wider (~16 km) than its western section were the valley is well marked by a narrow PTDZ of ca. 8 km. So, considering the values presented in Table II.3, probably the older sections of the EAFZ have been subject to a greater amount of extension, but the bulk of the C13 to C6 extension had also to be partitioned in other plate boundary structures located northwards.

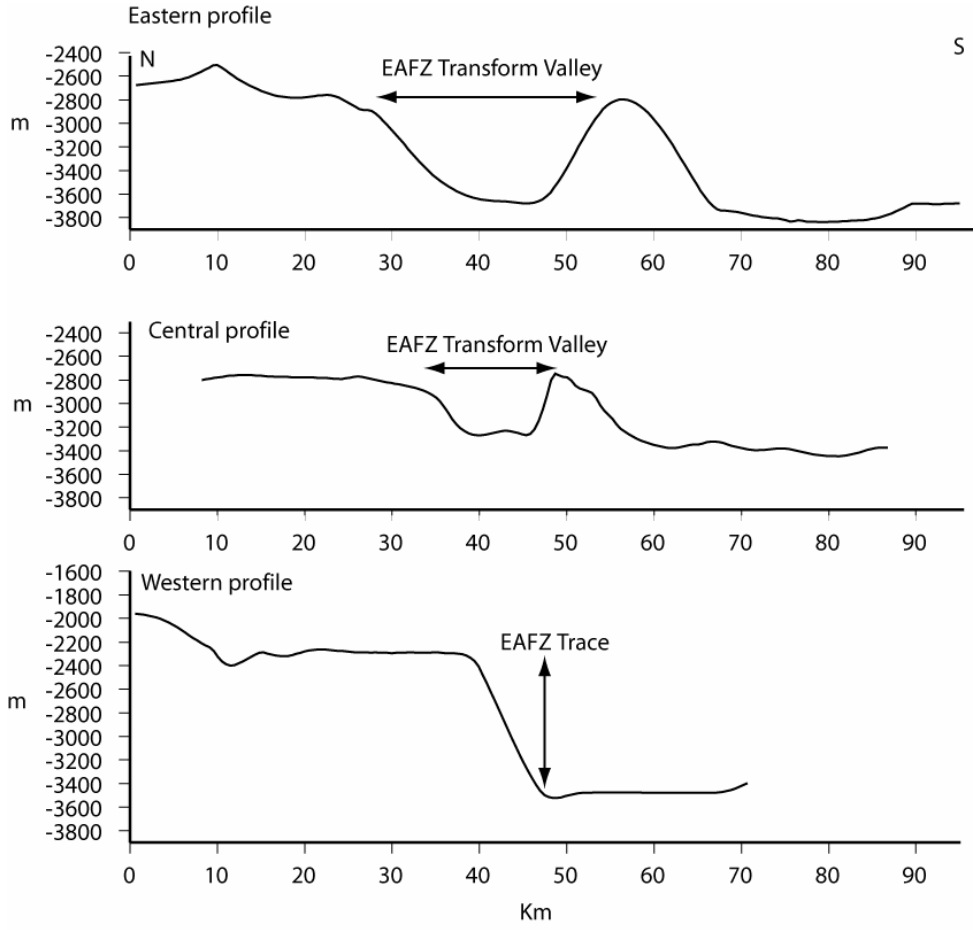

Figure II.10 - Topographical profiles across the EAFZ Note the progressive widening of the transform valley from the central to the eastern topographical profile. In the western profile, the transform valley dies out and only a major south facing scarp is present.

The transition between these two EAFZ domains is set at -27º54'W (Figure II.11). This location marks the beginning of a NW trending valley that roots into the EAFZ. and then inflects to a more WNW-ESE direction, terminating in wedge shape depression which cuts through Faial ridge, south of the condor Bank and defines the Princess Alice bank to the South.

This structure has been interpreted by Vogt and Jung (2003) as the morphological trace of the SATJ northward migration as a failed rift. Therefore, narrowness of the EAFZ west of this point, might represent the last increments of this structure as a major plate boundary fault. The lithosphere section imprisoned between this structure and the termination of the EAFZ trace might correspond to Azores lithosphere accreted onto the AF plate.

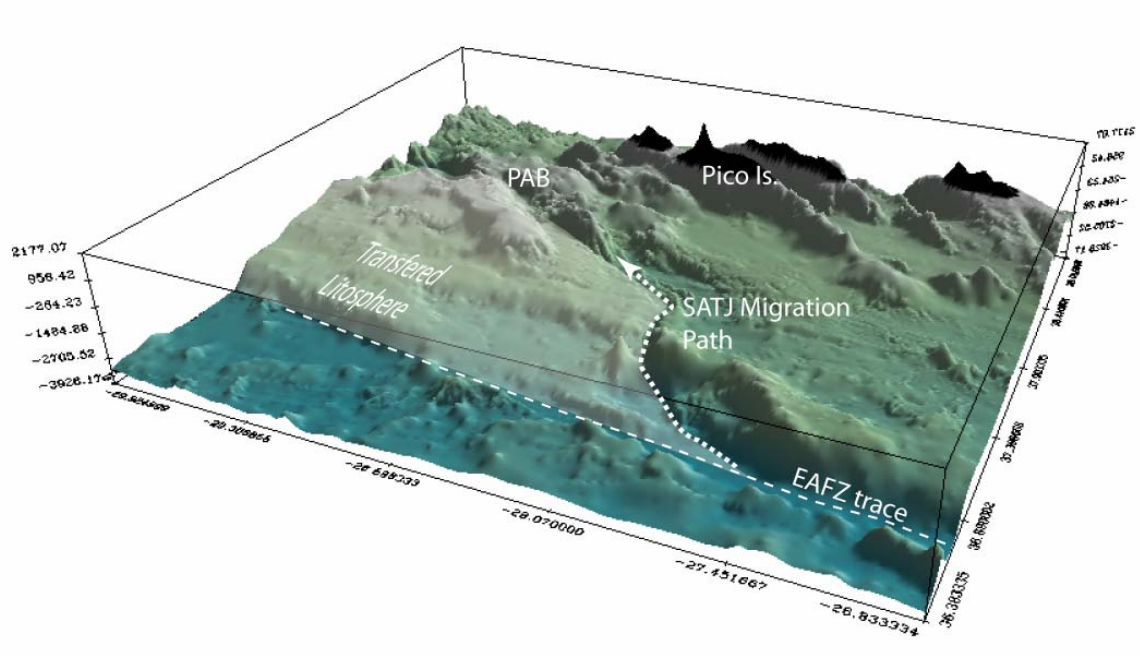

Figure II.11 - Shaded relief perspective view (facing NNW) of the EAFZ termination. Transparent polygon indicates possible Azores lithosphere accreted onto the AF plate located southwards. Doted line expresses possible SATJ migration path. PAB is Princess Alice Bank. See text for explanation.

Following an analogue procedure, we constrained the northern plate boundary between a stable Eurasian plate and the Azores domain by rotation of Pico FZ about NAM/EU finite Euler poles. Upon rotation, its position is to northerly with respect to the EAFZ. At C13, it lies in a point at the junction between the N-S striking Monaco Bank and the Western tip of S. Miguel Island. At C6, it lies in a point ca. 38º N 27º W, which pins a clear change in attitude of magnetic anomaly C6 from NNW-SSE to NNE-SSW as picked by Luis *et al.* (Figure II.6).

By analogy to the SATJ, the trace of rotated Pico using NAM-EU finite rotation poles tying this points is considered here as representative of the southern border of a kinematically stable Eurasian plate, and will be referred to as the NATJ – (Northern Azores Triple Junction).

The southern limit of a stable Eurasian plate, lying south of the Terceira axis, given the positions of rotated elements referred to above, cannot be linked to any clear first order morpho-tectonic signature in present day topography within the Azores plateau. This has two implications: either the present day topography was shaped more recently, possibly as a result of masking effects due to later tectono-magmatic events, or the NATJ was never a discrete feature during the all time span, but rather corresponded to a zone of distributed deformation.

The broad lens resulting from the mismatches in the ATJ closure (cf. Figure II.8 and II.9) provides an integral measure of Azores deformation during the ATJ evolution from 33.4 Ma to the onset of the SATJ migration, and leads to the hypothesis that an Azores domain, with a kinematic behavior independent of the two neighboring larger plates, has subsisted at least from anomaly 13 to anomaly 5 when EAFZ ceases its activity.

Moreover, as at C13 no ATJ closure can be achieved, right lateral transtension within this plate boundary surely started prior to this age.

It remains unclear if the response to this deformation in the EU/AF plate boundary was accommodated solely at the Mid-Atlantic ridge, for example by the re-arrangement of the segmentation pattern, with possible growth of segments, by re-orientation of existing ones and break-up of new non-transform discontinuities of higher orders, which would ultimately lead to geometrical repositioning of the MAR axis. If this has been the case, then the independent Azores domain grew solely from ridge dynamics and therefore some equivalent offaxis signature should be traceable in the North American plate. Lack of definition in existing data does not allow at present the verification of this hypothesis.

Another possibility can be considered: if Azores domain generation has resulted from tectonic-magmatic processes at the EU/AF plate boundary itself in the MAR off-axis domain. This could be achieved, for instance as re-activation of fracture zones as leaky structures or as formation of new fault zones within the active plate boundary domain. In this case, instability and northward migration of both Azores domain northern and southern limits would result from an intra-transform context, such as in some pacific micro-plates like Easter, Galapagos and Juan Fernandez (Bird *et al*.,1998; Bird *et al.,* 1999; Naar and Hey, 1991), as a tectonic response to ruling kinematics conditions for each time interval. The morphological evidences for the SATJ migration from the EAFZ, favor this second hypothesis; even so, some of the SATJ and NATJ dynamics through time can be accounted from magmatic pulses resulting from AHS activity as we shall refer to below in section II.4.

II.4 The Azores Hotspot

In the previous section, we considered the behavior of the ATJ along the time. We shall now consider the different models describing the nature and dynamics of the AHS and later we will address how they do mutually fit in.

In a time where there is a ongoing strong scientific community debate for or against mantle plume dynamics, relevance of mantle convection vs. plate tectonic controls, possible degrees of interaction with overlaying tectonic plates and even if plumes do exist at all (see for details www.mantleplumes.org), it is relevant to recall that the AHS remains a controversial topic in scientific literature.

The nature and dynamics of this mantle surge and the variations of the magma flux to the plateau is of key importance to understand the Azores geodynamic evolution and to constrain issues such as: 1) existence and style of hot spot trace paths across the plateau; 2) present day position and area extent of the AHS; 3) Spatial-temporal distribution of magma generation and constraints on the age of the plateau, its inner structures and the Azores Archipelago Islands; 4) degree of interaction with the Azores Triple Junction evolution through time, and therefore 5) relation with past and present plate boundary configuration between Eurasian and Nubian plates, current location and tectonic style of the Azores Triple Junction. Many of these points remain controversial or unanswered, even between those who share favorable views on the Azores mantle plume existence.

One point which remains nevertheless undisputed: the Azores volcanic platform results from an excess in volcanism/magmatism. Accordingly, the crustal structure of the Azores is equally anomalous (Escartin *et al.,* 2001; Searle, 1976; Miranda *et al.,* 1998;

Matias, in press). Only the sub-lithospheric causes of this magmatic excess remain controversial.

Numerous observations show evidence of an interaction between hot spots and Mid-ocean ridges at various levels: a thermal interaction, resulting in more crust being generated near hot spots, a geochemical interaction, implying a mixture of depleted mantle sources feeding the mid-ocean ridges and enriched mantle sources of the hot spot, and finally a dynamic interaction, responsible for the migration of second-order segments away from the hot spots, and of an asymmetry of the accretion processes (Müller, 1998; Hardarson *et al.,* 1997, Small, 1995). Frequent observations of spreading asymmetry and ridge jumps in sections of mid-ocean ridges close to hot spots suggest that mantle flow from the hot spot may control the distribution of stresses in the lithosphere above it (Ito *et al.,* 2003; Mittelstaedt and Ito, 2005)

For the Azores case, available publications tend to address the evolution of the AHS and ATJ as two independent realities, and little effort is made in the integration of their common history. Yet, it is recognized unequivocally by the generality of the authors, that both have interacted strongly at least from the past 20 Ma.

II.4.1 Nature of the Azores Hot-Spot (AHS)

The AHS has been interpreted in a diverse number of ways. The plateau bathymetric anomaly is attributed as te outcome of activity from: a plume detached head (Silveira and Stutzmann, 2002 and Silveira *et al.,* 2006; Courtillot *et al.,* 2003) a plume deeply rooted in the lower mantle (Montelli *et al.,* 2004) or with minor geochemical contributions from it (Madureira *et al.*, 2005); as a classical Hawain type hot-spot (Gente *et al*, 2003), a wet spot (Schiling *et al.,* 1975; Bonnati *et al*, 1990), an un-

specified mantle anomaly (Mitchell *et al.,* 2004); a plume related thermal/melt anomaly (Escartin *et al.,* 2001, Cannat *et al.,* 1999), or finally refuted as a plume related topographical expression (Anderson, 2001; Luis and Neves, 2006; Favela and Anderson, 2000).

These discrepancies illustrate well the lack of scientific consensus with regard to this region and the meaning of the processes which have acted upon it. One of the main arguments favoring the AHS is its influence on the MAR, an effect which has been relatively well studied (Schilling, 1985; Detrick *et al.,* 1995; Bourdon *et al.,* 1996; Cannat *et al.,* 1999; Escartin *et al.,* 2001). The AHS- MAR interaction is expressed by an asymmetrical bathymetric anomaly along axis extending from Kurtchakov FZ at 41º N at least to the Hayes Fracture Zone (at ~33.5ºN) (Goslin *et al.,* 1999), but it is arguable that it extends further south to the Kanes F. Z. (at 24ºN) (Escartin *et al.,* (2001). the MAR mid-valley is shallowest within the Azores. This bathymetry long wave-length variation is consistent with other gradients such as gravity anomalies (Detrick *et al.*, 1995, Luis *et al.,* 1998) and geochemical anomalies documented on basalts both in the axial domain (Dosso *et al.,* 1999, White *et al.,* 1976) and in the off-axis domain (Bougault *et al.,* 1985).

All these long wavelength variations suggest either that the mantle is anomalously hot and/or enriched (Cannat *et al.,* 1999). Modeling of the effect of hot-spots on ridge bathymetry and melt production is primarily a function of the plume flux (itself a function of temperature and size of the plume head), mantle viscosity, spreading rate and absolute motion of the ridge with respect to the plume (Escartin *et al*, 2001), considering the Azores context, Ito and Lin, (1995) calculated values of approximately 70º C for temperature anomalies related with the Azores plume.

Other contradictory views were presented by Bonatti (1990) based on the application of geothermometers on peridotite and basaltic material. Based on the high volatiles content for samples collected in the Azores region which reach two to three times normal MORB, he considered that this would have a significant impact in lowering the mantle solidus temperature curve therefore promoting high degrees of partial melting without the existence of a significant mantle temperature anomaly in the Azores.

Gravimetric modelling of the plateau (Luis *et al.,* 1998) and recent application of regional 3D admittance studies in the spectral domain (Luis and Neves, 2006) suggest that the plateau is regionally compensated and its shallow topography is supported by regional lithospheric flexure. These authors rule out the role dynamic forces maintained by mantle upwelling as the cause for the bathymetric surge.

II.4.2 Spatial location of the hot spot

There are no consensus on the areal extent and present location of the AHS nowadays. Tomographic models have been used to constrain the AHS position. Zhang and Tanimoto, (1992) report anomalously low S-wave velocities marking the hot spot influence in a large area, slightly east of the MAR. Silveira and Stuztmann, (2002) presented a first regional tomographic model with anisotropy retrieved from surface wave velocities. Their model reveals that the Azores related SV velocity anomaly fades at a depth of 150 km and is not linked with any deeply rooted structure (Figure II.12). Yang *et al*. (2006), using P wave tomography, also documented a generalized low velocity anomaly at a depth of ~100 km underneath the Azores. At higher depths (100-200 km) this anomaly becomes elongated along the NE-SW direction and at depths from 250 km to 400 km they position the anomaly related with the AHS in a pipe like structure NE of Terceira.

Other authors consider a location for the AHS 100 to 200 km to the east of the ridge in the Island of Faial (Schiling, 1991, Ito and Lin, 1995, Silver *et al.*,1998) or nearby Terceira Island (Moreira *et al.,* 1999; Madureira *et al.,* 2005), consistently the shallower and more volcanically focused domain within the Azores plateau. Escartin *et al*. (2001) places the AHS some 300 km east of the Princesa Alice in the vicinities of the S. Miguel Island, based on extrapolation of the HS2 model to times older than 3.2 Ma. Given this disparities we conclude that the current position and the lateral extent of the AHS plume head are not coherently described by the different aproaches and remain still uncertain.

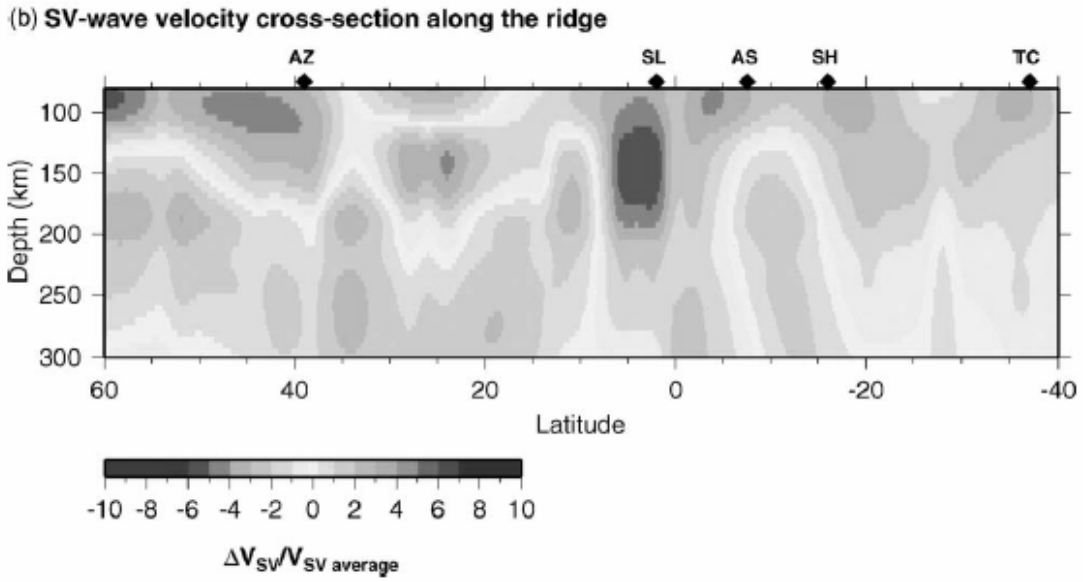

Figure II.12 - Cross-section of the S-wave velocity perturbation along the longitude 24ºW passing through the Azores (Silveira and Sutzmann, 2002). Note that the velocity anomaly fades at a depth of 150 km.

II.4.3 Dynamics of the Azores Hot Spot

Plume dynamics over time has always been constrained in a context of its interaction with the MAR and situated spatial-temporally within the kinematic framework given by

seafloor spreading on this ridge system. It's interaction with the ATJ third branch over time has always been subdued probably due to inherent complexities of this plate boundary. Below, we describe two contradictory models of interaction between the AHS and the MAR overtime:

The interaction between the hot spot and the Mid-Atlantic ridge appears to be responsible for a major thermal or magmatic event under the Mid-Atlantic Ridge 10 Ma ago, leading to the formation of part of the Azores Plateau, and an increase of crustal thickness between 5 and 8 km (Cannat *et al.,* 1999; Escartin *et al.,* 2001). This thermal anomaly has propagated southward along the Mid-Atlantic Ridge axis. Following a decrease in crustal production at the MAR since 5 Ma, the volcanic plateau was split into two branches, diachronically, forming the V-shaped structure marking the south of the present Azores plateau (Figure I.1). The decrease in crustal production at the MAR may have resulted from a reduction in the hot spot activity, or from a change in the dynamics of the interaction between the MAR and the hot spot.

No other event of this type has been recognized yet, in particular no other V-shaped volcanic ridge is observed within, or outside the main one. This model assumes that the AHS was centered along the ridge axis at the time of Chron 5, which corresponded at that time to the SATJ defined at the intersection between EAFZ, Pico FZ and the MAR in a RFF configuration. In subsequent times, while the melt anomaly migrated along the ridge axis. The considered fixed plume migrated NE into the Azores Plateau at a rate of ~20 km/Ma, following the southwestward absolute motion of the Ridge and adjoining plates, considering the HS2 reference frame. Southwestward migration of this thermal anomaly would have occurred at a rate of 60 km/Ma, according to those authors.

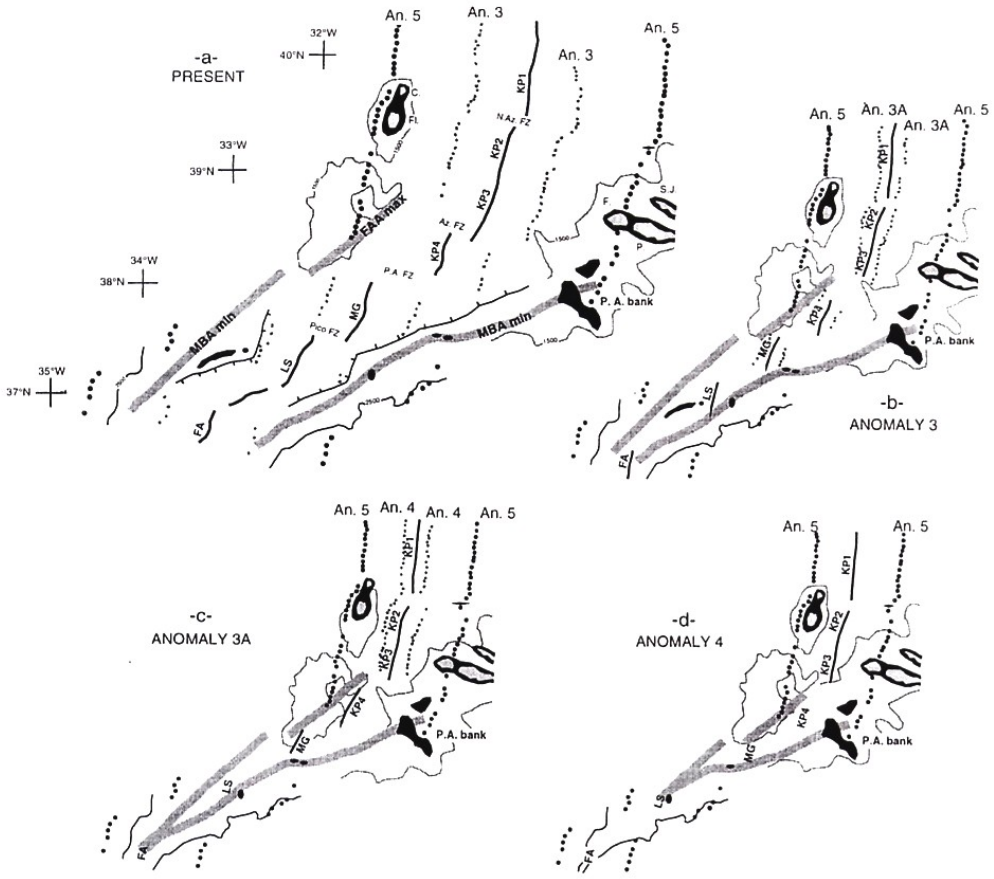

Figure II.13 - Sketches showing the location of selected bathymetry and gravity features from anomaly 4 (7.01 Ma) to the present. Thick black lines are MBA (Mantle Bouguer Anomaly) minima over the two edges of the West Jussieu Plateau (Flores ridge) and East Jussieu Plateau (Faial Ridge). Abbreviations: N. Az FZ – North Azores Fracture Zone, P.A. FZ – Princess Alice Fracture Zone, Az FZ – Açor Fracture Zone, P.A. Bank – Princess Alice Bank, C. Corvo Island, Fl – Flores Island, S.J – São Jorge Island, F – Faial, P. Pico Island, MG – Menez Gwen, FA – FAMOUS, LS – Lucky Strike (Cannat *et al.,* 1999).

Gente et al, 2003 have proposed a model constraining the interaction between the MAR and the AHS from 85 Ma to the present. They take Canpam (1995), earlier referred in this work as the kinematic reference model for their reconstructions. Plate kinematic reconstructions have revealed some key features and relations between the Azores plateau, Hot Spot activity and neighbouring structures like the Great Meteor on the African plate and the Corner Rise in the North American plate. However, as stated by the authors:

"*no precise inference should be drawn from our reconstructions on the detailed evolution of the Azores-Gibraltar line that marks the Africa-Eurasia Plate Boundary*".

Their model is sketched in Figure II.13 and can be summarised as follows: The interaction between the AHS and the MAR starts at 85 Ma and results in the formation of the Great Meteor seamounts (in the African Plate) and the Corner Rise in the American Plate (see Figure I.1 for location). Northeastward migration of this interaction along the MAR axis continues until anomaly 6 (20 Ma) resulting in the early stages of Azores Plateau formation. Between anomalies 6 and 5 (10 Ma) plume influence in centred in the Azores plateau and its interaction with the MAR gradually loses significance. At 7 Ma the Azores plateau is fully formed and the melt generation arising from plume activity ceases, this stage marks again the onset of normal seafloor spreading at the MAR north of latitude 38º. In the Southern part of the plateau Rifting of the Azores plateau started at C3 (4 Ma) and results in the formation of both Flores and Faial ridges (also referred as West Jussieu and East Jussieu plateaus) as independent morpho-tectonic features. The authors assume that the Azores plume is currently centred below Terceira Island.

II.5 Discussion

II.5.1 Interaction between the Azores Hot Spot and the Azores Triple Junction

Constraints on the formation of the Azores plateau and its inner structure are sometimes attributed to the kinematic evolution of the ATJ, others to the action of the AHS as we have just seen. It seems clear that their concurrence in space and time is bound to have promoted some degree of interaction between these two main processes.

If it is clear that the AHS, resulted in the formation of thicker than normal oceanic crust and the shaping of the anomalously shallow bathymetry; the geometry of the plateau, its internal structure, and the northeastern and southeastern limits within the EU/AF plate boundary (i.e Terceira axis and EAFZ) are clear tectonic features. This suggests that the surface expression of the excess in magmatism is tectonically controlled.

Considering both the kinematic constraints of the ATJ and the models for the evolution of the AHS, it results that the Azores deformation history started prior to any relevant spatial influence of the AHS trace in this plate boundary domain. The models used in section II.2.4 suggest that beginning of transtension started prior to anomaly 13 (i.e 33.4 Ma). According to Gente *et al.,* (2003) the position of the hot spot, considering an absolute reference frame, should be to southerly to bear important interactions or consequences to the Triple Junction.

The age of the plateau and intrinsically the age of the Terceira axis are still subject to considerable scatter in estimates. For example Canpam *et al.* (1995) sets an age for this features as early as 36 Ma age. Vogt and Jung (2003) have defined 24 Ma as its limiting age, Searle (1980) considers an estimate of 36 Ma. Given that the bathymetric anomaly does not surpass C6, in the North American Plate it is plausible that the bulk of its construction should have occurred prior to this age. As observed earlier, models considering the AHS evolution also point to an estimate of 20 Ma for the beginning of the most important period of AHS-MAR interaction which reaches a maximum at approximately 10 Ma (C5) and then gradually decreases activity from 7 Ma to the present.

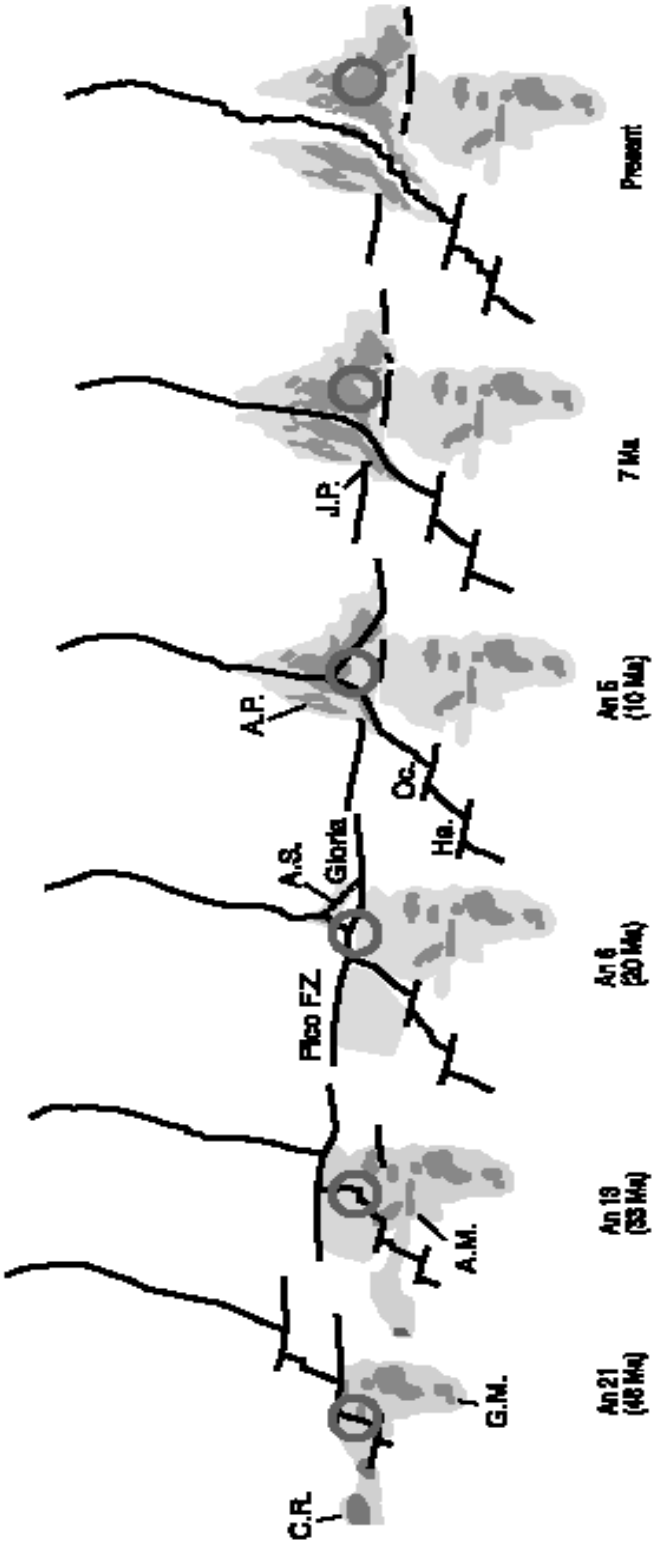

Figure II.14 - Schematic reconstructions of the relative movement between the Mid-Atlantic Ridge (MAR) and a hot spot supposed to be located under the Azores Archipelago and centred under Terceira Island. The hot spot (thermal anomaly) is assumed to be 200 km in diameter and is shown by a gray circle. C.R – Corner Rise, G.M. – Great Meteor, A.M. – Atlantis mound, A.S. – Azores spreading Center, A.P. Azores plateau, Oc – Oceanographer F.Z., Ha – Hayes F. Z. and J.P. - Jussieu Plateau.

Presented models in section II.2.3 differ essentially in the proposed mechanisms for the generation of the Faial and Flores ridges and the implications on the AHS dynamic through time. The model proposed by Cannat *et al*. (1999) considers that the rifting event leading to these main morpho-structures is essentially diachronical an directed south westward. Conversely, Gente *et al*. (2003) considered a more typical hot spot trace migrating progressively northward and associate the rifting of this plateau to a single event which started some 7 Ma ago when abnormal hot spot derived excess in magmatism ceased.

When considering the implications of both models addressing the possible consequences to the ATJ of the prevalence of hot spot related activity within the plateau in time, several limitations arise:

MAR generated magnetic anomalies, namely those that mark the onset of the plateau (C6 and C5) are still traceable within the plateau, as we have seen in section 1.2.1, and these seem inconsistent with widespread hot-spot influence of AHS on the plateau build up. To render the hypothesis valid, then the southern termination of anomalies 5 and 6, as picked by Luis *et al.* (1994), within the Plateau must be re-examined.

The magnetic anomalies of the Faial and Flores ridges are broadly positive, which seems to refute the dyachronical nature of these structures proposed by Cannat *et al*. (1999). Moreover from a geometric point of view, it is difficult to justify Cannat hypothesis that the plume was centred on the Ridge axis and was the key factor in the generation of the plateau. The plateau morphological asymmetry, with respect to the present MAR position, cannot be accounted by the referred ridge axis migration.

The prolongation westward of the EAFZ transform valley bordering the southern termination of the Faial ridge and the Azores plateau as an abrupt morphological step facing south is difficult to cope with a northward migration of the AHS, as its interaction with the EAFZ should blur its surface expression and not be limited by it. A more consistent behavior can be observed in the NAM plate where the Pico FZ terminates quite abruptly eastwards against the plateau.

Finally, the morpho-structure of Terceira axis itself, where deep basin occur, does not seem immediately linkable to a widespread excess in magmatism hot spot, relatable if this structure would have defined the northern boundary of the Azores plateau since at least anomaly C6 as represented in numerous models namely those of Gente *et al*. (2003) and Cannat *et al*. (1999).

II.5.2 Onset of SATJ northwards Migration

Considering Gente *et al*. (2003) model as a complete portrait of AHS dynamic through time, then what can we anticipate to be the response of the ATJ to the progressing AHS northwards?

Probably a combination of changing kinematic conditions depicted in section II.2 associated with the body forces resultant from topography build up, might have induced a tectonic response which resulted in strain re-localization and redefinition of the plate boundary, as AHS migration would proceed.

As suggested by Vogt and Jung (2003), the abandonment of the SATJ from the EAFZ and its progressive migration northward seems to have been crucial to the development of the Azores plateau internal structure. Vogt and Jung (2003) attribute the generation of the LVR, as a succession of failed rifts following this TJ migration, concomitant with

the progressive hot spot track also to the north. As we shall see later (see Chapter V) we favor a somewhat different interpretation as we consider that the western linear volcanic ridge domain has at present a significant tectono-magmatic activity and constitutes a part of inter-plate boundary zone.

Timing the onset of this migration is of key importance for the age relationship of morphological features within the plateau. We interpret the triple junction migration as a process that generated from a intra-transform setting between C6 and C5 and terminated post east Jussieu plateau formation. The fact that the valley that marks this migration cuts through a well shaped terrace and is not in-filled by magmatic products and the disruption itself of the Faial ridge, suggests, that the overall SATJ migration might have occurred in a magma-poor environment therefore at the at the onset of the MAR normal seafloor spreading, (i.e. ca. 7 Ma according to Gente *et al*., 2003).

The gradual migration of the SATJ converges to expectable NATJ position. Probably the changing in the kinematic conditions that supported this migration favored the rupturing of the Terceira axis as an intra-oceanic rift zone, therefore redefining the NATJ trace and plate boundary to a more northerly position along this structure. Though the starting age can be tentatively constrained by Gente's model, the end of such process, which resulted in the present definition of the EU/AF plate boundary dominantly along the Terceira axis is less easily definable. Probably, Luis *et al.,* 1994 model where the repositioning of the SATJ is achieved by discrete small ridge jumps to its present position, allegedly along the intersection of Faial-Pico strike with the MAR, remains valid (also see discussion in Chapter VIII).

The disparities observed in some sectors of the Azores plateau between main morpho-tectonic and magnetic anomaly features suggests that its present morphology and most

of its magnetic character associated with the Azores trend have been shaped in recent times, surely less than 7 Ma, and most probably less than 3 Ma as we shall see later in chapters IV and V of this manuscript, when we will analyze in more detail the present configuration of the ATJ and the EU/NUB plate boundary.

II.6 Conclusions

1) The rotations of a set of point elements within the plateau, inferred from calculated EU/AF stage poles, suggest an overall dominance of a transtensional or oblique extension regime from at least 33.4 (C13) to the present. From C13 to C6 any of these regimes would be dominated by extension along a near N-S direction. From C6 to the present extensional direction rotates to a direction closer to WSW-ENE or W-E according to the reference kinematical model chosen.

2) The EAFZ can be approached as the structural homologue of the Pico FZ considering NAM/WAF finite rotation poles. Therefore this structure acted as a southern plate boundary SATJ for most of the evolution of the Azores plateau since anomaly C13.

3) The northern trace of rotated Pico FZ Position using NAM/EU finite rotation poles (NATJ), does not correspond to any significant morphological feature. This implies that either a discrete plate boundary never evolve fully, and that the Azores kinematic block constituted an area of essentially distributed deformation, or that if existed this plate boundary was mask later by subsequent tectono-magmatic events.

4) No simple closure of the ATJ is possible at anomaly C13, implying that deformation associated with the Azores Triple Junction started prior to the 33.4 Ma. We need therefore to evoke an Azores domain with a kinematic behavior independent of the two larger plates. The expected position of the AHS implies little to no interaction of the hot

spot with the SATJ existed at this time, and that the onset of Azores domain and topography might have been, mainly tectonically controlled these early stages.

5) Strong interaction of the SATJ with the AHS started probably at C6 times (20 Ma) according to the models referred to in this study. After a period of intense melt production which reached a maximum at C5, rifting of the Azores plateau began around 7 Ma. Between C6 and C5 the EAFZ ceases to work as the SATJ, which departs from the EAFZ (in a intra-transform context) northwestwards. The migration process lasted to through times earlier than 7 Ma, as the most probable morpho-structure corresponds to a valley largely depleted from magmatism, and therefore generated after the maximum magmatic activity, AHS related.

Chapter III – Azores Hotspot Influence on MAR Seismicity

III.1 Hydrophone Arrays

One of the strategies designed to identify the effects of the AHS is the mapping of volcanic and tectonic activity along the MAR. This can be done very efficiently with the use of hydrophone arrays, a technique developed for submarine acoustic surveying that is now available for scientific use. In north Atlantic two autonomous hydrophone networks have operated in the past. A NSF network was deployed in February 1999 south of the Azores by NOAA/PMEL between latitudes 17ºN and 35ºN (Smith *et al.*, 2002 and 2003, Dziak *et al*., 2004), and was kept under operation until June 2005. The northern SIRENA (Goslin *et al.,* 2004) network was setup as a joint France-USA-Portugal cooperative effort. It operated between latitudes 40° 20' N and 50° 30' N, from May 2002 to September 2003. The two networks overlap in time for about 11 months, complementing one another therefore providing an earthquake monitoring of the entire Northern Mid-Atlantic Ridge axis from 16°N to 50°N during that time span.

The main objective of the SIRENA array deployment was the long-term monitoring of earthquake activity occurring at the Mid-Atlantic Ridge axis. Such observations enable an understanding of the spatio-temporal distribution of earthquakes along the MAR both in their tectonic segmentation context and in a broader scale as an indication of the interactions between the slow spreading MAR and the Azores plume.

The autonomous hydrophones are portable stand alone devices deployed at the water column to passively register ocean noise for time spans that can reach 1.5 years. The system is programmed to record 1s data at 100 Hz (1 to 40 Hz band pass). The hydrophone (Figure III.1) is an instrument with 1.8 meters long and 0.17 m wide consisting essentially of four components: the hydrophone itself and, packed within a titanium pressure case, a signal pre-amplifier, a battery pack and the data logger. The signal is digitized from the device amplifier and resultant data is buffered in the system RAM until full. Only then is the data recorded at one of several hard disk drives to economize energy. The system shutdowns automatically, after the last disk in the data logger is written.

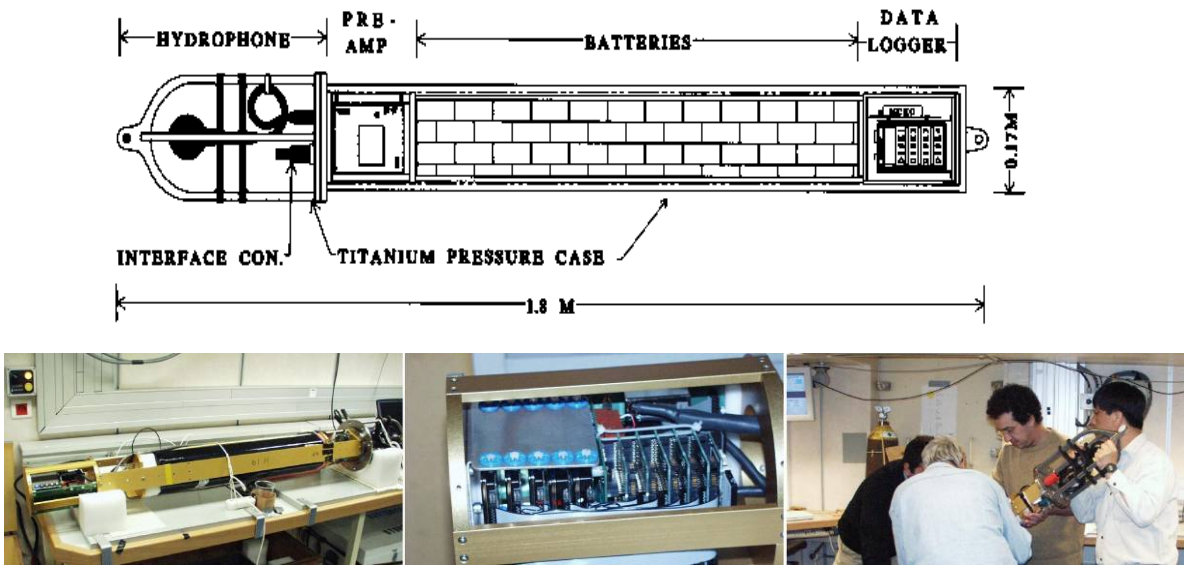

Figure III.1 - Hydrophone component scheme and corresponding component photographs. Left: hydrophone being prepared for deploy during SIRENA 1 cruise. Center: detail of the data logger. Right: hydrophone being introduced on the titanium pressure cage.

The mooring package is displayed in Figure III.2.A. From seafloor up it consists on an anchor attached to an acoustic release (Figure III.2B), in turn linked to the instrument by

a very low stretch mooring line, to minimize hydrostatic noise and pre-measured to place it at the correct water depth. The instrument is further attached to a set of floats which provide positive flotation to the set once the base anchor is released on bottom.

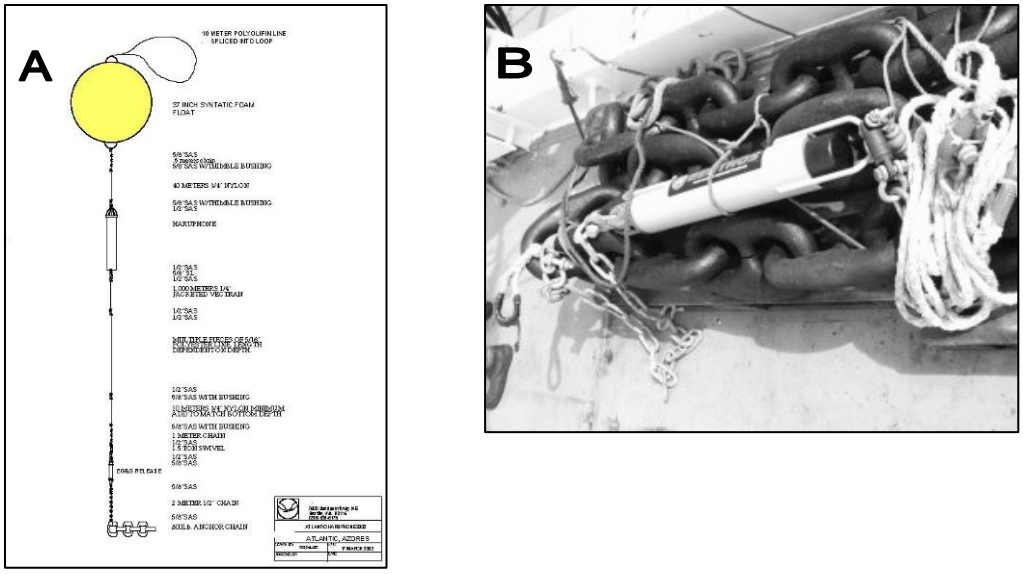

Figure III.2 - A) Diagram of mooring configuration. The hydrophone depth is given by the SOFAR channel axis (see section 2.2). B) Photograph of bottom anchor and acoustic release on deck.

III.2. The SOFAR channel

Autonomous hydrophones are deployed in the SOFAR (SOund Fixing And Ranging) channel. This ocean water layer is present in all the ocean basins, occurring in the Atlantic at depths between 700 and 1000 m. This channel forms at a minimum on a vertical sound velocity depth profile, resultant from the interplay between temperature and pressure variations with depth. The conjugate effect of sound velocity decrease at the thermocline and the sound velocity increase due to pressure below it, generates a minimum-velocity channel in which acoustic waves remain trapped (Figure III.3).

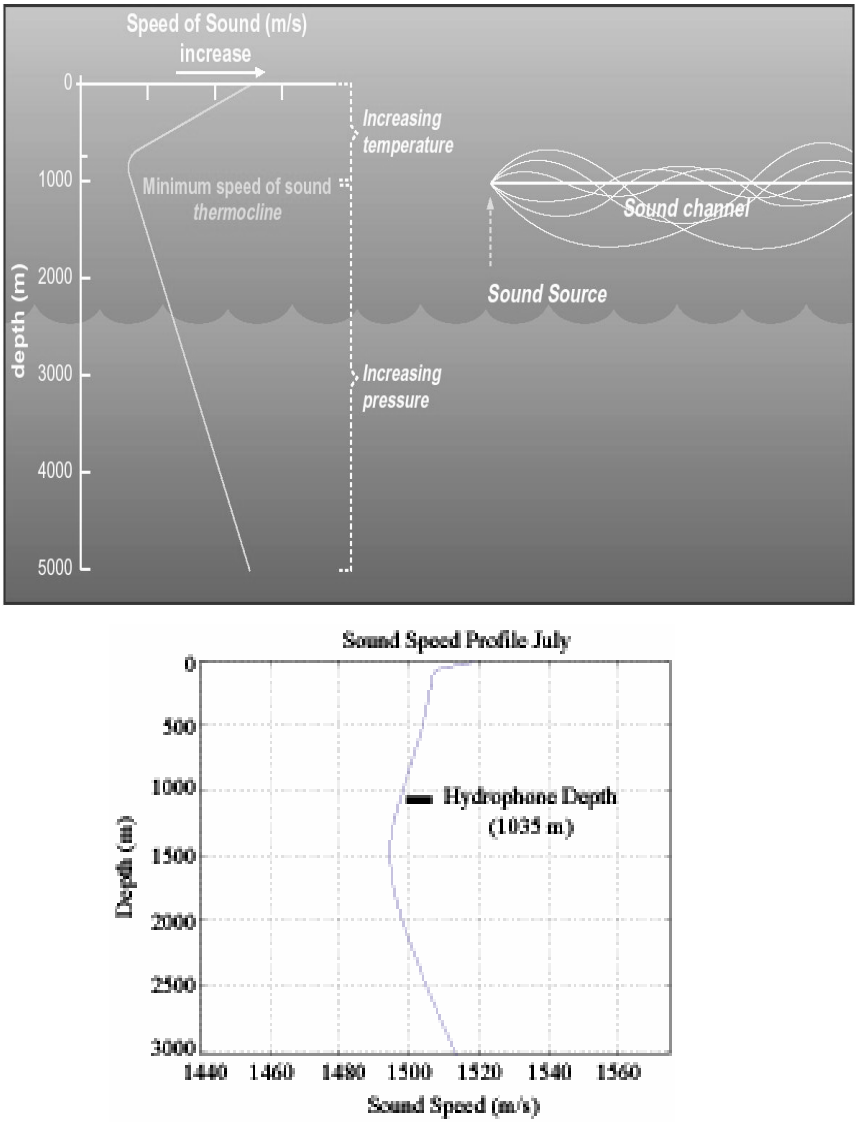

Figure III.3 – Top) scheme depicting SOFAR channel axis configuration and T-phase paths within it. (http://www.beyonddiscovery.org). Bottom) A measured velocity profile from the Southern network displaying hydrophone depth in the water column (Dziak *et al.,* 2004)

The refraction of sound waves from higher velocities above and below the sound channel axis bend the sound ray paths back towards the axis. Having no interaction with the sea surface nor the sea bottom, the SOFAR channel trapped acoustic phases suffer very low signal attenuation, which enables the acoustic waves to travel effectively over very long distances (up to several thousand km).

III.3 T phases

Seismic waves from tectonic events or volcanic tremors, when crossing the rough sea-bottom to water interface, convert into acoustic waves called T-phases; T stands for "Tertiary" as these waves travel more slowly in water (~1.5 km/s) than seismic waves do within the solid Earth, arriving in third after the P and S waves on land seismic stations and hydrophones. Hydrophones can only register P and S phases, provided that the seismic event is close to the instrument, as seismic phases attenuate rapidly within the crust (within 150/200 km for medium magnitude earthquakes). An exception to this is the ability for hydrophones to detect by direct incidence of P waves generated at distant epicenters from very high energy events. Due to their efficient propagation in the SOFAR channel, T-phases can be registered by the autonomous hydrophone, thousands of km away from their source area.

III.4 Data Analysis Interface

Data recorded in each array instrument is accessed via "Seasick", a NOAA developed data analysis interface. It enables the analyst to display the data from each instrument simultaneously on screen as a spectrogram (Figure III.4). In each channel Y axis is time, X axis is a frequency interval (from 0 to 140 Hz, but customizable) and a 10% cosine tapered amplitude spectrum of the signal record is color coded providing a measure by visual inspection of earthquake acoustic magnitude. Time frequency resolution on display of each scan line is customizable when justifiable but for a normal configuration a time resolution of 4 s has proven to be a good trade off between analyzing a large amount of data and getting accurate reduce errors in locations. Data is scrolled either synchronized in time or at each channel time and the operator checks by visual inspection for signals over the background ocean noise.

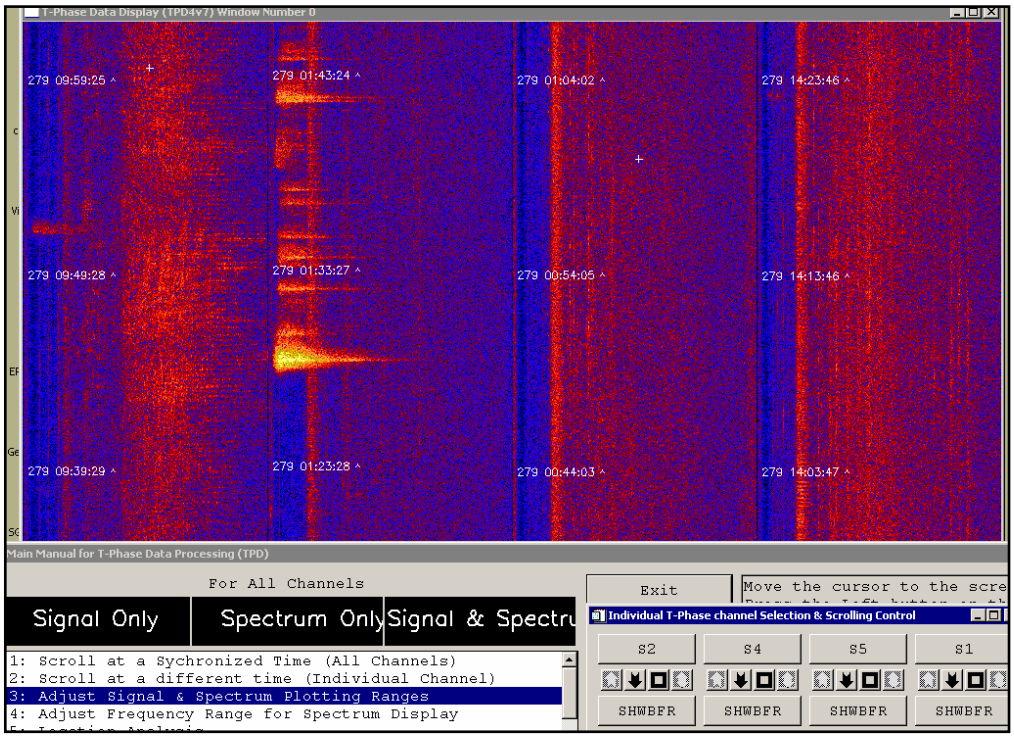

Figure III.4 - Screen capture of the interface from the program developed at NOAA, used to process the hydrophone data. In this example 4 hydrophones from SIRENA are displayed, along with the software main command window.

Picking earthquake signals is a simple but sometimes not straightforward task. The operator first performs a rough pick of the specific earthquake signal in each channel, and re-displays the histogram at a higher frequency resolution. By using criteria, normally based on the scan lines which present the smallest frequencies with higher amplitudes within the coda for that earthquake, a refined recalculation provides a more accurate prediction of position. This process is iteratively performed until the picking procedure allows minimization of the errors. When picked successfully, the calculated time, position, acoustic magnitude, and errors for this parameters as well as the number

of hydrophones used in the localization of the event are than stored on a *posit* files for posterior seismicity studies. The*Posit* files from several arrays around the world are made available on the NOAA website for download (http://www.pmel.noaa.gov/vents/acoustics/seismicity/seismicity.html).

The detailed description of the mathematical methods built-in on the program to provide T-phase source location and error estimates is out of scope of this work. Detailed information on this issue can be found in Fox *et al.* (2001). Here we just summarize the procedure briefly. Using built-in models of ocean sound propagation velocities, sound is propagated from a preliminary location to the hydrophones using interactively a non linear least square inversion method. Successive runs then, minimize the differences between predicted and recorded arrival times. Several solutions are calculated on each run to check consistency of initial source location; these consider the source location falling within the center of the array, outside the array from the direction of the hydrophone which registered the first arrival, and at the minimum residual error from a coarser grid. The location is taken from the solution presenting the lowest root mean square (RMS) residual error.

III.5 The SIRENA experiment

The SIRENA Project was set up in 2000, as a result of a cooperative agreement between UMR6538/CNRS (Brest, France; PI J. Goslin), the "Géosciences Marines Lab" from IPG Paris, the PMEL/NOAA (Pacific Marine Environmental Lab, Newport, OR, USA), the CGUL (Lisbon University Geophysical Center) and the CIMA (Marine and Environmental Research Center, University of Algarve – Portugal).

Two cruises have occurred within the framework of this project (Figure III.5): SIRENA1-2002 cruise aboard the R/V Le Suroit, starting in Ponta Delgada (Açores) on May, 16th and docking in Brest on June, 4th, 2002. Six hydrophones were successfully deployed during SIRENA1 on both flanks of the Mid-Atlantic Ridge between Kurtchatov Fracture Zone, immediately north of the Azores Plateau and a major discontinuity south of the Charlie Gibbs Fracture Zone (between 40º20'N and 50º35'N). (see report at http:// www-sdt.univ-brest.fr/ ~goslin/SIRENA/REPT).

A multi-beam survey of the ridge axis between latitudes 48°20'N and 50°05'N was completed. Together with previous surveys, in particular TRIATNORD (Goslin *et al*, 1999), these data provides complete bathymetry coverage from 40°20'N to 51°55'N (with the exception of the section between 46°N and 48°20'N, where only a few single-beam and multi-beam tracks cross the MAR).

The hydrophone array was recovered during the SIRENA II/D274 cruise, sailed by RRS Discovery from Govan, Scotland (Sept, 12th, 2003) to Ponta Delgada (Oct, 1st, 2003). Of the six hydrophones deployed in May 2002 (see site locations on Figure III.5), only five were recovered during SIRENA2/D274. We were not able to recover S3. Hydrophones S1, S2, S4 and S5 recorded data during the entire time they were deployed. S6 stopped recording data on the 12th day after its deployment. Despite this drawback, the four operational hydrophones occupy the four corner sites of the array and data analysis indicates they provide accurate locations of earthquakes that occurred within the array.

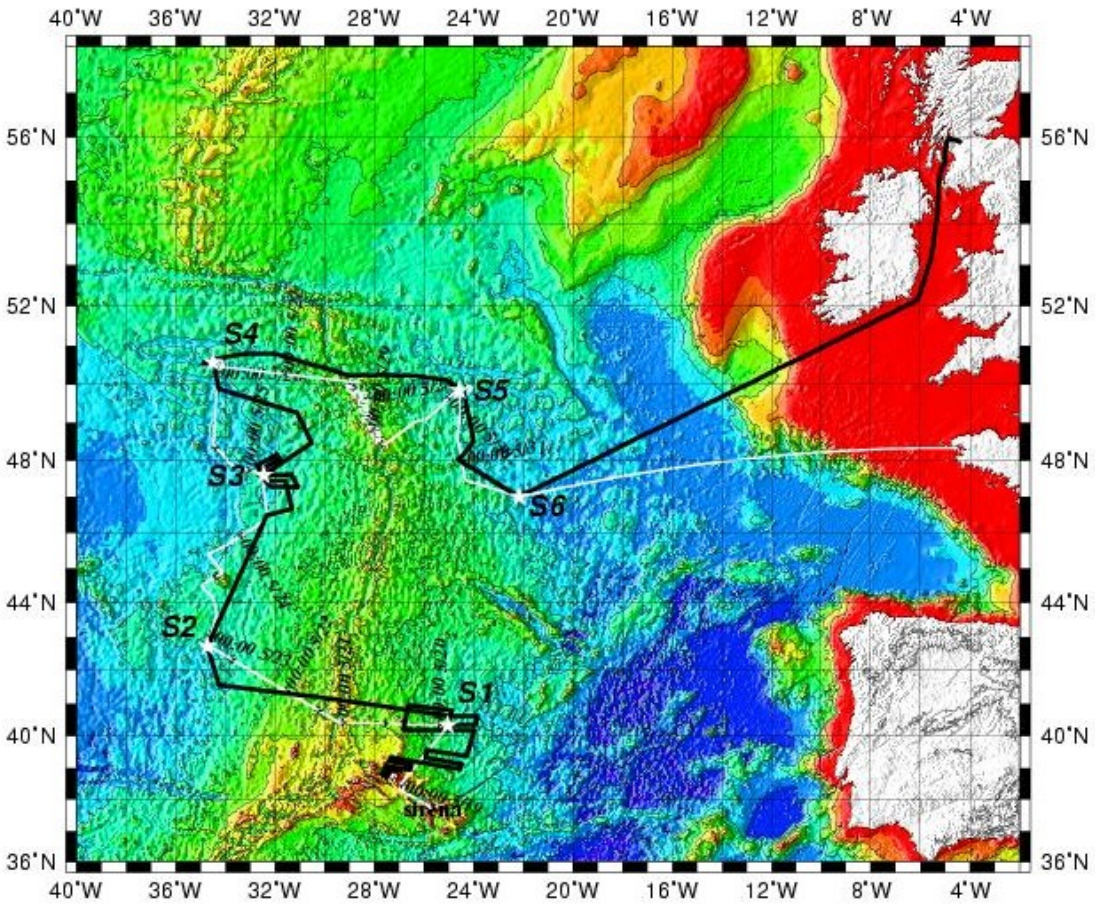

Figure III.5 - Ship tracks during the SIRENA1 (black) and SIRENA2/D274 (white) cruises. Indexed stars indicate the positions of the SIRENA hydrophone mooring sites.

III.6 SIRENA data processing

The hydrophone acoustic data analysis started in Brest in early November 2003. During that initial time we concentrated on acoustic data recorded within periods during which events were detected along the northern MAR by global seismic networks and listed in the USGS earthquake data catalog. Such an approach allowed for a first-order estimate of the performance of the hydrophone network and provided new results on the seismic activity of the MAR and on the Reykjanes ridge (Goslin *et al.*, 2004)

In general, even reduced to 4 instruments, the SIRENA array was able to detect and locate earthquakes from as far south as the Sierra Leone Fracture Zone (around 7°N) and as far north as the the Reykjanes Ridge (62ºN) . The Sirena hydrophone array has also observed seismic phases generated by distant earthquakes which have traveled through the lower mantle and core (Figure III.6). While hydrophones are capable of recording acoustic signals originating from thousands of miles away, the presence of the shallow and extensive Azores Plateau disrupts the SOFAR channel and acts as a natural barrier to sound propagation. Therefore this limits the ability of SIRENA network to detect many of the events occurring along the MAR axis in the opposite sections of the MAR with regard to the Azores Plateau and increases the location error of the earthquakes that are detected.

Mainly due to blocking effect of the Azores Plateau, we verified that a large number of events was recorded by only three hydrophones (S2, S4 and S5 see Figure III.7). Numerous events have large location errors and plotted in an abnormal off-axis region around 33ºW, 44ºN.

In order to get more constrained locations of these events, the SIRENA network data has been re-processed together with the "NSF array" deployed south of the Azores, during the common period of operation of both networks which extends from May 2002 (deployment of the SIRENA network) to April 2003 (last servicing of the South Azores network).

An evaluation of seismic events located with both networks suggests that this processing strategy has significantly improved the location of the events which occurred between latitudes 35°N and 41°N (the area between the two networks).

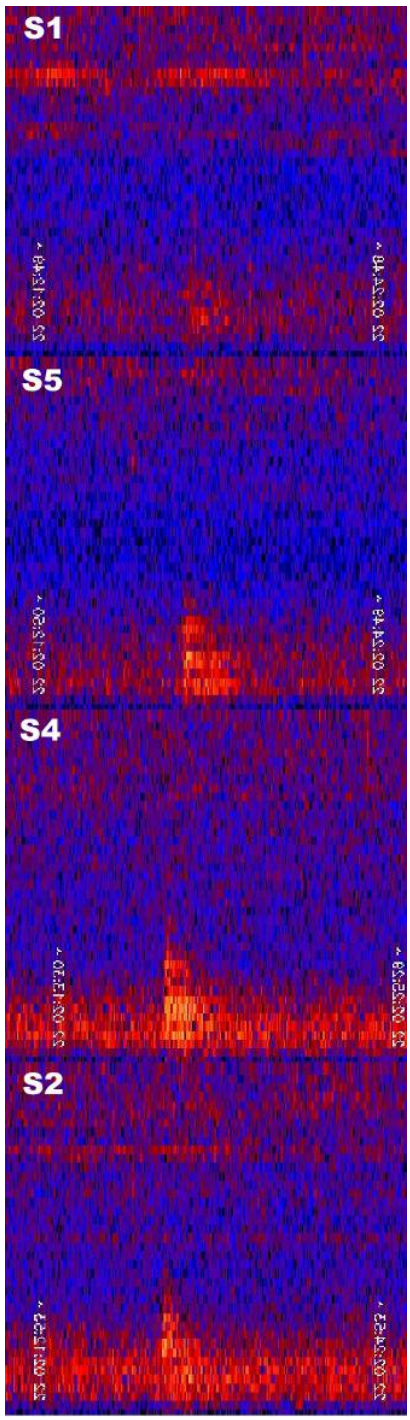

Figure III.6 - Example of hydrophone spectrograms displaying P phase arrivals from a large magnitude earthquake (Ms = 7.6) with epicentre at the Middle America Trench (104º06´W, 18º46'12''N). Frequency ranges 0–10 Hz.

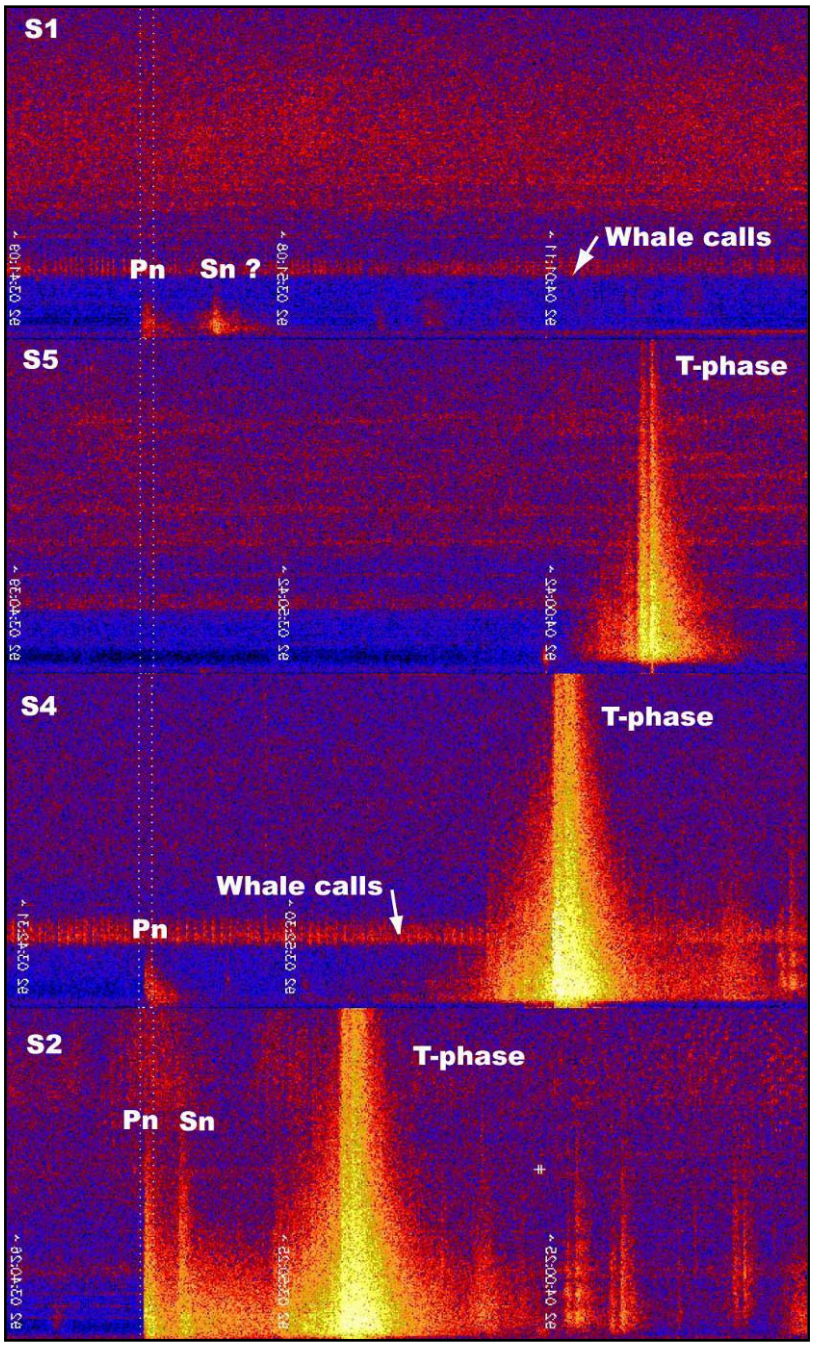

Figure III.7 - Spectrograms of the four hydrophones illustrating Pn and (Sn) arrivals from a clear tectonic event located in the Oceanographer Fracture Zone. Time is along the X-axis. For each channel, frequencies range from 0 to 124 Hz from bottom to top. S1 registers Pn and Sn seismic phases, however due to the Azores plateau blocking the SOFAR channel it is not able to record T-phase signals from the same event.

III.7 Comparison between hydro-acoustic and global seismological network data

Along the MAR 2973 earthquakes were localized between latitudes 10°N and 66°N from June, 1st, 2002 to 1st March, 2003 (Figure III.8). During the same period, land-based networks localised 98 events along the same section of the MAR (as listed in the NEIC catalog). The hydrophone arrays thus recorded and localized close to 30 times as many earthquakes as the land-based networks, thus exemplifying the large difference in detection threshold between autonomous hydrophones and land-based stations (Dziak *et al.,* 2004). Previous work along the 15°-35° N section of the Mid-Atlantic Ridge has shown that using autonomous hydrophones to detect earthquakes can lower the detection threshold of events from the 4.6 mb of global seismic networks to 3.0 mb (Dziak *et al.,* 2004), leading to a twenty-fold increase in the number of events detected. The data now processed jointly, confirms this. The hydrophone array succeeded in detecting - and precisely locating - about thirty more MAR events than the global seismological networks over the same time period. As an example, 66 small-magnitude earthquakes were detected and localized near 48°N, 27°W, while the global networks only observed a single event (with a magnitude m_b =4.6). Since these earthquakes are located within the hydrophone network, their location error is less than a few kilometers in latitude and longitude.

III.8 Large wavelength variation in seismicity patterns with latitude

The spatial distribution of the seismicity rate vs. latitude shows a remarkable first-order long-wavelength pattern: 1) the seismicity rate is low when approaching the Azores and Iceland (reaching values as low as 10 events/d°), while it peaks to 70 events/d° in the vicinity of the Gibbs FZ (Figure III.9a). 2) moreover, the latitudinal distribution of the seismicity hints at an asymmetric influence of the Azores hotpot on the MAR: 720

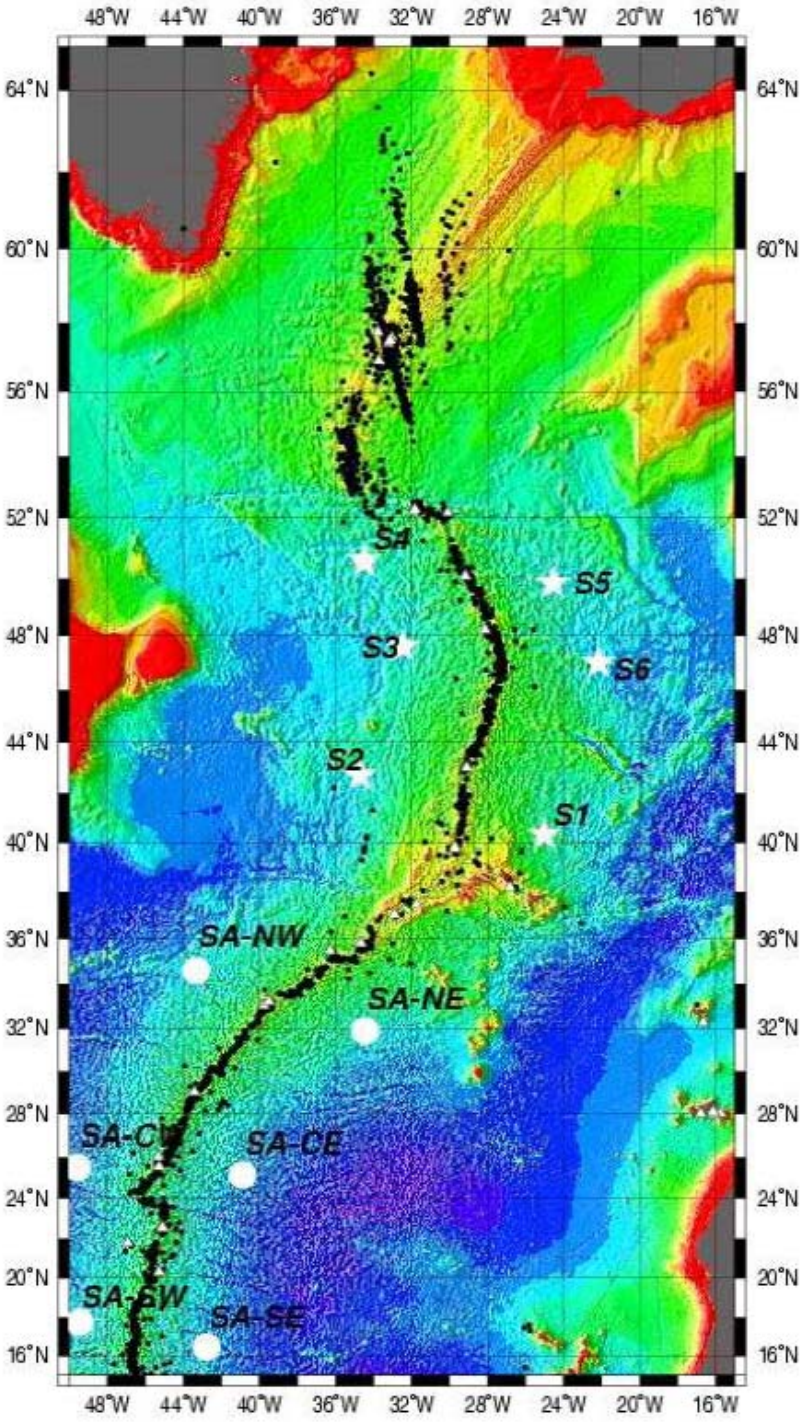

Figure III.8 - Earthquake epicenters from June 1st to feb 28th 2003. Black dots epicenters from hydrophones. White triangles events registered in the NEIC seismic catalogue. White circles point the hydrophone position from the NSF southern array. Triangles point the SIRENA hydrophone locations.

events have been localized inside the SIRENA array (between latitudes 40°20'N and 50°30'N), while 453 earthquakes have occurred south of the Azores, along a section of the MAR of similar latitudinal extent (28°N > 38°N).

The spatial distribution of the seismicity rates (Figure III.9a) along the MAR anti-correlates well, at long wavelengths, with the zero-age depths (Figure III.9c). These correlations fit in well with the now classical image of a hotspot-influenced slow spreading centre: globally thicker and more ductile crust would be emplaced along ridge segments closer to the hotspot, while the thinner, colder and more brittle crust emplaced along ridge sections free from the hotspot influence would produce a higher seismicity. Finally, the along-ridge seismicity distribution correlates with the Vs velocity anomalies at 100 km in the upper mantle (Figure III.9b). It is thus proposed that the thermal regime of the upper mantle, as it results in variations of the rheology and thickness of the crust, would be an important factor controlling the spatial distribution of the seismicty. The later could then be used as an additional tool to characterize the along-ridge asymmetrical influence of the Azores and Iceland hotspots on the MAR slow-spreading center, as it was proposed by Goslin *et al*. (1999). Our study thus confirms the asymmetry which was inferred earlier from global studies (e.g. Goslin *et al.,* 1998; 1999).

III.9 Time-wise seismicity distributions along the MAR

Similarly to what was observed for the spatial distribution of the seismicity along the Ridge, and even if a ten-month period cannot be considered as fully representative, time-wise distributions of the seismicity along the MAR (Figure III.10) show very different behaviours: 1) some sections of the MAR, which are considered as undergoing little influenced by the Azores hotspot (e.g. the 46°-49°N section) are the loci of more

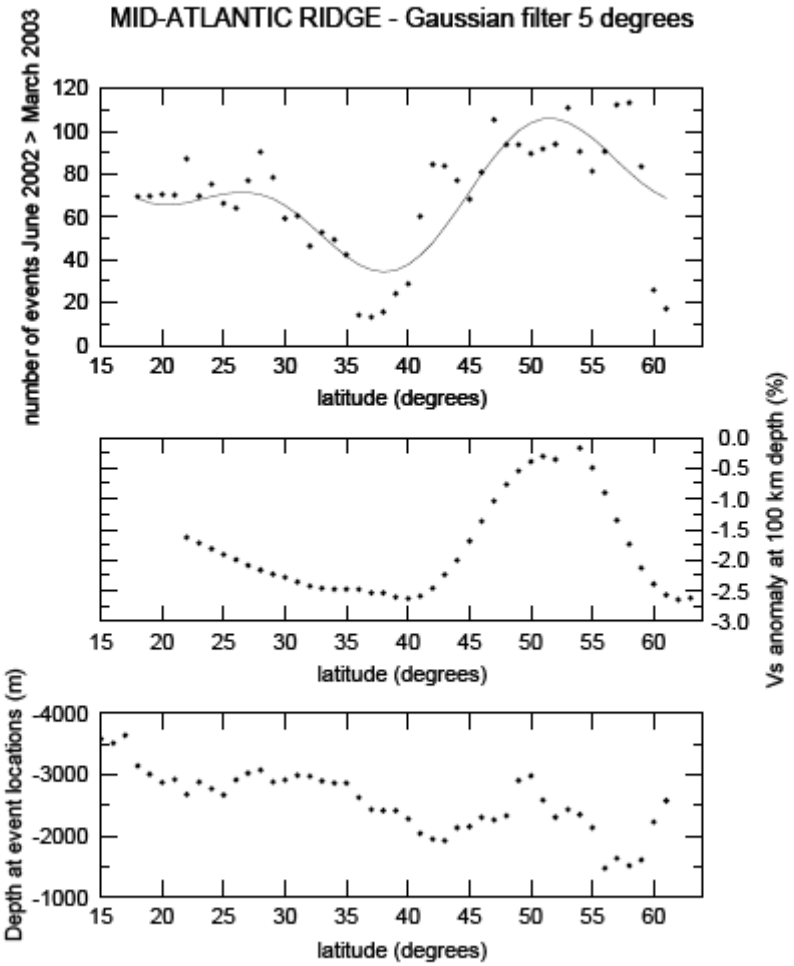

Figure III.9 - Plot of observables along the ridge filtered through a 5º Gaussian filter vs. latitude. Top) Seismicity rate. Event counts were binned in 1º bins prior to filtering. A Fourier regression model, fitted through the filtered values is shown as a thin line. Center) Upper mantle surface-wave Vs velocity at 100 km depths from the global tomography model of Ritsema *et al.* (1999). Bottom) Depths at epicenter locations, extracted from the predicted topography grid of Smith and Sandwell (1997). Note that the depth scale is inverted (deeper depths are to the top of the graph (Goslin *et al.,* in press).

intense seismic (tectonic?) activity 271 events were detected along this 3°-long section during a 10 month period). Along with such sections, the time-wise distribution is rather continuous and consists of several "super-sequences", each of these having a typical

one-month duration; 2) conversely, the less active (volcanic?) seismicity, which is observed along other sections (such as the 36°N-39°N section, centred on the Lucky Strike segment, along which only 36 events occurred during the same period) appears interrupted by long quiescent spells.

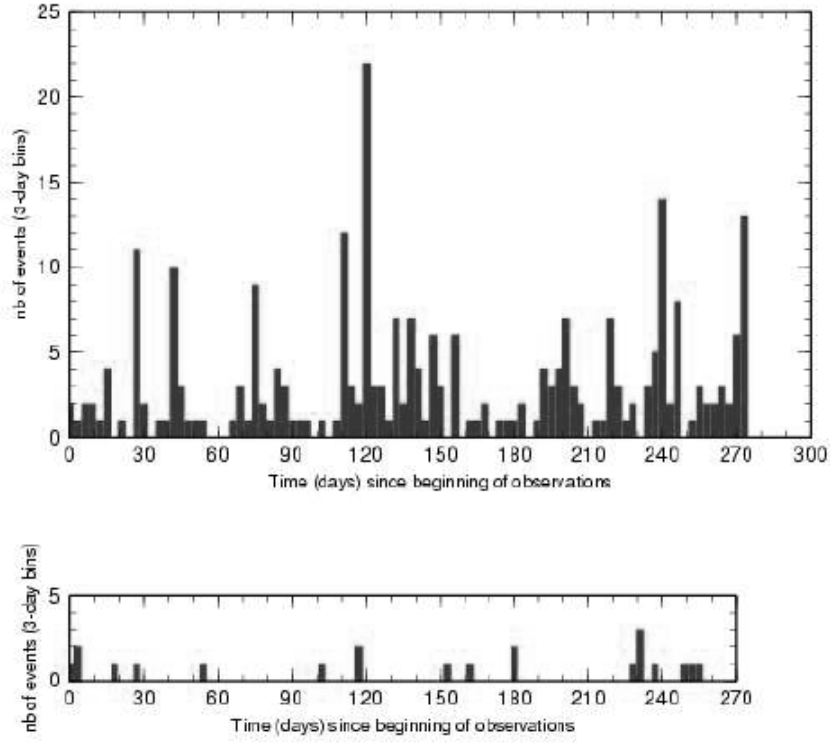

Figure III.10 - Top) Time-wise distribution of the number of events having occurred between June, 1st, 2002 and February, 28th, 2003 along a 3°-long section of the MAR, far north of the Azores (46°N - 49°N). The numbers have been binned into 3-day bins. Bottom) Same as before, but for a a 3°-long section of the MAR, close to the south of the Azores (36°N - 39°N). From Goslin *et al (2004).*

III.10 Discussion and Conclusions

Long-term monitoring of the seismicity along the Mid-Atlantic Ridge by two networks of autonomous hydrophones allowed the characterization of the spatial and temporal distributions of the seismicity along a 55º -degree-long section of the MAR. These

distributions bring new insights both on ridge/hotspot interactions and on accretion processes along a hotspot-influenced spreading center.

At long wavelengths, along-ridge seismicity rates appear closely correlated with other observables which characterize the thermal regime of the crust and upper mantle. These spatial correlations seem to confirm that the strong influence exerted on the MAR by the Azores plume extends over a long distance to the South and that its extension is more limited to the north of the hotspot.

At the ridge segment scale, time-wise epicentre distributions show that two different modes can be observed in the MAR seismicity: A high and constant seismicity rate would result from dominantly tectonic processes characterize colder sections of the Ridge. Conversely, a more episodic low-rate seismicity, which would be due to magmatic processes is observed near the centers of globally hotter - because they are located closer to the Azores hotspot?- segments.

It is however important to recall that the Azores plateau interrupts the SOFAR channel therefore inhibiting the accurate detection of hydro-accoustic events from the Azores plateau. This might lead to a biased analysis when transported to the Azores Plateau context. In the Azores, earthquake activity registered by local and global land based seismological networks, (as we shall address in the next chapter) is abundant in the some of the regions within the plateau, noticeably along the Terceira axis, as a result of tectonic and volcanic activity. In the Azores the thermal structure and consequently the lithosphere thickness along the Terceira axis are almost certainly quite different from those of the MAR north and south of the Azores, and probably progressively thicker

towards the Gloria fault (Bier, 2005), therefore favoring the onset of seismicity due to increase in thickness of brittle sections of the lithosphere.

Chapter IV - Defining the present day EU-NUB plate boundary

IV.1 Introduction

The determination of the Terceira axis segmentation pattern, the location of actively spreading segments and discontinuities, the areal extent of the plate boundary itself, are not easily definable. Poor definition of the plate boundary location arises probably from the combination of factors like the extremely reduced spreading rate promoting an unstructured pattern of magnetic anomalies or the highly discontinuous nature of accretion, and the complex tectonic pattern. For example, it remains unclear, due to absence of clear age relations which structures within the Terceira axis are actively deforming, and if accretion is taking place in the topographical highs or lows, in the submarine areas.

The beginning of GPS observation in the Azores with the installation in 1998 of the TANGO (Trans-Atlantic Network for Geodynamics and Oceanography) project (Bastos *et al.,* 1998) has enabled to study from the geodetic point of view the present day displacement field associated with the Azores Triple Junction.

In this chapter we review the models presented by different authors addressing the tectonic pattern of the EU-NUB plate boundary in the present day. We summarize the main seismo-tectonic observations and discuss new geodetic data presented by Fernandes *et al*. (2006). We first examine segmentation geometry by comparing the

observed displacement field with the predictions from two plate tectonic model based on geodetic data: DEOS2k (Fernandes *et al.,* 2003) and NUVEL-1A model (DeMets *et al.,* 1994). Finally, the observed relative velocity field is used to test a half-space elastic dislocation model for a synthetic plate boundary configuration. The results derived from this model are used to deduce the geometry of the present-day plate boundary and the width of the actively inter-plate region.

IV.2 Models based on morpho-tectonic and seismo-tectonic analysis

Based on sonar GLORIA images interpretations, Searle (1980) has presented a tentative segmentation pattern for this spreading center (Figure IV.1). This author considered that the present day position of the ATJ was located at the intersection of the North Azores Fracture Zone with the Terceira axis.

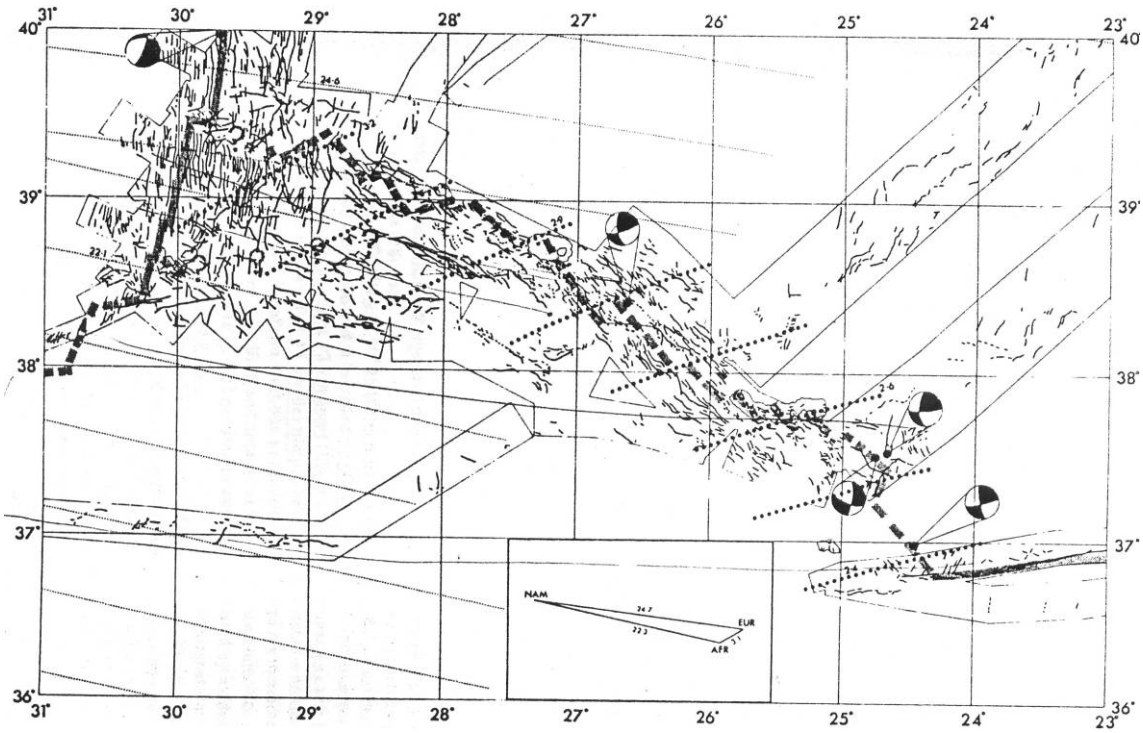

Figure IV.1 - Terceira axis segmentation pattern according to Searle (1980).

Recent improvements on the quality of the baseline data, namely on the regional bathymetric coverage (Lourenço *et al.*, 1998, Gente *et al.,* 2003) along with detailed tectonic work performed at Pico, Faial and S. Jorge Islands from the Central group (Madeira and Ribeiro, 1990) has led to models addresing the present day tectonic regime of the ATJ and the stress pattern within the Eurasian-African plate boundary.

Early views on the Terceira Axis as a simple rift system were considerably affected by a major earthquake event (magnitude 7.2) that took place the 1st Jannuary 1980 west of Terceira Island. (Hirn *et al.*, 1980). Contrary to what should be expectable, that is extension or oblique extension along normal faults parallel to the N120º strike of the Terceira axis, the aftershock sequence of this event was well constrained along a left lateral N150º pure strike slip fault (Hirn *et al.,* 1980) thus inconsistent with a simple spreading geometry. Madeira and Ribeiro (1990), considering the mapped fault families along the N150º and N120º, both displaying kinematic criteria ranging from dip slip to oblique slip faults to pure strike slip faults respectively as left lateral and right lateral, suggested that the tectonic regime was transtensional with a right lateral component and located the plate boundary at the S. Jorge channel (Figure IV.2).

A similar stress pattern, but a considerably different plate boundary configuration was proposed by Lourenço *et al.* (1998) using the fissural systems, represented by the linear volcanic ridges, as kinematic indicators (Figure IV.3). These authors, considering the marked rotation observed in these ridges within the plateau, their strike sub-parallel to the Terceira axis, the areal scatter of the earthquake activity within the western sector of the Azores plateau, and the prevalence of the Azores trend between 38º30' (West of the Condor Ridge) and the North Azores Fracture Zone, considered the ATJ, from the

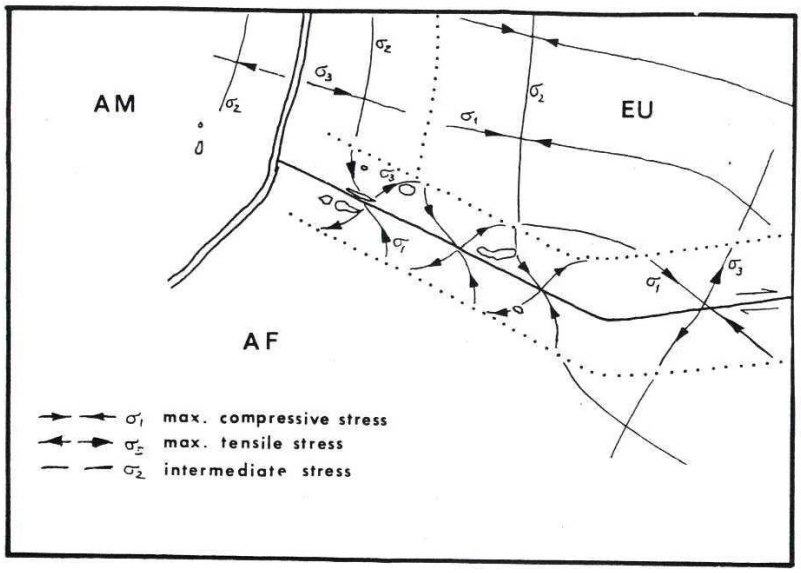

Figure IV.2 - Stress Pattern and tentative plate boundary location along a Leaky Transform fault at the S. Jorge Channel according to Madeira and Ribeiro (1990)

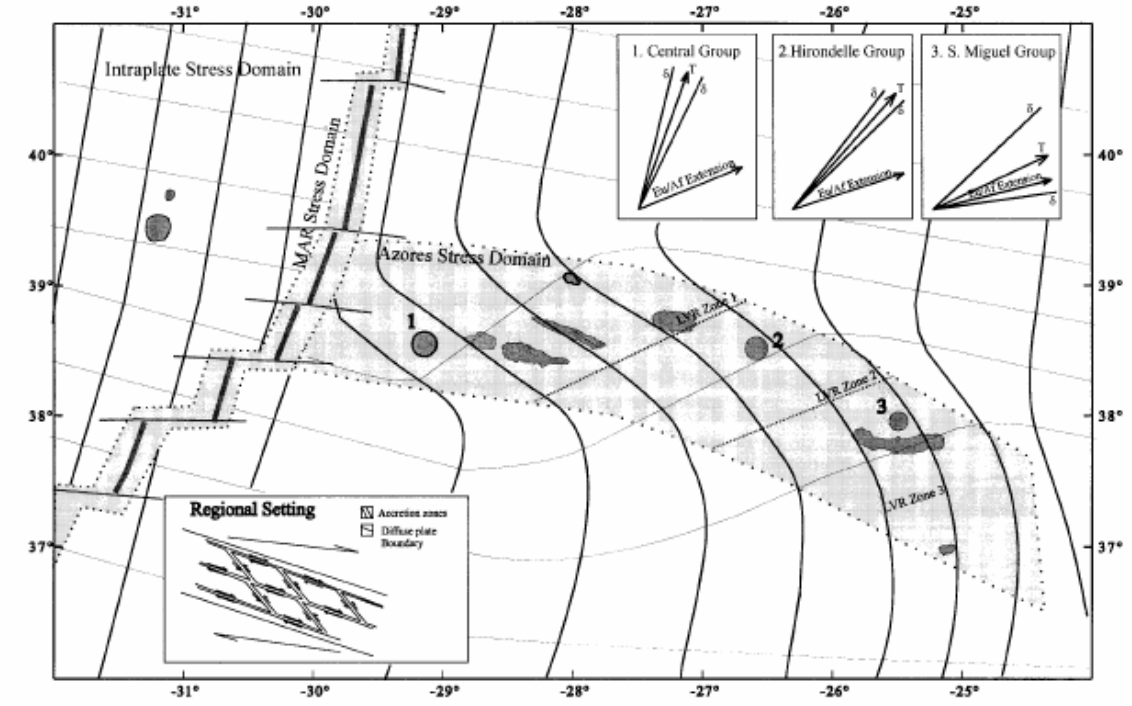

Figure IV.3 - Schematic stress pattern of the Azores Plateau according to Lourenço *et al.*, (1998). Dots represent the boundaries between the different LVR domains. Thicker lines represent maximum compressive stress orientation (σ1), thinner lines represent the minimum compressive stress orientation. The intermediate compressive stress is vertical. (Inset top) – T axis calculated from events occurring until 1998 along with calculated standard deviations, the kinematic orientation of the spreading axis calculated from Nuvel-1 model (DeMets, 1990) in the three individualised areas is also shown for reference. (Inset bottom) – Proposed schematic regional tectonic model for the Azores domain.

tectonic point of view, as a distributed feature. They also observed the right lateral transtensional character of the Azores domain which is interpreted as simultaneously acting as an ultra-slow spreading centre at the Terceira axis and a transfer zone which accommodates the dextral differential movement between stables Eurasian and African plates.

Miranda *et al.,* (1998) considering the earthquake distribution from local seismic network, data form a passive OBS survey and the focal mechanisms from Azores events, also inferred a transtensional regime from the tectonic fault system, where EU-AF inter-plate right lateral shear would be partitioned between the two fault systems in a framework of a tectonic block model (Figure IV.4). According to these authors, the interplay between the two faulting directions defines the current morpho-structure of the Terceira axis, where the basins are considered to coincide with tectonic blocks. The shear deformation along the plate boundary would be accommodated by rotation of the different fault controlled tectonic blocks.

More recently, Vogt and Jung (2003) returned to early views which approached Terceira axis as a classical rift system. They classified the Terceira axis as a young (< 1 Ma) intra-oceanic oblique spreading rift system. Noticing the extremely low spreading rates between EU and NUB predicted by NUVEL1A, and by comparing the first order morphological structures of the Terceira axis with other ultra-slow and super-slow ridge systems such as the Garkel, The Mohns- Knipovitch or the SWIR ridge systems, they conclude that the Terceira axis (designated by these authors as Terceira rift) is the slowest spreading environment in the world ridge system.

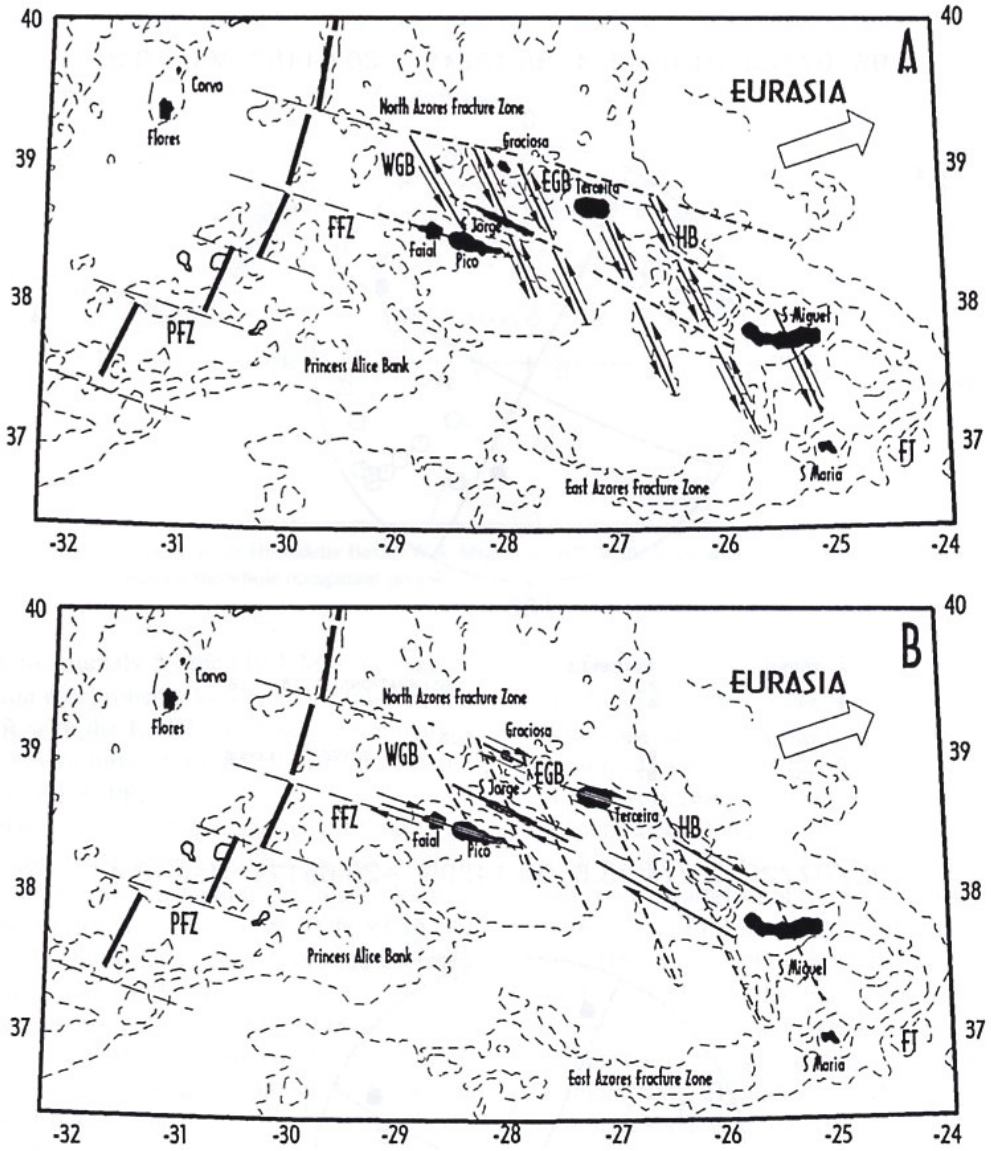

Figure IV.4 - Tectonic block model sketched by Miranda *et al (*1998). See text for details

In their view the plate boundary is located solely along the Terceira axis and, analogously to Searle's interpretation they locate the ATJ at the intersection of the Terceira axis with the MAR along the N. Azores Fracture Zone. Their interpretation of

Terceira axis as an oblique rift zone excludes the block tectonic model presented by Miranda *et al.* (1998) as Terceira axis basins are considered to correspond merely to segments of the rift valley which were not filled with volcanism.

Volcano-tectonic activity on the inner sectors of the plateau south of the Terceira axis is disregarded by these authors as significant and part of the plate boundary zone processes. Rather they consider that these structures are linked to and are a result of ATJ past northward migrating history in close link to the AHS migration northwards. They interpret their growth as a result of magmatism remnant of HS activity under short-lived presently abandoned rift axes. These interpretations and the significance of the linear volcanic ridges as a part of the actual plate boundary processes will be discussed more thoroughly in the next chapter.

IV.3 Earthquake data

IV.3.1 Epicenter spatial distributions

The Azores plateau displays quite a high level of seismicity but of low magnitude. The epicentral locations shown in Figure IV.5 comprise the time span between 1994 and 2004, and are taken from the ISC ("international Seismological Catalogue"). We opted to disregard epicenters from previous dates because 1994 was the year were the local based SIVISA network entered in operation and corresponds to a better azimuthal coverage and better constrained epicenter locations. Nevertheless, the period chosen covers the time span of GPS TANGO network observations and provides a good reference on how active processes distribute across the plateau.

The seismicity displays some amount of scattering but is largely aligned along the Terceira Axis in a band ca. 80 km wide for its central and eastern part., essentially

confined within its northern and southern walls. In the western sector the band of seismicity widens to about 180 km, and is limited to the south by Condor volcanic ridge and the northen wall of Terceira axis between Terceira and Western Graciosa basin.

It is worth noting that the majority of epicenters are located on submarine areas. The Islands generally display few occurrences. Islands such as Pico, S. Jorge, Graciosa, Terceira and S. Maria are earthquake depleted. Exceptions to this scenario are S. Miguel and Faial Islands. In the case of Faial, the earthquake cluster located NE of the Island corresponds to main shock and aftershock sequences resulting from the 1999 destructive earthquake that struck the Island, with epicenter NE of the Island (See section IV.4). The earthquake activity in S, Miguel is of low magnitude swarm like type and is probably related with volcanic activity at two volcanic systems within the Island, The Sete cidades caldera on the NW tip of the Island and the Fogo Caldera a volcano located near the center of the Island within the NW-SE trending Congro graben. Both systems have been displaying signs of activity in recent times.

Other spatial clusters of activity along time are mainly focused, despite the scatter, seawards west of volcanic ridges: Condor, Pico-Faial S. Jorge and within Terceira axis: West Graciosa Basin and at the SE Terceira ridge between D. João de Castro bank and Terceira Island

IV.3.2 Focal Mechanisms at the Azores

There are limited moment centroid solutions available at the Azores. These are presented in Figure IV.5 following Harvard CMT convention. The vast majority of the solutions are of low magnitude pure normal faulting events or with a minor component of right lateral strike slip along N120º planes (Grimison and Chen, 1986; Bufforn *et al*,.

1988). These events present normally traction T axes directions nearly perpendicular to the Terceira axis at each location. This progressive rotation of tectonic directions from WNW-ESE to nearly N-S at the intersection of the Terceira axis with the Gloria fault was already recognized by Luis (1996) and Lourenço *et al.,* (1998).

Two thrust events are documented in the Azores region. One is located north of the D. J. Castro bank and was re-evaluated by Buforn *et al.* (1988) as a dominantly right lateral strike slip event along a nearly East-West direction or conversely a left lateral strike slip along a N-S fault plane. Another thrust event is located SE of S. Miguel near the formigas islets. Its significance remains unclear, but might be related with structural complexities at the intersection between the Terceira axis and the Gloria fault.

The highest magnitude events registered instrumentally that have occurred in the Azores are of pure left lateral strike slip faulting along directions ranging NW-SE to N-S. This faulting direction was first interpreted by analysis of aftershock epicenter distributions (Hirn *et al.,* 1980) following the highly destructive M = 7.2, Terceira, 1st Jannuray 1980 earthquake with epicenter at the Eastern Graciosa Basin.

IV.4 The Faial 1998 earthquake

This earthquake occurred on July 9th 1998, with epicenter at the sea 10 km NE of Faial at a SIVISA computed location of 38º38.05'N 28º31.38' W (Senos *et al.,* 1998). This event had a Mw = 6.1 and caused 8 casualties and 1500 homeless. Figure IV.5 displays the focal mechanism for this event. Two conjugate planes determined are: Strike N61º dip 82º and rake -180º and strike 151º, dip 90º, rake -8º.

Soon after the main shock, the seismological network was up-graded and documented with very detail the aftershock sequence that followed, registering thousands of small

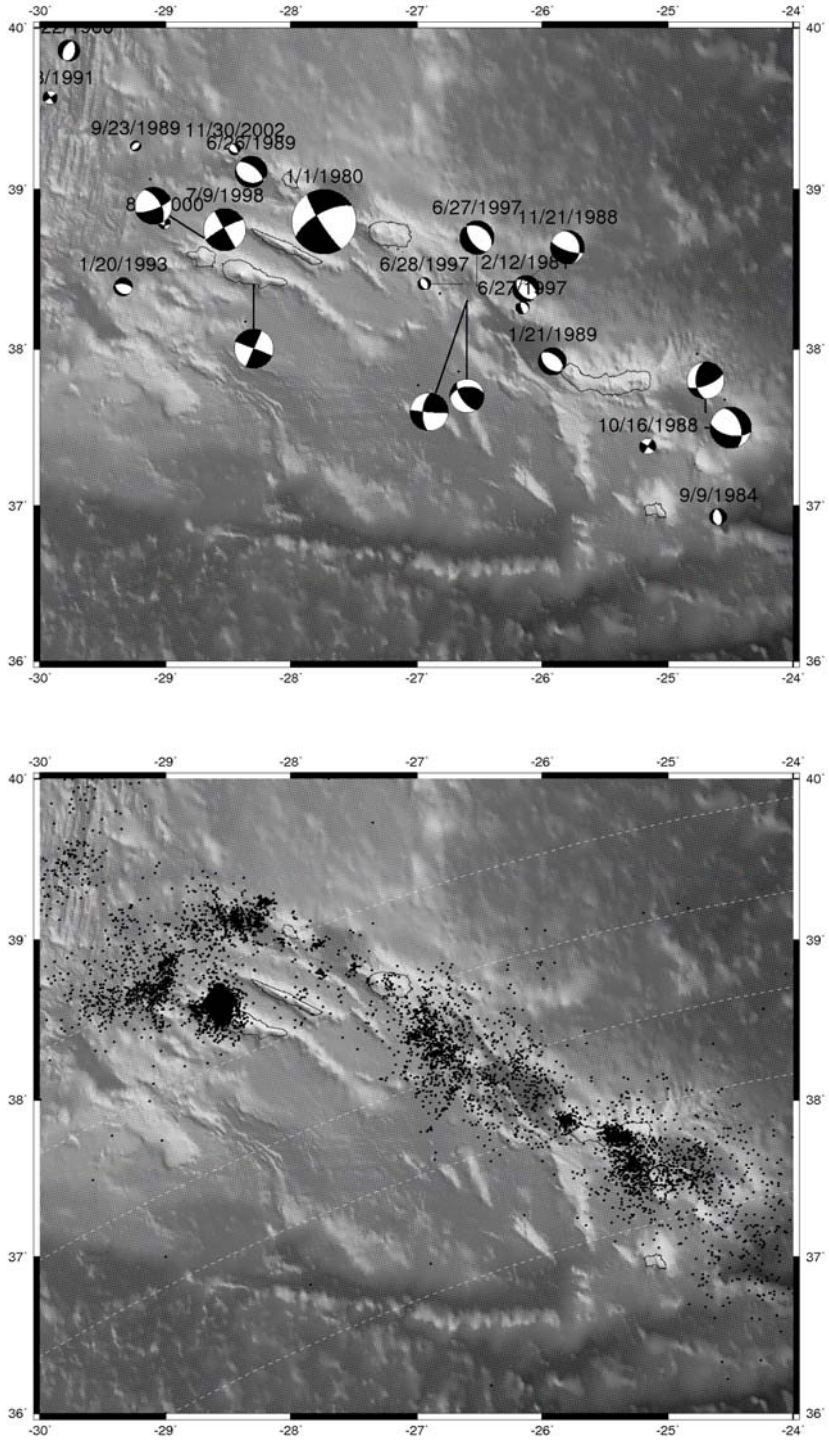

Figure IV.5 – Top) Moment centroid solutions from NEIC for most significant earthquakes detected in the global and local networks see text for details. Bottom) Recent Earthquake Epicenter distribution across the Azores plateau from years 1994 to 2004 taken form the ISC catalogue. Dashed white lines are predicted transform directions from NUVEL1A for Nub/Eu plate boundary.

magnitude events (Dias, 2006). The resulting epicenter distribution pattern displays a major alignment along the N151º direction but is cut trough by epicenter alignments which follow the other conjugate nodal plane direction. Fernandes *et al*. (2002) using GPS data from the TANGO network, isolated the co-seismic displacement component and modeled the dislocations provided by the two possible fault solutions in an homogeneous elastic half-space. Results from their modeling procedure did not provide any additional tectonic constraints, as both fault solutions provided equally satisfactory fits to the observations.

More recently, Dias (2006) performed a complete re-evaluation of the earthquake sequence following the main shock and aftershock epicenters have been re-located and focal mechanisms resultant from that event have been revised and up-graded from previous publications on the subject. Considering the aftershocks epicentral distribution, they cluster in two nearly ortogonal tectonic directions following the main shock rupture. Focal mechanisms display a complex pattern, and in any case, both possible fault planes are clearly discordant from the orientation of Faial Island main faults (Figure IV.6). Ruptures in the N60º direction, are dominantly oblique right lateral normal faulting events. On the contrary focal mechanism distributed along the N160-N170º vary between dip slip normal events and others which display a marked left lateral strike slip component. The significance of these strike slip events, for the tectonics of the present day tectonics of the Triple Junction will be dealt with in chapter VIII.

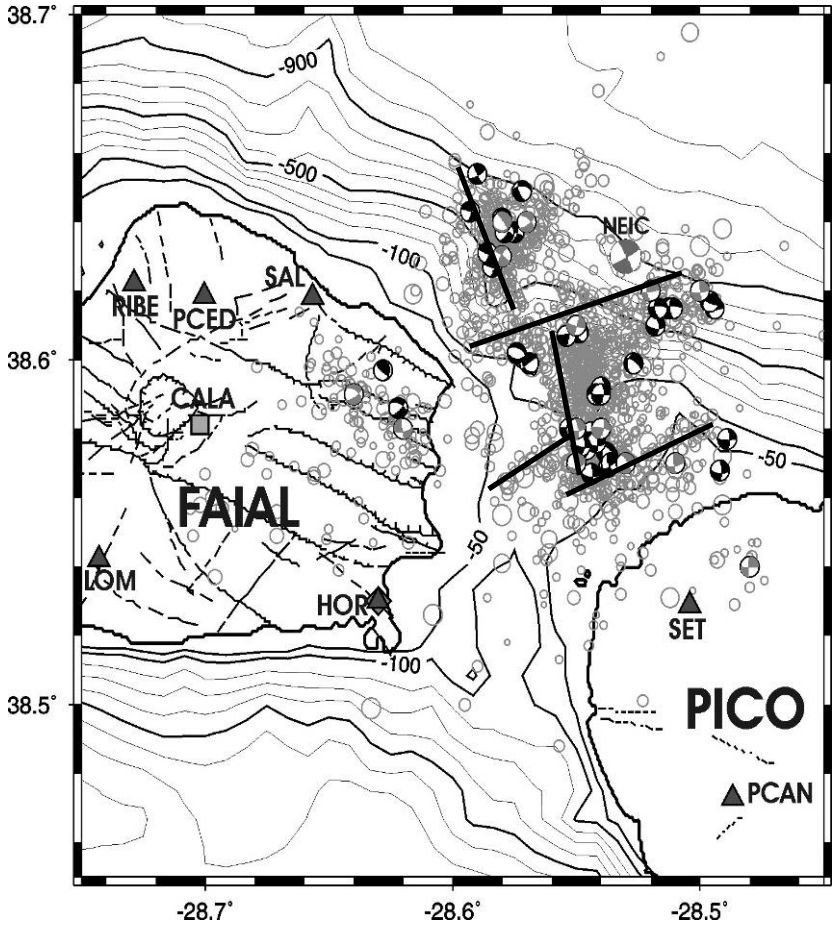

Figure IV.6 - Re-location of the events registered in July 1998 following the Faial earthquake. All plot events have epicentres calculated with a minimum of 4 stations (to better constrain the hypocenter depth). Black focal mechanisms correspond to singular events. The gray focal mechanisms are composed. NEIC corresponds to main shock centered on the epicentral relocalization performed by Dias (2006).

IV.5 Geodetic Data

IV.5.1 The TANGO experiment

The initial TANGO network consisted of one station per Island (cf. Figure IV.7) and was re-occupied with an approximate triennial periodicity until 1997. In 1999, DEOS

(Department of Earth Observation and Satellite systems) and AOUP (Astronomical Observatory of University of Porto) initiated a collaboration with the aim of maintaining and expanding the original network. In September-October 1999, 26 new sites were observed for the first time on the Central Group of the Azores Archipelago. In addition, two permanent GPS stations were installed on Faial (2000) and Terceira (2001). In 2001, CGUL (University of Lisbon Geophysical Center), in collaboration with DEOS and AOUP, added 30 new GPS stations in Terceira (May 2001, see Navarro *et al.,* 2003) and Faial and Pico (October 2001) Islands. These stations are being observed every year to address the intra-Island displacement field over the Central Group. Figure IV.7 presents the actual GPS network in the Central Group of the Azores Archipelago. This will be referred to here as the Extended TANGO network.

Results from the initial TANGO network for the period 1988-1997 were already presented by Bastos *et al*. (1998). A new evaluation of the TANGO network for the 1993-2000 period was presented by Fernandes *et al*. (2004). The 1988 and 1991 TANGO campaigns were not considered due to their low quality. The average opening rate of the Middle Atlantic Ridge at the latitude of Graciosa/Corvo Islands was re-evaluated as 23 mm/yr, consistent with global kinematic models, such as NUVEL-1A (DeMets *et al.,* 1994), and with local studies based on marine magnetic anomalies (Luis, 1996).

IV.5.2 GPS Results

The processing schemes for data used in this chapter are detailed in Fernandes *et al.*, 2006. They use daily solutions from each campaign and combine them into a single campaign solution. Table IV.1 lists the overall r.m.s. of the residuals for the reference stations used in each campaign. The overall residuals in all campaigns range between 1

mm and 3 mm in the horizontal components and, between 4 mm and 8 mm in the vertical component.

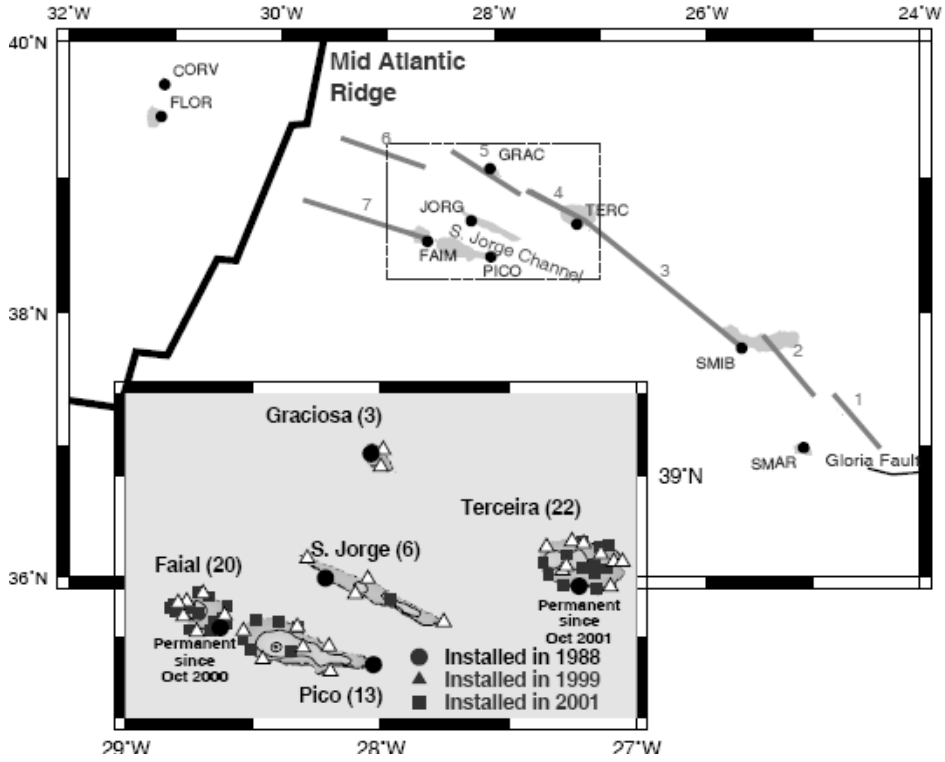

Figure IV.7 - GPS sites in the Azores Archipelago observed since 1988 (the Central Group is evidenced due to the large number of stations recently installed). Gray lines show the location of the segments used in the elastic modeling procedure).

A procedure was then followed to retrieve the velocity solutions relative to a geodetic reference model, the ITRF (International Terrestrial Reference Frame) 2000 (Altamimi *et al.*, 2002). This model defines a set of coordinates and velocities for a series of fiducial points on the Earth surface therefore providing a frame to which the velocity solutions for each campaign can be compared.

Table IV.1 - r.m.s. of the residuals on the mapping for each campaign

Campaign	North	East	Up	Number of
	Mm	mm	mm	Reference Stations
Nov 1993	2.7	2.8	6.5	12
Oct 1994	2.6	1.7	8.3	11
May 1997	2.0	2.5	7.7	17
Oct 1999	1.6	3.1	5.6	18
Oct 2000	1.6	2.5	4.0	17
Apr 2001	2.9	2.7	5.7	15
Oct 2001	1.3	3.1	6.1	15

The velocities relative to ITRF2000 of the six stations in the Central and Eastern groups of the Azores - that correspond to the longest observation periods - are plotted in Figure IV.8. In the same Figure, velocities computed from kinematic plate models, assuming stable Nubia or stable Eurasia behaviors are also plotted relative to ITRF2000. This is done for DEOS2k (Fernandes *et al.,* 2003), NUVEL-1A (DeMets *et al*.,1994) and REVEL (Sella *et al.,* 2002) models.

The time-series for Faial station (FAIM) is not shown. As discussed by Fernandes *et al*. (2002), there is a sudden slope change between the 1997 and the 1999 observations due to the co-seismic elastic deformation associated with the 1998.08.09 Faial earthquake. Therefore, due to the short time-span after the earthquake, the FAIM site is disregarded in our analysis.

Concerning the Island of Santa Maria, the available time series matches well with stable "Nubian" behavior. The other "end-member" of the displacement field corresponds to the Island of Graciosa: the available time series matches well the predicted "Eurasian" behavior. This observation (like the previous one) does not depend on the choice of the global plate kinematic model (cf. Figure IV.8).

All other stations display an intermediate behavior that can be seen as a weighted average between pure Eurasian and pure Nubian behavior. Even Terceira, which is close to the northern border of the Azores plateau, displays this intermediate behavior. If the Pico and S. Jorge stations are compared, they show similar motions. Therefore, most of the relative divergent movement must be accommodated between S. Jorge and Graciosa Island. Nevertheless, it is clear for this analysis that inter-plate displacements as measured from GPS are not confined to the Terceira axis.

IV.5.3 Half space Elastic dislocation modeling

The observed displacement field for the Azores Islands may be due to both elastic and inelastic processes. The viability of a purely elastic model with slip on buried dislocations (considered as the active plate boundary) can be investigated, if an a-priori location of the boundary is available. The most diagnostic information to locate the active spreading area comes from magnetic anomalies. Luis (1996) made a large-scale aeromagnetic survey that allowed the identification of a series of magnetic highs, following the alignment of the Islands that was interpreted as neo-volcanic axes. The segmentation pattern deduced from magnetic data is represented in Figure IV.7.

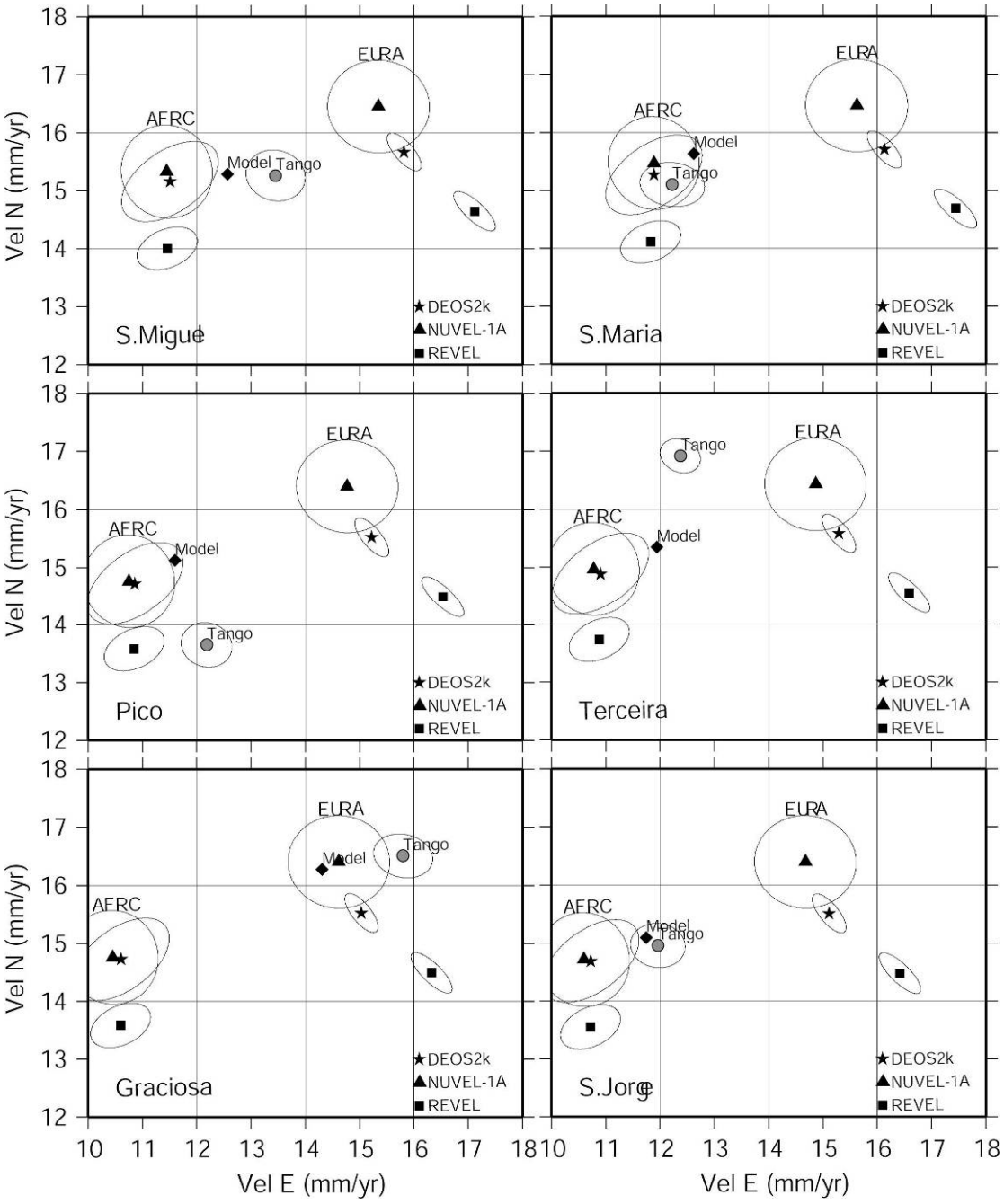

Figure IV.8 - Horizontal motions for the six TANGO sites with longest observation periods in the Central and Eastern groups. Estimated motion (circle) is fitted through the successive station positions obtained from the campaign solutions. Predicted motions according with the DEOS2k (star), NUVEL-1A (triangle), and REVEL (square) models correspond to those of stable Eurasia and stable Nubia. Elastic model prediction (diamond) uses DEOS2k for boundary conditions. Uncertainties are shown as 95 % confidence ellipses.

Here we tested two segmentation patterns: one where the plate boundary consists of 6 segments which follow the Terceira axis and intersect the Mid-Atlantic Ridge near the North Azores Fracture zone corresponding to the segmentation models proposed by Searle (1980) and corroborated by Vogt and Jung (2003) referred to hereafter as one axis model, and one that considers a Triple Junction further south following the westward prolongation of Faial-Pico direction towards the Mid-Atlantic Ridge corresponding to the segmentation pattern solution proposed by Luis *et al.,* 1996, based on magnetic anomalies and kinematic premises (Table IV.2), this will be referred to as the two axis model.

The elastic models were computed using the half-space approach (Okada, 1985). Each boundary segment has rectangular shape; its top follows the magnetic lineation and is located at the locking depth of 8 km. This depth defines the base of lithosphere deforming elastically due to continuous inelastic inter-plate strain below. The slip vector for each fault is determined from the projection of the DEOS2k and NUVEL1A relative velocity models between NUB and EU plates at the segment centre considering a fixed Eurasian Plate (Table IV.2).

The predicted displacement grids (the inter-plate displacements) from the elastic model are referenced to the segments used in the modeling procedure. These are subsequently converted into a tectonic plate reference frame. The Nubia displacement field with relation to a fixed Eurasian plate, predicted with Nuvel1A or Deos2K, is calculated and subtracted from the model grids. The resulting grid (see Figures IV.9 and IV.10) presents the interplate expectable deformation zone between stable Eurasia (where the displacement is overall null) and stable African plate where beyond the inter plate domain) the displacement is maximum for the given plate boundary configuration and

reference kinematic model. Finaly the resulting grid is sampled at GPS station locations, and values for displacement components are compared with TANGO observations (See Table IV.3 for model results).

Table IV.2 - Plate boundary segments characteristics used in the modeling procedure. ID corresponds to segment labels used in Figure V.1. Az – Azimuth, L – Fault Length, D – Fault Dip, SS and T are respectively right lateral strike slip and traction displacements according to Nuvel1A and Deos2K kinematic models.

	Central Point (UTM)					Nuvel1A (cm)		Deos2K (cm)	
ID	X (m)	Y (m)	AZ (º)	L (m)	D (º)	SS	T	SS	T
1	713832	4118156	138	59564	90	0.234	0.299	0.183	0.351
2	656123	4163233	139	65916	90	0.234	0.299	0.175	0.361
3	553319.5	4228639	129	170097	90	0.213	0.35	0.229	0.339
4	463328.5	4294153	118	53287	90	0.213	0.35	0.288	0.301
5	406832.5	4321541	123	66438	90	0.284	0.335	0.255	0.335
6	323556.5	4339289	110	72224	90	0.284	0.335	0.319	0.281
7	306736	4285451	108	104308	90	0.318	0.288	0.324	0.268

The predictions from the dislocation model are shown in Figures IV.9 and IV.10. A zero slip had to be affected to the candidate boundary segments 5 and 6 (cf. Figure IV.7). This is a direct consequence of the fact, already noted, that GRAC station displays an almost pure Eurasian behavior (cf. Figures IV.8). Therefore, only the segment 7 can be considered active during the time-span of the TANGO network.

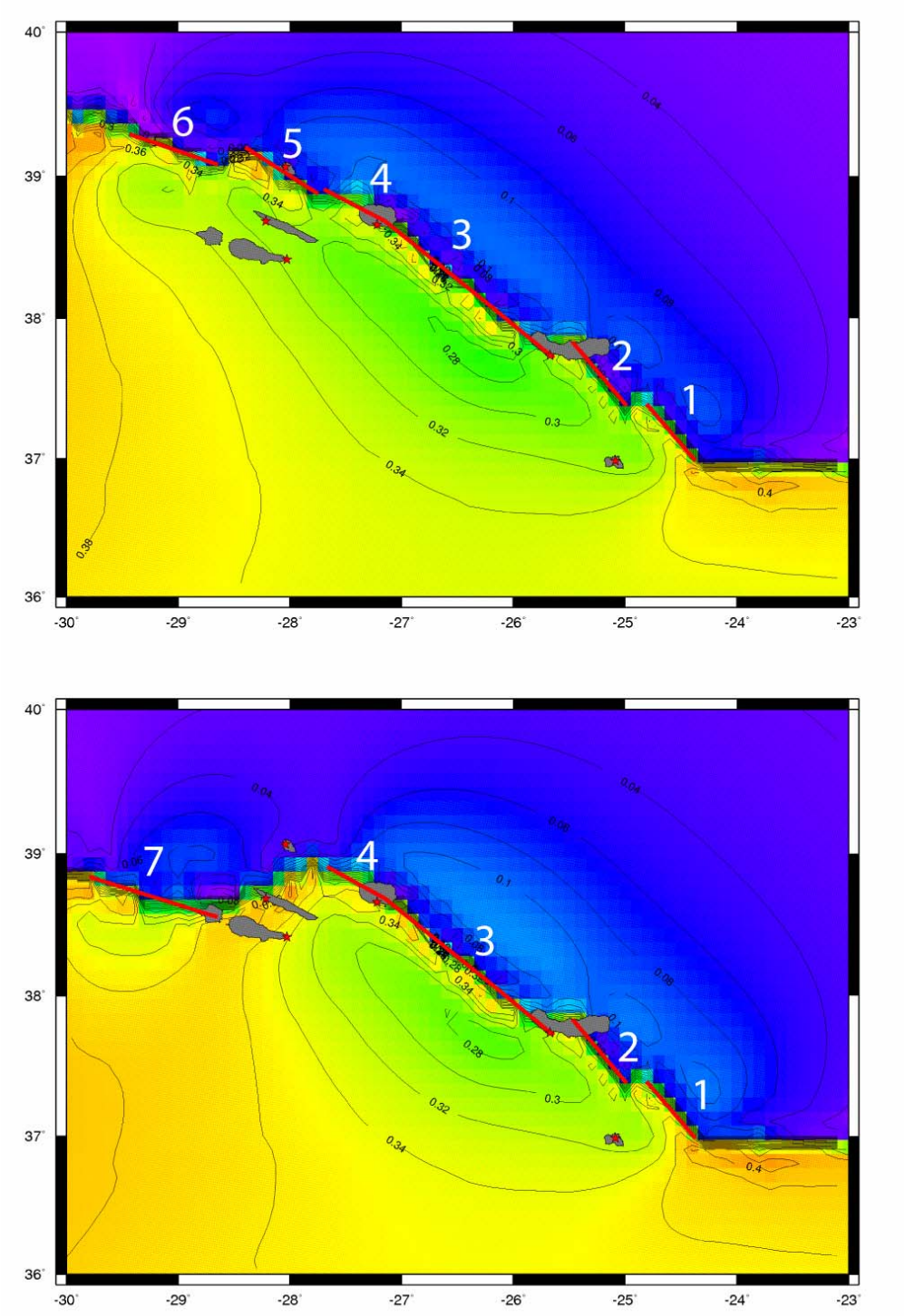

Figure IV.9 - Elastic dislocations considering an homogeneous elastic half space, a fixed Eurasian plate and Deos2K kinematic model as the plate boundary displacement constraint below the locking depth. Top) one segment configuration. Bottom) two segment configuration. Displacement units in millimeters. Red stars are Tango GPS Stations.

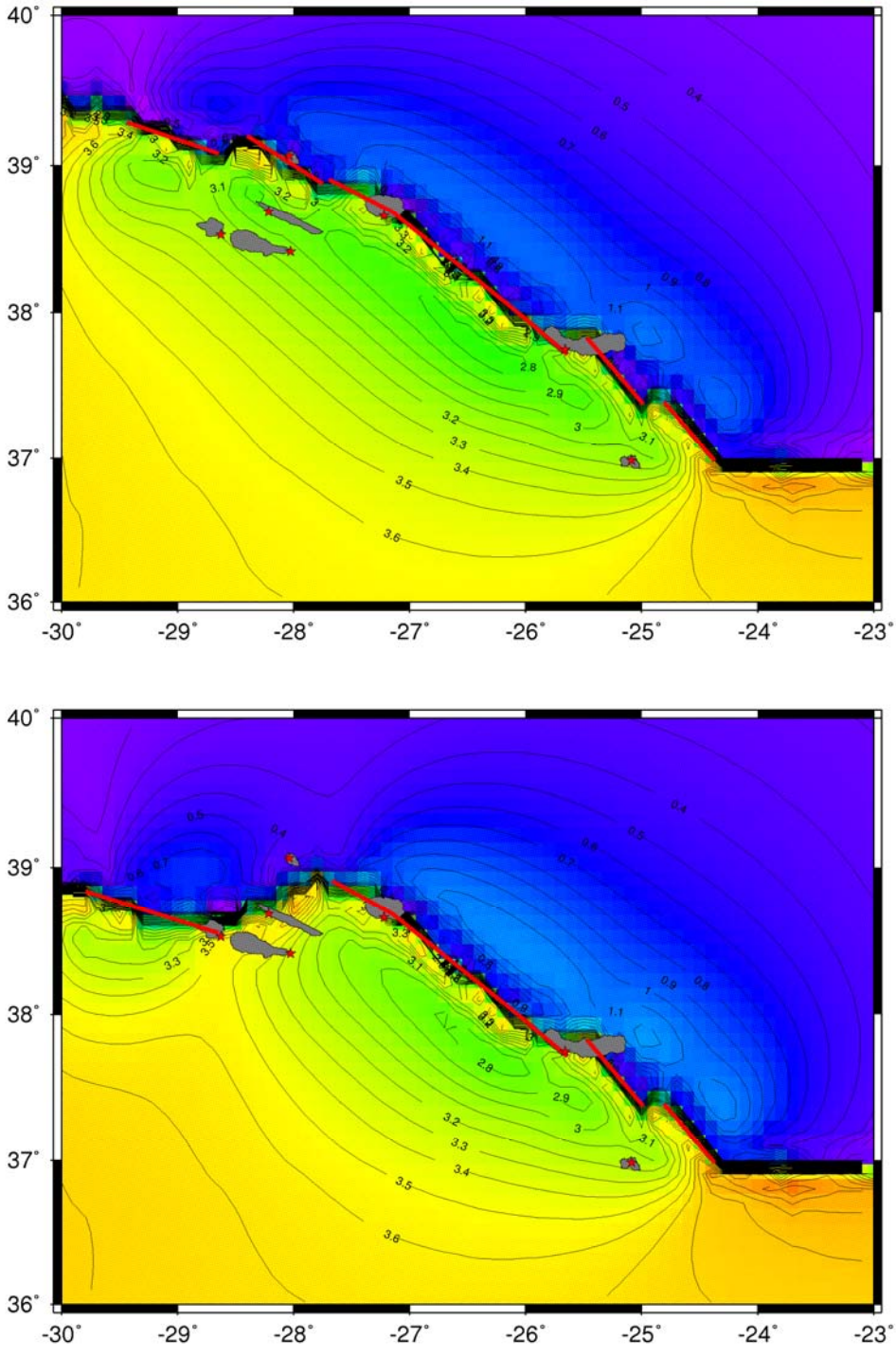

Figure IV.10 - Elastic dislocations considering an homogeneous elastic half space, a fixed Eurasian plate and Nuvel 1A kinematic model as the plate boundary displacement constraint below the locking depth. Top) one segment configuration. Bottom) two segment configuration. Displacement units in cm. Red stars are Tango GPS Stations

Table IV.3 - Listing of the modeling results, Tango observations and residuals (Observed – Modeled) for the TANGO stations considering a fixed Eurasian plate. Results from Nuvel 1A and Deos2K are very similar. Note that the two axis configuration fits better the observations than the one axis configuration.

Configuration	GPS station	Lon	Lat	Model (X)	Model (Y)	Tango (X)	Tango (y)	Residual (X)	Residual (Y)
Two axis (Nuvel1A)	GRAC	-28.0389	39.0652	1.26462	0.84873	0.954	0.716	-0.31062	-0.13273
	SJORGE	-28.218	38.6827	-0.03283	0.47785	-2.969	-0.828	-2.93617	-1.30585
	PICO	-28.0293	38.4155	0.31947	-0.86489	-2.855	-2.145	-3.17447	-1.28011
	SMIG	-25.6728	37.7359	0.60506	0.50256	-2.176	-0.665	-2.78106	-1.16756
	TERC	-27.2233	38.6586	0.19897	2.08124	-2.722	0.994	-2.92097	-1.08724
	SMAR	-25.0906	36.9832	-0.70721	-0.0295	-3.707	-0.861	-2.99979	-0.8315
Two axis (Deos 2K)	GRAC	-28.0388	39.0652	0.74146	0.70753	0.435	0.605	-0.30646	-0.10253
	SJORGE	-28.218	38.6827	0.37245	-0.18863	-2.427	-1.276	-2.79945	-1.08737
	PICO	-28.0293	38.4155	-0.91073	-0.36683	-4.009	-1.42	-3.09827	-1.05317
	SMIG	-25.6628	37.7477	1.93658	0.29022	-0.914	-0.835	-2.85058	-1.12522
	TERC	-27.2233	38.6586	2.12557	1.39662	-0.686	0.366	-2.81157	-1.03062
	SMAR	-25.0906	36.9831	-1.20278	-0.1391	-4.26	-0.896	-3.05722	-0.7569
One axis (Nuvel 1A)	GRAC	-28.0389	39.0652	1.71739	0.86343	0.954	0.716	-0.76339	-0.14743
	SJORGE	-28.218	38.6827	-0.0479	0.268	-2.969	-0.828	-2.9211	-1.096
	PICO	-28.0293	38.4155	0.13307	-1.09897	-2.855	-2.145	-2.98807	-1.04603
	SMIG	-25.6728	37.7359	0.60086	0.50763	-2.176	-0.665	-2.77686	-1.17263
	TERC	-27.2233	38.6586	0.12669	2.12193	-2.722	0.994	-2.84869	-1.12793
	SMAR	-25.0906	36.9832	-0.70846	-0.02756	-3.707	-0.861	-2.99854	-0.83344
One axis (Deos 2K)	GRAC	-28.0388	39.0652	1.16294	0.71881	0.435	0.605	-0.72794	-0.11381
	SJORGE	-28.218	38.6827	0.35997	-0.43041	-2.427	-1.276	-2.78697	-0.84559
	PICO	-28.0293	38.4155	-1.09369	-0.58113	-4.009	-1.42	-2.91531	-0.83887
	SMIG	-25.6628	37.7477	1.93241	0.29555	-0.914	-0.835	-2.84641	-1.13055
	TERC	-27.2233	38.6586	2.0545	1.43608	-0.686	0.366	-2.7405	-1.07008
	SMAR	-25.0906	36.9831	-1.20446	-0.13704	-4.26	-0.896	-3.05554	-0.75896

IV.6 Azores plate boundary configuration by geodesical constraints

The spatial distribution of the deformation associated with the Eurasia-Nubia plate boundary remains poorly understood. The divergence between the two mega-plates seems to be accommodated (during the last 2 Myr) in a confined region that follows the S. Miguel-Graciosa and the Pico-Faial lineaments, along which the high-amplitude magnetic anomalies have been mapped (Luis, 1996). The fine-scale geometry of this active plate boundary area is still unclear, and one of the main objectives of this work was to get information from the GPS velocity field distribution to better understand its broad structure.

Figures IV.8 and IV.11 show that two stations (Graciosa and S. Maria) display a clear kinematic behavior, with a displacement that follows respectively the Eurasian and Nubian velocity vectors retrieved from DEOS2k. This result is consistent with the fact that no significant active tectonic active structures are known north of Graciosa or south of Santa Maria (Lourenço *et al.,* 1998). Moreover, Santa Maria lacks any documented neo-tectonic activity. In the case of Graciosa, we must still keep in mind that there is historical volcanic and seismic activity locally. Thus, even if the behavior concerning the last decade matches "pure Eurasia" and even if most of the present day Eurasia-Nubia divergence in this sector of the boundary is accommodated further south, it still lies on an active deformation area. This seems to corroborate, at least from the geodetic point of view, the model of broad segmentation proposed by Luis *et al*. (1998).

It should be emphasized that a time-scale problem exists in comparing current day plate boundary configuration from GPS measurements with that deduced from plate tectonic models that integrate the past 3 Myr (DeMets *et al.,* 1994). The short time-span covered by the TANGO measurements implies that interpretations can be highly susceptible to

longer term changes in the strain pattern. In this regard, many factors, such as fault stress locking during inter-seismic periods, co-seismic induced deformation and swarm activity, not necessarily associated with expressed volcanic phenomena, can all be accounted for as transtensive strain, and thus condition the configuration and mechanics of the inter-plate deformation zone.

From Figure IV.11, which shows both the main topographic features along the Azores plateau together with the mean velocities deduced from the GPS array, it can be seen that most of the deformation (that appears in the GPS mean velocities as a change between Nubian velocities at south to Eurasian velocities at north) is mainly restricted to the highly tectonized area that includes the Islands themselves, as well as the neighboring submarine topographic highs.

The presented preliminary results (mean velocities) concerning the Extended-TANGO network show consistency with the motions deduced from the longer time-series. Table IV.4 lists the weighted averaged of the motions for each Island considering all observed stations (the associated uncertainty is the weighted r.m.s. of the residuals). Due to large uncertainties, the differences observed to date cannot, at present, be interpreted in terms of intra-Island tectonics. Further observations are needed to detect the interaction between intra- and inter-Island tectonics.

IV.7 Conclusions

Vogt and Jung (2003) suggested that the Terceira Rift is the world's slowest spreading-axis plate boundary. The Azores Plateau would have been formed by successive NE jumps of the oblique spreading axis, where the present Terceira Rift is the latest stage. These authors also suggest that the Azores Triple Point is located in the prolongation of

the Terceira Rift (ca. 39.4°N, 29.7°W) but they do not provide any supporting evidence. In fact, they consider that the location proposed by Luis *et al*. (1994) at the Faial latitude might also be a second active triple point. The GPS data seem to support the southern location of the triple point deduced from magnetic modeling by Luis *et al*. (1994).

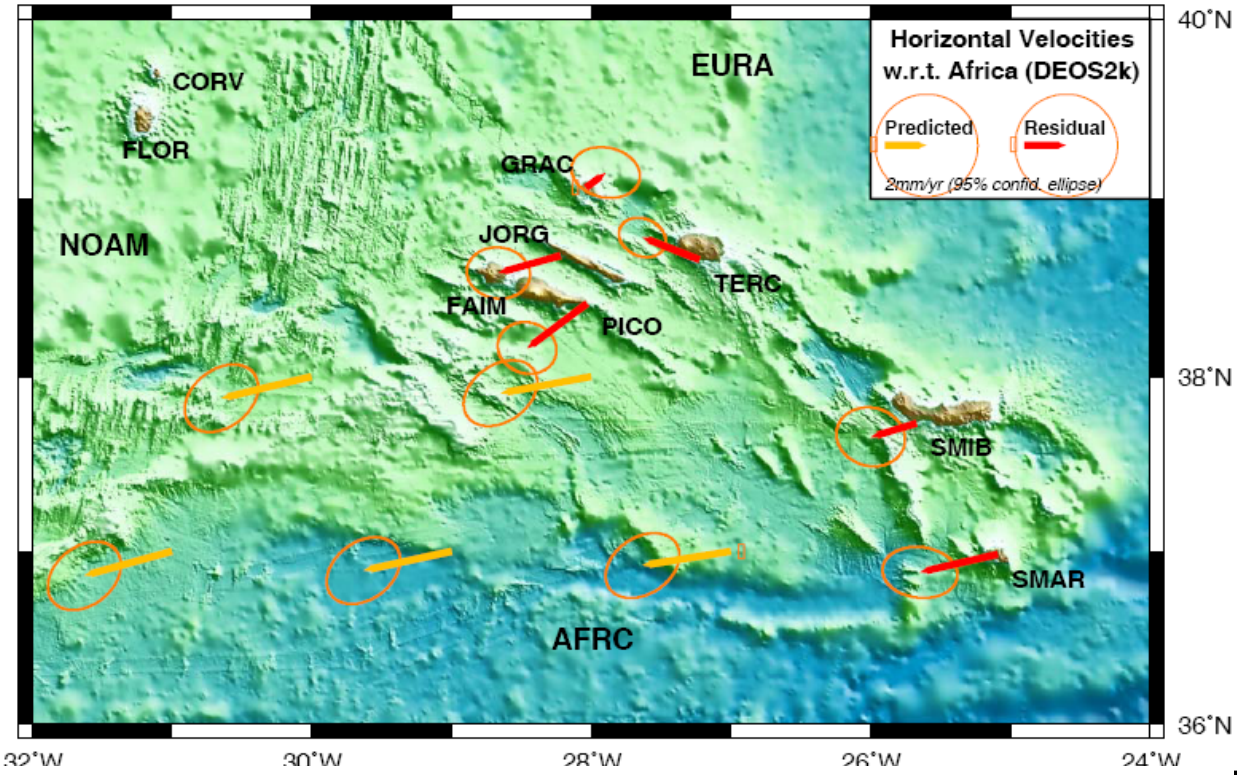

Figure IV.11 - Relative motions with respect to stable Eurasia (as predicted by DEOS2k). Residual motions (observations minus predictions) for the initial TANGO sites in the Central and Eastern groups (red). Predicted relative motions for points located in stable Nubia (purple). On the background is shown the bathymetry from Lourenço *et al.* (1998).

The velocity field for the period 1993-2001 for GPS sites located on the Azores Islands can be considered as good estimate of the displacement field for the area close to the western segment of Eurasian-Nubian plate boundary. The values for the averaged

velocities are compatible with the mean velocities deduced from global models for both plates.

Table IV.4. Comparison between the averaged horizontal motion (in mm/yr) computed using the new stations observed since 1999 (first two columns) and the TANGO station (two last columns) in each Island of Central Group. It is also listed the number of new stations per Island. The initial TANGO motion for Faial (FAIM) was not computed due to the co-seismic displacement caused by the 9 July 1998 earthquake.

Island	Averaged Motion		# Stations since 1999	Initial TANGO motion	
	East	North		East	North
Terceira	12.2±1.4	14.6±0.7	9	12.4	16.9
Graciosa	17.1±0.1	14.5±0.1	2	15.8	16.5
S. Jorge	13.1±1.6	13.1±1.6	4	12.0	15.0
Pico	11.7±2.1	12.5±3.1	6	12.2	13.6
Faial	9.2±2.4	13.5±1.2	7†	---	---

Within the accuracy of the available geodetic data, we conclude that the relative displacement between Eurasia and Nubia along the Azores plate boundary is mostly accommodated within a relatively short lithospheric band that follows the Islands alignment and the neighboring submarine topographic ridges. End members of this system appear to be the S. Maria and Graciosa Islands, which display "Nubian" and "Eurasian" behavior, respectively. All other sites are located along the presently active interplate deformation zone.

An elastic half-space approach was used to model the expected velocity field for this active boundary zone. Elastic predictions for all TANGO stations are close to the observations, if a locking depth of 8 km is considered. Two major spreading axes, an eastern one running from S Miguel to Terceira and a western one from Faial to the Mid-Atlantic Ridge, can be inferred. The candidate boundary segment that goes along the Graciosa Island was mostly inactive during the occupation period of the TANGO network.

Chapter V - LVR as active tectono-magmatic features of the EU-NUB plate boundary

V.1 Introduction

As seen in the previous chapter, GPS velocity solutions and forward elastic modeling favor, from the geodetic point of view, an interpretation consisting in a plate boundary divided in two broad segments: one defining the ATJ configuration exclusively centered at the Faial-Pico, and another axis located from Terceira southeastwards along the Terceira axis towards the Gloria Fault. This is valid taking both DEOS2K and NUVEL1A kinematic models as reference.

However, the short time span in geodetic observations only provides a snapshot of present day kinematic context. The existence of seismo-tectonic and volcanic activity along the westernmost sectors of the Terceira axis, implies that geologically the plate boundary is not confined to MAR-Faial-Pico segment and if both segments coexist in time, some active transfer zone is bound to exist between this two overlapping axis.

The area enclosed in between these two axis is characterized by a series of sub-parallel linear volcanic ridges (Lourenço *et al.,* 1998) (see Figures V.1 and V.2), dividing flat terraces with a uniform depth of 1200 m bsl. This domain encompasses the S. Jorge Island, The Faial-Pico itself and two co-planar linear volcanic ridges designated by "*Condor Mar*" and "*Condor Terra*", It will be referred to hereafter as the LVR Sector 1.

These ridges have a characteristic spacing of 30 to 40 km and a uniform axial orientation of N120º.

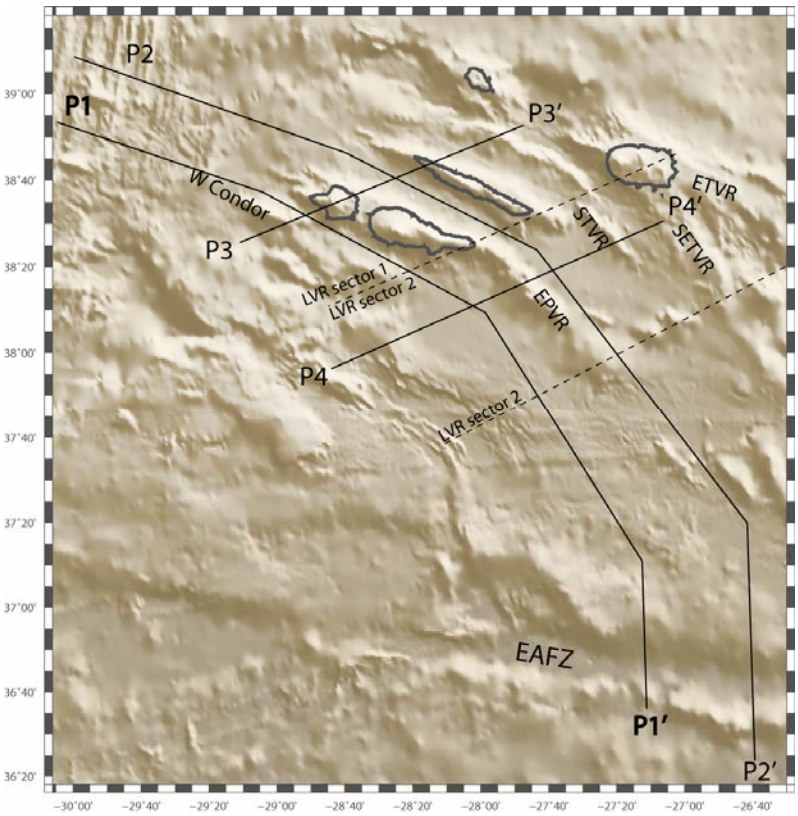

Figure V.1 - Shaded bathymetry of LVR sector 1 and 2. EPVR – East of Pico Volcanic Ridge; ETVR – East of Terceira Volcnaic Ridge; SETVR Southeast of Terceira Volcanic Ridge; STVR – South of Terceira Volcanic Ridge. Continuous lines and P1 to P4 denote bathymetric/topographic profiles displayed in Figure V.2.

Further East, a second set sub parallel volcanic ridges (Sector 2) is observed. It comprises the East Pico Volcanic Ridge (EPVR) the South Terceira Volcanic Ridge (STVR) and a undesignated volcanic ridge further SW. When compared to sector 1, the LVR present a similar spacing (about ca. 30 km) and a marked rotated axial orientation (N140º). The EPVR is the submarine prolongation of the Pico Island south-eastwards, the STVR on the contrary does not have any correspondence to LVR sector 1 structures. The flat terraces separating these LVR are 500 m deeper than those of sector 1. They lie

at a depth of ca. 1700 m bsl and become 200 m shallower between the EPVR and the STVR, at the vicinities of the Terceira axis.

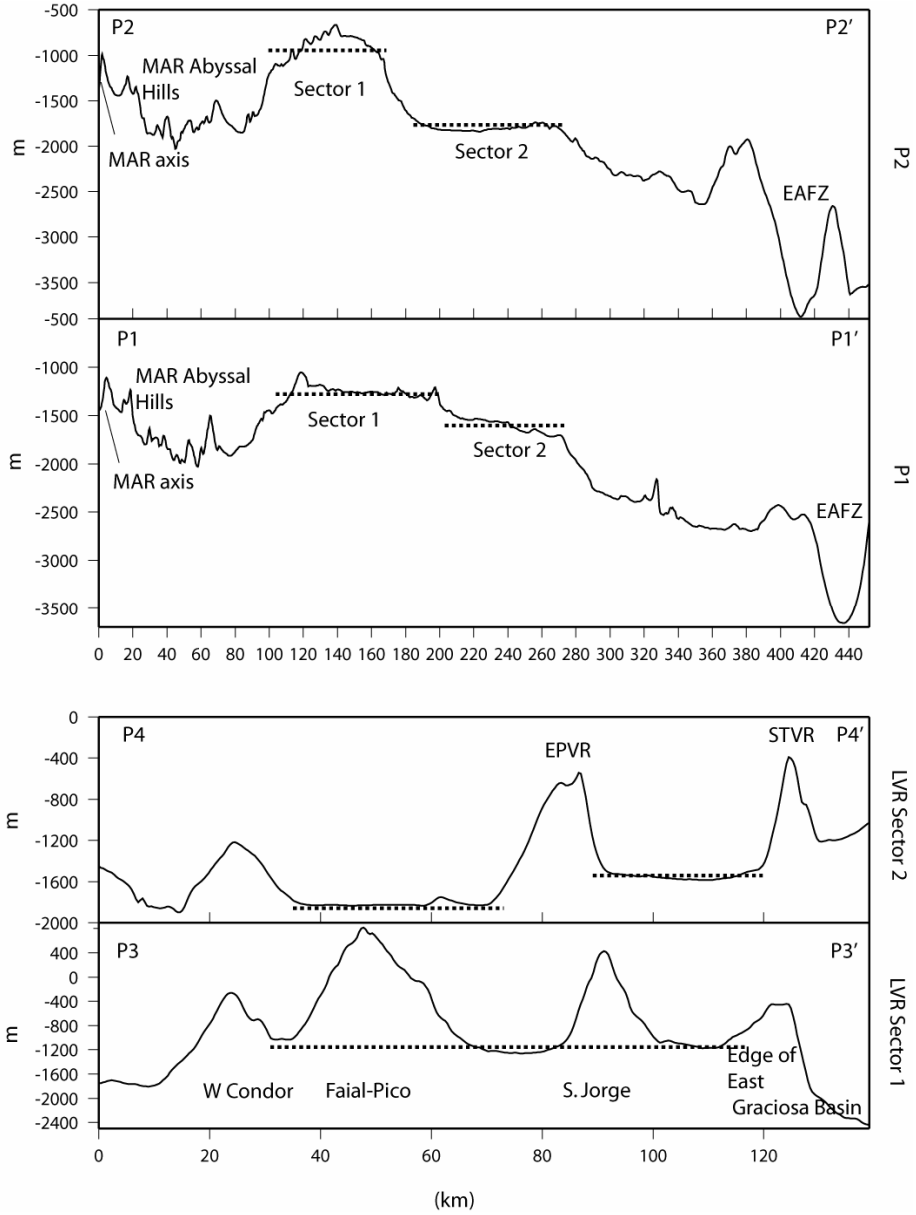

Figure V.2 - Topographic profiles of LVR sectors considered in this chapter. See Figure V.1 for profile location.

It is unclear if LVR Structures present in Sector 2 are apart of the Transfer zone as suggested by Lourenço (1998), or if they correspond to already inactive structures linked to the past evolution of the Plateau.

In this chapter we make used of previously published magnetic data, and sonar TOBI images acquired during the Azzorre 99 cruise, to study the structure and geological nature of the Azores plateau seafloor in both sectors. Given the uncertainty in the relative ages of the structures (as previously discussed in Chapter II), we foccus analysis in characterizing structures which prove either from magnetic anomalies or by neotectonic indicators to be currently active.

Our goal is three folded: 1) to characterize the seaflor geology of the different volcanic ridges. 2) To verify if any qualitative age progression exists amongst them in each individual sector and between adjacent sectors. 3) To evaluate the tectono-magmatic nature of the plate boundary processes and the dynamics of the transfer zone.

V.2 Data

V.2.1 Marine Magnetic data

To evaluate more thoroughly the nature of the seafloor, especially in what concerns distribution of recent volcanism within the Azores Plateau, and to validate geological interpretations of the sonar images, we produced a new magnetic map which complements that of Luis, 1996 presented in chapter II (cf. Figure II.6).

This new map has the advantage of the magnetometer being closer to the source magnetic layer as it results exclusively from marine magnetic observations and has therefore a higher resolution more suitable to complement finer scale TOBI sonar images interpretations. This map integrates new data retrieved from the AZZORRE99

cruise and both SIRENA magnetic surveys performed east (Sirena I and II) and west (Sirena II) of Terceira Island. These data set was complemented with other magnetic data retrieved from the NGDC marine data base (Figure V.32). The resulting magnetic anomaly map reduced to the pole is presented in Figure V.4

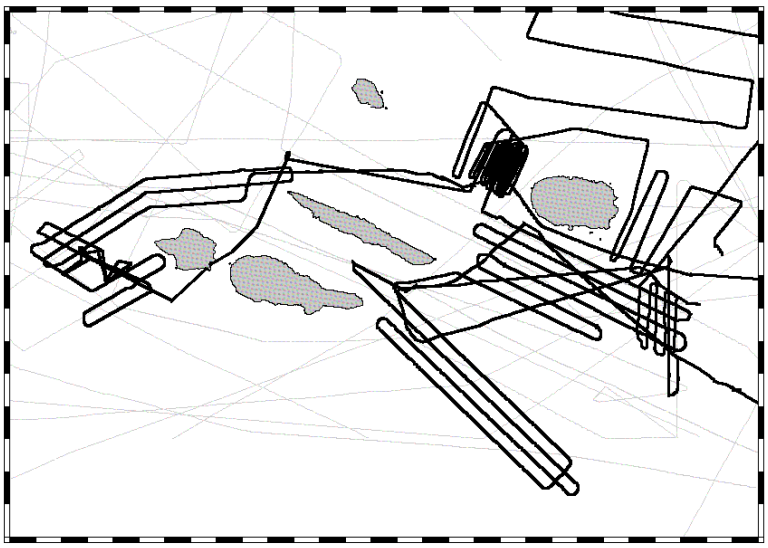

Figure V.3 - Magnetic survey ship tracks plot. Tracks in light gray are ship tracks retrieved from the NGDC marine data base. Thick black lines correspond to surveys performed during the Azzorre 99, Sirena I and II cruises.

V.2.2 The AZZORRE 99 TOBI Cruise

The Azzore 99 cruise (Ligi *et al.,* 1999) was held in July 1999 on board of the R/V Urania (CNR), as a joint Italian (IGM; PI Marco Ligi) – English (Oxford Univ.; PI Neil Mitchell); (SOC; TOBI Team) - Portuguese (Lisbon Univ.; Algarve Univ.). TOBI operations at sea were financed by the EU under the EASSS program (European Access to Sea Floor Survey System), ship time was funded by the Italian CNR. Post cruise data processing and training for cruise participants at the SOC –England was also financed by the EU.

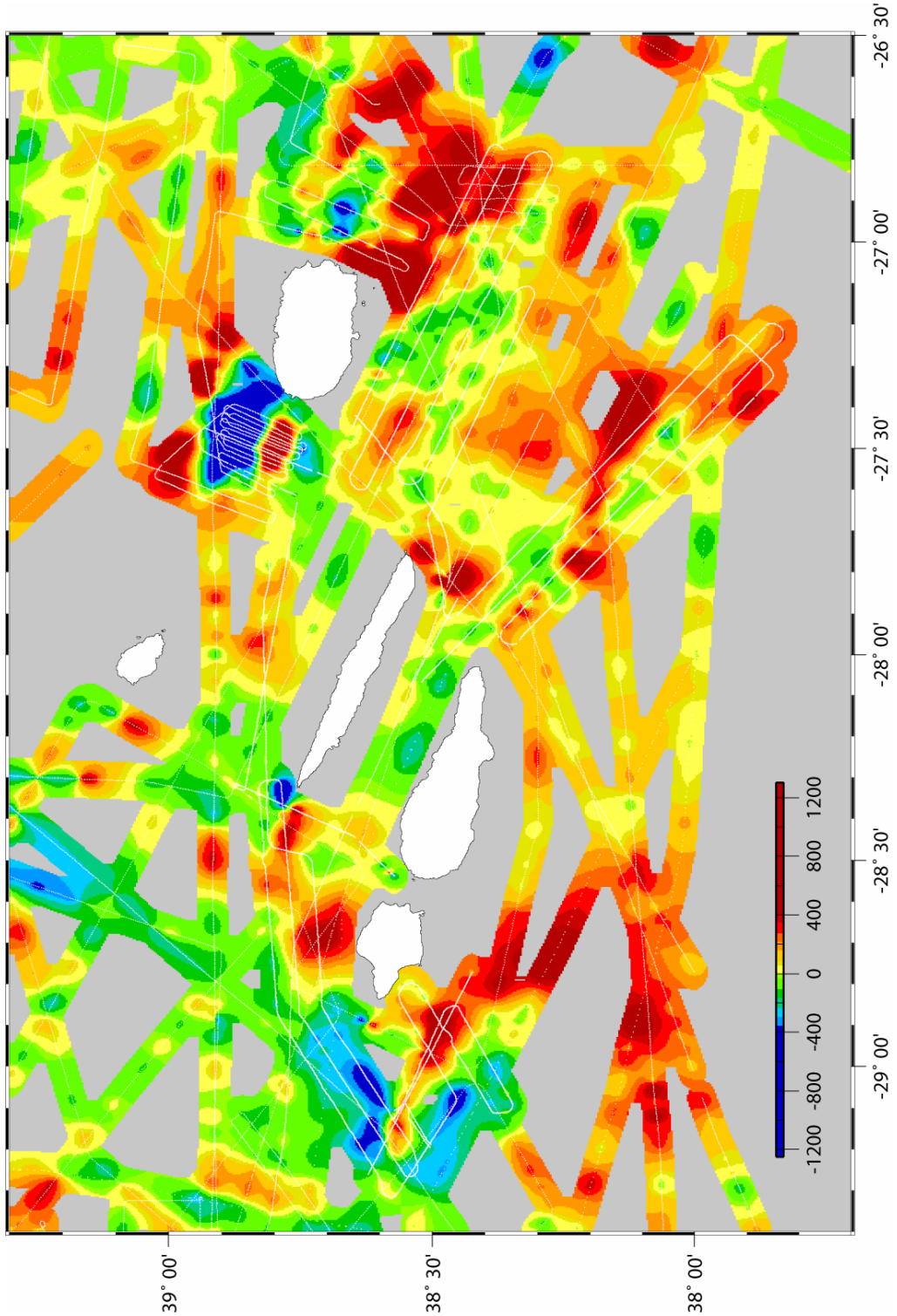

Figure V.4 - Magnetic anomaly map reduced to the pole, covering the LVR area. Data sources NGDC and the cruises: AZZORRE 99, SIRENA I and II (Goslin, 2004) Scale: magnetic anomalies; units: nT.

The cruise surveyed the linear volcanic ridges in the Azores.. It consisted of two legs with a stop at Faial Island for partial crew turn-over. The first leg allowed 10 days of continuous coverage of TOBI sonar, chirp sonar, bathymetry and surface magnetic data, southeast of Pico, S. Jorge and Terceira Island. The second leg provided equivalent data on a region comprising the Condor Ridge and the West of Faial and S. Jorge submarine prolongations. The sonar data acquired covers a total of 5 complete LVR and the west sector of S. Jorge and Faial LVR (Figure V.5). The general quality of the data is fairly good with the exception of the shallow portions on the top of the Condor Ridge (south of Faial). The analysis of the mosaic corresponding to the SETVR will be performed in the next chapter.

TOBI Sonar is a multi-sensor platform tow-yawed between 200 and 500 m from the bottom. It was equipped with a two sided 30 kHz sidescan sonar, a 7.5 kHz sub-bottom profiler, a CTD, a three-axis fluxgate magnetometer and a range of vehicle attitude sensors (i.e pitch, roll and heading from a gyro-compass). The instrument is towed with a 200 m umbilical behind a depressor weigth detaching the instrument from ship movement. TOBI position was achieved by using the ships' Simrad-Konsgberg HPR-1507 system and a long-range (6km) transponder, that was mounted 45 deg. below the TOBI's depressor. Sonar has a total swath width of 6 to 8 km, and footprints of 4x 7 m near the fish track but higher for the outer beams

Each mosaic results in a 8 bit image (256 tons of gray) where white pixels portrait high backscaterring surfaces and black pixels correspond to acoustic shadows. These images were drapped on top of bathymetric digital terrain models. The magnetic anomaly map was overlain on top of the composition to further constrain the interpretations.

V.3 Magnetic anomalies and Acoustic Facies interpretation

V.3.1 LVR Sector 1

The available mosaics show quite clearly that the bulk of active volcanic activity in the Azores western sector is concentrated in LVR, these structures correlate strongly with positive magnetic anomalies. Furthermore their surroundings are almost exclusively composed of a greyish homogeneous facies interpreted as pelagic and volcanic sediment and turbidite fans.

The main volcanic facies present are homogeneous high backscatter surfaces probably related with massive flows, hummocky textures related with pillow mound formation, and individual circular volcanic cones sometimes with visible craters, that can reach several tens of meters high. They occur both oriented along LVR major axis direction, parallel to fault scarps, or as individual cones with a somewhat more random spatial distribution.

It is possible to observe a high backscatter surface prolonging from the Capelinhos 1957/58 eruption site in the western tip of Faial for about 20 km towards WNW. This high backscattering surface is cut by a well marked lineation interpreted as a major fissure which aligns up with the Western Faial fissural system. (Figure V.6).

Due to its shallow depth the axial structure of the Condor ridge is poorly imaged. Figure V.7 displays a high backscattering surface, suggesting a recent nature of the volcanic terrain which contrasts with the surrounding greyish areas interpreted as pelagic or volcanic sediment. The western tip of this 40 km long LVR consists of a highly

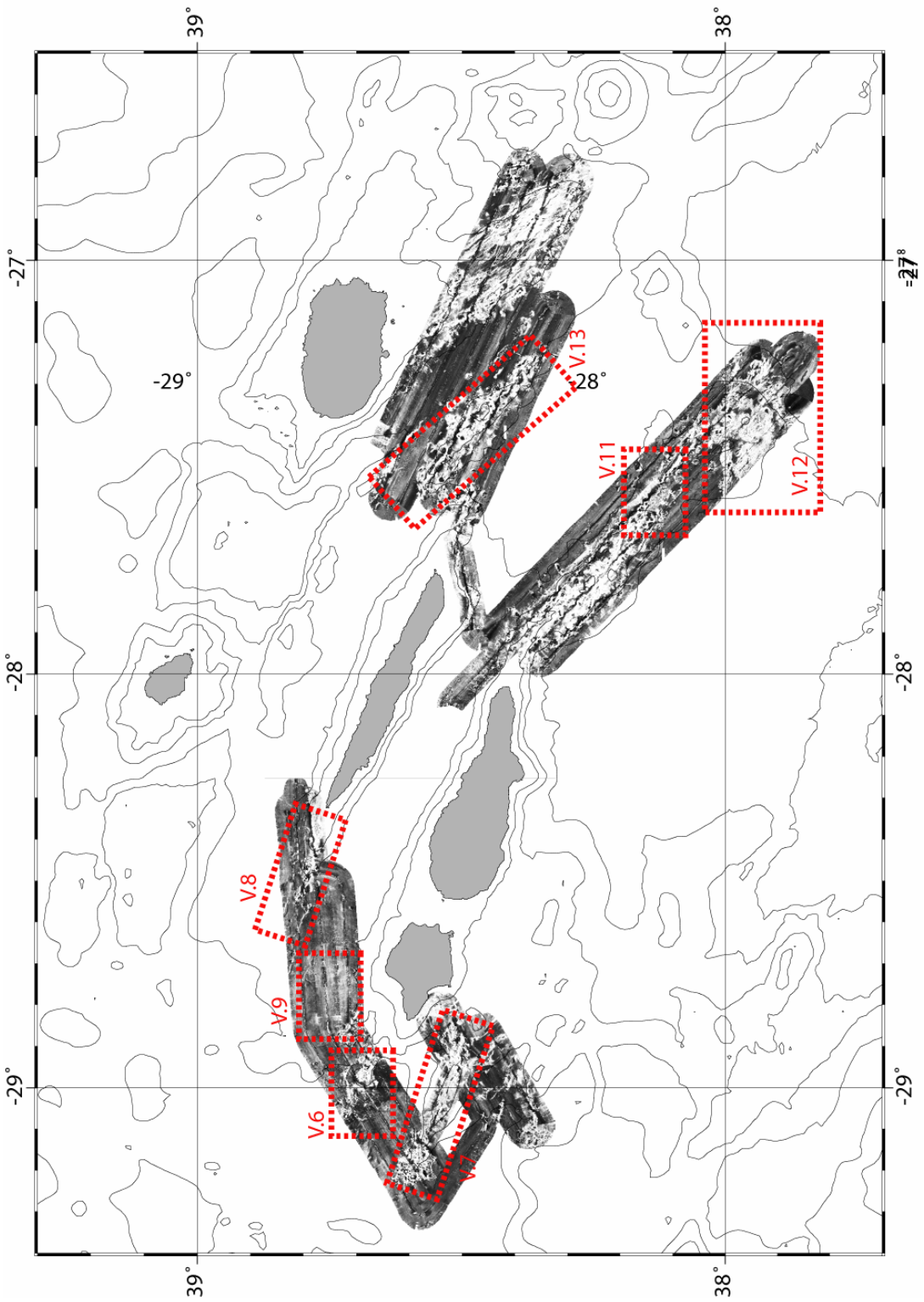

Figure V.5 - TOBI Mosaics surveyed during the Azzorre 99 cruise. Bathymetric contours each 500 m are overlain for morphological reference. Dashed red boxes and numbers refer to figures numbers which are presented below.

irregular pattern of high backscattering acoustic facies, probably related with a combination of mass wasting debris at the slopping tip of the LVR and some volcanic constructs like individual pillow mounds and more complex hummocky structures. No clear tectonic structures are here visible.

Both LVR and corresponding tips correspond to marked positive anomalies probably Brunhes and their surroundings are a wide area of negative polarity (probably Matuyama), which in the case of West condor ridge define two elongated magnetic anomaly lows parallel the axis of the LVR. It is not clear if in this case, the negative bands were generated at the axis of the W Condor ridge and than rafted sideways. However, given the flatness of the W Condor ridge surroundings and the lack of significant tectonic or volcanic structures we come to an interpretation where the W Condor ridge has simply grown over a negative polarity basement.

The seawards prolongation of the S. Jorge Island shows features which are somewhat distinct from the observations of Faial western sector (Figure V.8). The prominent inland fissural system aligned along the Island central axis prolongs seawards in the same direction for about 12 km. The submarine extent of the Island western tip displays a series of acoustic echoes which, probably due to its shallow depth, are poorly imaged. Further west these terminate abruptly towards the centre of a 200 m deep graben. Faults defining this graben structure are clearly outlined on the sonar image, they have the same orientation of the S. Jorge Island and present little segmentation. There is no indication of strike slip component and this are interpreted as dominantly dip-slip faults.

They extend for about 20 km to the image limits and cut thru seabed sediments, the base of the fault scarp is irregularly bordered by a confined area of intermediate non-

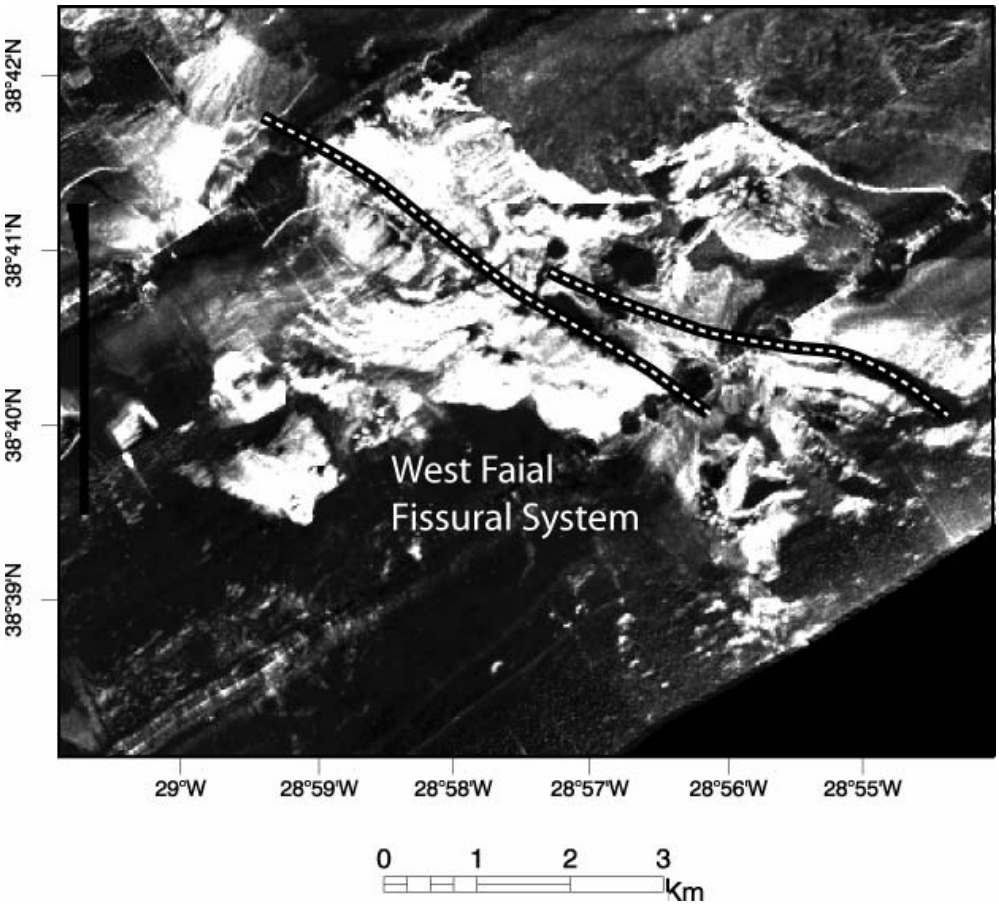

Figure V.6 - TOBI sonar image of West seaward prolongation of the Faial Island. Lines in image corresponds to a major fissural system 11 km long, the submarine prolongation of the Faial fissural system on land. Note: lines are slightly shifted to the north to allow a clearer view of the structures in image.

-homogeneous backscatter which suggests existence of fresh talus deposits and that these structures are currently active. Further evidence of activity exists at the centre of the graben. Here, four acoustic echoes are present in the graben centre, aligned and parallel to the graben bounding faults, some display circular sections. We interpret these features as possible indicators of subsurface volcanic phenomena and a clear suggestion of recent activity within the fissural system with possible ongoing propagation of the LVR westwards.

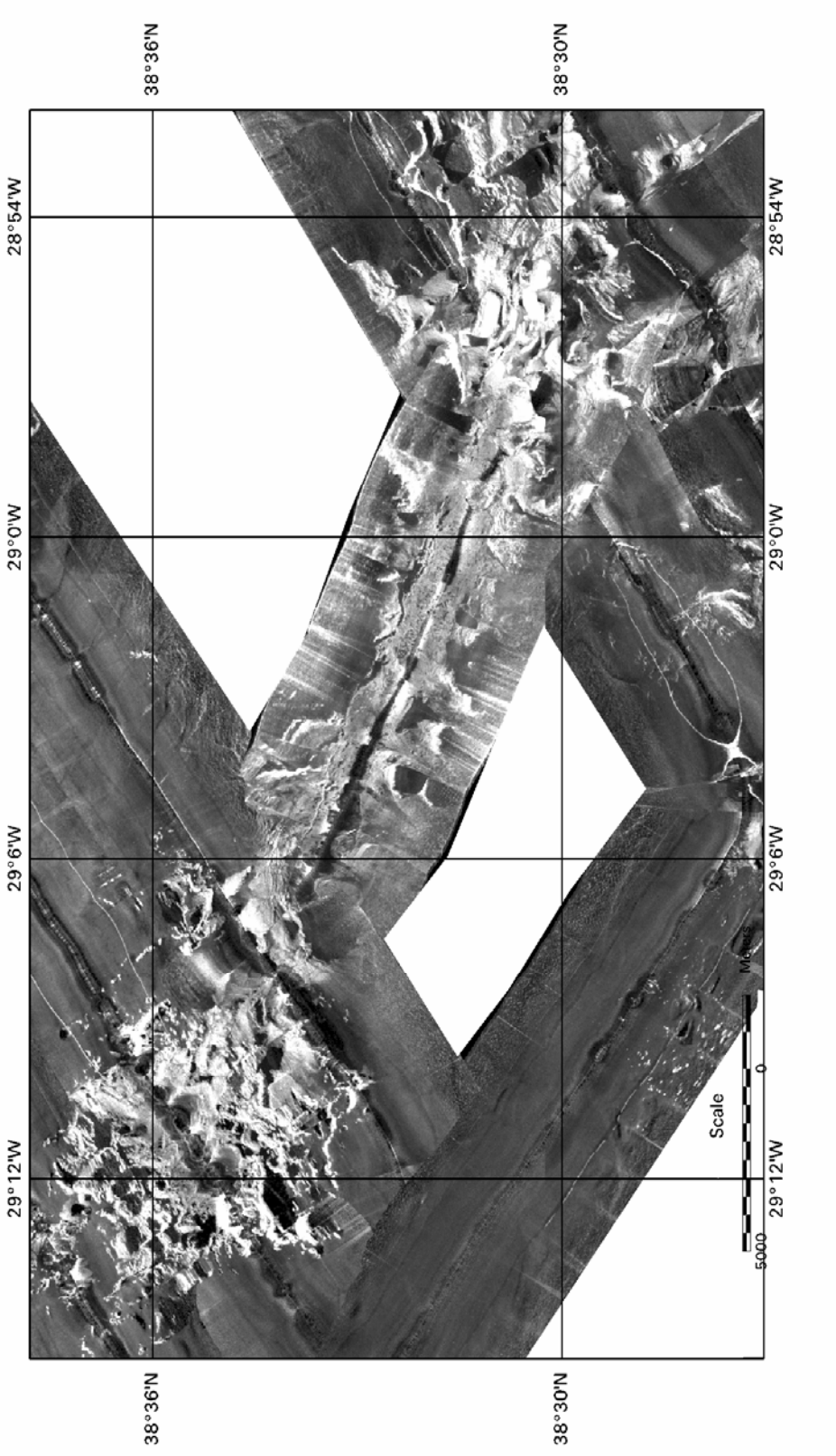

Figure V.7 - TOBI image of the Condor ridge (South of Faial). Note the constrast between the high backscatter irregular pattern in the WNW (deeper area) with the surrounding featureless sediments.

At ~28º44'W, 38º44'N, in the Northern flank of the Faial Island, an area of homogeneous grey acoustic facies, interpreted as sediments, sometimes displaying "rippled" surfaces indicating mass wasting transport is disrupted by a set of fault scarps displaying cross cutting relations which indicate recent tectonic activity. Two overall orientations are observable: one at N120º corresponds overall to the trend of Faial Island and the other around N35º. Cross cutting relations between both fault system suggest that the latter is older and currently being disrupted by the N120º one

This area corresponds to a broad roughly circular positive free air anomaly (ca. 53 mgal) and a positive magnetic anomaly well expressed in Figure V.3, nevertheless no obvious volcanic structures are here present. The draping of the sonar image over the lower resolution bathymetry reveals some more details of this area. Despite the significant sediment cover, this area corresponds in fact to a circular up-lifted seafloor, about 200m height, with a roughly flat top (Figure V.9).

Given the positive potential field anomalies and the circular basal section of the relief, we interpret it as possible resulting from the subsurface emplacement of a magmatic diapir. The divergent normal faults which are visible in the northern and southern flank of this structure could be the result from flexural faulting due to diapir emplacement near the surface.

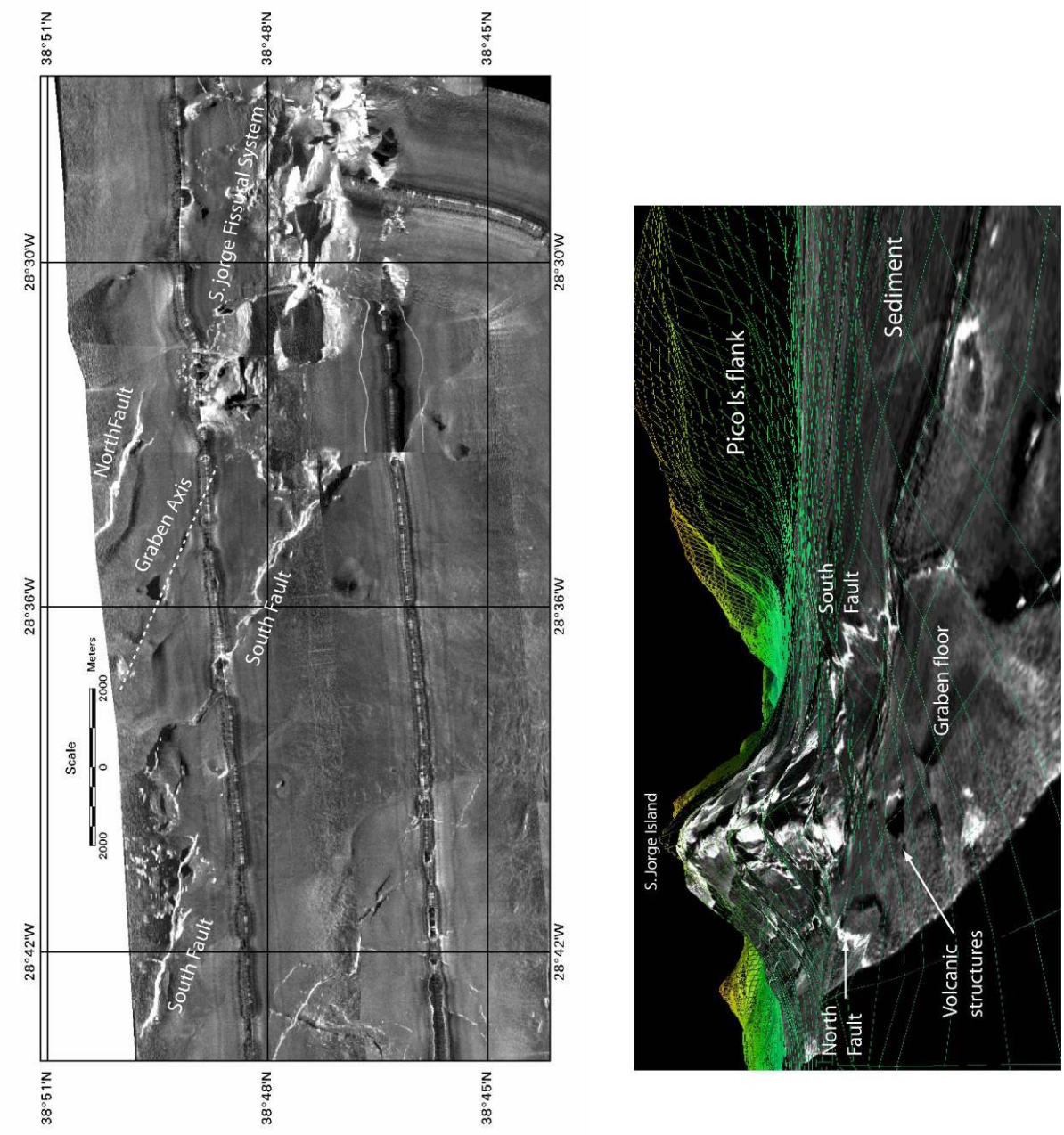

Figure V.8 - S. Jorge seaward prolongation. Left) The fissural system gives rise to a significant graben structure. Right) perspective view facing ESE of the same structure, bathymetric mesh is overlain over the sonar image to allow spatial referencing. See text for discussion.

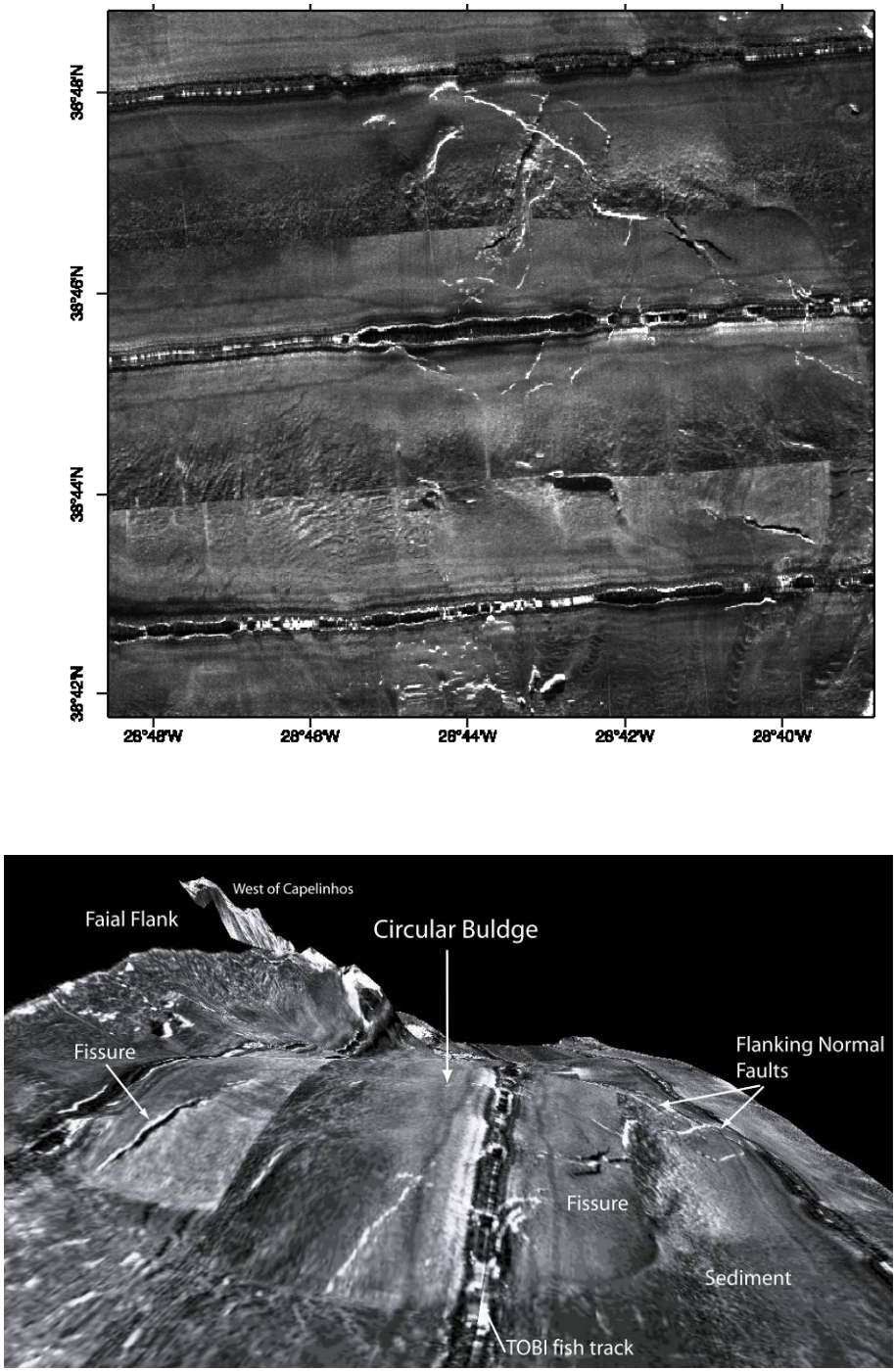

Figure V.9 - Top) sonar image in plan view displaying a tectonised sedimented area north of the Faial Island. Bottom) Drapping of the Sonar image over the bathymetry reveals that these faults are associated with a circular buldge. See text for details. View perspective: facing West. Vertical exaggeration 4x.

V.3.2 LVR Sector 2

Contrary to LVR in sector 1, the features within this sector, display a much more complex morpho-tectonic and magnetic structure. Magnetic inversions along strike are often visible, especially at the EPVR in the southeastern prolongation of Pico Island, where interaction between faulting and volcanic edifices exists at least spatially.

The EPVR despite being a continuous morphological ridge 80 km long, is in fact a composite structure with an heterogeneous morpho-tectonic character (Figure V.10. From Pico Island Eastern tip to a point located at 27º30'W, 38º06'N the surface of the ridge presented two slightly negative polarity areas. One of these areas defines in plan view a narrow corridor oriented NNE-SSW, the corresponding sonar image in this area does not show any significant change in seafloor geology, as the top of the ridge remains a fairly continuous although heterogeneous high backscattering surface suggesting recent volcanism. Some of this effect can be accounted for if one considers a context where products of a Brunhes magnetic chron eruption, overlay and cover negative anomalies of Matuyama or older ages

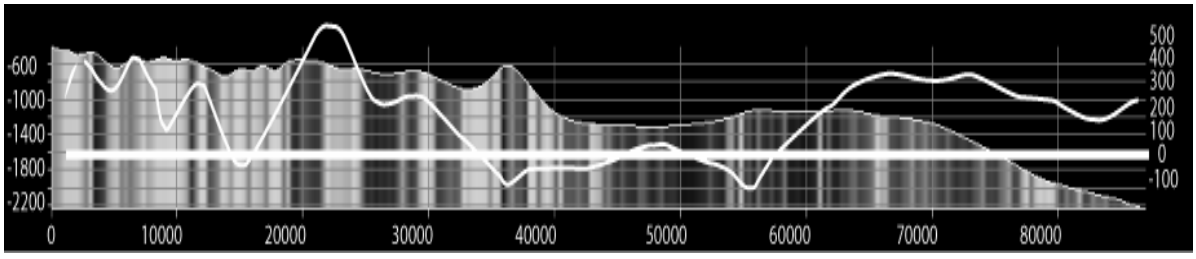

Figure V.10 - Topographical and magnetic anomaly profiles along the EPVR. Gray shades correspond to acoustic backscatter from sonar image along the profile. Dark is low backscattering surfaces, white is high backscattering surfaces. Magnetic anomaly profile is the thick white line. Bathymetry is in meters (left axis), Magnetic anomaly in nanoteslas (right axis). Distance along profile is equally in meters.

The second negative anomaly, on the contrary, represents a clear change in seafloor geology (Figure V.11). Here the seafloor is punctuated by numerous small cones aligned along the LVR axis. An assertion of individual cones height was provided by some sections of TOBI bathymetry in the inner half of the swath, where it is possible to observe individual cones reaching 60 m high. Lack of significant sedimentation suggests that these structures are very recent and are growing over older basement.

The EPVR as described above terminates at 27º30W and 28ºN in an area of smooth bathymetry at 1400m bsl. From this point southeastwards, the relief broadens and raises to a flat terrace at 1200 m bsl. TOBI images display a much more complex signature in this domain (see Figure V.12).

Acoustic facies range from very low backscattering surfaces as before representing pelagic/volcanic sediments in the EPVR surrounding areas; intermediate backscattering surfaces, interpreted as volcanic terrain with probably higher sediment content displaying numerous faults and lineations. Areas with these acoustic facies are essentially confined to the center-left of this domain; and finally high backscattering surfaces, the geometry of which allows its constraint as individual or composite volcanic edifices or ridges and major fault scarps. These are grouped essentially in two clear corridors one along the 38ºN parallel and the other trending ENE-WSW defining the southern limit of the EPVR, further ENE aligned with this corridor (see Figures V.4 and V.5), two seamounts are present which express as two broad negative anomalies. Taken together this regional lineament marks the eastern end of LVR sector 2, and deepening of Azores plateau to the east.

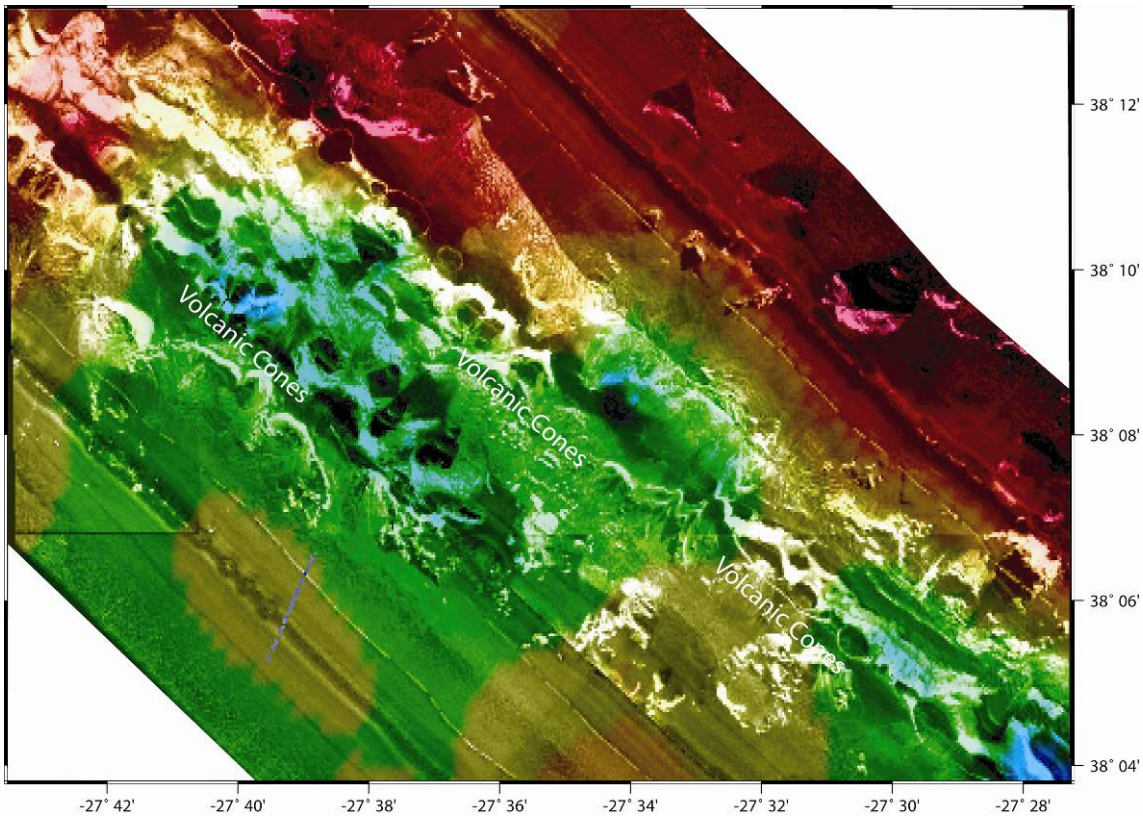

Figure V.11 - Section of the magnetic anomaly map reproduced in Figure V.10, overlain over the TOBI sonar image. It is possible to verify the existence of numerous volcanic cones aligned along the EPVR axis on negative magnetic anomaly basement. The high backscattering acoustic facies and the overall shape of the volcanic cones suggest that these are recent and currently active features.

This domain present three fault families interacting spatially and isolating depressed blocks with little or no observable deformation. To differentiate the faults families and discriminate more significant faults from other lineations or small fault scarps, we opted to trace representative faults in Figure V.12 with a thicker trace.

Based on their orientation range, we consider the following fault families: N140º-156º (hereafter referred to as (A)); N100º-107º (analogously as (B)); N54º-70º (C). Finally it is worth mentioning one single fault striking N9º which seem to have regional significance as it separates a domain with strong positive magnetic anomalies to the

east, probably reflecting MAR generated crust, from a western domain with very low amplitude magnetic anomalies.

Analysis of fault geometrical relations provides some constraints on the kinematics of the different fault families. With the exception of faults belonging to (B) which seem to prevail over the others, cross-cutting relations are not clear and no prevalence of one family over the others seems to exist.

Faults from (A) sometimes isolate semi-circular terraces limited by normal faults dipping in the same direction, these structures can be observed, both in a point at ca. 27º14'W, 37º57'N and ca. 27º24'W, 37º55.5. The S shape, in plain view, of such structures and the prevalence of apparent normal components suggest that these are oblique slips with a left lateral strike slip component. The left lateral component can be additionally constrained by the analysis of a structure at ca. 27º30'W, 37º56'N, where a fault striking N148º cuts through a series of sub parallel lineaments If these are secondary faults subsidiary of the main shear then their shape in plane view also suggests presence of a left lateral strike slip component.

Faults belonging to family (B) define a northern deformation corridor. These faults at that location present two broad segments with a right lateral en-echelon pattern.. This direction is also associated to the major volcanic ridges in the sonar images.

The (C) fault family is less prevalent than the previous ones in map view, and there are no major fault scarps associated with it. Nevertheless, several TOBI sonar lineations suggest its presence across the all domain. The most relevant fault of this system is about 10 km long and its mid point is located ca. 27º22'W 37º56'N, again relation between this fault and minor secondary structures, especially at the westernmost

sections, points to some component of right lateral strike slip. Finally the same direction (as referred to above) is defined by a major SE facing topographical step, corresponding to the Eastern limit of LVR 2. To SE of it, the seafloor deepens to 2000m bsl, and high backscatter relief's become absent.

The last LVR we shall consider in this section is located South of Terceira and will be referred to as STVR (South Terceira Volcanic ridge). This structure is 35 km long and 700 m high, and is sub parallel to the EPVR. The magnetic signature in the STVR comprises both negative and positive low amplitude fairly uniform magnetic anomalies with no obvious pattern of variation along strike. This is particularly relevant as the seafloor north and south of this structure presents higher amplitude positive anomalies but no distinct morphological structures when these are compared with both sonar and bathymetric images.

Its geological character as observed from the sonar images (Figure V.13) is similar to that of the northwestern part of the EPVR. Aligned along the STVR axis, numerous small individual volcanic cones are present often displaying a small crater and sometimes linking and forming ridges which seem analogue to AVR's (Axial volcanic ridges) occurring at Mid-Ocean Ridges. The ridge is dominated by volcanic processes as no clear faults are traceable from the TOBI images. The flanks of this structure are highly degraded and present numerous slump scars, the mass wasting deposits resulting from this slope instability processes suffer little transport and remain confined as lobate fans at the base of the LVR.

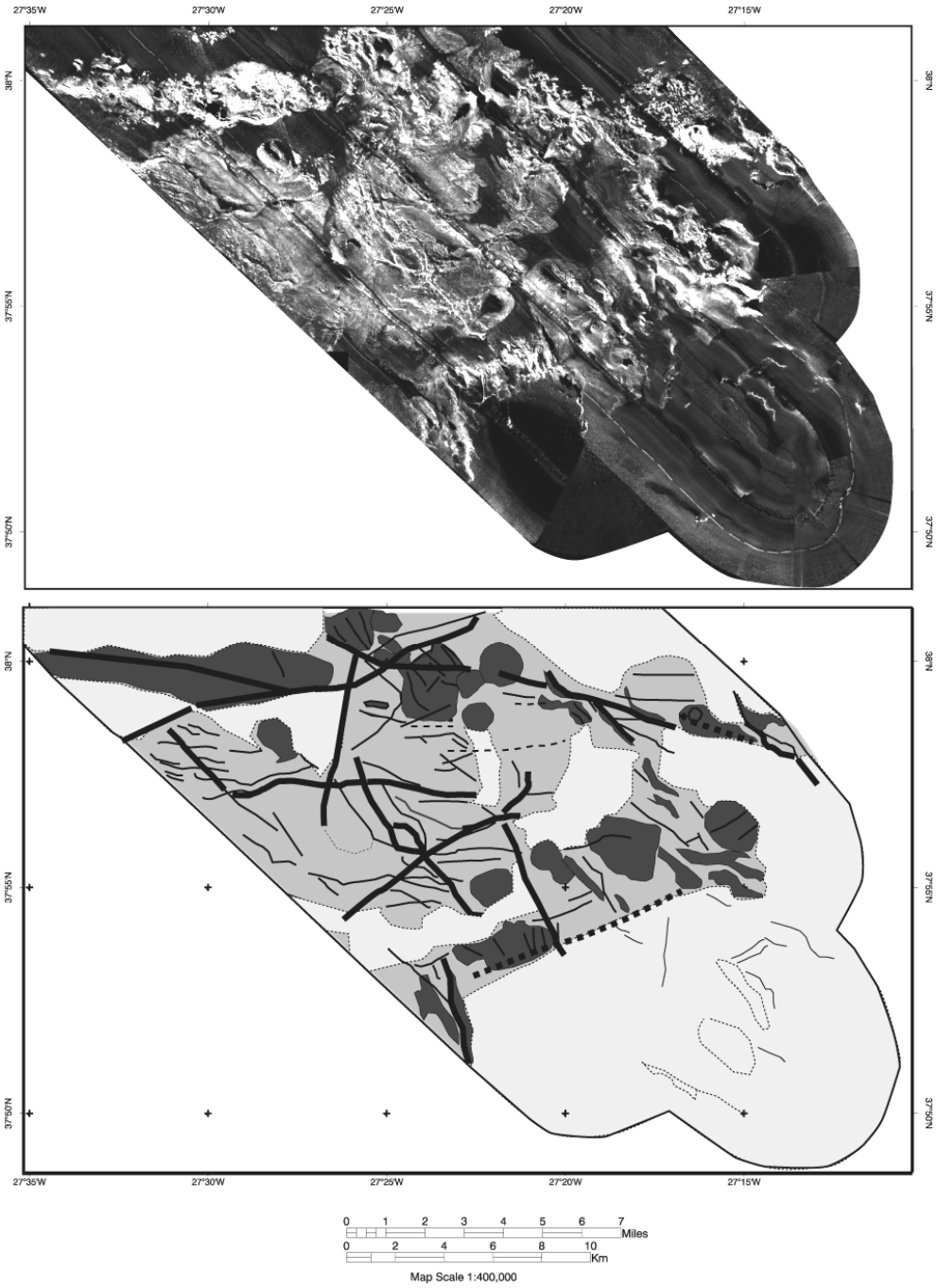

Figure V.12 - Acoustic facies and tectonic interpretation of EPVR south-eastern termination. Light grey corresponds to low backscattering pelagic/volcanic sediment; Medium grey, intermediate backscatter surfaces corresponding to tectonised volcanic terrain. Dark Gray represents high backscatter targets such as fault scarps and individual volcanic edifices as well as young undifferentiated recent volcanic terrain. Faults and lineations: Thick lines represent faults representative or different fault families. Stippled lines correspond to interpreted lineations even if no clear faults planes are recognizable

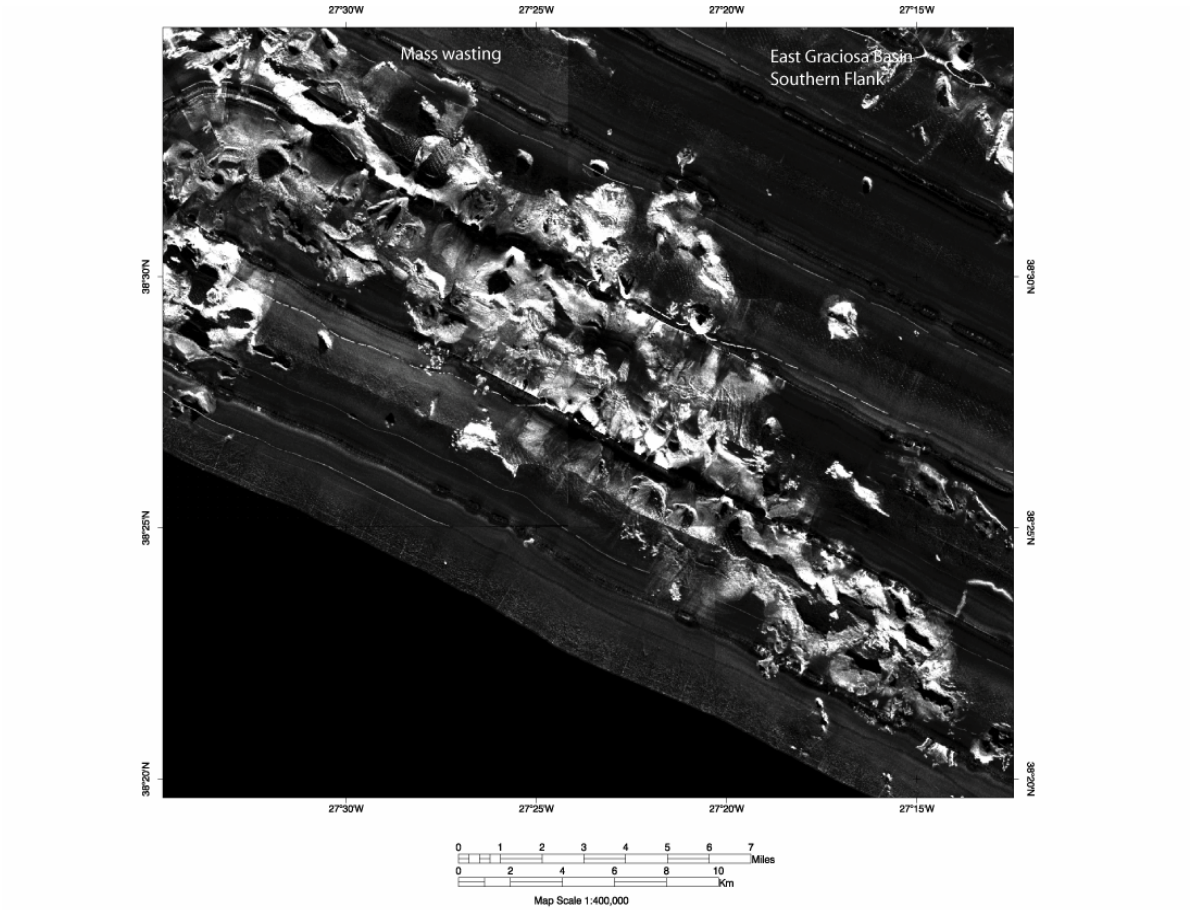

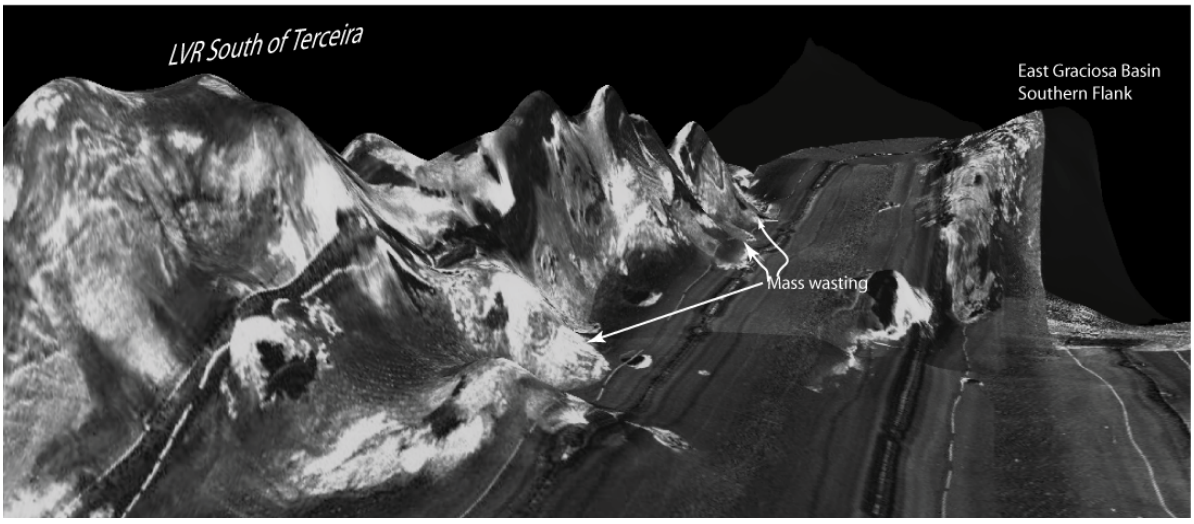

Figure V.13 – Top) sonar image in plan view of the STVR. The ridge is volcanically dominated and numerous isolated or composite volcanic features are easily recognizable. Bottom) TOBI sonar image draped over the bathymetry depicting slumps and mass wasting deposits at the base of the ridge. View perspective facing WSW. Vertical exaggeration 4x.

V.4 Conclusions

The major characteristics of the Azores Linear Volcanic Ridge systems can be summarized as follows:

1. All volcanic ridges imaged with TOBI sonar, regardless of their magnetic signature present recent volcanism of fissural type aligned along their strikes.

2. Sector 1 LVR seem to be overall more recent than those of sector 2, it shows more active volcanic features and displays consistently positive magnetic anomalies along their strike. The LVR from sector 2 present a more complex magnetic anomaly pattern sometimes masked by possible MAR generated magnetic anomalies. All the LVR studied in this chapter present a clear dominance of volcanic processes, little tectonisation is observed.

3. The western terminations of sector 1 LVR display evidences of ridge propagation westwards, these comprise graben development west of S. Jorge tip, submarine prolongation of the fissural system in Faial, more robust volcanic activity on the western tip of condor ridge, and widespread earthquake activity as also detailed in section IV.3.1.

4. As observed in the easternmost areas of the EPVR, the transition between LVR sectors corresponds to domains of higher tectonisation where fault families seem to define a somewhat irregular and complex shear zone and where essentially three fault families were recognized.

5. The three fault families identified in that area are co-relatable by strike with the expected orientation respectively of MAR transform zones and LVR1 strikes.

Oblique faults with a possible sinistral strike slip component as those which ruptured during the Terceira 1980 and Faial 1998 earthquakes (see section IV.4) and finally those which correspond to secondary ruptures at nearly 90º with the previous ones during the same Faial earthquake. The tectonic significance of these later orientations had never been discussed in previous works until the Faial event (Dias, 2006, Fernandes *et al.,* 2002) despite their morphological signature across the plateau having been noted by Lourenço *et al.,* 1998). They individualize the studied LVR sectors, and surrounding flat terraces which become deeper towards east. This direction as we shall see in the next chapter is also recognized inland at Terceira Island.

Chapter VI - Tectonics on the Terceira Island and neighbouring basins

VI.1 Introduction

The northern limit of the plateau consists of the Terceira rift. Its morphology is characterized by a series of deep rhombic to square shape basins in plane view separating the Islands and other major volcanic constructions which express as shallow submarine banks. The distribution of the central volcanoes along the rift is relatively regular, with major, active edifices every 80 to 100 km (Formigas, Grande Norte, São Miguel – Sete Cidades, João de Castro submarine volcano, Terceira – Stª Barbara and Graciosa main central volcano). Spreading centers with this characteristic spacing characterize the second-order segmentation of most ultra-slow to slow-spreading mid-ocean ridges (Briais and Rabinowicz, 2002; Rabinowicz and Briais, 2002). It is possible that the distribution of the recent volcanic activity along the Terceira axis reflects a control of the magma feeding by mantle processes, or by melt migration processes. Vogt and Jung (2003) compared the morphological characteristics of the Terceira axis with other ultra-slow spreading systems such as the South-West Indian Ridge (SWIR) or the Gakkel ridge and classified it as an oblique, hiper-slow rift system. The Terceira axis is considered, by these authors as a young (possible <1Ma) and wide oblique graben structure disrupted and segmented by the equispaced volcanic centers.

As we discussed in Chapter II, the nucleation age for the Terceira axis has never been totally constrained. Its complex magnetic structure, and lack of magnetic anomalies older than Matuyama (Luis, *et al.,* 1996), does not allow its classification as a fully developed oceanic spreading system or otherwise as a young intra-oceanic rift system.

The magnetic and morpho-tectonic structure of the Terceira axis, varies significantly between the Western half of Terceira Island and adjoining East graciosa Basin and the Eastern half of Terceira Island and the North Hirondelle Basin (Figure VI.1). The separation between these two domains is defined by the intersection of the Terceira Island with the prolongation to NE of the limit between LVR sector 1 and 2. West of Terceira, the Serreta ridge, disrupts the eastern flank of the East Graciosa Basin. The most recent volcanic eruption in the Azores occurred on this ridge. East of the Island, several linear volcanic ridges with heterogeneous magnetic character converge into the Island plateau and define a broad v-shape morphology. To the present day it has never been clear, if accretion takes place in a single or in several neovolcanic axis in this plate boundary, and, as pointed by Searle (1980), if main plate boundary processes are located in the bottom of the basins or associated with the linear volcanic ridges that border them.

In this chapter we use all available altimetric/bathymetric data sources both in Terceira, the East Graciosa Basin and the North Hirondele basin, to create an integrated Digital Terrain Model (DTM). This map is used to interprete the tectonic pattern and its variations within the context of Terceira axis as a plate boundary. By comparing observations from both basins and in different sectors of the Island, we aim to verify if the tectonic observations can be explained by a single tectonic regime (i.e right lateral transtension) or if strain is accommodated differently in the domains to the west and

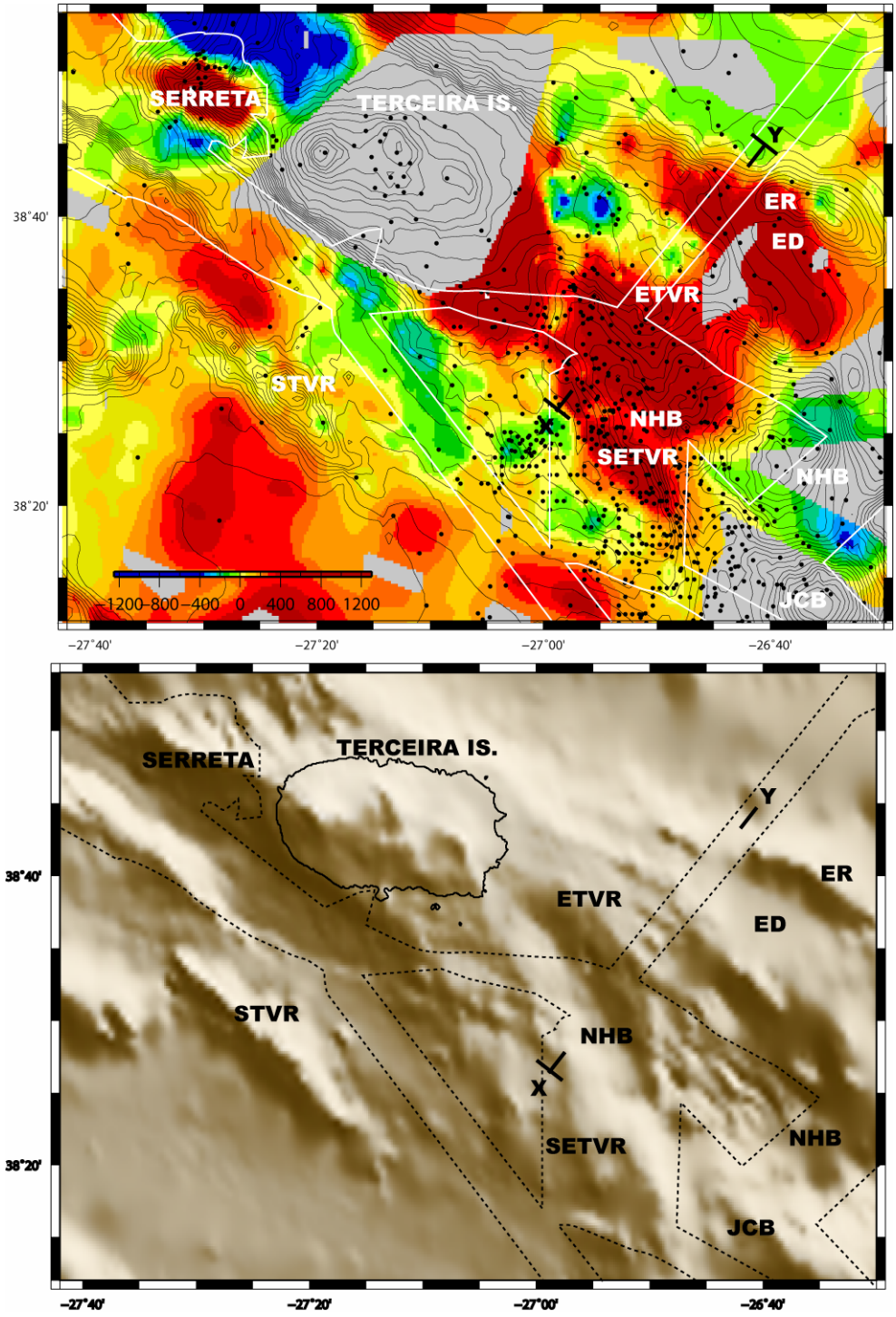

Figure VI.1. Top) Baseline data on the study area. Basemap is the magnetic anomaly map presented in Figure V.3. Black lines are bathymetric/Altimetric 100 m contours from Lourenço *et al.* (1998). Back dots are earthquake epicenter locations from ISC between 1994 and 2004. Whitelines are gathered swath bathymetry enclosing envelopes from different cruises. XY refer to the location of the profile discussed in section VI.4.2. STVR – South of Terceira Ridge; SETVR - Southeast Terceira ridge; NHB - North Hirondele Basin; JCB – João de Castro Bank; ETVR – East of Terceira Volcanic Ridge; ED – Edge Depression; ER – Edge ridge (see text for details). Bottom) Corresponding shaded bathymetry.

East of Terceira Island. We finally attempt to draw a complete tectono-magmatic framework for this area.

VI.2 Data and strategy

The compilation of bathymetric data acquired prior to 1998, presented by Lourenço *et al*. (1998) was updated since, with other swath bathymetry data more focused around the Terceira Island (Figure VI.2a), namely: 1) the SIRENA cruise (PI Jean Goslin) provided a small Simrad EM300 survey gridded at 60x60m in the submarine ridge located southeast of the Terceira Island (SETVR). The Serreta ridge, NW of Terceira, was mapped over the Serreta eruption area by the R/V KNORR (Voyage 161, leg 4) using a Seabeam 2100. MARCONNI contracted a inter-Island EM12 survey for optical cable festooning and finally a EM12 transit from TRIATNORD cruise was gridded at 100x100 m resoluton (Goslin *et al.,* 1999). Island topography was retrieved from digital terrain models (DTM) from IGEOE and gridded at 30 x 30 m resolution. The resulting map is presented in figure VI.2b. The swath bathymetry coverage is still rather limited especially in the northern flank of the Terceira axis. It is possible to observe a sharp contrast in the information provided by the higher resolution data sets, notably the SIRENA, Knorr and the Island DTM with respect to background bathymetric image from Lourenço *et al.,* (1998).

The map is analysed together with very high resolution (4 m x 4 m) orto-photo maps covering the Island, to retrieve a regional lineation map. This map comprises confirmed or possible faults and volcanic alignments and unassigned lineations retrived from the ortho-photo maps and from the DTM. The orientation of all digitized features was analyzed and grouped in sets based on characteristic ranges of orientations. Fault

kinematic constraints were interpreted based on the spatial relations between the different sets and validated by direct field observations.

The analysis of bathymetric data was complemented with geological and tectonic interpretations provided by high resolution sonar images acquiered during the Azzorre 99 cruise over the SETVR (See chapter V).

VI.3 Terceira Tectonics

VI.3.1 Geological setting

The Terceira Island is the third largest Island in the Azores Archipelago with an area of 402 km2. and is approximately 29 km long in the W-E direction and 18 km wide in the N-S direction (Figure VI.3). The Island is made up of four overlapping strato-volcanos with summit calderas, build up of volcanic sucessions ranging from basaltic to trachyte lava flows and pyroclastic deposits (Self, 1976; Calvert *et al.,* 2006; Nunes 2000). From west to east, the volcanos St. Barbara, Guilherme Moniz and Cinco Picos are ligned up along a fissural system materialized by alignments of scoria and pumice cones of essentially basaltic nature following the same strike. St. Barbara is the most robust volcano and its summit marks the highest point of the Island (1021 m). Located to NE of St. Barbara, the Caldera of Pico Alto is a cluster of trachyte domes and short trachyte flows in close association with The Guilherme Moniz northern flank. From these four polygenetic volcanos only St. Barbara and Pico Alto are considered active (Self, 1976). The later is considered the source for the extensive pyroclastic deposits belonging to the Lages Ignimbrite covering the NE extent of the Island (Nunes *et al.,* 2000) and which erupted some 19 to 21 Ka (Self *et al.,* 1976; Calvert *et al.*, 2006). Age relations have been established from geological mapping (Zbyszewski *et al.*, 1971) and volcanic

stratigraphy studies (Self, 1976, Nunes, 2000). K/Ar dating (Feraud *et al.,* 1980) for the top of the different calderas yield values ranging from less then 30 Ka in Stª Barbara to 300 Ka at the "Serra do Cume" ("Cinco Picos"). More recently Calvert *et al*. (2006), performed seven new $^{40}Ar/^{39}Ar$ on Terceira Island, there main results point to a E-W progression in strato-volcano growth. Cinco Picos argon ages yields 370 Ka to 380 Ka for end of volcano growth and formation of the large 7 x 9 km caldera later covered by basalts from the fissural system. The interior of the caldera also presents some volcanic cones related with this system. Guilherme Moniz was active from 270 Ka to 111 Ka. The vast majority of Pico Alto eruption, according to the same authors took place in the interval between 9000 and 1000 years BP. Finaly the Argon age of 29 Ka for the St. Barbara volcano is consistent with that obtained by Feraud (1980).

Historical eruptions have occurred associated both with St Barbara volcano and the fissural system. Hot springs "furnas de enxofre" exist in the center of the Island. In 1761 two occurrences are documented. The event started by an explosion on the Misterio dos Negros location. East of this site, and shortly after the explosion a basaltic flow designated by "Mistério dos Biscoitos" occurred, flowing from the fissural system along the Northern flank of the Island (Zbyszewski *et al.,* 1971). Other recent eruptions at the centre of the Island and linked with the fissural system displayed an isotopic age of approximately 2115 years (Zbyszewski *et al*, 1971). At sea, volcanic activity has been concentrated NW of the Island in a submarine shallow ridge striking WNW-ESE named Serreta. This was the location of the 1867 and 1999 eruptions (Luis *et al.,* 1999). (see section VI.4.1).

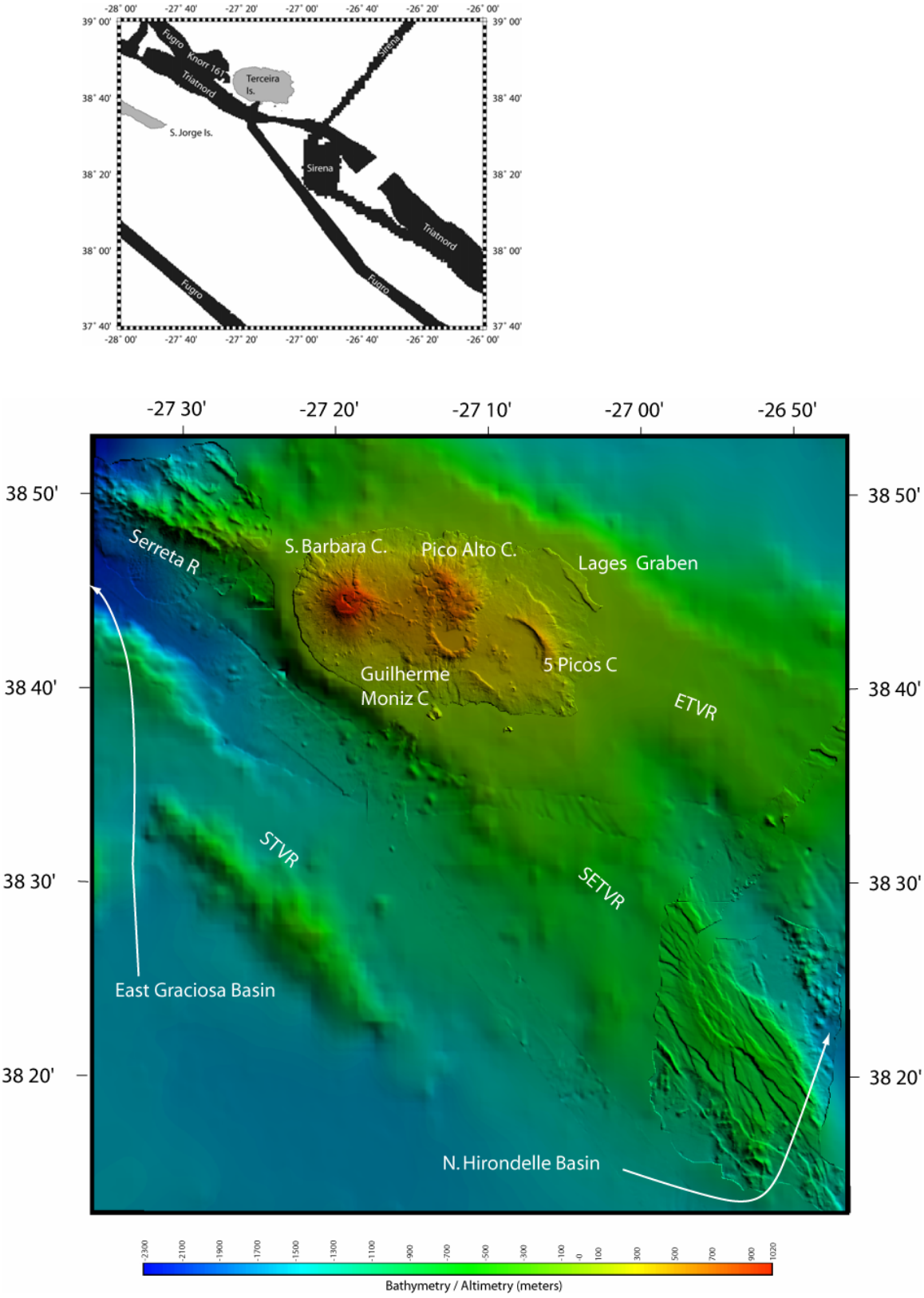

Figure VI.2 - Top) Swath bathymetric tracks (black polignons) used to update the compilation from Lourenço *et al.* (1998) around Terceira. Bottom) Resulting bathymetric and topographical map of the study area. Labels designate structures discussed in the text.

Tectonic structures with clear morphological expression are visible in the southern and Northeastern coasts. These are respectively a series of NNW-SSE normal faults and the NW-SE striking, Lages graben. These will be addressed bellow.

Figure VI.3 - Terceira Geological map (adapted from Nunes, 2000).

VI.3.2 Volcano-tectonic lineations in Terceira Island from DTM and ortophoto maps interpretation

The Terceira lineation map is presented in Figure VI.4. The main directions present on the Island are grouped in three different azimuthal classes: lineations labelled as FLT comprise: confirmed faults from field analysis and inferred faults from linear steps in morphology. Volcanic lineations (VLC) consisting on: volcanic cone alignment

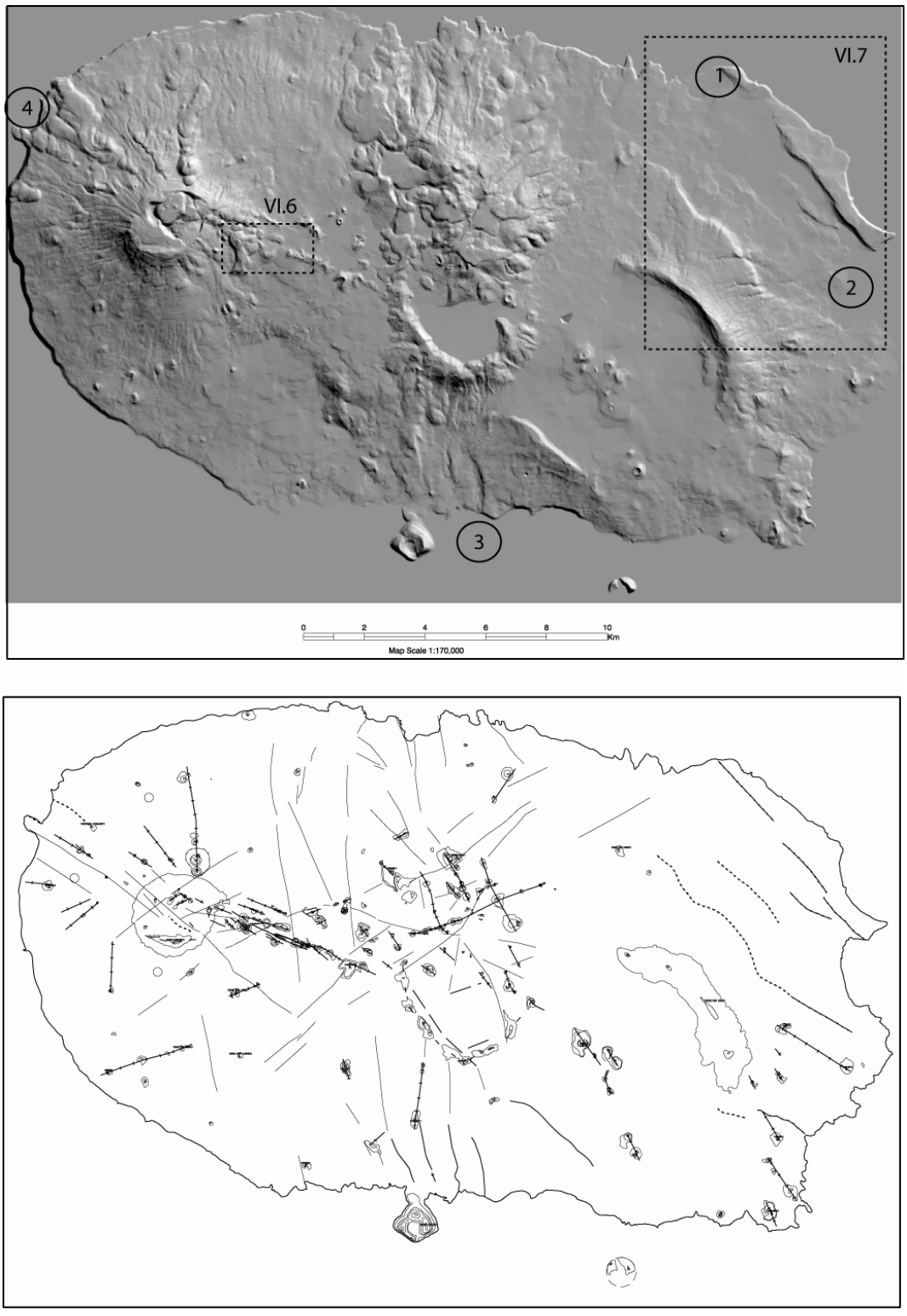

Figure VI.4 – Top) Terceira shaded relief map. Sun azimuth 45º and elevation 30º. Vertical exaggeration 3x. Bottom) Terceira lineation map. Numbers refer to field stations discussed in the text.

mapped fissures, elongation direction of individual volcanos and field measurements of dike strikes. Finally a set of lineations retrieved from the coupled analysis of the DTM and the ortophotomaps but which could not be assigned to either of the previous classes, during field work are attributed to a generic unassigned lineation class (LIN). The bulk rose diagram plot of these sets lineations is presented in figure VI.5).

Despite some scatter in the plot, we verify that measured azimuths group in three main domains: The dominant structural direction is N140-160º (12% of overall data) and corresponds to the expression of the fissural system on the eastern side of the Island, and the en-echelon configuration of some of the individual cones within this system on the western side, which, in turn, presents a dominant N110-120º direction (Figure VI.5 and Figure VI.6).

Volcanic lineations strike (Figure VI.5), plot over the range span of the strikes of FLT and LIN. This seems to attest the tectonic control on volcanism in this domain. The fissural system present in all extent of the island follows both N110º-120º and N140º-160º trends. The fissural system controls the position and elongation of several cinder and scoria cones which are generally located south of the main fissural system (Figure VI.6).

A clear separation between the two fissural domains is provided by a previously un-recognized orientation set varying between N50º to N70º (8%). These lineations are very discrete and no clear planes were observed in the field, nevertheless they seem to have controlled some flows on the eastern flank of Pico Alto and Guilherme Moniz Caldera, as some of these flows are oblique to the maximum gradients within their

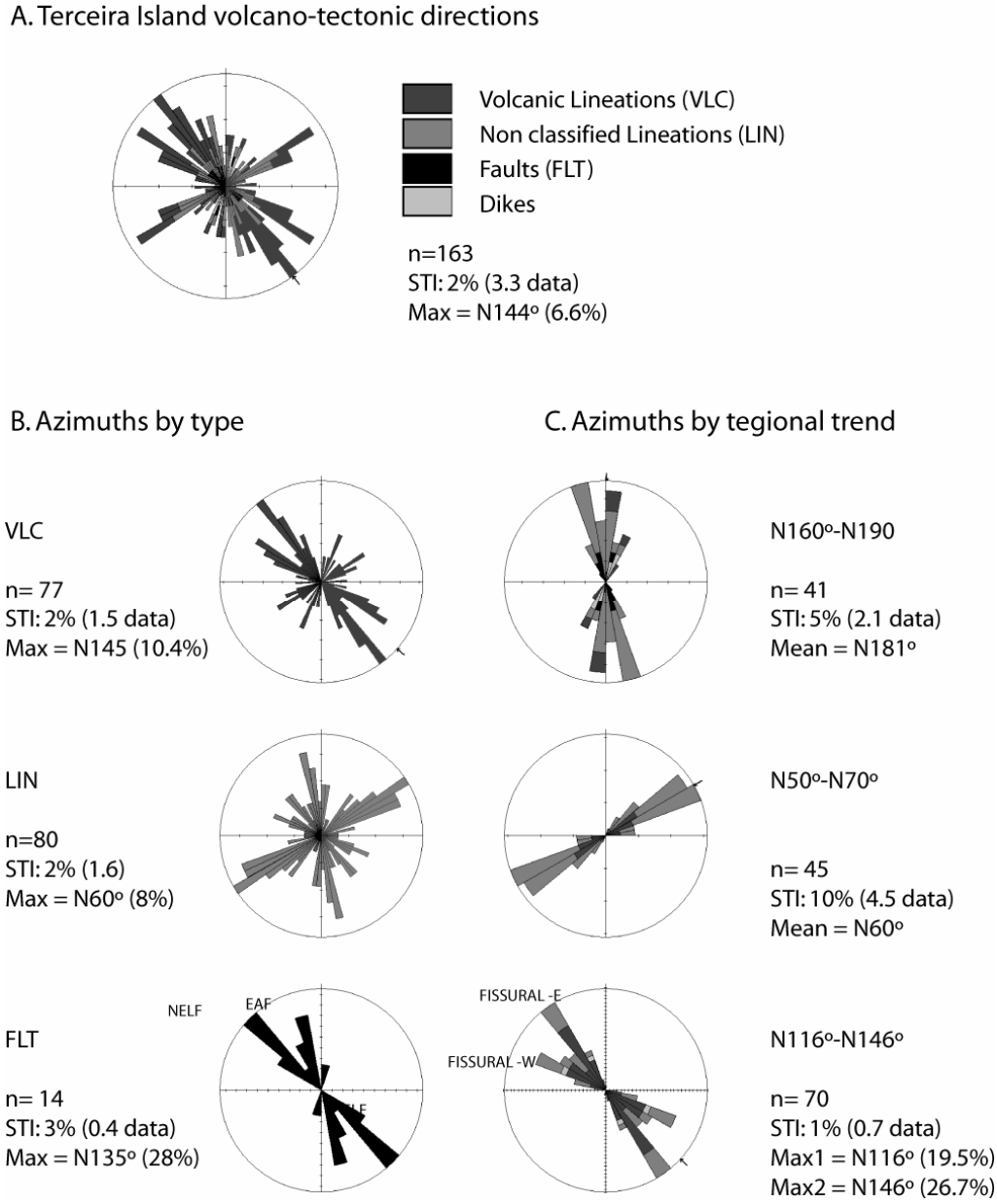

Figure VI.5 - Stereographic plots of azimuths from all elements retrieved from the Terceira lineation map along with field measurements of faults and dikes. A) Bulk of Terceira volcano-tectonic directions. B) Azimuths by lineation type. C) Azimuths grouped by trends recognized across the Island. Legend: n = number of events; STI – Scale of tick intervals; Labels refer to features discussed in the text.

flanks. Figure VI.6 displays some of this lineations present in the SE flank of St. Barbara volcano.

These lineations seem to be the inland continuation of the morphological set which separates LVR1 from LVR2 sectors. They also divide the Island in two different morpho-tectonic domains. To the East, Island topography is smooth, tectonic structures prevail, and the sole central volcano has been largely eroded and is now materialized by the Serra do Cume and the (fault controlled?) linear Serra da Ribeirinha. To the west, the robust St Barbara volcano with a altitude of 1021 m dominates, eventually masking existing faults. The set of measured azimuths within the St Barbabra volcanic edifice reveal partially a radial pattern around the main caldera of this volcano.

Identified Faults (Figure VI.5) trend essentially in two main directions one corresponds to the Lages graben (N130º-140º) and the other is represented by several faults east of Angra city which are dominantly in the N160º-170º azimuth interval.

We note that some linear segments on the Island coast are parallel to these structural orientations and probably represent tectonic controls on coastal erosion. Careful inspections of Island cliffs have however yielded little tectonic data.

VI.3.3 Meso-scale observations

Forest, extensive areas of agriculture land and the intrinsic nature of the volcanic terrain rather limits the ability to detect tectonic structures in the field. Identified fault planes provided little kinematics indications. The vast majority of identified faults lie on the eastern side of the Island. Some could be observed on the southern coast cliffs by apparent vertical offsets in lava sequences co-relatable on the hanging wall and the footwall across the fault plane.

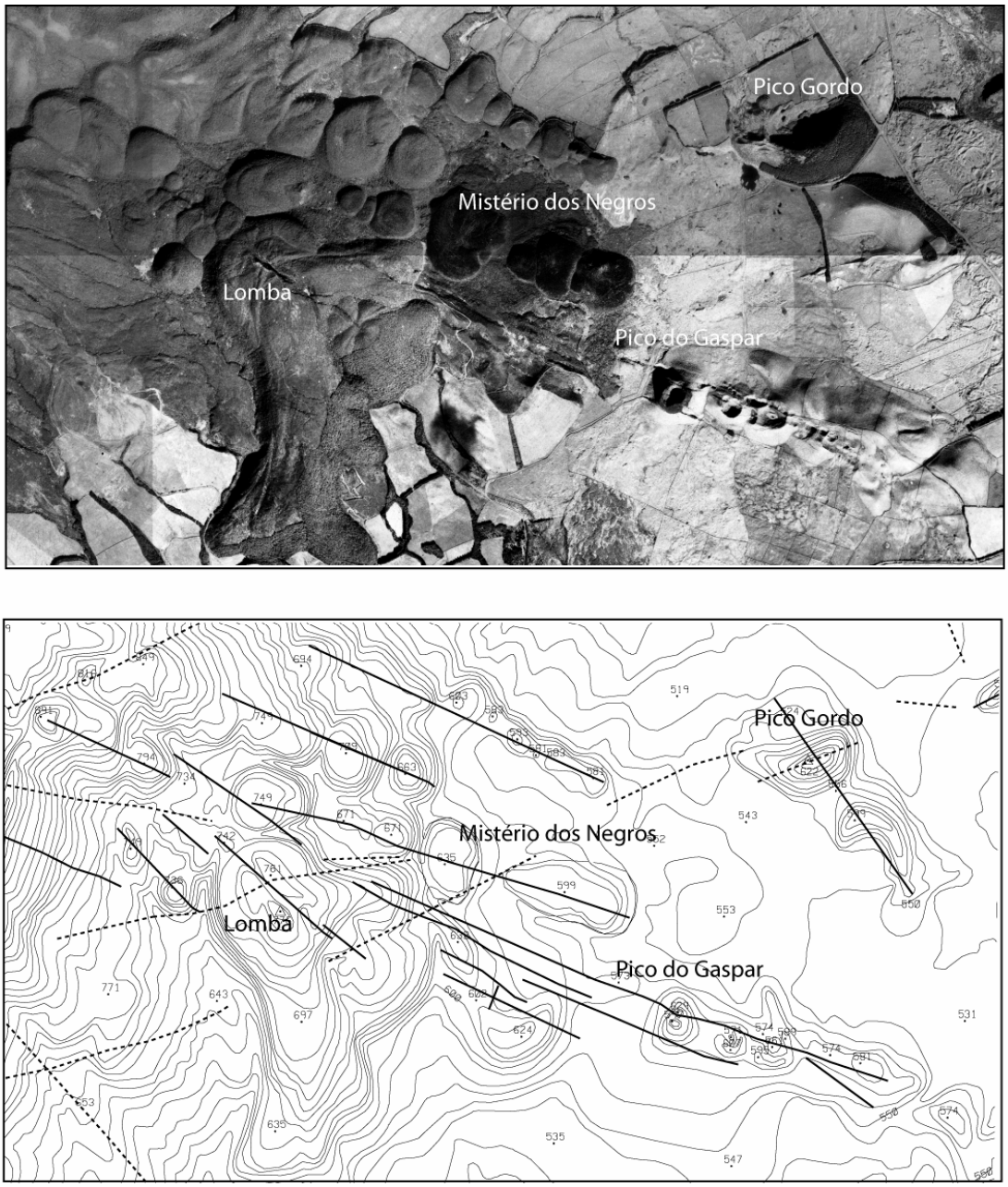

Figure VI.6 - Top) Ortophoto map image of the fissural system. Main volcanic cones and Trachytic domes are labelled. Bottom) Corresponding lineations plotted over the DEM contour map. Contours interval 10m. The lineations belonging to the fissural system dominate but are intersected by N60º trend lineations. (see Figure VI.3 for localization)

The faults in the Island, group in two main areas (see Figure VI.4) for location: the Lages Graben faults and The East Angra faults. These are briefly documented below. Additionally it is worth mentioning a set of brittle structures associated with the onset of a trachytic lava flow in the Ponta da Serreta promontory. Despite constituting a somewhat off-topic, we opted to address them in this manuscript as an illustration of the peculiarities that can arise from tectonic studies in volcanic terrains.

VI.3.3.1 The Lages Graben

The Lages Graben, the most evident tectonic feature in Terceira Island, is a 10 km long, 3.5 km wide and trends N130º. This feature may extend further SE through the seafloor. The surface of the graben is covered by a ignimbrite deposit dated of 18 Kyr BP (Before Present) by Feraud *et al.* (1980). The Lages Graben North-Eastern bounding fault (NELF) is well expressed in topography. The NELF in plan view presents three sinuous segments with a tight en-echelon configuration. Further to SE, near Praia da Victoria, within the graben, a secondary fault is traceable from the topography and has been mapped in the Terceira Geological Map (Zbyszewski *et al.,* 1971)

Each segment displays a well defined SW facing scarp. At the tips of the segments the scarp is strongly attenuated and is retreated to its adjacent scarp traces therefore defining bridge structures (Figure VI.7). The bridge structures can result from 1) the en-echelon nature of the fault; 2) interaction with intersecting faults and 3) soft linkage at adjacent fault segment tips (Hossack, 1983). We were not able to verify any of these possibilities during field work.

The NELF fault zone is exposed in an outcrop on the Island's NE coast (station 1 in Figure VI.4 and VI.7). It presents a well exposed section of the fault damage zone (see

Figure VI.8). It consists on a 5 m wide zone of tectonic brecciation. Within this zone two clear sub-parallel fault traces are present. The SW one is sub-vertical. The NE one is a normal fault plunging about 60º to SW, which displacement defines the graben scarp. The vertical fault plane within the NELF fault damage zone, it is not consistent with a pure dip slip displacement for the NELF, and suggests: 1) that some amount of strike slip component should present in that fault and 2) that the imposed strain is accommodated by slip partitioning between these two planes, one acting solely as strike slip fault and the other as pure dip-slip fault.

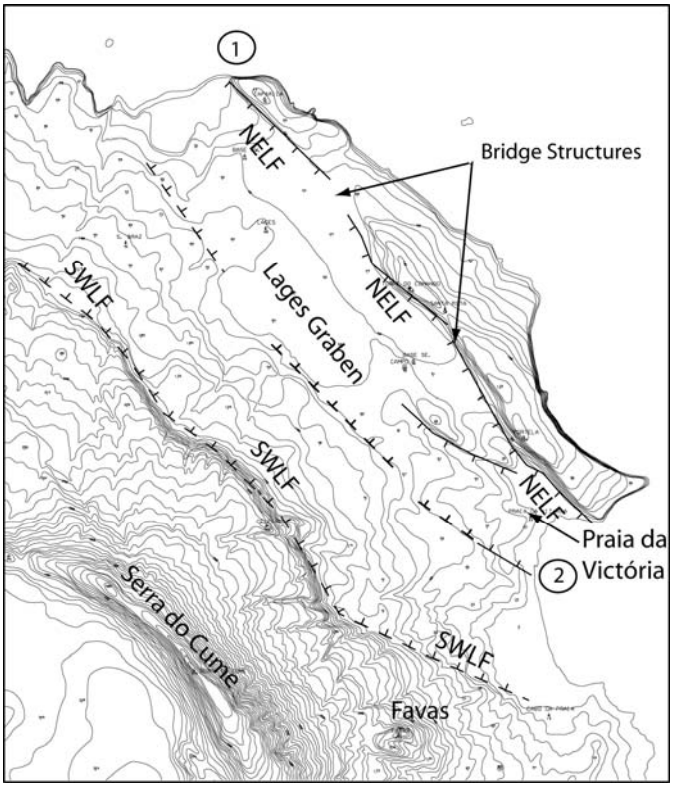

Figure VI.7 - Contour map of the Lajes Graben . Contours interval 10 m. Major identified (continuous lines) or interpreted (stippled lines) fault traces are plotted. Numbers refer to field observation stations.

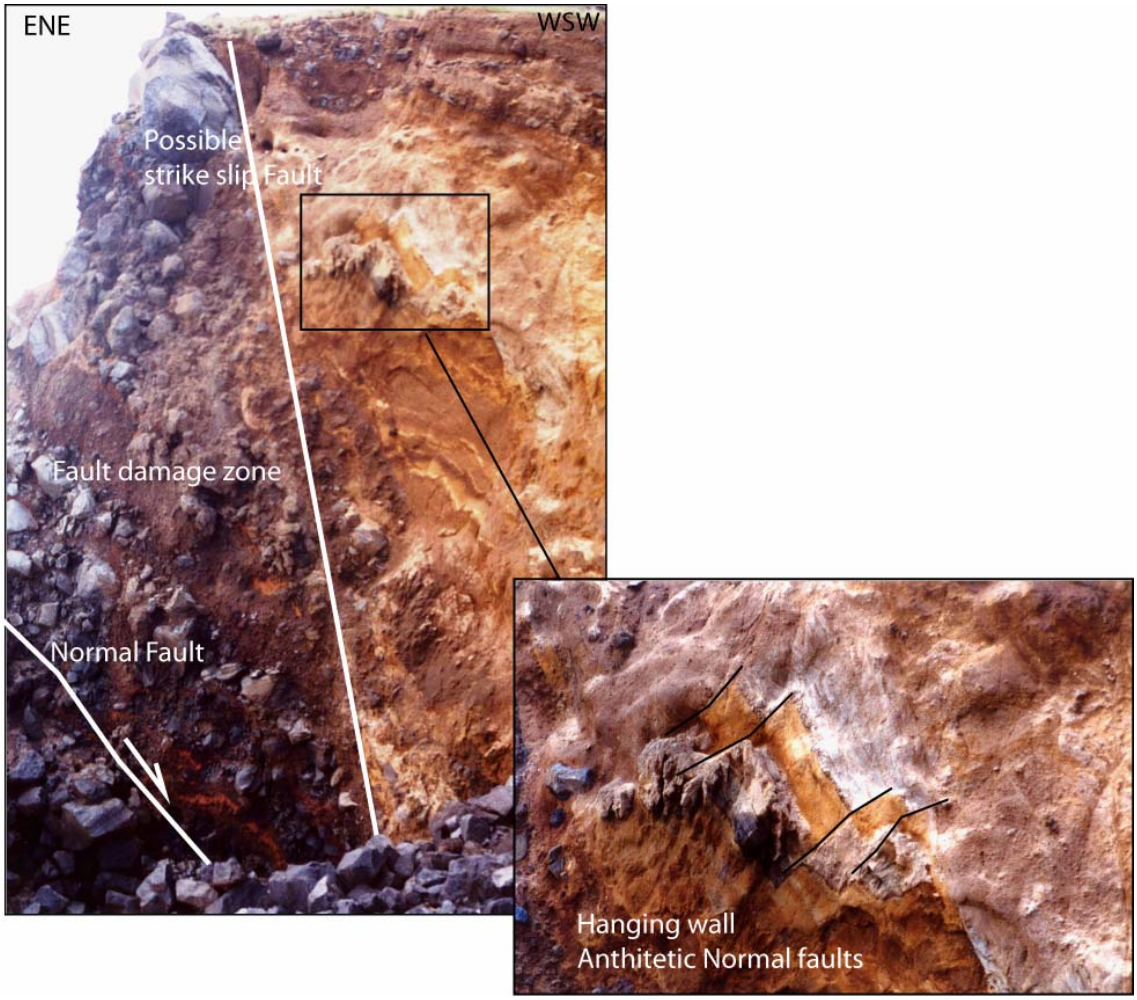

Figure VI.8 - Photo of the NELF damage zone. Fault planes are identified by white traces. Inset) Overview of hanging wall deformation.

The hanging wall block consist on a yellowish pyroclastic infill and is disrupted by a set of closely spaced antithetic rotational normal faults which constitute the testimony of the last increments of the NELF growth. The infill sequence and the fault itself are sealed by a thin top layer of dark brown pyroclastic materials.

The SWLF fault is less well exposed. The clear step observed in topography consists on a contact between a trachyte flow unit and the graben floor. We performed, where possible, a series of transects across this morphological step, normal to the possible fault trace, which did not result in any clear fault plane identification. We noted nevertheless that, to NE of the main morphological step, the bottom of the graben is reached by a succession of small step like terraces, providing faint lineations in the DTM retrieved images and contour maps (Figure VI.4). Confirmation of these as fault related, is achieved in the western sector of the Praia da Victoria bay cliff (station 2 in Figure VI.7). Here, faults crop out and a complete geological cross section on the SW graben bounding faults is displayed. (Figure VI.9). The overall SW-NE oriented cross section displays a cylindrical fold in pyroclasts, with 20º deeping flanks and axial plane nearly E-W. It is unclear if this fold is simply the result of cohesive ash fall deposition over a possible positive paleo-relief in the sub-surface or whether it results from tectonic processes. Further NE from the fold, a horst structure is present, defined to SW by a 60º deeping normal fault, striking N144º (F2 in Figure VI.8), thus subparallel to the SWLF; and to NE by a fault (F1) striking N80ºW and dipping 75º northwards. Analogously to the NELF, the dips of this fault exclude them as having simple dip-slip components, and suggest existance of some sort of strain partitioning, with presence of oblique or strike slip components. Considering the regional fault kinematics, it is conceivable that F1 is associated with right lateral strike slip. In this case the observed fold could also form, as a consequence of space problems, at the intersection between both fault systems. Verification of this hypothesis however, was not possible, as we were not able to detect any occurrence of faults to SW of the fold.

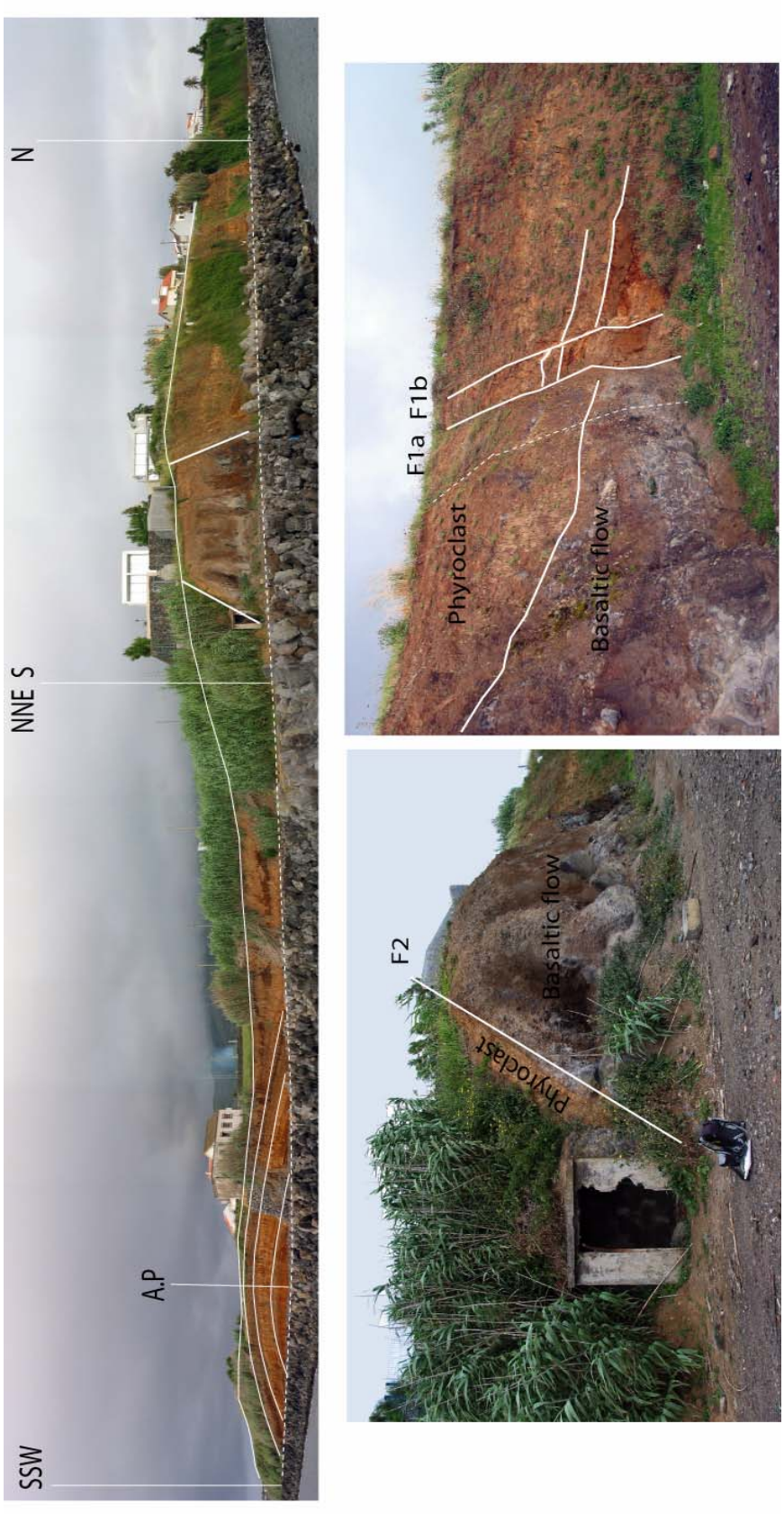

Figure VI.9 - Praia da Victoria geological cross-section displaying faults belonging to the SWELF system.

VI.3.3.2 The East Angra Faults

Located to the North and East of Angra do Heroismo City, The East Angra faults are a set of sub-parallel faults striking N!60º to N170º (see Figure VI.4 for location of station 3). These faults are well exposed in the Southern Terceira coastal cliffs (Figure VI.10), They are expressed in the topography as tens of meters setps. In the Coastal Cliffs, we could verify that these faults present a clear normal component. In a recent paper, Navarro *et al.* (in press) evaluated these faults as having a left lateral component; In fact, after the 1980 Angra do Heroismo main shock, some epicenters of the aftershock sequence layed along these faults (Hirn *et al.,* 1980) and were probably related with some stress transfer mechanisms (Ribeiro personal comn.). Fault plane inspection did not yield any clear kinematic indicators.

Several fractures following the strikes of the East Angra Faults are detected all along the East of Angra do Heroismo coast. Some of this fractures control the installation of sub-vertical dykes, which in some cases display evidences of subhorizontal magmatic flow. An example is presented in Figure VI.10.

Taking as a reference the produced lineation map, we consider these faults to be the southern prolongation of the N-S lineations observed in the Island Northern coastal areas and in the northern flank of Guilherme Moniz Cladera. The rectilinear west edge of this caldera system also suggests some control from the same fault system. We consider that this system of lineations and faults, constitute abyssal hill fabric reactivated within the Azores stress field.

Figure VI.10 - Examples of East Angra Fault traces exposed on the the Terceira southern coastal cliffs. Photos of Faults are ordered from W to E.

VI.3.3.3 The Serreta trachytic flows

In this section we present clear tectonic-like structures, which were developed and are confined within the Ponta da Serreta trachytic flow (site 4 in Figure VI.4). Its tectonic pattern when considered as a whole is consistent with the regional tectonic stress field, however, in fact it translates the dynamic history of the cooling flow.

The Serreta trachytic flow (Ponta da Serreta) is several tens of meters high and is capped by a lava clinker (Figure VI.11). Orto-photo with 0.5 x 0.5 m pixel resolution and DTM were used to constrain the lava surface structures. Structural lineation map (Figure VI.12) displays the trend of arcuate ridges, with typical wavelengths of 30 to 45 m, resulting from lava cooling and compression induced by lava gravitational flow. To the N, a set of WNW-ESE lineations mark the right lateral sheared border of the flow.and and correspond to vertical tear faults accommodating differential movements within the flow.

Figure VI.11 - Side view photograph of the Ponta da Serreta Spur, displaying main volcano-tectonic features (see text for details).

The structures observed in the Ponta da Serreta seacliff are brittle to ductile shear zones developing low angle frontal (synthetic and antithetic) and lateral ramps; deformed columnar disjunction and other brittle planar discontinuities. Ductile-brittle transition in a context of progressive deformation within viscous flow is given by the deformed prisms. Flow front is characterised by brittle reverse faults and extensional fractures (Figure VI.11).

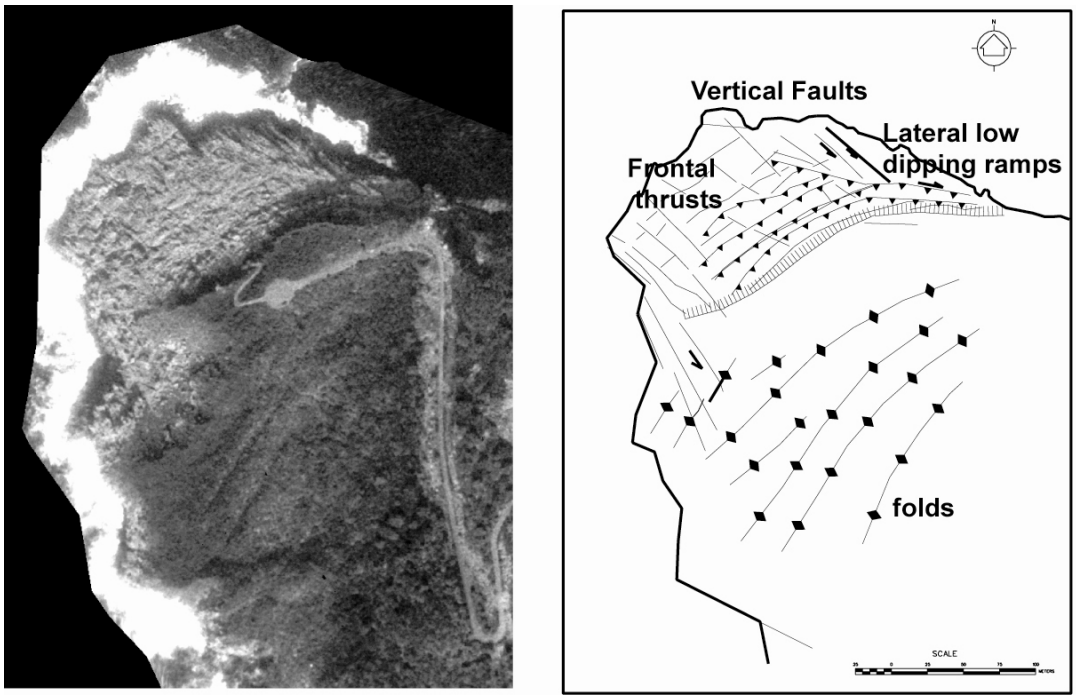

Figure VI.12 - Left) Ortophotomap of the Ponta da Serreta Spur. Right) corresponding structural map.

At the meso-scale, structures express distinct strain mechanisms imposed by significant rheological variations, resulting from drastic centrifugal thermal gradients. Flow core, corresponding to the front of the outcropping lava lobe, presents dominantly ductile deformation. It displays a fan like pattern of stretching lineations materialized by alignment of feldspar crystals growing upon complex magmatic foliations. Ductile to brittle transitions within volcanic flow are observed from either co-planar or oblique discrete fault surfaces developing in lava lobe outer shells and they are interpreted as incremental colder pulses postdating quasi-coeval magmatic foliations and sharing a common kinematic history for the entire flow unit (Figure VI.13).

Identified fault kinematic criteria are fault grooves and striations sometimes presenting cross-cutting relations, and ranging from dip slip to oblique slip both with normal and reverse components (Figure VI.13). The stereographic plot of existing fault planes and fault kinematic criteria is consistent with a local stress field generated by the gravity flow of the freezing lava (Figure VI.14).

In summary, impressive fault structures in the brittle-ductile transition can develop within a trachytic volcanic flow. These develop in a context of progressive deformation due to the cooling lava. The physical similarity between such cooling induced structures and those produced by a regional tectonic stress field (as discussed by Madeira and Ribeiro, 1990 and Lourenço *et al.,* 1998) imply that interpretation of volcanic lavas outcrops from past terrains have to be evaluated in a careful manner as they might produce erroneous tectonic interpretations.

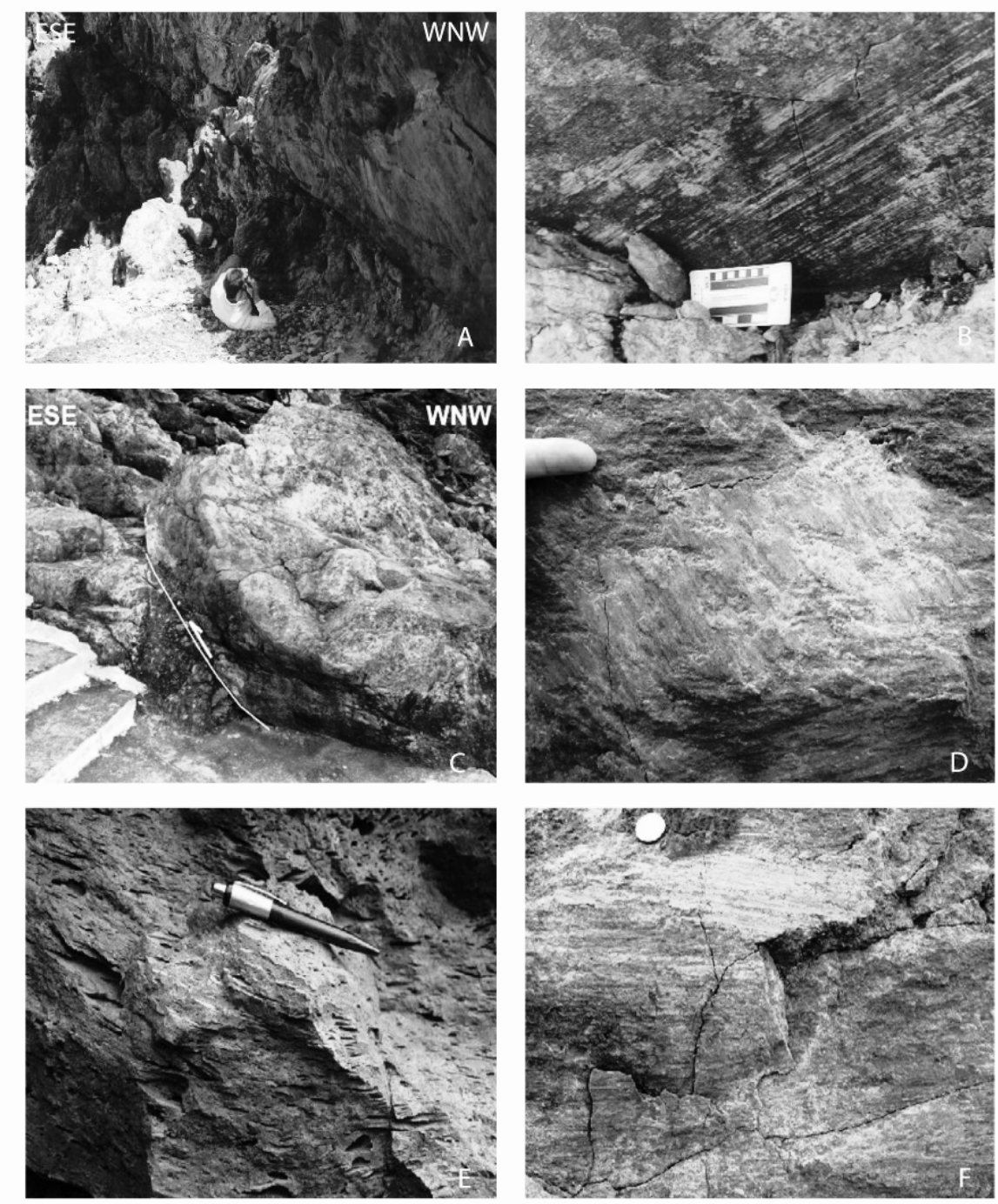

Figure VI.13 - Series of photos from the Ponta da Serreta (station 4) A) Low angle right lateral fault with a thrust component. B) Detail of the thust fault zone striae. C) N150º backthrust. D and F Fault plane striae sometimes displaying cross crutting relations (as exemplified in D). E) Vesicule elongation follows the same trend of the fault plane striae.

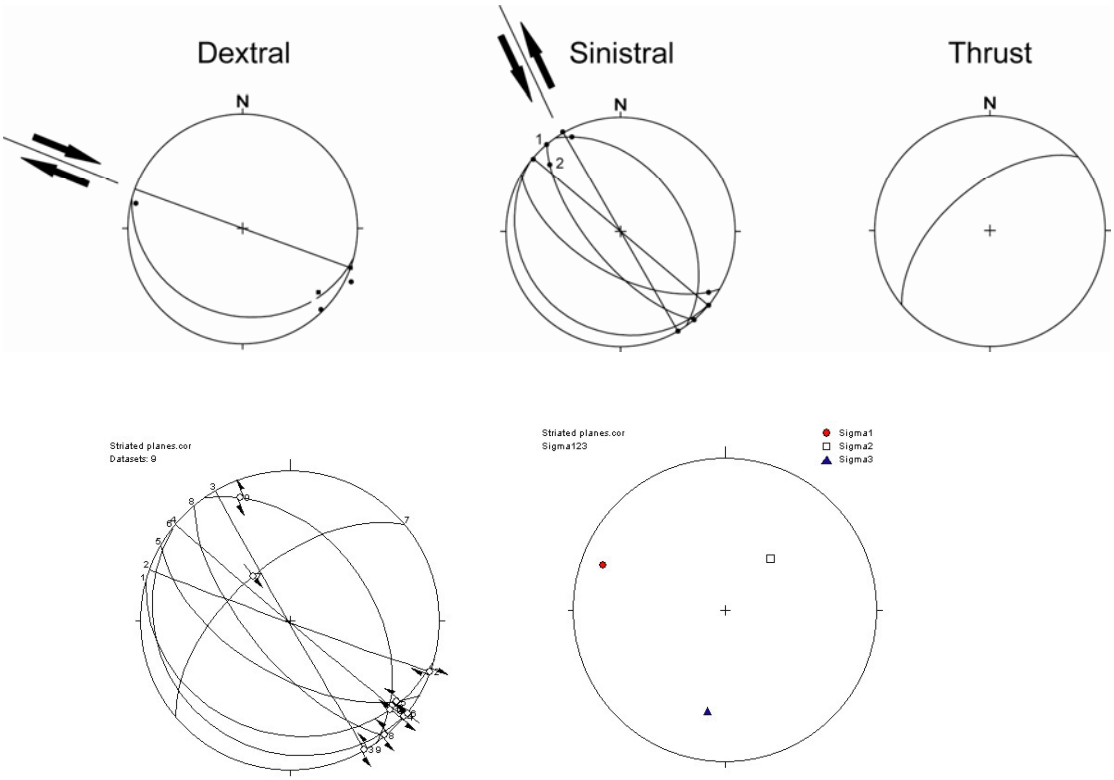

Figure VI.14 – Top) Stereographic plots of Serreta fault planes and slip lines. Bottom) Principal Stress axes retrieved from stress inversion using dihedral computations (Angelier and Mechler, 1977) with TectonicsFP software (Ortner *et al.*, 2002).

VI.4 Tectonic interpretations from the adjacent basins

VI.4.1 West of Terceira: The Serreta Ridge structure

The Serreta ridge is a shallow submarine feature, extending from the west coast of Terceira Island for about 20 km along the WNW-ESE direction, therefore parallel to both flanks of East Graciosa Basin and also to the sector 1 LVR, described in the previous chapter. The Serreta ridge flanks are higly assymetrical. Its southern flank deepens to the base of the East Graciosa Basin defining a slope of more than 1000 m, on the contrary the northern flank base lies at a westward dipping slope, which follows

roughly the same westward inclination of the Serreta ridge axis. Therefore the northern flank Serreta presents a fairly uniform height of ca. 500 m. The spatial relation of Serreta structure with the main St. Barbara volcano seems analogue of what was observed between the Capelinhos fissural system and the Faial Island central caldera. The axis of Serreta is well aligned with the inland fissural system, suggesting that the St. Barbara volcano has grow over and masked it.

Northwards, sub-parallel to the Serreta ridge, two more ridges are present (Ridges 2 and 3) (Figure VI.15) both with a length of approximately 8 km and an average height of respectively 400 m and 200 m. Ridge 2 aligns with a massif trachytic flow on land, suggesting a structural control of the valley where this flow is present. Ridge 3 has no obvious prolongation in land.

The three main ridges present a similar morphology and are spaced at equal intervals of 4 km. Despite some limitations in the areal extent of the survey, their configuration suggests a rigth lateral en-echelon pattern along N65º. Contrary to Serreta Ridge which displays a strong positive anomaly of about 1000 nT, the other two neighbouring ridges present negative anomalies of respectively ca. -50 nT and ca. -1060 nT. If these are contemporary features, as their morphology suggests, than they are growing on strong reversely magnetized basement of the Terceira axis. Other possibility, given their magnetic anomalies, is that they are older features. In this case, their orientations suggesting a fairly homogeneous stress field along recent times in this domain.

The three ridges are formed by several segments linked together either due to bending of continuous ridge tips towards one another, or by possible splay formation from the dominate ridge segment. These linkage zones are areas of disturbed relief. In the Serreta

ridge crest, linkage areas result in formation of a series of flat round or square depressions aligned along the main ridge direction and limited overall by several minor ridges.

Other features present in this domain are smaller, more discontinuous ridges parallel to the main ones, and a semi-circular depression present between ridges 1 and 2 which can possibly be a degraded small caldera arch. Near the western tip of the Serreta Ridge and also scattered in the imaged area, numerous small elevations punctuate the sea floor, similarly to what have been observed west of Condor Ridge.

VI.4.1.1 Serreta 1998-2001 Eruption

The 18th December 1998, after a period of some micro-seismic activity registered by the local seismic network, local fisherman observed sea surface manifestations of a submarine eruption. This phenomenon, located at 38º46.8'N 27º28.6'W (Figure VI.16), was confined to the ridge crest of Serreta. The beginning of the eruption was focused in three different areas, developing later to a number of six different focalised areas. Nevertheless all these manifestations were consistently aligned along a NE-SW direction (Gaspar *et al.,* 2003). The eruption had constant activity throughout 1999, and localized emanations or micro-seismic activity have been reported in the area until 2001.

It comprised plumes of smoke emanating from cooling floating lava ballons (Gaspar *et al.,* 2003), as big as 3m in length consisting on vitreous basalt (figure VI.17). The eruption was high in volatile content, as the debris normally presented empty cavities formed by gas accumulations, at the surface. As cooling occured, seawater entering through the cracks and gas liberation promoted plunging or sometimes explosion of the

debris (floating time: 15 minutes in average). This eruption was not continuous; it pulsed between periods of moderate activity and others of relatively quietness with total lack of volcanic activity at the sea surface.

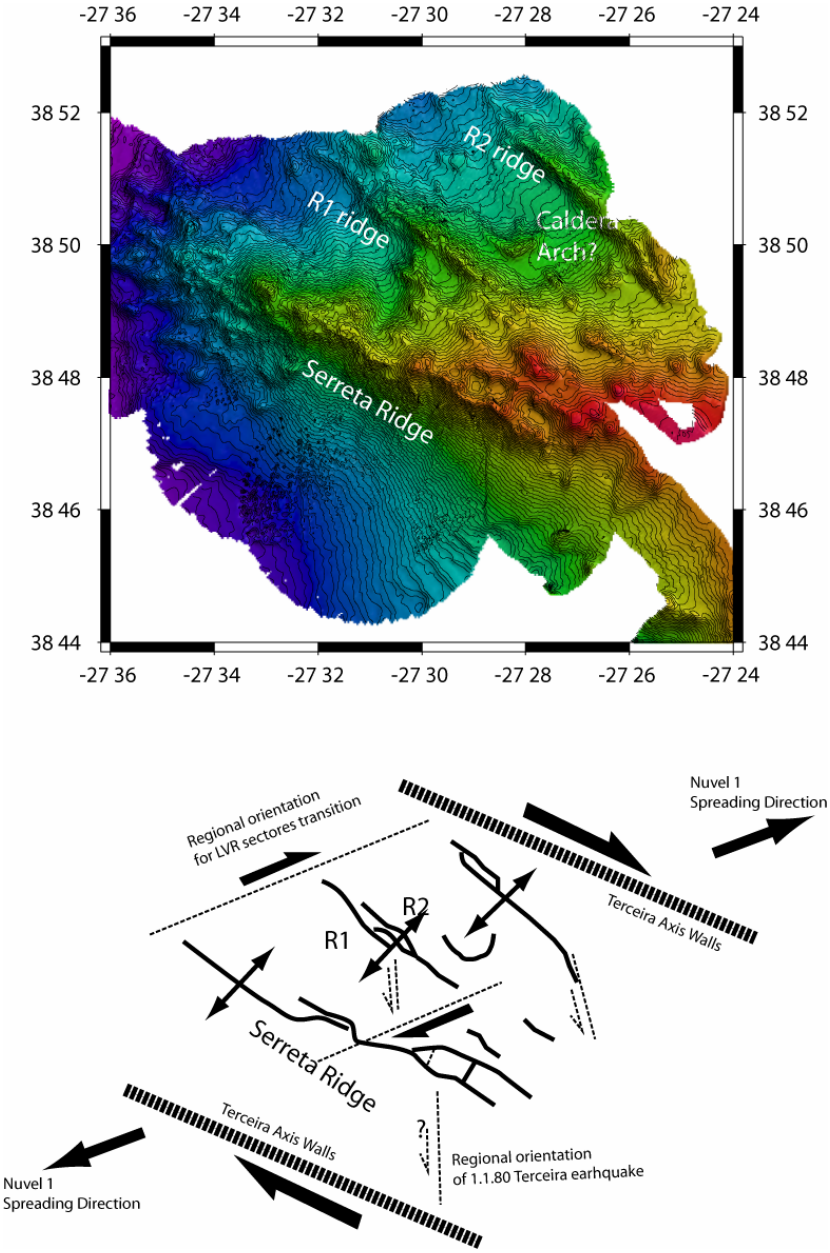

Figure VI.15 - Model depicting possible tectonic interpretation for the Serreta Ridge Area. Ridges would act as dominantly tension cracks with possibly a minor right lateral component. Shear components would be largely accommodated in N150º faults and N65º transfer zones.

During the 500 years of human settlement in Azores, a significant number of submarine eruptions have already occurred, sometimes evolving into ephemeral Islands (a complete synthesis of Azores eruptions may be found in the paper of Weston (1964). The eruption site was very close to the location of other submarine eruption which occurred in the year of 1867. The later was preceded by premonitory tremors that lasted five months culminating with violent earthquakes and explosive volcanism that lasted only a week and produced damage in the Terceira Island. On the contrary, the Serreta eruption has lasted for longer time and seems to have been much more effusive in character and, given the geometry of the sea-floor manifestations, of a fissural nature.

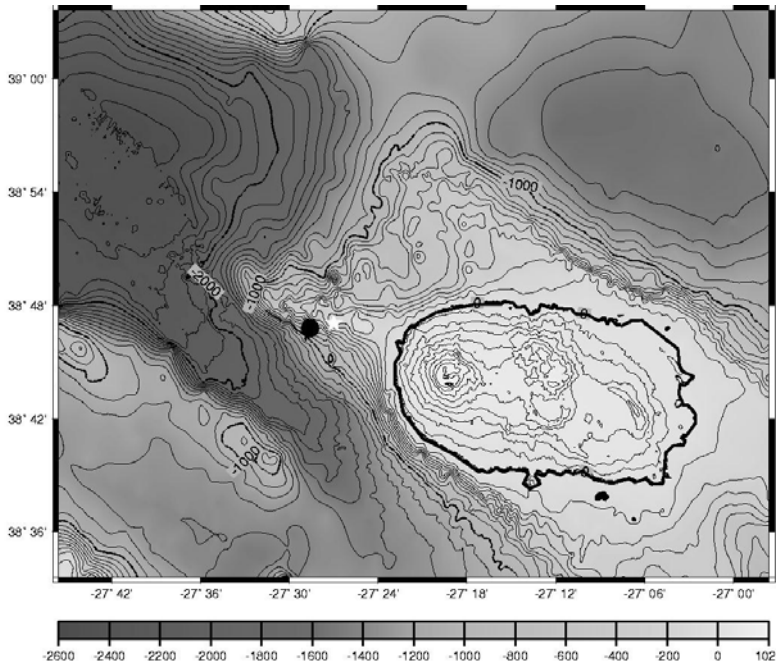

Figure VI.16 - Bathymetric/altimetric map of Terceira Island and East Graciosa basin. Black circle and white star are respectively the 1999 and 1867 Serreta submarine eruption sites.

Using sparse echo-soundings collected by the Portuguese Hidrographic Institute prior to the onset of the eruption, and multi-beam data collected by the Knorr, after the eruption main episodes, we are able to trace, at least qualitatively, the changes in the seafloor topography (See Figure VI.18). The pre-eruption survey displays an ortogonal "bay" like relief which interrupts the Serreta ridge crest. This bay is open southwards. The most significant change in the topography at the eruption site, is visible in the post eruption survey as that "embayment" is now closed into a square section depression and the Serreta ridge becomes a continuous feature. Despite the different resolutions of the surveys, profiles from both surveys, across this new feature, yield sufficient bathymetric correlation on the sections off the eruption location to allow characterization of bathymetry change. The profiles suggest that the eruption probably started a a depth of around 450 m bsl and created a continuous relief about 120 m high, overall. The slope of the southern flank probably became steeper as suggested by the profiles. The orientation of the newly formed ridge does not match the reports of NE-SW but observation suggest that some leakage from a NNE-SSW ridge east of it but in close proximity might have occurred (Gaspar *et al.,* 2003)

Figure VI.17 – Left) photograph of a "lava ballon" sample. Right) Photograph of a series of lava ballon at the sea surface during one of the Serreta eruption events (Source: http://www.volcano.si.edu, Photos by CVUA, *Centro de Vulcanologia da Universidade dos Açores*).

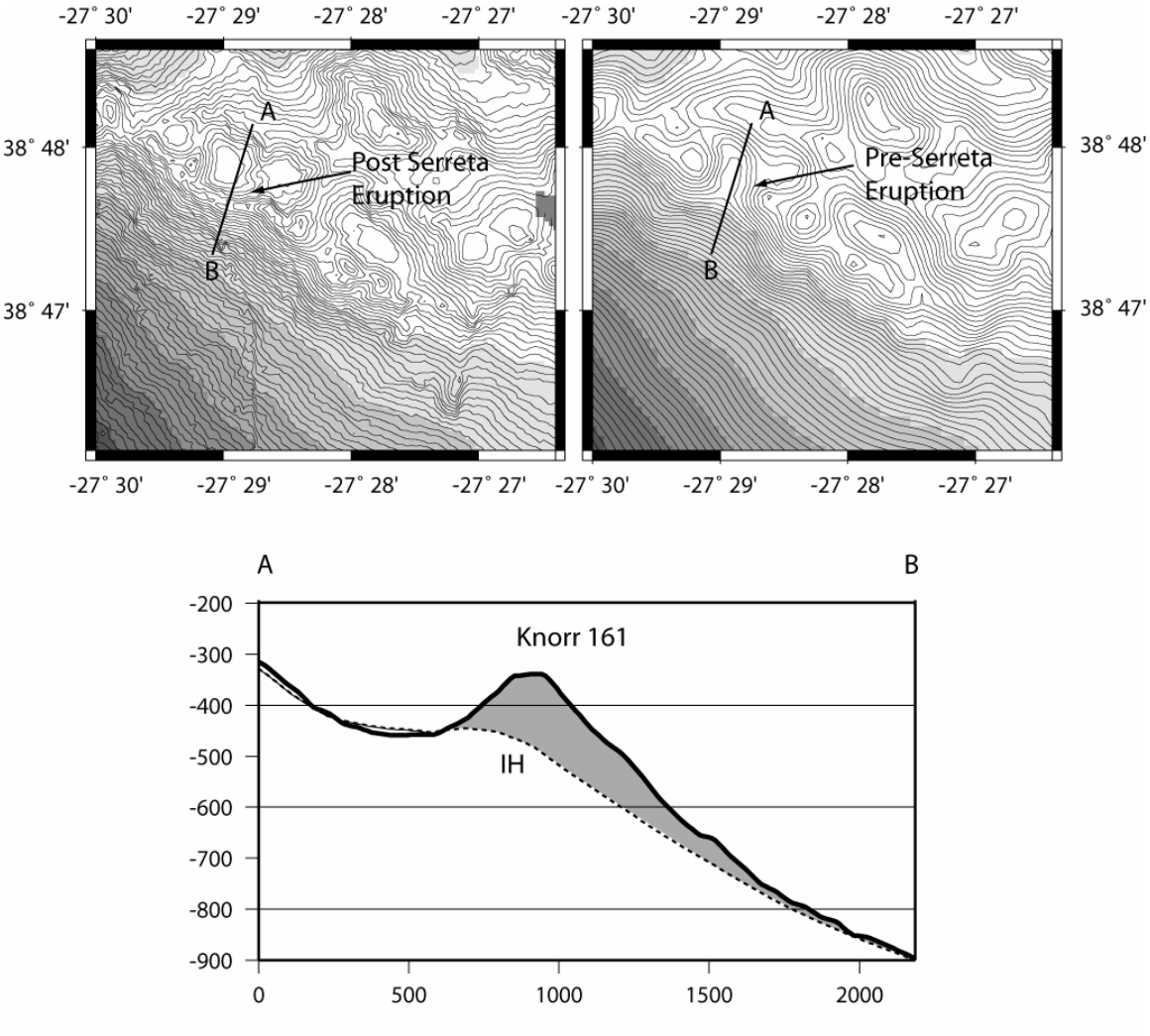

Figure VI.18 – Top) Pre (rigth) and post (left) eruption bathymetry of the Serreta ridge, contours each 20 m. Bathymetric grids are respectively from a dense echo-sounder survey made by the Portuguese Hydrographic Institute, and a swath bathymetry survey made by the Knorr in transit over the area. A-B designates topographic profiles shown in the bottom figure. The eruption had a significant bathymetric impact, linking two adjacent ridge segments and leading to the individualization of a 130m deep basin. Bottom) Grey shade ilustrates the qualitative difference in bathymetric profiles due to the submarine eruption.

VI.4.2 East of Terceira: Geological inferences from a transect across the Terceira axis.

Contrary to the observations in the Terceira Island and the East Graciosa basin, the domain comprising the North Hirondelle Basin and the adjacent off-Terceira axis domain, displays a much more complex pattern with areas dominated clearly by volcanic processes whereas others display high levels of tectonic deformation and

others still display relatively flat surfaces with little evidence of volcano-tectonic activity. The orientation of the main morphological features, changes drastically when compared to the Serreta domain or to the western part of the Island, but is consistent with the observations on its eastern side.

The transition form NHB to the South Hirondelle Basin (SHB) defines a step in morphology which orientation corresponds to the prolongation northeastwards of the eastern transition from LVR sector 2 to deeper areas (see section V.3). The João de Castro Bank, a shallow (~13 m bsl) caldera system lies over this probable tectonic limit.

From the gathered swath bathymetric data, we only have a profile, which crosses the all extent of the Terceira axis, perpendicularly to it. The profile is located at the northwestern limit of the NHB (see Figure VI.1 for location). Its analysis, combined with magnetic data, provides some constraints about the Terceira axis major morpho-structural features (See Figure VI.19). From Northeast to Southwest the transition from the abyssal plain into the Azores plateau is defined by an asymmetric ridge. The northern flank of this structure is about 900 m high defines the edge of the plateau (we designated it as ER – Edge of plateau Ridge). The southern flank of this structure is about 300m high and bounds a 400 m depression elongated parallel to the Regional Terceira axis strike. This graben like basin (hereafter called ED – Edge of the plateau Depression) lacks any significant seismo-tectonic activity but presents nonetheless high magnetizations, in the order of those observed further SE in the seismically active portion of the Terceira axis. The single passage of swath bathymetry reveals that the floor of this depression is disrupted by normal faults striking N130º-140º (n= 9) parallel to the ER, and two volcanic cones about 200 m high are partially imaged.

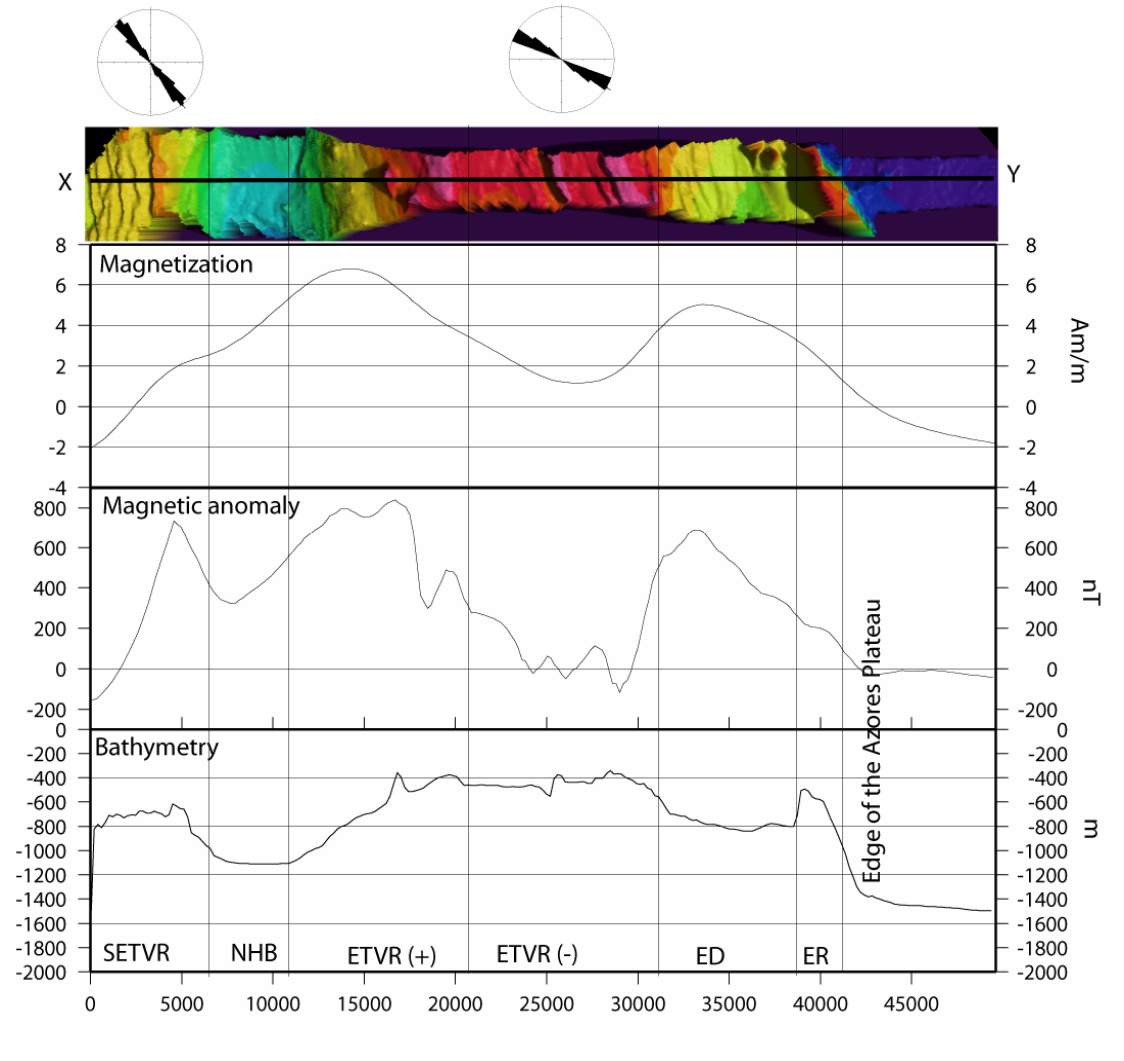

Figure VI.19 - Series of profiles performed over a single passage of EM300 swath bathymetry data across the Terceira axis (see Figure VI.1 for profile location). Based on their morpho-tectonic and magnetic signature several domains have been identified: SETVR -SouthEast Terceira Volcanic Ridge; NHB – North Hirondelle Basin; East Terceira Volcanic Ridge (positive); East Terceira Volcanic Ridge (negative anomalies

The following topographical high, here referred to as the East Terceira Volcanic Ridge Ridge (ETVR), shows two distinct areas based on the orientation of tectonic structures and its magnetic character. The first of these areas tends to have negative or near zero magnetizations and corresponds to a rough surface deepening towards East. Normal fault scarps imaged by the single passage confined to this areas of low magnetization have a distinctive orientation from the previous ones, as they strike between N110º and N114º (n=4). Volcanic structures are absent. Further Southwest the ETVR becomes strongly positive (locally in the profile it reaches ca 7 Am/m) and dominated by volcanic processes. This is confirmed, as we shall see below, by the far NE portion of the Sirena bathymetric map and the AZ99 TOBI mosaic, where in the prolongation of this domain towards SE, numerous volcanic cones cover deeper portions of the NHB (see Figure VI.2 for spatial reference).

The NHB, in this profile is bound between the ETVR and the Southeast Terceira Volcanic Ridge (SETVR). In pratice, it prolongs towards the Terceira Island as a V-shaped depression, where its apex, at around 300 m bsl, defines the geometrical convergence between both marginal ridges.

VI.4.3 The SouthEast Terceira Ridge (SETVR)

The amount of data over this ridge, either from swath bathymetry from Sirena I cruise (Lourenço *et al.,* 2003) and the TOBI mosaic that was performed during the Azzore99 cruise (Ligi *et al.,* 1999), makes one of the most documented submarine structures in the Azores apart from the Islands themselves. For instance GLORIA images from Searle (1980) see Figure VI.20, would only provide a hint on the high level of tectonic deformation here present, and in terms of regional bathymetry, (as observable in Figure VI.2) despite reproducing the overall shape of the ridge, it does not provide any

indication at all of relevant tectonic features. These data on the SETVR proofs the importance of having a wider swath bathymetric coverage of the Azores Plateau.

The ridge presents a NW-SE orientation, it is seismically active (see Figure VI.1) and corresponds mainly to Brunhes magnetic epoch. The bathymetry and sonar maps reveal a clear partition between tectonic processes, centred in the ridge, and volcanism present at the bottom of the North Hirondelle basin.

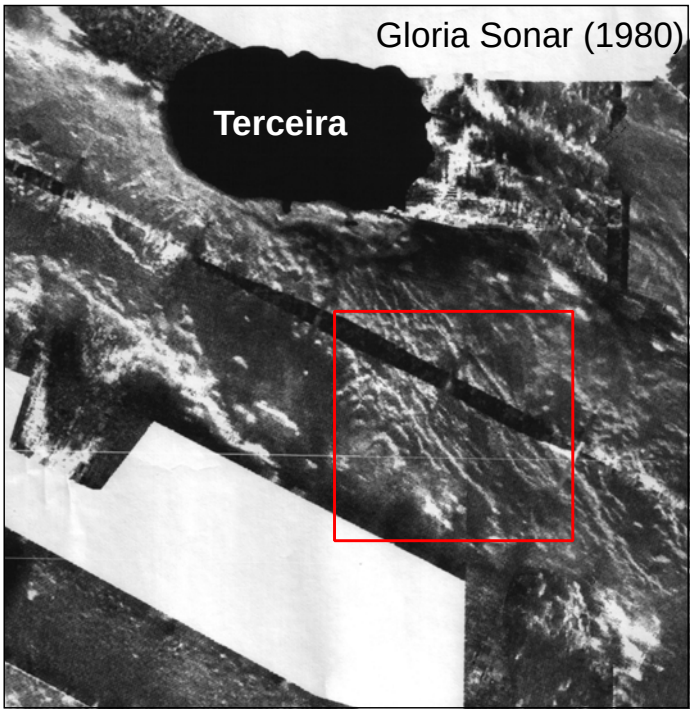

Figure VI.20 - Gloria sonar image from Searle, (1980), over the SETVR. Red square indicates the area now covered with both TOBI and EM300 swath bathymetry.

The acoustic facies interpretation from TOBI is presented in Figure VI.21. We have defined essentially 5 different acoustic facies: Clusters of bright linear, or otherwise linear acoustic shadows (for faults facing away from sonar ensonification direction), are classified as tectonic terrain, polygons of faults identified within this domain were digitized. High to medium backscattering surfaces, with irregular textures sometimes forming hummocks or with identifiable conic or with basal circular sections have been classified as volcanic terrain. If a significant number of faults were present disrupting bright backscaterring surfaces, these domains were classified as tectonised volcanic terrain. Sediment terrain corresponds to areas of homogeneous low backscatter. Finally, making additional use of swath bathymetry to help interpretation process and define more sharply the base of the ridge, areas of talus deposits and mass wasting deposits were mapped. In the first case, outlined by narrow bands, at the base of fault scarps, with variable degrees of backscatter, characteristic of talus deposits. Corrugations in sediment facies in the dowdip direction and flanking fan like shapes in plan view, typical of slump deposits (Figure VI.22-3) were indistinctly classified as mass wasting deposits.

The SETVR axis is a broad high backscatter surface of volcanic nature, given its high amplitude magnetic anomaly. All the areal extent of the ridge is disrupted by a strand of sub-parallel but highly anastomosed normal faults striking between N130º and N150º. At 27ºW, 38º25N, in the SW ridge axial flank, a distinct rhombic shape topographic low is present, defined by a continuous low backscattering sedimented surface which correlates with a negative magnetic anomaly. This low is fault controlled in its Southern and Northern limits. Its Eastern and Western flanks, correspond to sharp N-S contacts

between low and high backscaterring surfaces, which are cut through, by faults belonging the same dominant fault system in the SETVR.

The top of the SETVR consists on an arched demi-.horst, and it is interpretable either as volcanic structure remnant (caldera system?), existing prior to onset of the tectonic stage in the ridge or otherwise a giant scar from the gravitational collapse of the northeastern flank. Both ridge flanks display gullies and mass wasting fans at the base of the slope (Figure VI.22-3). The ridge vicinities are almost exclusively composed of a grayish homogeneous acoustic facies interpreted as pelagic and volcanic sediment. The numerous untectonized volcanic cones, present to NE, in the northern flank of the North Hirondelle basin (see Figures VI.19 and VI.22-1), form alignments sub-parallel to the ridge main strike and contrast with the densly fractured pattern observable in the SETVR. The high magnetization values observed in the areas covered by this volcanic constructs suggests that this is the current neo-volcanic axis in this domain. Limited data, limits our ability to constrain its areal extent along the plate boundary.

Faulting geometries their inter-relationships and fault orientations, in the SETVR, provide clues concerning their kinematic behaviour. Some faults present horse-tail terminations. Fault splays often link to neighbour faults defining extensional duplexes (Figure VI.22-2), relay ramps and fault wedge basins and highs of roughly rhombic shape (see Figure VI.22-4). These faulting patterns observed in the SETVR are conformal with right lateral oblique extension component. Typical wrench structures like strike slip pull-apart basins are not observed in this domain.

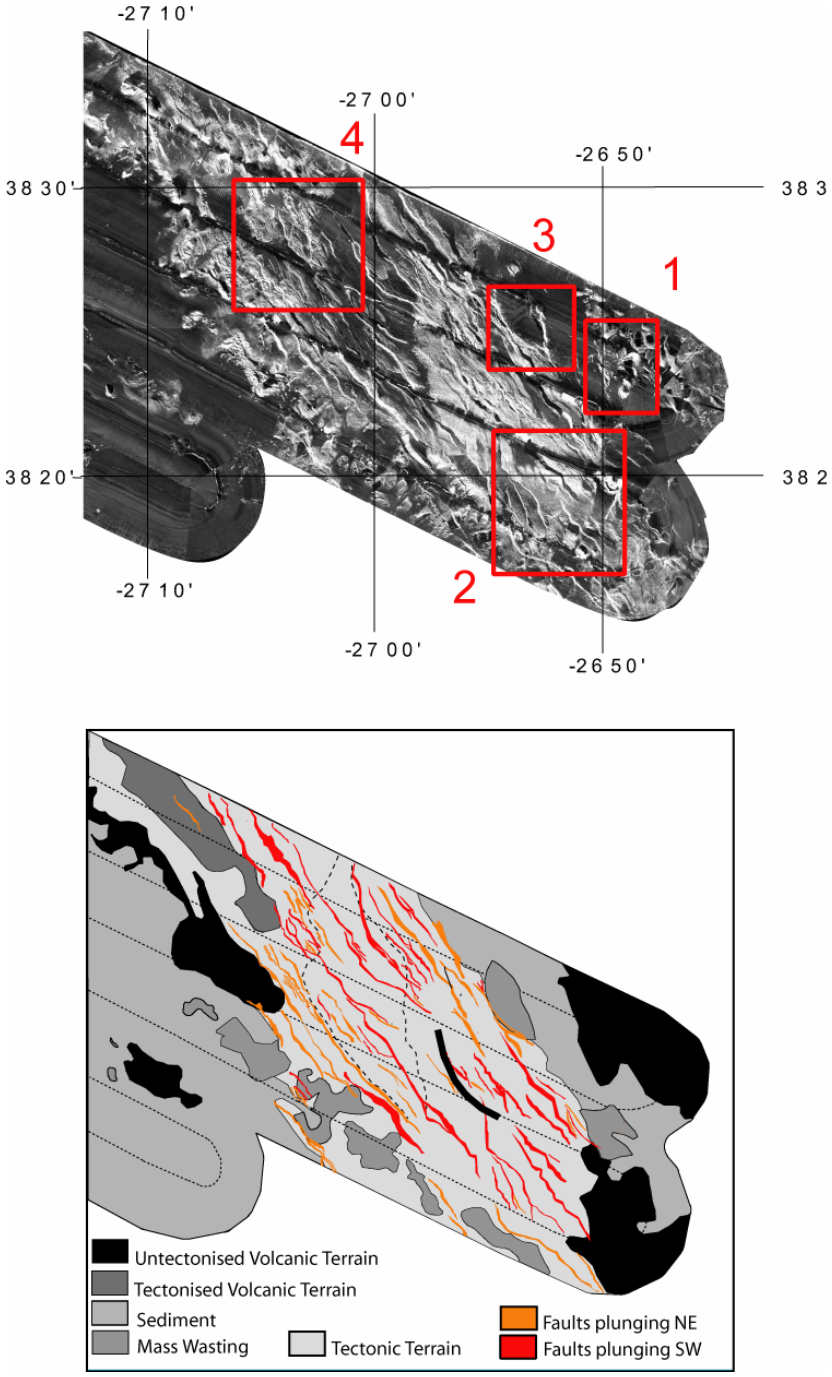

Figure VI.21 – Top) TOBI mosaic of the SETVR. Red poligons and labels are areas of interest depicted in Figure VI.22. Bottom) Accoustic facies interpretation (see text for details). Stippled lines delimitate a rhombic shaped depression discussed in the text.

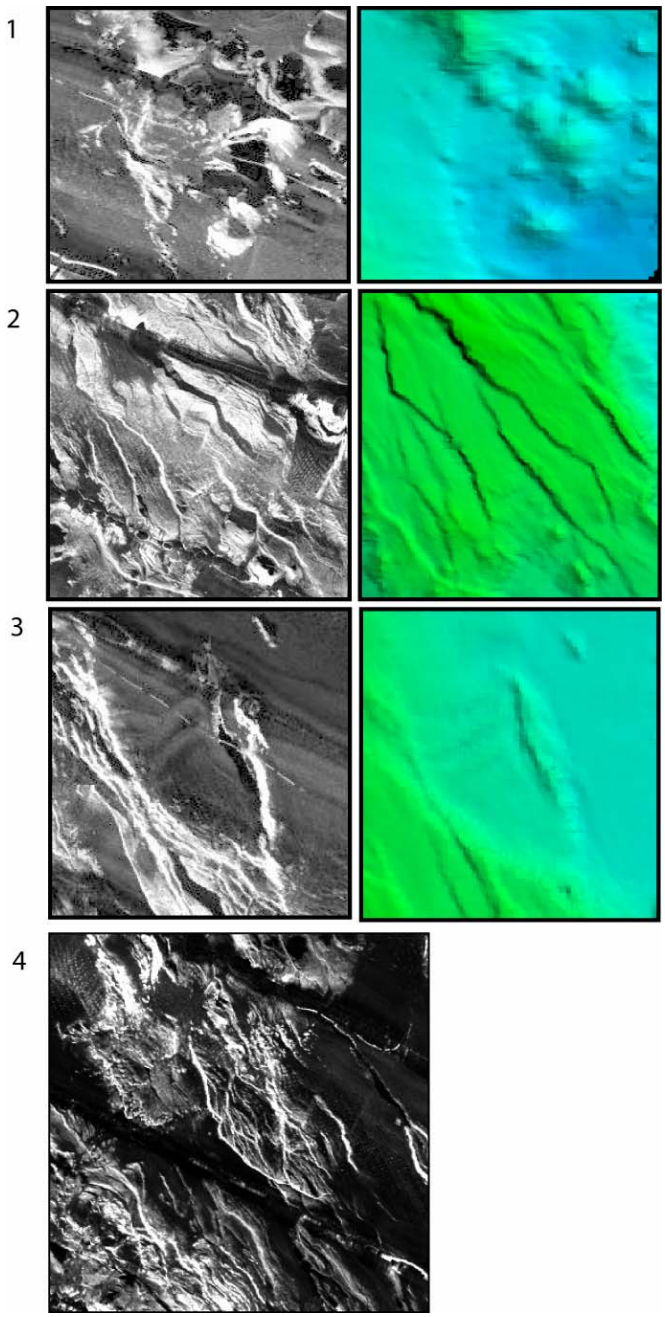

Figure VI.22 - Left) TOBI sample images; Right) Corresponding EM300 swath bathymetry images. 1. Cluster of volcanic cones located in the North Hirondelle Basin aligned sub-parallel to the SETVR. 2. Strandle of normal faults disrupting the SETVR surface. Note the Zig-zag pattern of some faults (see section VI.4.3.1 for details). 3. Slump scar and corresponding mass wasting deposit in the SETVR northeastern flank. Note the flow corrugations and the frontal thrust in the frontal edge of the slump. 4. Complex fault pattern at a normal fault intersection relay zone.

VI.5 Discussion and conclusions

In this chapter we have addressed the tectonic pattern, and the partition between volcanic and tectonic processes in the Terceira axis, between the East Graciosa Basin and the North Hirondelle Basin.

The distribution of tectonic and volcanic processes varies significantly across the studied sector of the Terceira axis. In Figure VI.23 we present a tectonic model that summarizes our main observations. West of Terceira, volcanic accretion seems confined to the Serreta ridge, expressing as fault controlled fissural volcanism. The East graciosa basin floor is barren in volcanism and clear cut tectonic structures, nevertheless a left lateral strike slip N150º faulting direction is bound to play a significant role in the plate boundary strain accomodation. Linkage of bathymetric observations with inland data is straight forward for the Serreta ridge as the submarine prolongation of the fissural system inland, clearly expressed between the Guilherme Moniz and St. Barbara calderas.

The Island of Terceira displays a complex tectonic pattern where four tectonic directions were recognaized often controlling volcanic cone morphology, dikes, lava flows paths and possibly same sections of the coast line. These are according to strike:

1) WNW-ESE. Corresponding to the fissural system in the Island west of Guilherme Moniz Caldera. Possibly corresponding to tension fractures with some minor rigth lateral displacement provided by the en-echelon arrangement of individual cones elongation axis.

2) N-S. Expressed by the East Angra faults; interpreted as possible reactivation of MAR generated fabric. This system ruptured as left lateral Strike slips in the 1980 Terceira earhquake.

3) NNW-SSE. Expressed by the Lages Graben and the Cinco Picos Caldera fissural system. Co-existance of vertical and 60º dipping fault planes belonging to this fault family suggest that some strain partitioning should exist associated with it.

4) ENE-WSW lineation family. These devide the Island in two halfs with distinct morphologies. Volcano-tectonic orientations also denote the clear change in orientation of the fissural system between the Island western and eastern halfs. Furthermore as discussed in Chapter V, this fabric seems to have a regional significance related as a relay zone parallel to the opening direction between AF (Nub) and Eurasia as constrained by NUVEL1A kinematic model.

The seafloor structure East of Terceira displays a higher magnetic and morpho-strucutural complexity than the submarine domain west of it. The linkage of submarine observations with the East of the Island is less clear mainly because of data availability limitations.

The Lages Graben follows the same strike as the SETVR pervasive faulting. In SETVR, the faulting pattern seems dominanted by right lateral oblique extension. Faulting on the ETVR follows a strike close to the Island fissural system. The observed active submarine fissural volcanism is concentrated in a region parallel to the SETVR but lying deeper and between this two ridge systems. Furthermore consistent high magnetization values and lack of tectonization leeds us to the conclusion that this fissural volcanism materializes the neo-volcanic zone in the submarine domain east of

Terceira Island. Linkage of these submarine volcanic occurrences with those of Cinco Picos Caldera, fissural system inland, cannot be verified and probably they are a part of different accreting segments.

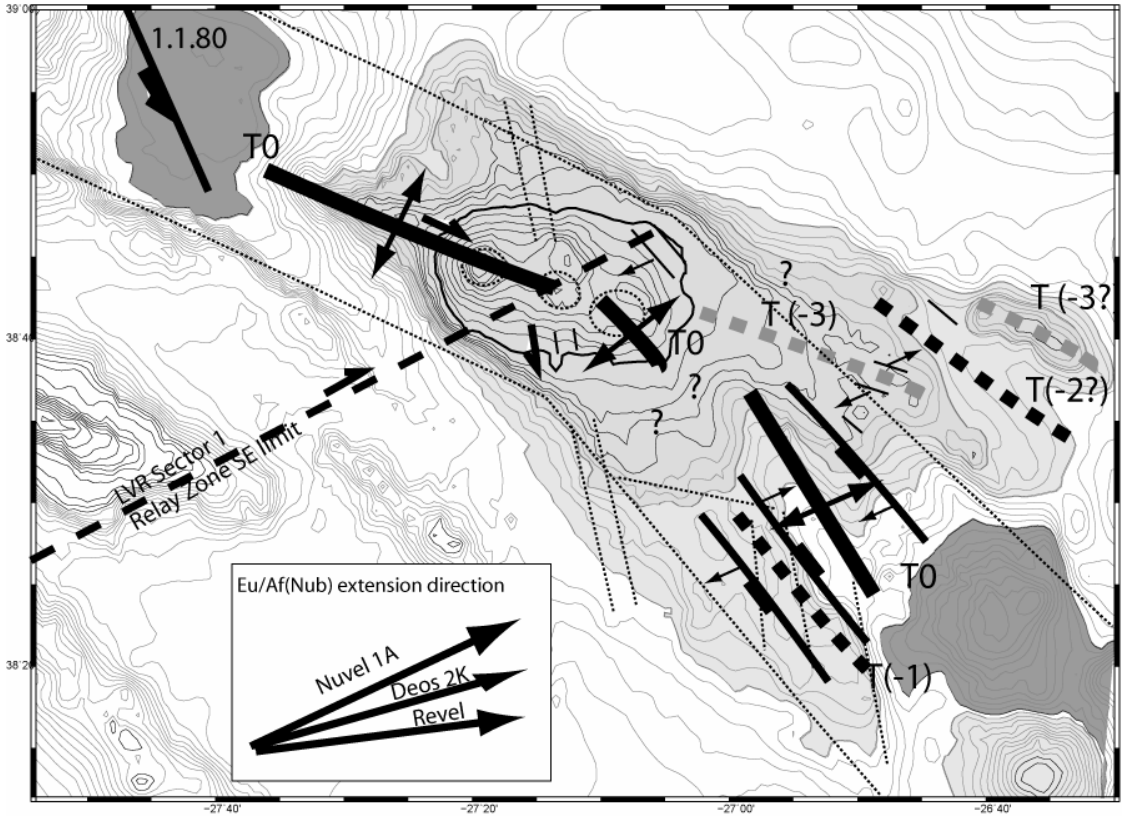

Figure VI.23 - Summary of main tectonic observations in the study area. Ligth gray contours are shallow area. Dark gray contours are deep bathymetric areas. Dash gray lines are axis of negative magnetic anomalies considered abandoned accretion units. Short dashed black lines are positive magnetic anomalies considered volcanically inactive. T labels refer possible timing sequence for activity of those acretion units, where T0 refers to the present day. Black line defines the Terceira axis neo-volcanic zone. Long dashed lines mark the SE limit of sector 1 LVR hypotetised as corresponding to a relay zone. Stippled lines are possible MAR related reactivated fabrics. Arrows indicate interpreted bulk sence of displacement in the fault. West of relay zone, faults probably accommodate deformation by deformation partition. East of the limit faults are considered to present oblique dextral slip.

Considering these observations, and assuming that the bulk of inter-plate tectonic processes are focused in the Terceira axis in this sector, how is accretion accommodated in this domain? Is it full seafloor spreading or is intra-oceanic rifting still taking place as suggested by Vogt and Jung (2003)?

Existance, both in the Island and in the SETVR of N-S striking fault segments and the point source style of volcanism which resulted in the construction of the Island, probably at the intersection of tectonic structures (Self, 1976; Lourenço *et al.,* 1998) leads us to the conclusion that Terceira axis "basement" can be in fact tectonically subsided MAR generated seafloor due to rifting of lithosphere resultant from EU-NU plate boundary processes without effective seafloor spreading. We envisage, therefore that the extremely slow nature of extension within the Terceira axis, has resulted in vertical stacking of volcanic products along main active tectonic trends. The Brunhes and Matuyama magnetic anomalies, documented within the Terceira axis would represent the last volcanic expression within that system. In this case, the spatial arrangement of magnetic anomalies within the Terceira axis, and the main orientation of the principal volcano-tectonic features, can provide some clues on the sucession of magmatic and tectonic accretion events and their spatial distribution across this plate boundary.

Searle (1980) stated that it was unclear form the studied GLORIA images, if the plate boundary corresponded to the topographical highs or lows. Considering the strike of faults imaged on the ETVR subparallel to the Western Terceira Island fissural system strike and its overall orientation, we consider that this must have been initially a single accreting segment and the older one (See also section II.2.6), probably corresponding to reactivation of a MAR transform (axis at T-3 time in Figure VI.23). Magmatic activity essentially ceased in Matuyama age. The ER follows the same strike of the ETVR and presents a similar magnetic anomaly character suggesting that it has been active during the same T-3 period.The timing for ED generation is also unclear. Probably it was formed in a recent time (axis at T-2 time?) and active volcanism and minor earthquake

activity suggest that is still an active feature, despite never having evolved fully to a an acretion axis. Activity then jumped into the SETVR resulting in the construction of this ridge by volcanic processes (at T-1 time). Subsquently as extension proceeded volcanic processes get focalized in the southeastern edge of the ETVR, materialising the present day acretion axis (T0 axis). All the across axis domain, notably the SETVR and ETVR, undergo mainly concomintant oblique extension.

We interpret these clokwise jumps in accretion axis as the result of two conjugate factors:

1) Variations in the thickness of the lithosphere brittle layer. As magmatic processes proceed, progressive topography build up and therefore increase in load as well as crustal thickness, could lead to a re-organization of the magmatic plumbing system and reactivation of subparallel pre-existing structures but in a thinner and weaker brittle layer, therefore more favourable to rupture as volcanic conduits

2) The prevailing kinematic conditions through time. As referred in Chapter IV, the extension at this plate boundary has progressively rotated from NE-SW to more E-W directions (as constrained respectively by Nuvel-1A and by GPS models). This modification of kinematic constraints could have resulted in changement of the tectonic regime from right lateral transtension dominated by wrenching, still prevailing in the studied western domain to oblique right lateral extension in this eastern domain. In the latter with consequent reactivation of NW-SE left lateral faulting directions as oblique normal faults. We suggest that the Terceira axis neovolcanic axis, at least in this sector, is re-organizing and fitting the current kinematic conditions.

Chapter VII - Geodynamic inferences of 1957-58 Capelinhos Eruption (Faial)

VII.1 Introduction

Geodetic monuments were installed for the first time on Faial Island in 1937. Fifty years later they were reoccupied with triangulation and trilateration and, just before the 9 July 1998 earthquake, they were once again observed, now with GPS instruments. In spite of the significant volcanic and seismic events during this period, a quantitative assessment of the Island's deformation has never been attempted. In this section, we summarise the results of re-processing of geodetic data covering a time span of 60 years, to assess the long-term deformation pattern of the Island recently presented as a form of a paper (Catalão *et al.*, 2006). We show that displacements are large over the western part of Faial Island, and mainly limited to the 1937-1967 period; in the eastern part of Faial Island the displacement field is below the accuracy threshold of conventional geodetic techniques for the whole time span. Most of the Island deformation, as we shall discuss below, probably was accommodated in a single event, corresponding to the 1957 Capelinhos eruption and subsequent earthquake activity. This unique data allows constraining the dynamics of active volcanic processes and how they contribute to inter-plate deformation at the Azores. Its generalization also provides clues on modes of growth of the LVR at least for sector 1.

VII.2 The eruption and associated earthquake activity

Since the arrival of the first settlers, in the early XV century, several aerial eruptions have been reported in most of the Islands. Faial Island in particular was the site of a few historical eruptions; the last one and the best described is the Capelinhos eruption. This eruption started on the 27th of September 1957, 1 km offshore the western tip of Faial Island. During about 1 month (until 30 October) intensive explosive activity was observed, with uninterrupted emission of bombs and scoria. A small Island was formed, built up with tephra and basaltic lapilli reaching 600 m in diameter on the base and a height of 80 m above sea level. On the 30th October the explosive volcanic activity ceased and the Island collapsed. Subsequent activity led to the construction of an ash arc, which reached 150 m height in 1958. Contact between the active chimney and seawater was responsible for the high explosive character of the eruption in the first 7 months of the eruption. There is a large photographic survey and many written information concerning this eruption (Castello-Branco *et al.,* 1959, Machado, 1958a, 1958b, 1959a, 1959b, Machado *et al.,* 1959, Machado *et al.,* 1962, Zbyszewski *et al.*, 1959).

On May 13th, 1958, there was a readjustment of the volcanic edifice inducing a seismic crisis with more than 450 events recorded. In some places macroseismic intensity reached X, in the Modified Mercalli scale (Machado, 1959a). Three source areas were identified: one immediately southwest of the central caldera, other northwest, at half distance between the caldera and the active crater. The focal depth was estimated by Machado (1959a) to be approximately 1 km. A series of fractures was observed with subsidence parallel to the N105 cinder cones alignment and uplift along sea cliffs. A long narrow belt parallel and along the north side of the cinder cones was depressed

during these crises (Machado *et al.,* 1962). These shallow events had low magnitudes, as they were not felt on the SE of Faial (Machado *et al.,* 1962). There are no records of these earthquakes because there were no permanent seismographs in the Azores. Activity ceased on 24 October 1958. The seismic information is poor: only 3 seismic stations were installed in the Azores, one at S. Miguel (since 1902) another at Faial (since 1902) and the third at Terceira (since 1932). Faial was inoperative at the time of the eruption and a new seismograph was installed at Horta during the crisis.

Topographic changes were noticed and several surveys conducted to evaluate their magnitude (Machado *et al.,* 1959). Most of the measurements were limited to the Capelinhos area and devoted to volume computation. Machado *et al*. (1962) describes significant height changes in the south and west of the Island as a result of whole event. Changes reached 0.5 m uplift in Vale Formoso (see site VFOR on figure VII.1 for location) and 1.5 m subsidence along pre-existing faults, in the central area of Faial. Some quantitative data referred by Machado *et al*. (1962) point to a relative displacement of about 1.2 m between north and south side of west of Faial and surface movements were considered irregular better describing a warping movement than a single graben subsidence.

VII.3 Geodetic Data

Geodetic observations on the Azores have been carried out since 1937 by the Portuguese Geographic Institute (IGP). Their network covers the whole of Faial and Pico Islands. It consists of 135 monuments – 62 in Faial and 73 in Pico - forming a 2-3 km triangular mesh (see Figure VII.1).

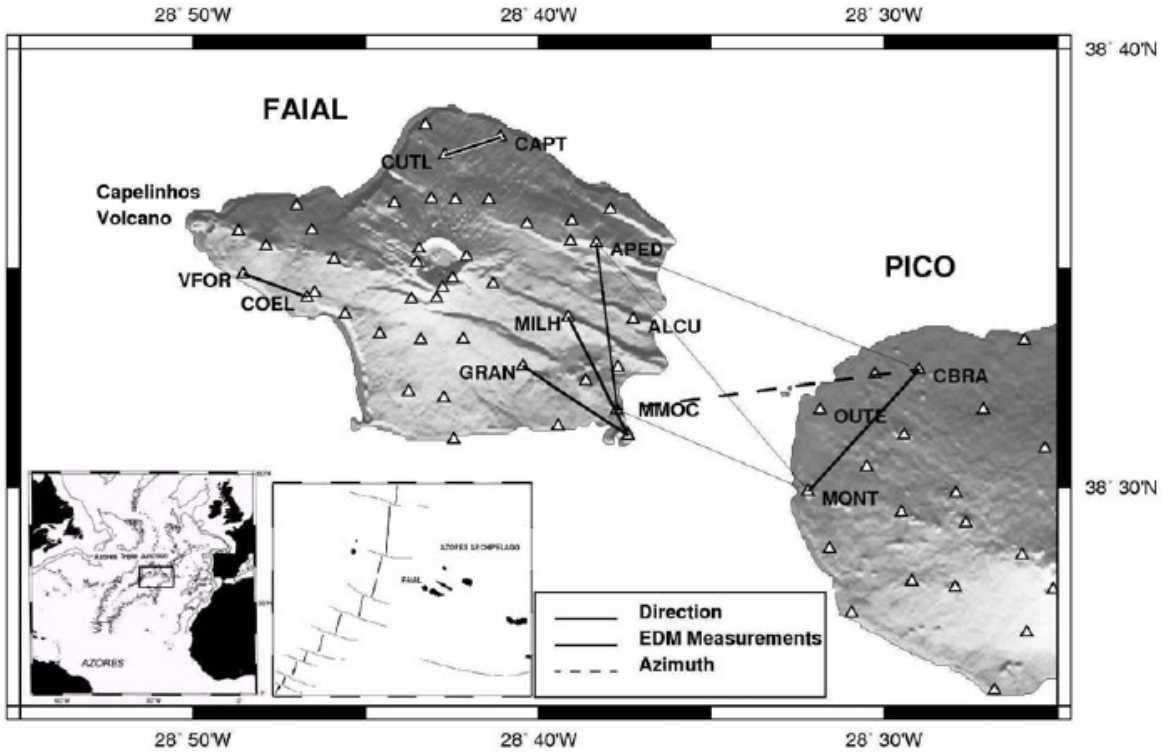

Figure VII.1 - Location of Faial Island in the Azores Archipelago. Faial is the western Island of the central group that is closest to the Mid-Atlantic Rift. The Capelinhos volcano is located on the coast in the westernmost part of the Island. Geodetic network on Faial and Pico (triangles), directions and azimuth between Faial and Pico measured in 1937 and Electronic Distance measurements (EDM) made in 1967.

This network was built in 1937- 1942. It is based on well-cemented pillars, about 1.2 m high, set firmly into the ground. The network covers the whole surface almost uniformly with a local cluster around the Faial summit crater. The network has been surveyed to the best available standards of the time in six different operations since 1937, as shown in Table VII.1.

Five different types of observations were made: triangulation, trilateration, azimuth, levelling and GPS. Two global occupations have been made, in 1937-1942 and 1995-1997, giving a time span of about 60 years between the first, made with traditional methods, and the second, with GPS. In Faial, intermediate observations were made in

1967, with several distances measured with an electro-optical device; in the 1987 campaign, the Faial geodetic network was almost completely observed with directions and zenith distances (planimetry and altimetry).

Catalão *et al*. (2006) evaluated triangulation, trilateration and GPS measurements obtained in the Islands of Faial and Pico between 1937 and 1997 and estimated the total displacement field for a set of 58 points well distributed over both Islands. Their full data exploration strategy and processing schemes description is out from the scope of this work, for more details the reader is refered to Catalão *et al.* (2006). Here we only present a brief summary of this topic:

Table VII.1 – Observation epochs and number of geodetic observations.

Method	Epoch					
	1937	1942	1967	1987	1995	1997
Distance	1	1	10 / 3			
Triangulation	335 /10	343		313 / 4		
Azimuth	1	1				
Levelling	62	73		35	20	
GPS (baselines)					180	212
Island	Faial / Pico	Pico	Faial /Pico	Faial/Pico	Pico	Faial
Number of sites	62 / 2 a)	73	12 / 5	52 / 3 b)	76	61

a) Only the CBRA and MONT vertices were observed on Pico Island

b) Only the CBRA, MONT and OUTE vertices were observed on Pico Island

To integrate all existing geodetic data and to derive the most reliable deformation field for the Capelinhos eruption, Catalão *et al.* performed the analysis in three steps. First, for each epoch and each Island, they obtained the geodetic parameters (coordinates) loosely constrained to the MMOC site from terrestrial observations and GPS data. Second, he compared distance observations made in 1967 with computed distances

derived from single epoch solutions constraining the deformation process in time. In the third and last step, loosely constrained single epoch surveys were combined into a single solution which general constraints in position and velocity were imposed, reducing all observations and parameters into a uniform reference frame.

The projected distances were compared with the computed distances derived from each single-epoch network adjustment and are presented in Figure VII.2 as a function of time. Distance measurements made in 1967 at some sites on Faial, show large baseline variations before 1967 and moderate or null variations after that, suggesting no systematic trends related to any secular relative deformation between these sites. The main ground deformation is confined to the period 1937-1967 and is most probably the result of the Capelinhos eruption and associated volcanic and tectonic ground deformation processes. In this case, derived site velocities may be interpreted as mean velocities integrated over time, and as a consequence are dependent on the chosen interval range.

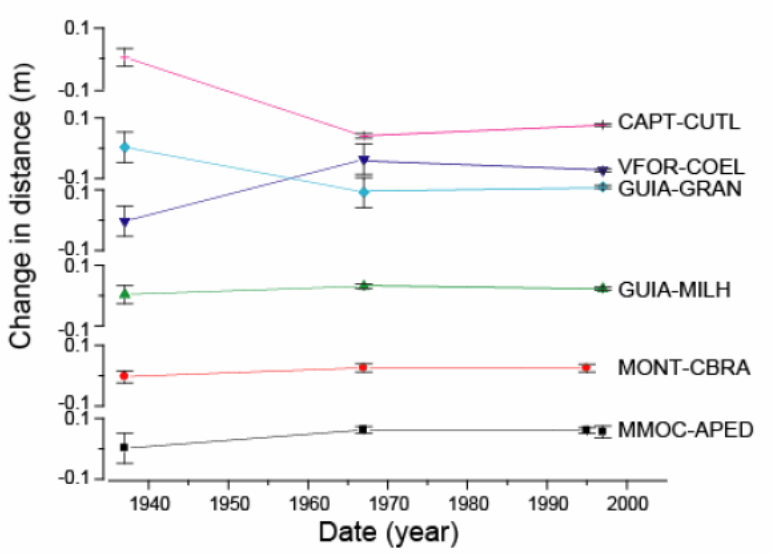

Figure VII.2 - Line length less a constant nominal length plotted as a function of time. The line length was measured with AGA-6A in 1967 and was computed from site positions for the 1937, 1995 and 1997 campaigns (Catalão *et al.*, 2006).

The leveling data used in this study was collected in 1937 and in 1987 for Faial Island. No leveling data was used on Pico Island. Orthometric heights were determined purely by trigonometric heighting for most of the geodetic vertices. The starting point was the MMOC site with its known true orthometric height determined by conventional differential levelling from the tide gauge. A set of 36 sites are common in both epochs and the vertical deformation was computed for each site, from which a vertical deformation contour map was derived and presented in Figure VII.3.

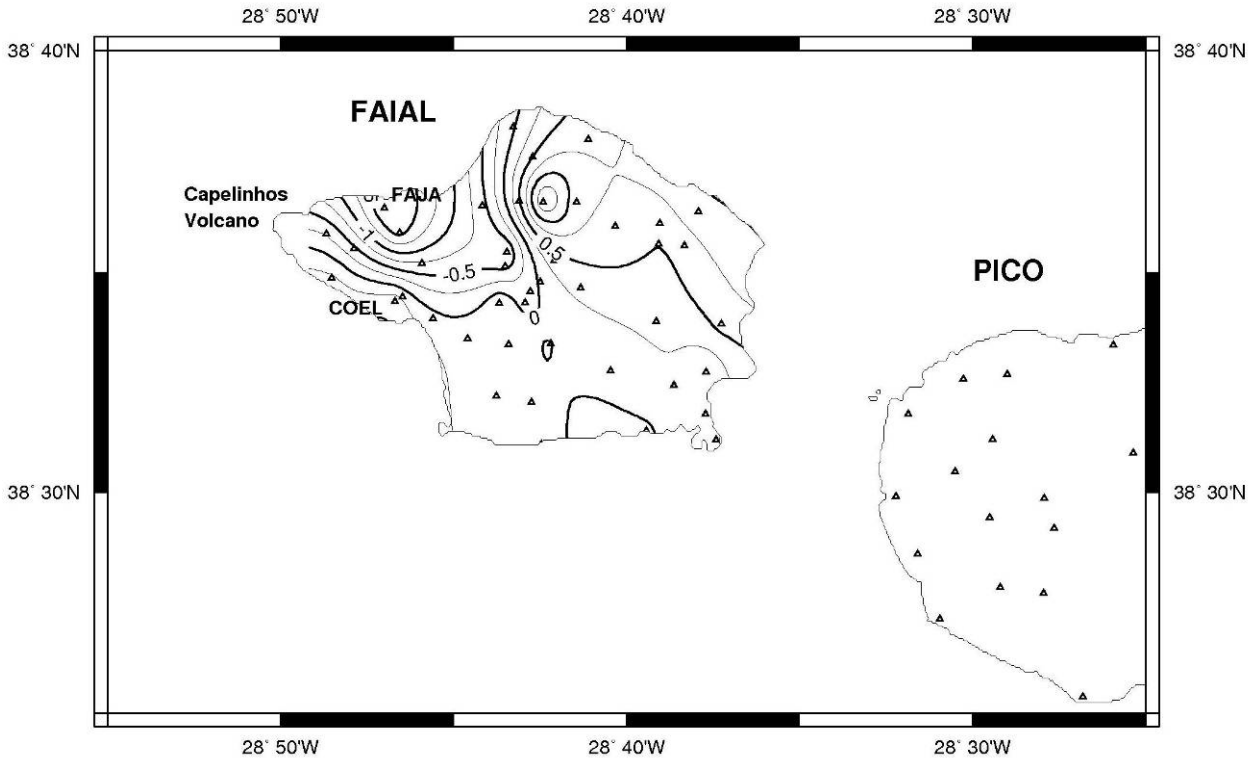

Figure VII.3- Vertical deformation obtained from 1937 and 1987 epochs (Catalão *et al.*, 2006)

The first thing to note from this map is the almost perfect agreement between neighboring sites producing an almost smooth surface, and showing a high spatial coherence of these movements. Moreover, the results are in agreement with Machado *et*

al. (1962) for the west side of Faial, revealing a large depressed area from the summit crater that reaches a maximum of -1.75 m vertical displacement at the FAJA site, and on the south coast a vertical uplift of about 0.5 m at the COEL site. From the north flank of the Faial crater spanning the entire north coast of Faial, a vertical uplift of 1.0 m is observed with a maximum of 1.5 m on the north crater flanks.

Finally, the single-epoch observations were integrated by Catalão *et al.* (2006) into a multi-temporal adjustment to derive the deformation field in the period 1937-1997.There are two possible intervals: 1937 to 1987, with only conventional geodetic data, and 1937 to 1997 with conventional geodetic data and GPS. Catalão *et al.* processed both periods and two sets of displacements were derived, corresponding to the 1987 and 1997 epochs. Both solutions were compared and it was found that residual displacements between them were within the 95% confidence error ellipses. In Figure VII.4, the computed displacement for the 1937-1987 period with 95% confidence interval ellipses is depicted. This period has more common sites than 1937-1997 due to the network reconstruction in 1997.

It is important to note that the resulting displacement field for the Faial-Pico network has been found in the joint solution of conventional and GPS geodetic observations in a frame of reference attached to the MMOC site in the south-east of Faial Island, which was strongly constrained in position and velocity in the adjustment of the geodetic network. This was the only strong constraint. This means that the computed displacements between 1937 and 1987 are relative to the MMOC site.

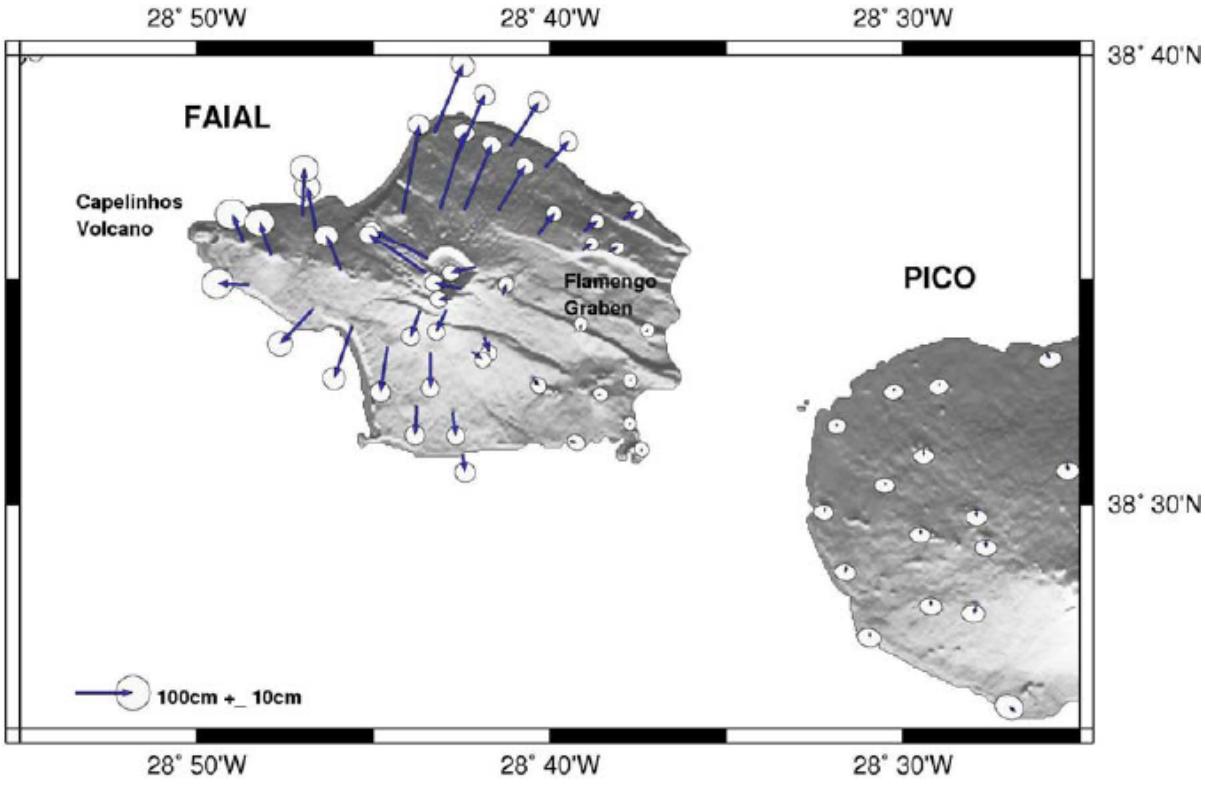

Figure VII.4 - Displacements obtained from simultaneous adjustment of the 1937 and 1987 geodetic networks. Error ellipses are computed with a 95% confidence interval (Catalão *et al.*, 2006).

VII.4 Elastic modelling

To model the observed geodetic displacements it was assumed that ground deformation was elastic and caused by the intrusion of two sub-vertical dikes in-depth. Dyke emplacement was simulated by a set of rectangular tensile dislocation sources in an elastic, homogeneous and isotropic half-space (Okada, 1985). The medium is assumed to have rigidity equal to 30 GPa. Inversion was made using the non linear generalized inverse algorithm developed by Briole *et al*. (1986), which allows the estimation of fault and slip parameters that best fit geodetic data. We first used field data reported by Machado *et al*. (1962). For the inversion, all three components of the displacements were used. The parameters for each rectangular dislocation model are length, width,

strike and geographic location of the centre of dislocation plane at its top, as well as dip-slip, strike-slip and opening dislocations. The reference surface is considered to be sea-level.

Table VII.2 - Elastic model fault parameters

Parameters	Fault 1	Fault 2	Fault 3	Fault 4
Latitude	38º 36'10''	38º34'46''	38º35'09''	38º34'36''
Longitude	-28º43'50''	-28º43'44''	-28º46'53''	-28º47'50''
Length (m) 2X	4426	1800	2463	3102
Strike (Degree)	107	110	109	116
Dip (Degree)	50	70	90	46
Strike Slip (cm)	-54	0	145	109
Dip Slip (cm)	181	0	0	142
Traction	0	309	232	0

Initial fault parameters were based in Machado *et al*. (1962) descriptions of the May 1958 seismic crisis. In the inversion process we constrained the geometry of the dislocations sources to follow the surface traces of eruptive fissures and invert for their geometry, kinematic solutions and location. Four plane sources were used. Fault planes

laying along the fissural system west of the summit caldera were constrained to be essentially pure opening; the other two fault planes sub-parallel to the previous ones, located north and south of the system were constrained respectively as dominantly normal fault dipping south, with a minor right lateral shear component, and dominantly normal fault, dipping northward, with a minor left lateral component. These can be viewed as the collapse of the caldera, corresponding to the May 1958 seismic crises.

Source parameters obtained from inversion are presented in Table VII.2 and their projection on the horizontal plane is shown in figure VII.5.

Reduced chi-square was determined from the network adjustment (12 cm for the horizontal components). The χ 2 / n values obtained after adjustment were 0.98 assuming the aforementioned uncertainties. A misfit of 1.0 indicates that the data errors are statistically consistent with the residuals. In this case the goodness of the fit is very promising and we have a reduced chi square almost equal to 1 considering the a posteriori 12 cm standard deviation for latitude and longitude displacement components. The mean square error for the best fitting model is 14.5 cm in longitude and 13.8 in latitude, implying there is still un-modelled signal. This model explains 94% of the planimetric displacement but only 42% of the vertical displacement. The misfit is scattered throughout the network, showing residual local vertical displacements that we interpret as block falling that cannot be modelled by a simple elastic model. The model fits the summit and northwest subsidence rather well and also the large horizontal displacements along the coast. However, it underpredicts the uplift on the north flank.

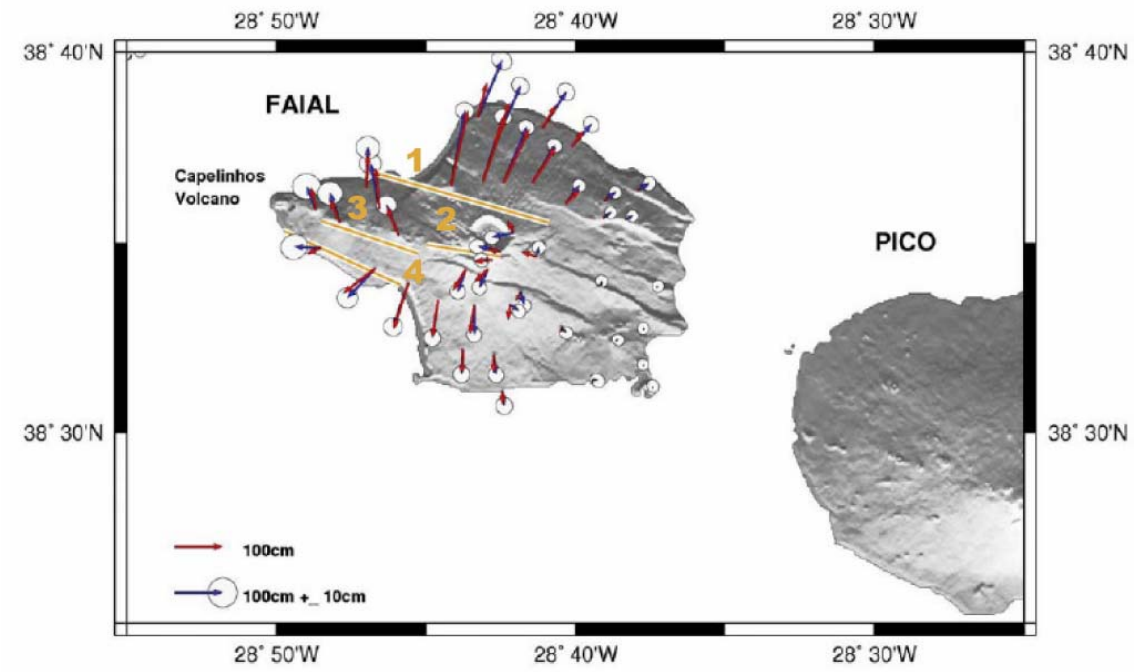

Figure VII.5 - Map of the displacements obtained from the measured geodetic network (directions and distances). Blue arrows are the observed displacements and the red arrows are the displacements computed from the forward rectangular source model with four rupturing elements.

The horizontal displacements show rapid seaward displacement in the north and south flanks with a scattered behavior over the caldera. The greatest displacements occur along the north coast. The velocity pattern around the summit is clearly influenced by a local source of deformation displacing all summit points to the west. This pattern is consistent with a dike intrusion near the summit caldera. Stations on the north flank show significant uplift of about 1 m. There is a dramatic decrease in the displacements in the south-east of Faial that correlates well with the normal fault system of Flamengos graben. The displacements in this region and on Pico Island are almost within the confidence error ellipses, indicating a non-deformated area consistent with the trilateration observations made in 1967 and the GPS observations from 1997. In fact the

eruption and the subsequent seismic crises did not affect either the east of Faial nor Pico Island.

Most of the deformation is spatially constrained to the central and western zones of Faial Island. Northern and western stations have average displacements of 1.5 m (relative to MMOC), while stations on eastern Faial and Pico show no significant relative motion. It is known (Machado *et al.,* 1962) that the eruption and associated seismic crises were hardly felt in Pico, this is confirmed by the geodetic data therefore no significant deformation has affected Pico Island since 1937.

Vertical displacements show subsidence of the north-west zone with a maximum of -1.5 m and coastal uplift on the south-west zone with a maximum of 0.5 m. This uplift along the south coast constrains the fault position and argues in favour of normal faulting along this fault. There are three stations with significant subsidence along the north-west coast.

As we have only a few occupation epochs during the whole time span we cannot completely discriminate the time variation of the displacement field. However, we know that displacements were smaller than the accuracy of conventional geodetic techniques during the 1967-97 period, and also that the magnitude of the displacements deduced from our work agree well with the independent measures presented by Machado *et al*. (1962) for the deformation generated by the 1957-58 events. We can conclude that surface displacement observed between 1937 and 1997 is mainly a consequence of a single series of events related to the Capelinhos dyke emplacement event and related eruption as suggested by our modeling procedure.

Chapter VIII - Physical models of rifting and transform faulting in a wedge-shape lithosphere

VIII.1 Introduction

Most of the physical processes that must be evoked to support tectonic interpretations in the Azores are not well understood as in the case of rifting and transform fault generation. In the Azores mantle processes which contribute for the formation of rifting in the Terceira axis and transform fault generation can be driven both by plates divergent spreading and by the Azores Hot Spot dynamics in space and time. As this interaction between the Azores Hot Spot and Azores lithosphere is not yet fully understood, physical modelling as shall be presented bellow is a usefull tool to provide constraints on the relevance of some of those factors. In this chapter we disregard plume related mantle processes and foccus our attention in ridge push as a driving force for ortogonal transform fault generation and for spreading to occur.

The way in which mantle processes contribute to plate tectonics has long been a subject for debate. After more than 30 years of studies of oceanic ridges, several objections were raised to the early views in which plate motions are fundamentally a result of mantle convection (Cox & Hart, 1986) and lithospheric plates ride passively on a moving asthenosphere. Molnar (1988) considered that flow in the asthenosphere is no

more than a trigger for plate motion. Davies (1992) suggested that plates govern the flow and that they are integral parts of the convection process. More radically, Stüwe (2002) calculated that differential stresses at the base of the lithosphere are too small to transmit forces from the asthenospheric mantle to the lithosphere. On petrologic arguments, he also concluded that the ascending paths of convective cells are not directly under oceanic ridges.

There is growing support for the idea that tectonic plates are active components of global convection. According to this view, plate tectonics are an example of self-organization (Anderson, 2001 and 2002), whereby forces at the edges of plates directly influence processes in the convecting mantle. The recognized forces are ridge push, slab pull, trench suction and basal drag (see Turcotte and Schubert, 1982). Balancing them are shearing, slab bending, friction on transform faults, and continental collision (e.g. Forsyth and Uyeda, 1975; Richter, 1977; Chapple and Tullis, 1977, Cox & Hart, 1986, Favela and Anderson, 2000).

First order oceanic transform faults tend to be geometrically simple; on the whole they are parallel to plate motions, disturbed only by significant changes in kinematic conditions (Fox and Gallo 1984 and 1986; Carbotte and Macdonald, 1994; Hey *et al*., 1995). Non-transform discontinuities also exist, but they are ephemeral, and result from local interactions (MacDonald, 1986 and 1988; Grindlay *et al*, 1991; Grindlay and Fox, 1993). Transform faults that strike at 90º to adjacent ridge segments are common in nature, for example in the Mid-Atlantic Ridge south of the Azores, the Hayes and Oceanograper Fracture Zones display such a configuration. Within the ATJ domain, there are no clear first order transform linked with the Eu-Af plate boundary, however we have here presented reported co-seismic ruptures in orthogonal planes, as shown by

Faial 1998 earthquake, and orthogonal geometrical relations is fault patterns namely in the East of Terceira Island and adjoining North Hirondelle Basin or across the LVR sectors. These geometrical relations are not accountable from classical theories of fracture mechanics.

In this chapter, we investigate the structures that are formed in ridges, straight or offset. The presence of a heavy wedge-shaped lithosphere above a buoyant asthenosphere leads to isostatic compensation, forming ridges and abyssal plains. The topography of the ridge results in ridge push. This is a driving force for extension on the ridge, as well as for transform motion at ridge offsets.

VIII.2 Background on physical models of ridges and transform faults

Physical modelling has been successful to some extent in reproducing ridges and transform faults. Oldenburg and Brune (1972, 1975) obtained good likenesses, using paraffin wax as a model material. They concluded that equivalent structures in nature result from tensile forces that originate through buoyancy forces acting in plates, rather than through underlying viscous drag.

O'Bryan *et al.,* (1975) published results based on the wax model of Oldenburg and Brune, and the Cox "tennis ball experiment" (Cox, 1973). They produced realistic ridge and transform geometries and suggested that transform faults orthogonal to the ridge would result from upward propagation of a zigzag pattern at the base of the lithosphere or top of the asthenosphere. Ragnarsson *et al*. (1996) used similar wax models to address ridge dynamics and structure. They concluded that, above a critical spreading velocity, a transient segmented ridge and orthogonal fracture zones form.

Shemenda and Grocholsky (1991, 1994) used a wax-like hydrocarbon, forcibly cooled from above, to simulate both melt and a semi-brittle upper layer subject to horizontal tension. In their experiments, a ridge resulted from an unstable, non-stationary and asymmetric three-dimensional process. They were not able to produce orthogonal transform faults, but rather transfer zones, which grew in width or ceased to be active as a function of adjacent ridge dynamics.

Dauteuil and Brun (1993) used analogue models consisting of brittle and ductile layers to study the structural pattern of the highly oblique Mohns Ridge. Mart and Dauteuil (2000) used similar layers, isostatically compensated, to model obliquely rifting systems. In both sets of experiments, the resulting fault pattern included en-echelon ridges, normal to the extension direction, and intervening zones of oblique strike slip. Mauduit and Dauteuil (1996a and 1996b) and Dauteuil *et al.,* (2002), using isostatically compensated two-layer models of sand and silicone putty, altered the lithospheric strength in the transform zone. The resulting fault zones were narrow, when the lithosphere was strong; and wider and more complex, when the lithosphere was weak. In nature, Dauteuil *et al*. (2002) concluded that spreading rates and offset lengths are the main factors controlling lithospheric strength at transform faults.

Tentler (2003) used centrifuged models, in which up-rise of lighter and weaker ductile material (an analogue for the asthenosphere) promoted passive rifting in an overlying brittle layer. In some experiments, propagating cracks interfered longitudinally and developed into "overlapping spreading centres". Tentler (2003) suggested that such overlap might lead to orthogonal ridge-transform configurations in true mid-oceanic ridges.

None of the above analogue modelling strategies has focussed specifically on the interplay between gravitational forces, rifting and the generation of transform faults between offset spreading segments. To do so we must investigate the problem by means of physical models in which the driving forces for the development of axial rifts are gravitational in origin. They come from density jumps at a dipping interface, rather than from a convecting mantle. Although in nature the role of heat is essential, in that it governs the thickness of a cooling lithosphere, we do not model its conduction or advection. Instead, we assume that, as a result of cooling and spreading, the lithosphere is a wedge of small apical angle. We test the mechanical response of such a wedge and then of an offset between ridge segments. In some experiments, the offset is purely geometrical, whereas in others we have reduced the frictional resistance by using artificially embedded faults. The underlying question is, can gravitational forces explain the common occurrence of major oceanic transform faults, which are orthogonal to adjacent ridge segments?

VIII.3 Dynamics of a spreading oceanic lithosphere

The oceanic lithosphere can be considered as a thermal boundary layer and its base as an isotherm. To calculate the shapes of isotherms, we follow Turcotte and Schubert (2002): if the oceanic lithosphere cools in the same way as a semi-infinite half-space, its temperature at a time t is given by (Turcotte and Schubert, 1982, equation 4-113, page 160):

$$(T - T_m)/(T_m - T_s) = \text{erf}\ \{z/2(\kappa\, t)^{1/2}\} \qquad (1)$$

In equation (1), the terms on the left and right are dimensionless, T is the current temperature at the base of the lithosphere, T_m is the temperature deep in the

asthenosphere (in other words, the original temperature, before cooling), T_s is the surface temperature (which we assume to be constant), z is the depth (in mm), κ is the thermal diffusivity (in $mm^2\ s^{-1}$), t is the age of the lithosphere (in s), and erf is the error function.

If the lithospheric wedge moves at a steady velocity u in a horizontal direction x, then t = x/u and equation (1) becomes the parametric equation of a parabola (Figure VIII.1). For T_m-T_s = 1200 ºK, u = 3 cm/yr and κ = 1 $mm^2\ s^{-1}$, the lithospheric segment that formed between 10 Ma and 35 Ma is up to 86 km thick and has an average basal slope of about 3º. As the lithosphere moves away from the ridge, it cools, and its density ρ increases in the following way (Turcotte and Schubert 1982, equation 4-173, page 179):

$$\delta\rho = -\rho\,\alpha\,\mathrm{d}T \qquad (2)$$

Here α is the volumetric coefficient of thermal expansion. For an initial mantle density of ρ_m = 3.3 x 10^3 kg m^{-3}, a constant coefficient of α = 3 x 10^{-5} °K^{-1}, an initial temperature of 1480 °K, and a final temperature of 280 °K, the final lithospheric density is $\rho_l \approx 3.4 \times 10^3$ kg m^{-3}.

As the lithosphere becomes heavier, it requires support. If isostatic compensation occurs in the asthenosphere, the theoretical depth w of the ocean is (Turcotte and Schubert, 1982, equation 4-202, page 182):

$$w = 2\,\rho_\mu\,\alpha\,\{(T_m - T_o)/(\rho_m - \rho_w)\}\ (\kappa x/\pi u)^{1/2} \qquad (3)$$

Here ρ_w is the density of seawater. According to this equation, the depth of the ocean increases with the square root of the distance from the ridge axis. The result is in good agreement with most observations.

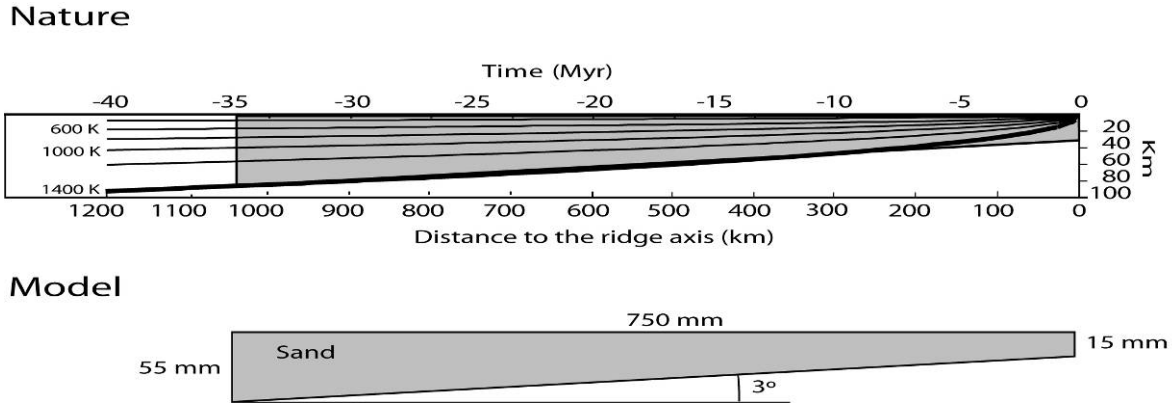

Figure VIII.1 - Thickness of oceanic lithosphere in nature and experiment. In nature (top), isotherms are for cooling of an infinite half-space (Turcotte and Schubert, 2002), moving at 3 cm/yr. Base of lithosphere is at 1400ºK. Segment of triangle (grey polygon) is approximation to true shape, for lithosphere between 10 Ma and 35 Ma. Basal slope is 3°. In experiment (bottom), sand has same triangular shape and basal slope.

The elevation of the ridge establishes a pressure head, or ridge push, which drives horizontal motion of the lithosphere. The process can be thought of as gravitational sliding. The lithospheric plate slides downward along the slope between the ridge crest and the adjoining ocean basin. By assuming that the weight of the lithosphere causes equal horizontal and vertical stresses (in other words, a true pressure) and by balancing the horizontal forces, we may predict the ridge push (Turcotte and Schubert, 1982). It is the resultant of three forces (F_1, F_2 and F_3, Figure VIII.2A). The first (F_1) results from pressure in the asthenosphere and is equal to the depth-integrated pressure (F_5) acting on a vertical plane. The second (F_2) results from pressure in seawater and is similarly equal to a depth-integrated pressure (F_4). The third (F_3) is due to the weight of the lithosphere.

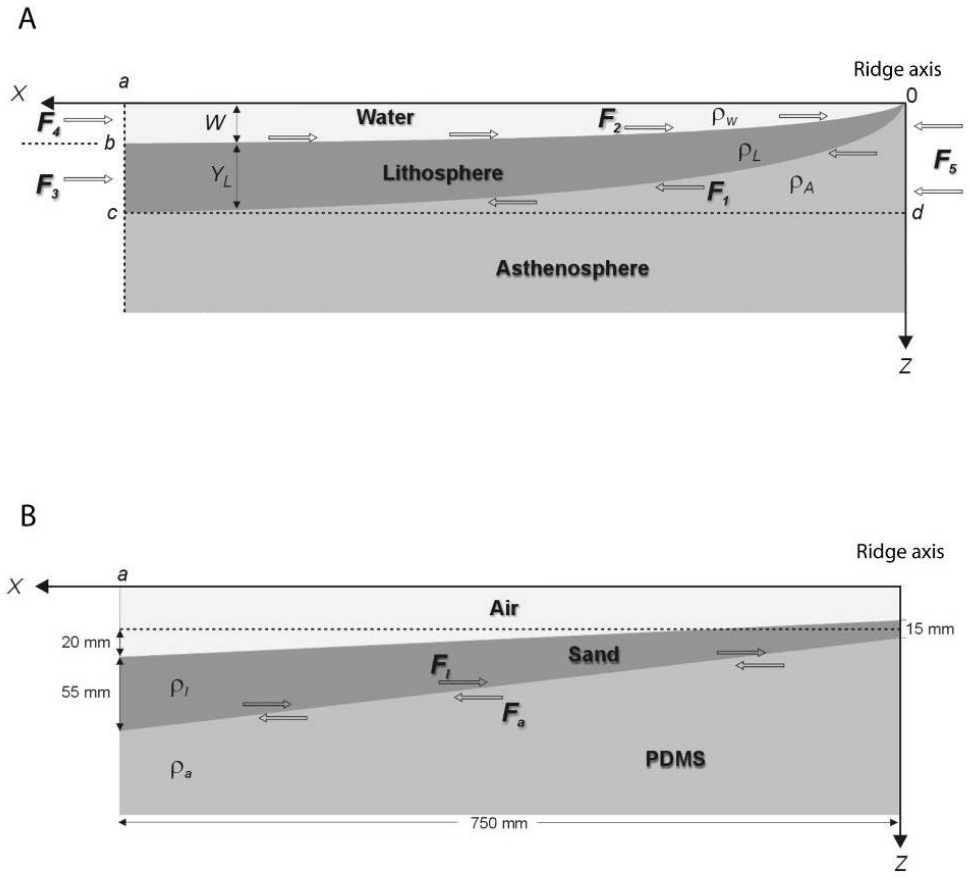

Figure VIII.2 - Theoretical subsidence and ridge push in nature and experiment. In nature (A), subsidence w is due to variable thickness (y_L) and density (ρ_L) of lithosphere, as well as density of seawater (ρ_W) and asthenosphere (ρ_A). Ridge push is resultant of horizontal forces (F_1, F_2 and F_3) acting on lithosphere. In experiment (B), air replaces seawater, lithosphere is triangular segment of sand, and asthenosphere is of PDMS. Subsidence equals one half of lithospheric thickness. Ridge push is resultant of horizontal forces (F_l and F_a) acting on lithosphere. For further details, see text.

The resultant ridge push F on the lithosphere becomes (Turcotte and Schubert, 1982, equation 6-376, page 288):

$$F = g\,\rho_m\,\alpha\,(T_m - T_o)\,\{1 + 2\,\rho_m\,\alpha\,(T_m - T_o)/\pi\,(\rho_m - \rho_w)\}\,\kappa t \qquad (4)$$

Here g is the acceleration due to gravity (9.81 m s^{-2}). According to equation (4), the ridge push is directly proportional to the horizontal distance from the ridge axis, and therefore to the age of the lithosphere. For a density of water of ρ_w = 1.0 x 10^3 kg m^{-3}, a temperature difference of 1200 °K, and values of the other parameters as before, the total ridge push on an oceanic lithosphere, which is 100 Ma old, is ca. 3.8 x 10^{12} N m^{-1} (Turcotte and Schubert, 1982, page 288). This is a force per unit length, parallel to the ridge. On a lithosphere that has moved at 3 cm/yr for a distance of 1050 km, so that it is 35 Ma old, the ridge push is ca. 1.4 x 10^{12} N m^{-1}.

If the only stress that balances the ridge push is a horizontal shear stress, acting on an area (1050 km by 1 m) at the base of the lithosphere, its magnitude is ca. 1.3 x 10^6 Pa. If the viscosity of the asthenosphere is 10^{20} Pa s (Turcotte and Schubert, 1982), the corresponding rate of shear beneath the lithosphere is ca. 1.3 x 10^{-14} s^{-1}. If the plate velocity is 3 cm/year (ca. 1 x 10^{-9} m s^{-1}), and if this attenuates linearly with depth, it must do so down to at least 130 km. As this depth is conservative for the asthenosphere, we conclude that the ridge push is sufficient to cause plate motion. Any excess ridge push is available for causing a longitudinal stress gradient in the lithosphere or for driving strike-slip motion on transform faults.

VIII.4 Model configurations and scaling

All the experiments (except Model B) were done in a wooden box, 2300 mm long, 500 mm wide and 150 mm deep (Figure VIII.3). Thin sheets of transparent polyester (Mylar) covered the walls. At the two ends of the model were motor-driven L-shaped pistons, 90 mm high and 500 mm wide. They rested and could slide on end walls, 60 mm high and 1500 mm apart.

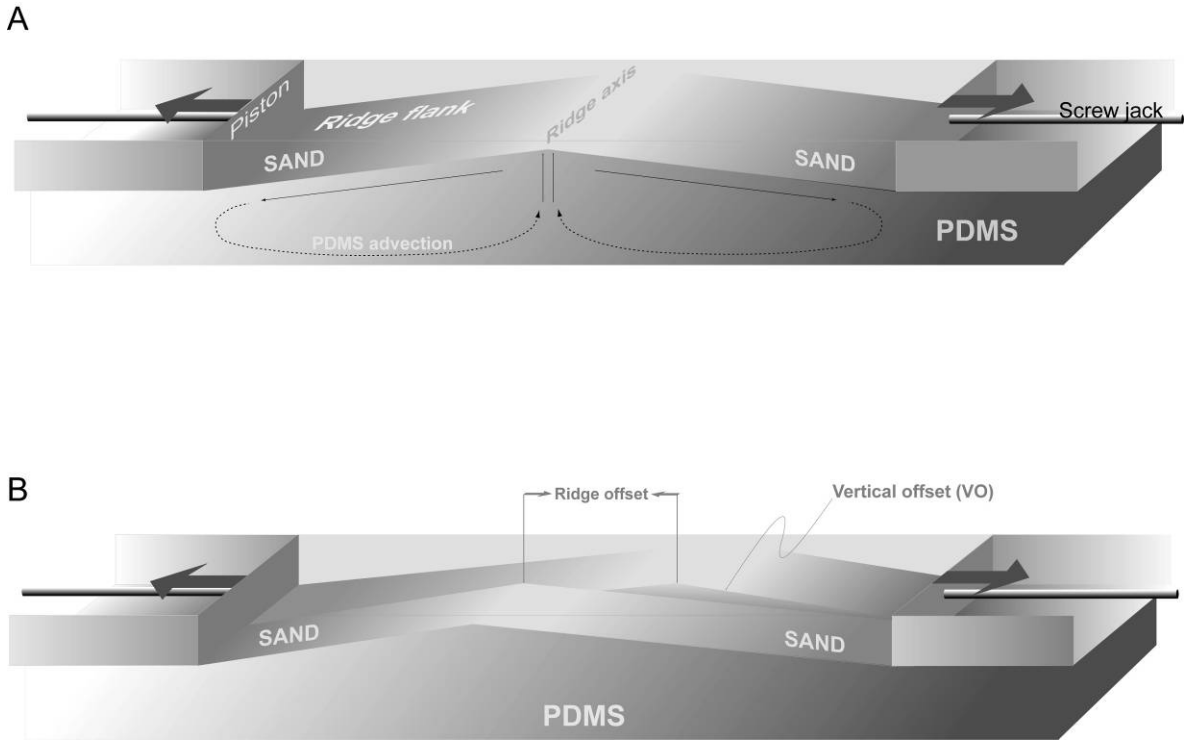

Figure VIII.3 - Experimental configuration (in schematic oblique view). Models consist of only one spreading ridge (A), or of two spreading ridges (B) and one orthogonal vertical offset (VO). Model lithosphere (sand) rests on model asthenosphere (PDMS).

The model materials were (1) dry quartz sand from Fontainebleau, France, for the lithosphere and (2) transparent silicone polymer, polydimethylsiloxane (PDMS), for the asthenosphere. These materials are readily available and their properties are well known. The sand yields according to Coulomb criterion: the angle of internal friction is about 40° and the cohesion is negligible (see Mourgues and Cobbold, 2003). The PDMS is a Newtonian fluid and its viscosity is about 10^4 Pa s.

Our models took no account of heat advection, thermal contraction, or consequent variations in density. Instead, the density of the model lithosphere was constant, as was that of the model asthenosphere. The density of the sand was approximately 1.5 x 10^3

kg m^{-3} and that of the PDMS was about 1.0 x 10^3 kg m^{-3}. Thus the density ratio was 1.5 - far greater in the models, than it is in nature. As we shall see later, this high viscosity ratio led to abnormally high values of isostatic subsidence and ridge push.

We did seven experiments, in two basic layouts: (1) a single symmetric ridge with no offset (models A, C and D; Table VIII.1 and Figure VIII.3A), and (2) two ridge segments, trending N-S and offset E-W, with or without an embedded fault (models E, F and G; Table VIII.1 and Figure VIII.3B).

Table VIII.1. Model configuration.

Model	*Configuration*	*Objectives*	*Results*
A	**Symmetric single ridge**	Effects of friction at side walls	Figure 5
B	**Half-ridge**	Velocity during unrestricted gliding	Figure 7
C	**Symmetric single ridge** (lithospheric thickness: 10 mm)	Style of axial rifts as function of lithospheric thickness	Figure 8
D	**Symmetric single ridge** (lithospheric thickness: 20 mm)	Style of axial rifts as function of lithospheric thickness	Figure 8
E	**Ridge-transform-ridge** (no embedded transform fault)	Development of transform faults	Figure 9
F	**Ridge-transform-ridge** (planar rigid embedded transform fault)	Development of transform faults	Figure 10
G	**Ridge-transform-ridge** (flexible long embedded transform fault)	Development of transform faults	Figure 11

We adopted a model ratio of length, $L_r = L_m / L_n$ that was nominally equal to 7 x 10^{-7} (Table VIII.2, Figure VIII.1). From nature to model, all stresses necessarily scaled down by a factor of $\sigma_r = \rho_r L_r$. Taking $\rho_r \approx 0.45$ for the lithosphere, and $L_r \approx 7 \times 10^{-7}$, we obtain a stress ratio of $\sigma_r \approx 3.2 \times 10^{-7}$. In nature, the viscosity of the asthenosphere is of the order of $\mu = 10^{20}$ Pa s. As the viscosity of the PDMS is of the order of 10^4 Pa s, the viscosity ratio for our experiments was $\mu_r = 10^{-16}$. From this and the stress ratio, the time

ratio was $t_r \approx 3.1 \times 10^{-10}$ (1 second in an experiment was equivalent to about 100 years in nature; 100 hours were equivalent to about 37 Ma).Thus the velocity ratio was $u_r = L_r/t_r \approx 2.3 \times 10^3$ (0.13 mm/minute in an experiment were equivalent to 3 cm/year in nature). Finally, because ridge push has dimensions of N m^{-1}, its model ratio, in principle, was $F_r = \sigma_r L_r \approx 2.2 \times 10^{-13}$. In practice, the ridge push was abnormally high in the models, as will be explained later.

Table VIII.2. Parameters and scaling.

Parameter	***Length***	***Viscosity***	***Lithosphere Density***	***Basal Shear Stress***	***Time***	***Velocity***	***Ridge Push***
Symbol/units	L /mm	μ /Pa s	ρ_l / kgm^{-3}	σ /Pa	t /s	u / ms^{-1}	F / Nm^{-1}
Value in model	750	$1x10^4$	$1.5x10^{-3}$	0.416	1	$2.3x10^{-6}$	0.3
Value in nature	1050×10^6	$1x10^{20}$	$3.3x10^{-3}$	$1.3x10^6$	$3.2x10^9$	$1x10^{-9}$	$1.4x10^{12}$
Ratio (derivation)	$L_r=L_{model}/L_{nature}$	$\mu_r=\mu_{model}/\mu_{nature}$	$\rho_r=\rho_{model}/\rho_{nature}$	$\sigma_r=\rho_r L_r$	$t_r = \mu_r/\sigma_r$	$u_r= L_r/t_r$	$F_r = \sigma_r L_r$
Ratio (value)	$7x10^{-7}$	$1x10^{-16}$	0.45	3.2×10^{-7}	$3.1x10^{-10}$	2.3×10^3	2.2×10^{-13}

VIII.4.1 Models of straight ridges

To make these models, first the PDMS surface was shaped into a single linear symmetric ridge (Figure VIII.3A). The height of the PDMS was 100 mm at the ridge axis and it decreased linearly to 60 mm at the end walls. A layer of Fontainebleau quartz sand was laid over the PDMS and its upper surface was scraped horizontal. The thickness of the sand wedge was therefore ca. 55 mm against the pistons and ca. 15 mm at the ridge axis (except in models C and D, where it was ca. 20 mm and 10 mm, respectively). The model wedge, on each side of the ridge, was 750 mm long and 500 mm wide, representing a prototype wedge that was 1050 km long, 700 km wide and up to 86 km thick. In cross-section, the wedge was triangular and its apical angle was close

to 3°. This was a simplification that made it easier to construct the models. The underlying PDMS represented an asthenosphere, 164 km deep.

In a matter of minutes after construction the shape of the model changed as a result of isostatic compensation. At the axis, where the heavy lithosphere was relatively thin, the upper surface rose. On the flanks, where the lithosphere was thicker, it sank. However, at the lateral boundaries, the lithosphere did not move, because it was in dry frictional contact with the sidewalls and end walls. Nowhere did the model asthenosphere have the opportunity to extrude, as a result of the pressure that the heavy lithosphere exerted upon it.

For ideal isostatic compensation of a perfectly triangular wedge, the subsidence w is directly proportional to the thickness h of the model lithosphere and to the density ratio:

$$w/h = \rho_l/\rho_a - 1 \qquad (5)$$

In a perfectly triangular wedge, where the density is 1.5 x 10^3 kg m^{-3} for the lithosphere and 1.0 x 10^3 kg m^{-3} for the asthenosphere, the theoretical subsidence is one half of the lithospheric thickness. In our models, which were segments of triangular wedges, the theoretical subsidence was w ≈ 27.5 mm at the far end, and w ≈ 7.5 mm at the near end (Figure VIII.2B). Thus the theoretical relief was 20 mm, representing an abnormal value of almost 30 km in nature.

In a perfectly triangular wedge, the ridge push F is equal to the difference between the vertically integrated pressures in the asthenosphere (F_a) and the lithosphere (F_l):

$$F = F_a - F_l = g\rho_a\int^{h+w} z\,dz - g\rho_l\int^{h} z\,dz = (g/2)\{\rho_a (h + w)^2 - \rho_l h^2\} \qquad (6)$$

Substituting equation (5) into equation (6), we obtain, for the theoretical ridge push on a triangular wedge:

$$F = (g/2)\,(\rho_l/\rho_a)\,(\rho_l - \rho_a)\,h^2 \qquad (7)$$

For the same densities as before and for a wedge segment, the ends of which are 55 mm and 15 mm thick, the estimated ridge push at the far end is ca. 10.3 N m^{-1}. However, in our models it may have been smaller than that, because sidewall friction impeded full isostatic compensation.

Because ridge push has dimensions of N m^{-1}, it should scale down by a factor of $F_r = \sigma_r L_r \approx 2.2 \times 10^{-13}$. As the ridge push in the prototype is ca. 1.4×10^{12} N m^{-1}, in the model it should have been ca. 0.3 N m^{-1}. The estimated value (10.3 N m^{-1}) was about 30 times greater, partly because of the triangular shape of the model lithosphere, but mainly because of the abnormal density contrast and consequent topographic relief.

VIII.4.2 Models of offset ridges

In the second layout (models E, F and G), the ridge was offset vertically and orthogonally (Figure VIII.3B). To construct the models, the PDMS surface was shaped into two N-S ridges. The amount of offset was 300 mm. The ridges were asymmetric, the apical angles being ca. 2.2º for the short flank and ca. 5º for the long flank. These dimensions were for convenience in constructing the models. However, they meant that the lithospheric thickness was over-estimated on the short flanks and underestimated on the long flanks.

There were three variants to the layout (Figure VIII.4).

In Model E, there was a vertical offset, but no embedded fault (Figure VIII.4A).

In Model F, there was an embedded fault, consisting of two Mylar sheets and an intervening thin glass plate (Figure VIII.4B). The Mylar sheets spanned the distance (300 mm) between the two ridge segments. Downward, they penetrated no more than 5 mm into the PDMS. Upward, they reached into the sand as much as 5 mm above the ridges. The glass plate was also 300 mm long, but it reached the bottom of the box.

In Model G, there was an embedded fault, consisting of two longer Mylar sheets, but no intervening glass plate. One end of each sheet was at a ridge axis, whereas the other end went well beyond the other ridge axis (Figure VIII.4C). Between the ridges, the Mylar sheets were in mutual contact, whereas beyond the ridges they were in contact with PDMS or sand.

The Mylar sheets were in dry frictional contact, with each other (Model G), with the glass plate (Model F) and with the sand. Although for these contacts we did not measure the frictional resistances, we observed that they were less than the internal friction of the sand. In contrast, all materials adhered strongly to the PDMS. In Model F, the glass plate rendered the embedded fault inflexible.

In a matter of minutes after construction, the shape of the model changed, as a result of isostatic compensation. At the ridge axes, where the heavy lithosphere was relatively thin, the upper surface rose. On the flanks, where the lithosphere was thicker, it subsided. At the lateral boundaries, the lithosphere did not move, because it was in dry frictional contact with the sidewalls and end walls. For similar reasons, uplift was less pronounced along the trace of the ridge offset, than it was on the ridges or their immediate flanks.

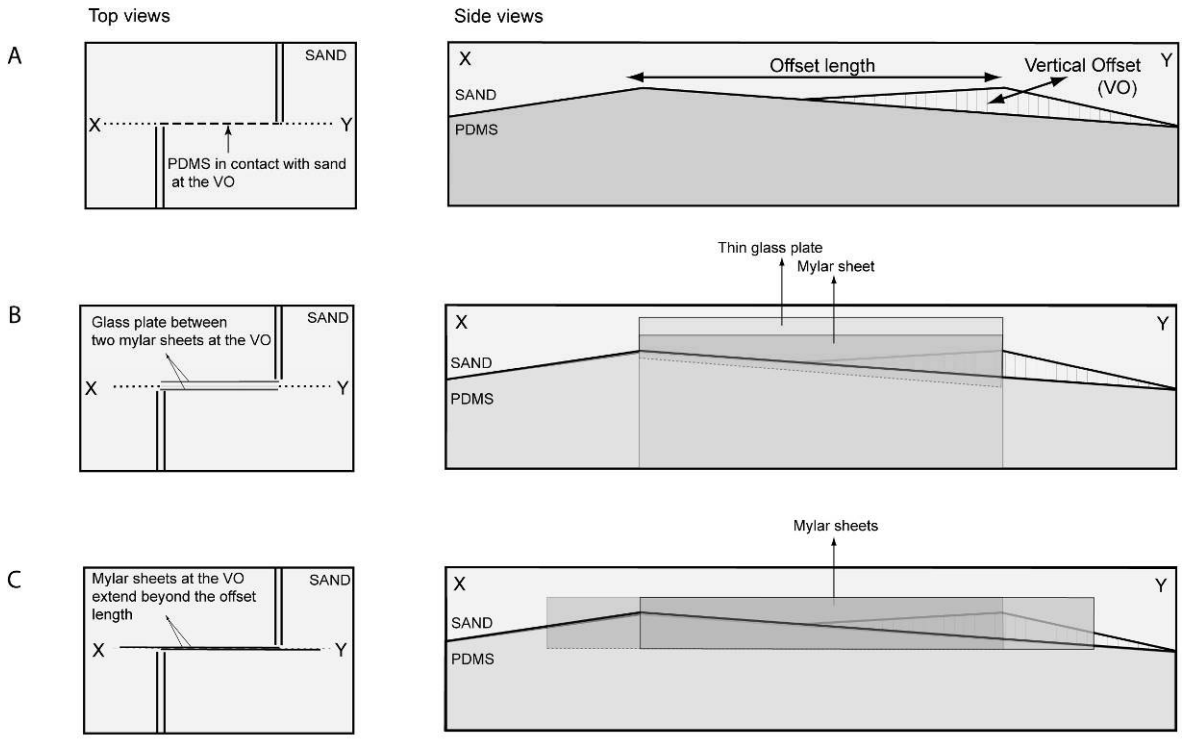

Figure VIII.4 - Three initial kinds of transform fault in models (top views and side views). In Model E ridge has vertical offset and there is no embedded fault (A). In Model F, embedded fault consists of two flexible Mylar sheets and one intervening thin glass plate (B). In Model G, Mylar sheets extend beyond offset and there is no glass plate (C). All interfaces are in dry frictional contact, except against PDMS.

VIII.5 Experimental results

VIII.5.1 Model A. Half-ridge, unconfined gliding, sidewall friction (Figure VIII.5).

In Model A, the lithosphere consisted of a single ridge flank. As long as the end walls provided confinement, the lithosphere did not move. However, when the experimenter removed part of the wall, at the far end of the box, the lithosphere glided down slope. As a result, normal faults formed in the axial region (Figure VIII.5). However, the sand was in dry frictional contact with the plastic sidewalls and the PDMS adhered to them strongly. This lateral resistance resulted in shear zones, containing Riedel faults.

To reduce the sidewall friction, we fixed four Mylar sheets (Mylar 1, Figure VIII.6) to the end walls, in such a way that they ran along the sidewalls. Another four Mylar sheets (Mylar 2) were fixed to the sidewalls, but in lower positions, so that they partly overlapped the upper sheets. On withdrawing the end walls and the attached upper Mylar sheets at a constant rate of 20 mm/hr, we found that no shear zones developed against the sidewalls.

VIII.5.2 Model B. Unconfined gliding, no sidewall friction.

Model B was built outside the apparatus, on a rigid plate dipping at 3°. The model consisted of a triangular wedge of sand, resting on a layer of PDMS, 3 cm thick. All lateral boundaries were free. Under its own weight, the lithosphere glided down slope. The experiment lasted one hour.

The upper part of the model glided slowly, whereas the lower part glided more rapidly. As a result, the entire model was subject to extension. The velocity at a point in the centre of the model increased slowly, up to a value of about 120 mm/hour (Figure VIII.7).

VIII.5.3 Models C and D. Straight ridges, confined gliding, limited sidewall friction

In models C and D, a piston moving at 10 mm/hour limited the rate of gliding of the model lithosphere. The result of gliding was extension in the ridge axis (Figure VIII.8). When the extension had reached 1%, an axial rift formed. To avoid the PDMS welling up unduly and to simulate the formation of oceanic crust by cooling, we deposited thin layers of sand episodically in the axial rift. The thickness of this sand exerted a strong control on the development of extensional faults in the axial rift.

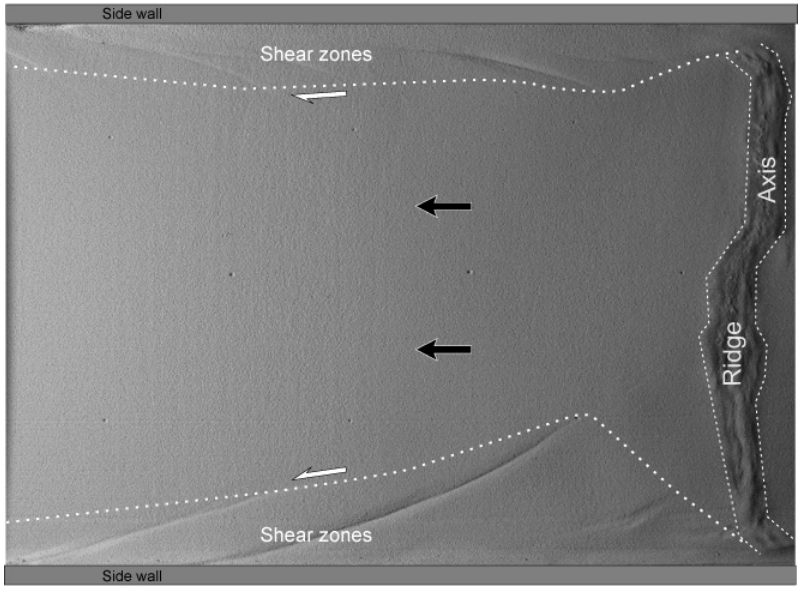

Figure VIII.5 - Unconstrained gliding and effect of sidewall friction, Model A. Photograph is from top. Ridge push caused spreading in ridge (right), rigid gliding of ridge flank (arrows) and lateral shearing, due to sidewall friction.

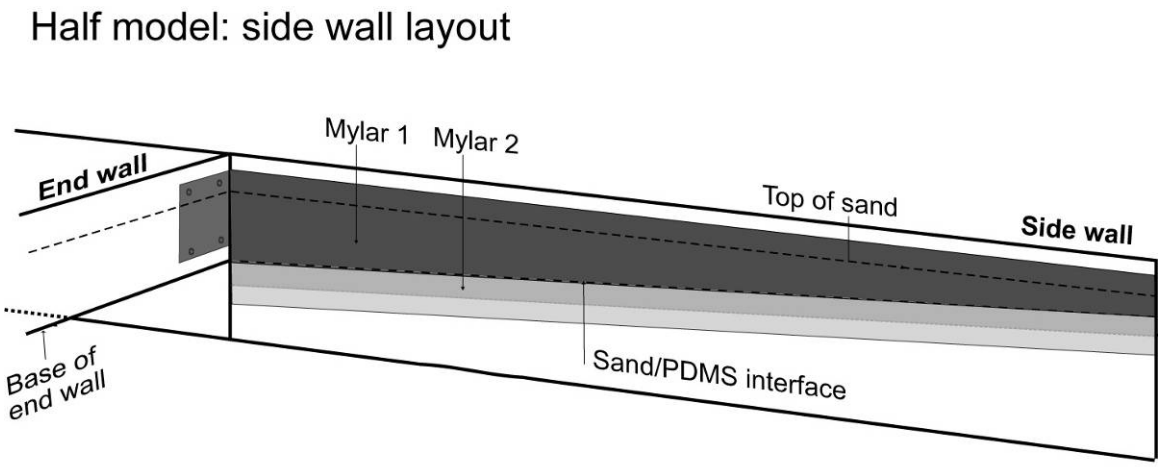

Figure VIII.6 - Use of Mylar sheets to reduce sidewall friction (schematic oblique view). Mylar 1 (dark grey) is attached to piston and moves with it, sliding between sidewall and Mylar 2 (semi-transparent light grey). Top of Mylar 2 is at same height as interface between sand and PDMS.

In Model C, the thickness of sand in the axial rift did not exceed 10 mm (Figure VIII.8). Extensional faults were irregular in strike and they were not sharp. Early faults soon became inactive and new faults took over from them, but the pattern remained irregular.

In Model D, the thickness of sand in the axial rift reached 20 mm. Extensional faults were sharper and more regular in strike. The amount of slip on the faults was also greater. In the early stages of deformation, two major faults were active, defining a valley. Later, these faults rafted out and became inactive. New faults formed on the ridge axis, where the extension concentrated. Thus the final result was a series of parallel normal faults, of which only the innermost ones were active.

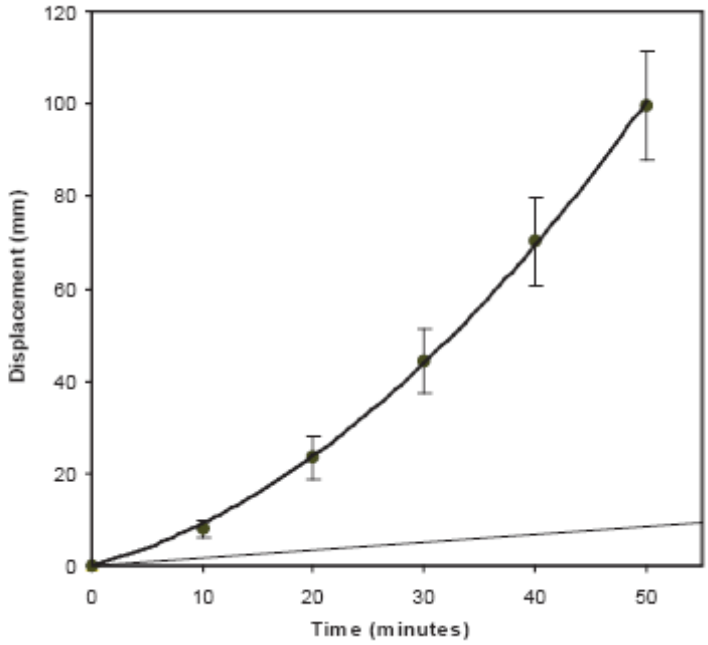

Figure VIII.7 - Displacement versus time for unconfined gliding, Model B. Data points are for average displacement of ridge flank. Error bars are standard deviations for each time interval (10 minutes). Velocity attained 2 mm/minute. In confined gliding (thin line), piston moved much more slowly (0.2 mm/minute).

VIII.5.4 Model E. Offset ridge, no embedded fault

In model E the ridge was offset laterally by 300 mm. However, there was no embedded fault. As before, normal faults formed along the axis of each ridge segment (Figure VIII.9). Normal faults propagated towards the offset trace (OT), curving into it, and parallel to the topographic gradient. A broad transform zone (TZ) developed. Initially, the zone contained two left-lateral Riedel faults, at 17° to the offset trace. These developed into normal faults, bounding oblique transform valleys. At ca. 0.7% of axial extension, a left-lateral strike-slip fault formed almost at right angles to the ridge axis (arrow, Figure VIII.9). However, the entire transform zone continued to be active and it remained oblique to the offset trace. The structures were typical of a trantensional context and did not resemble a sharp transform fault, as occurs in nature.

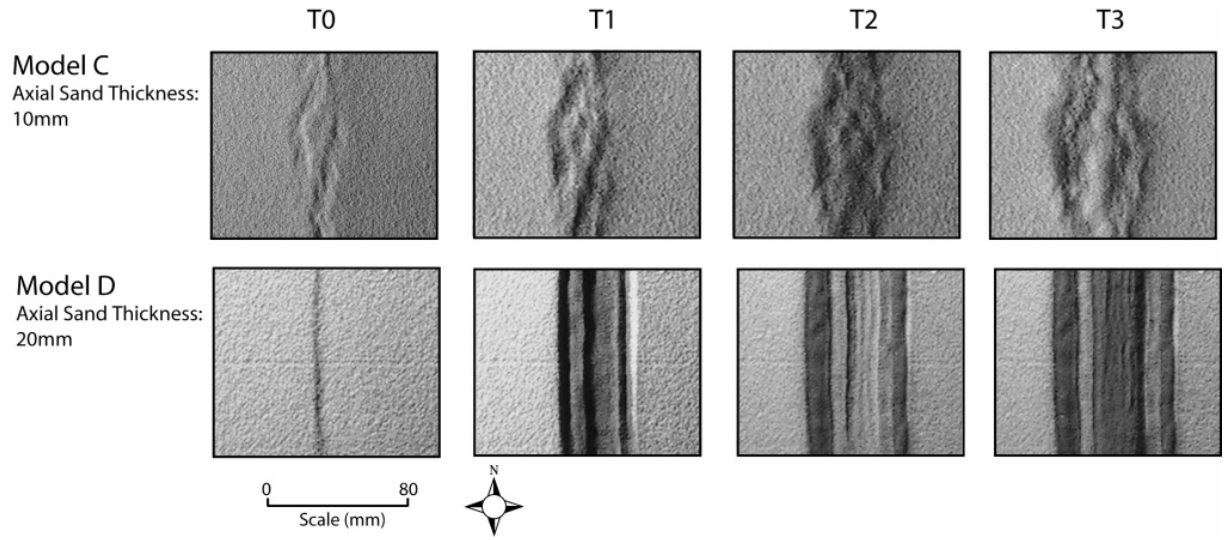

Figure VIII.8 - Progressive development of ridge, models C and D (no offset). Photographs (from top) show four stages in development of relief. Initial thickness of sand in ridge was 10 mm (Model C) or 20 mm (Model D).

VIII.5.5 Model F. Offset ridge, rigid planar embedded fault (Figure VIII.10).

In Model F, the embedded fault consisted of two Mylar sheets and an intervening glass plate. The fault was therefore rigid and inflexible, but it allowed slip. At ca. 5.1%, 6% and 7.2% of axial extension, sand was added to depressions in the transform zone (Figure VIII.10).

In the initial stages of the experiment, two axial rifts formed, as before. However, this time the rifts propagated as far as the offset trace, remaining straight. At about 0.6% of axial extension, a narrow transform zone appeared, on one side of the offset trace, and at about 79º to the ridge axis. It contained two left-lateral faults. At about 5% of axial extension, the southern fault propagated eastward, intersecting the outer bounding fault of the axial rift (arrow 1, Figure VIII.9), whilst the northern fault splayed and propagated westward. A pure left-lateral strike-slip fault (arrow 2, Figure VIII.9) cut across the transform zone. At ca. 6.7% extension, a new oblique-slip fault (left-lateral normal) formed on the northern side of the transform zone (arrow, Figure VIII.9, 6.7% extension). Thus the transform zone became straighter, but it remained oblique to the offset trace. Again, the structures were typical of trantension, as in Model E.

VIII.5.6 Model G. Transform with long flexible embedded fault

In Model G, the embedded fault consisted of two Mylar sheets but no glass plate. The fault was therefore inextensible but flexible.

In the early stages of the experiment two axial rifts formed as before. Again, they propagated as far as the offset trace, remaining straight. However, this time a single, discrete fault formed along the offset trace, at right angles to the ridge axis (Figure

VIII.11A). The fault slipped steadily and there were no appreciable changes in its position

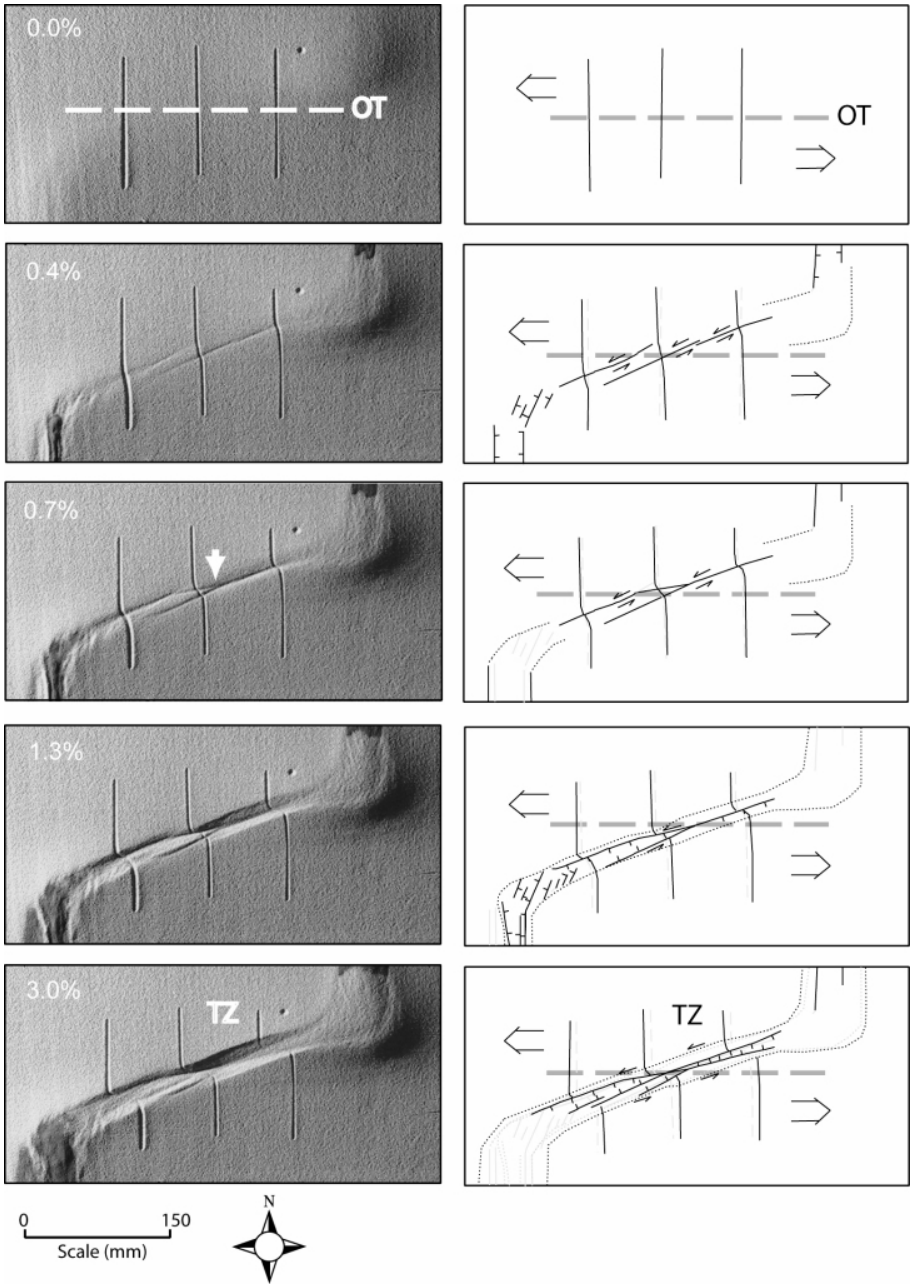

Figure VIII.9 - Progressive development of transform zone, Model E (offset ridge, no embedded fault). Photographs and line drawings show five stages in development of faults and in displacement of surface markers. Percentages (top left) are for extension normal to ridge axis. Dashed grey lines indicate original trace of offset (OT). Arrow indicates appearance of left lateral strike-slip fault within transform zone (TZ). Initial ridge offset was 300 mm.

In the early stages of the experiment two axial rifts formed as before. Again, they propagated as far as the offset trace, remaining straight. However, this time a single, discrete fault formed along the offset trace, at right angles to the ridge axis (Figure VIII.11A). The fault slipped steadily and there were no appreciable changes in its position or orientation. No strike-slip motion occurred elsewhere. Such a kinematical configuration is typical of transform faults in nature (Figure VIII.11B)

VIII.6 Discussion

VIII.6.1 Straight ridges

In the experiments, horizontal ridge push resulted in lithosphere gliding and the development of axial rifts. It is likely that ridge push caused a component of horizontal compression, which was insufficient to generate reverse faults, but sufficient to obstruct the formation of extensional structures, other than the axial rifts. Thus the experiments yielded realistic structures and kinematics, which were closely comparable to those in nature.

In the experiments, both the magnitude of the ridge push and the velocity of gliding were an order of magnitude too large, as compared with the values obtained from scaling. The exaggerated values were almost certainly due to the strong contrast in density between model lithosphere and asthenosphere. Despite these exaggerations, the experiments confirmed that ridge push is capable of (and sufficient for) driving plate motion and generating axial rifts. There is no need to invoke other forces, coming for example from thermal convection in the asthenosphere. However, this does not mean that some such additional forces do not exist in nature.

In the experiments, the shapes of the axial rifts depended on the thickness of sand. Where the axial sand was thin (so that the asthenosphere was shallow), the ridge was an area of distributed extensional deformation, where bounding faults were short-lived and had small scarps; where the sand was thick, the axial rift was straight and wide, and the two bounding faults were long-lived, taking up most of the extension and developing prominent scarps. On the Mid-Atlantic ridge, faults have a similar pattern (Shaw and Lin, 1993), which has been interpreted as a function of the thermal regime. In cold domains at the ends of ridge segments, the lithosphere is thick and strong, and faults are long- lived. In contrast, at the segment centres, where the lithosphere is weaker and thinner, faults are closely spaced and short-lived, and they have smaller displacements.

There are several explanations for abyssal hills on ridge flanks (see Edwards *et al.*, 1991 and references therein). Amongst the possible structures are half-grabens, resulting from block tilting.

In Model D, fault blocks rafted away from the active axial domain and became tilted, between faults dipping toward the ridge axis. Thus Model D accounts well for the structural fabric of abyssal hills in nature.

VIII.6.2 Offset ridges

In Model E, where the thickness of the lithosphere was offset and the ridge push acted in opposite senses on each side, why did a transform fault not form at 90º to the ridge axis? We suspect that various factors worked against it. First, the amount of isostatic uplift was smaller at the offset ends of the ridges, than it was elsewhere along them. Therefore the ridge push must have attenuated toward the offset trace. Second, the

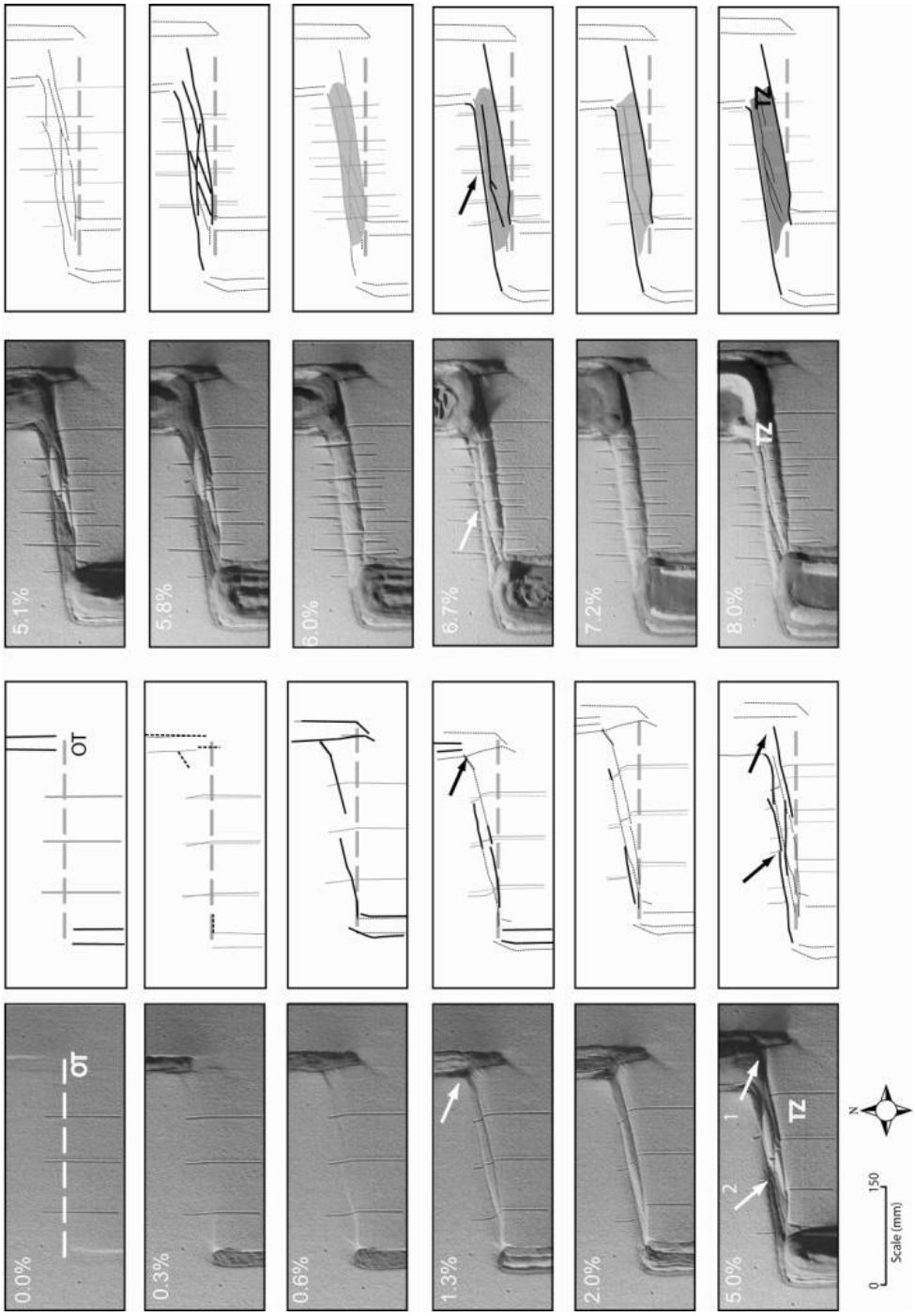

Figure VIII.10 - Progressive development of a transform zone, Model F (offset ridge, planar rigid embedded fault). Photographs and line drawings show twelve stages in development of structures and in displacement of surface markers. Percentages (top left) are for average extension normal to ridge axis. Dashed grey lines indicate original trace of offset (OT). Arrows refer to structures described in text. Thick black lines indicate newly formed faults. Grey lines indicate faults that formed in preceding stage. Grey polygons enclose areas of sedimentation. Initial ridge offset was 300 mm.

model lithosphere was as strong along the offset trace as it was elsewhere. Therefore the shear force due to ridge push may have been insufficient to cause failure in strike-slip mode, parallel to the offset trace. In contrast, transtensional failure along an oblique transform zone, linking the more uplifted segments of the ridges, may have occurred more readily.

In Model F, where a rigid planar fault was embedded within the ridge offset, why did a transform fault not form at 90º to the ridge axis? We suspect that the reasons are similar to those for Model E. Even though the embedded fault was potentially less resistant to slip than the non-ruptured sand, we believe that transtensional failure on an oblique transform zone occurred more readily than strike-slip along the embedded fault. That the oblique zone formed to one side of the offset trace, instead of crossing it, may have been because the glass plate was rigid. The reduction in available space may have forced the transform zone to form at a higher angle to the ridge than it did in Model E.

In Model G, the Mylar sheets slipped readily but they were inextensible. No oblique zone could crosscut them; but why did one not form to the side, as in Model E? We suspect that isostatic uplift occurred all along the ridges, as far as the embedded fault, which may have slipped vertically at that stage. This may have happened all the more readily that the embedded fault reached well onto the outer flanks of the ridges. Thus the resulting relief may have been more similar to what it is in nature, where it forms incrementally. Once the relief was of the required shape, the distribution of ridge push may have been sufficient to cause slip on the embedded fault.

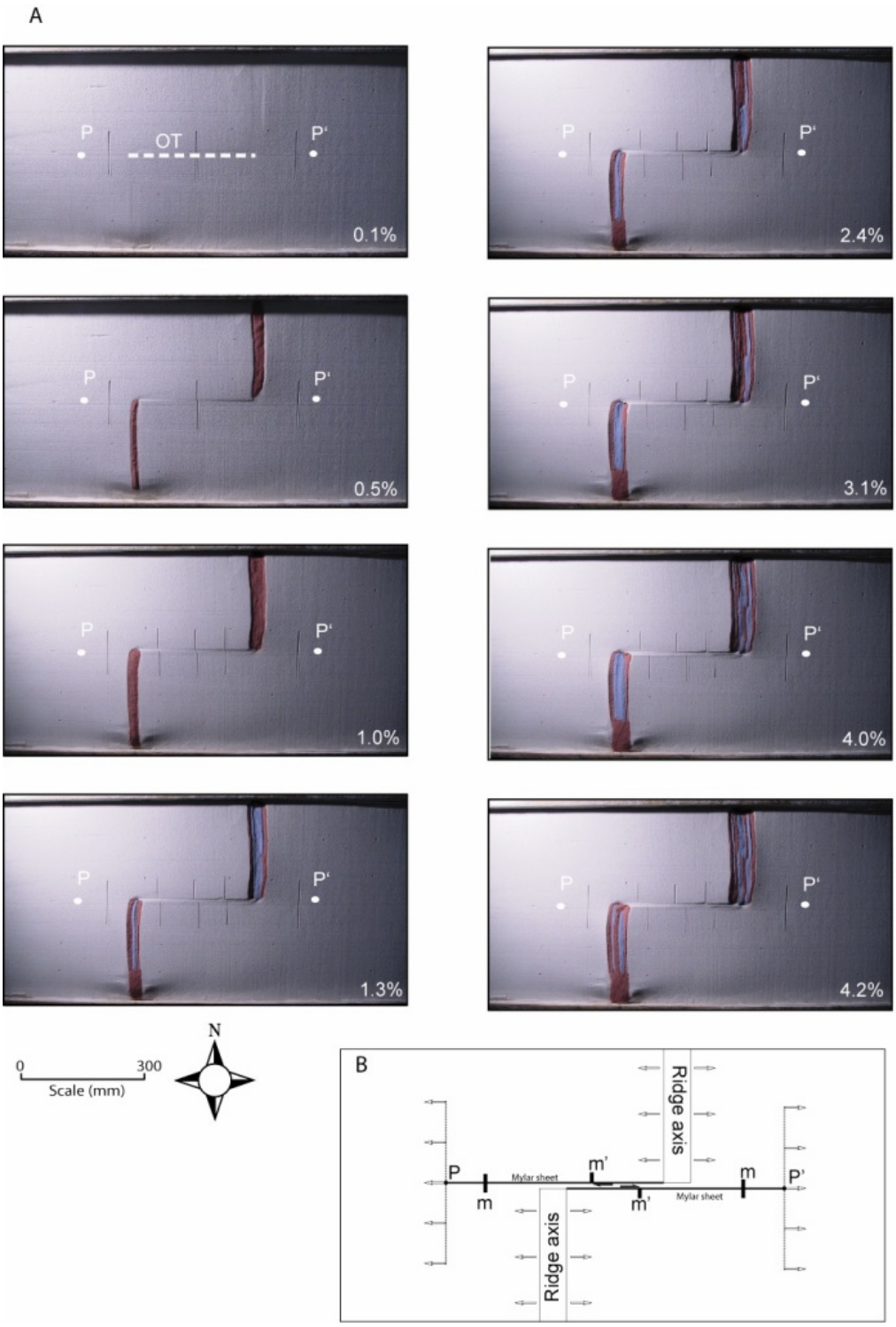

Figure VIII.11 - Progressive development of transform zone, Model G (offset ridge, flexible embedded fault). Photographs (A) show eight stages in progressive development of structures and in displacement of surface markers. Diagram (B) illustrates kinematical aspects. Initial offset of ridges was 300 mm. Points (P and P') mark ends of Mylar sheets, beyond offset trace (OT). During deformation, distance P -P´ increased, external marker lines (m) underwent no offset, and internal marker lines (m') became offset across transform fault.

In nature, although the brittle upper crust is relatively strong, well-formed faults appear to be very weak (Sibson, 1994; Scholz, 1996; Behn *et al.,* 2002). In particular, the resistance to slip along transform faults is considered to be extremely small (Zoback, 1991). However, the reasons for this are not entirely clear. Various possibilities have been suggested.

The coefficient of internal friction is smaller in the fault gouge than it is in the wall rock (Parsons, 2002).

As a result of fluid overpressure (Byerlee, 1990) or seepage forces (Mourgues and Cobbold, 2003), the effective stresses in the fault zone are smaller than they are outside.

Transform faults form at the onset of cooling and they remain weak, as a result of thermal contraction (Collette, 1974; Turcotte, 1974).

A biaxial stress field promotes extension and fault unlocking in a direction parallel to the ridge axis (Zoback, 1991; Gudmundsson, 1995).

Long-term interaction with other faults ("fault unclamping") reduces the normal stress on a transform fault (Parsons, 2002).

Presence of serpentinites within the principal transform displacement zone or at ridge transform intersections (Escartin *et al.,* 1997, Hirth *et al., 1998*, Escartin *et al.,* 2001b).

Our experiments do not provide any clues as to which of these potential mechanisms operates in nature. However, the experiments do indicate that transform faults must be weaker than the surrounding oceanic lithosphere.

Chapter IX – Discussion and main conclusions

The Azores are a region subject to a unique geodynamic setting in the world, it comprises: An area of anoumously thick oceanic crust expression of a non-conventional Hot Spot, an unstable triple Junction, geometrically and kinematically complex, and a plate boundary which displays the slowest spreading rate in the world ridge system.

During the course of this work, we analysed the spatio-temporal variability of the large and small scale processes which interact in the Azores domain, these can be broadly systematized as ATJ-AHS for large spatio-temporal scales (Plateau scale) and in seismo-tectonic and volcano-tectonic events for smaller spatial working scales (Islands and surrounding deeps) at the present day.

For the large scales, we discussed possible scenarios of interaction between the ATJ and the AHS through time as described independently by different authors for the kinematic evolution of the Azores. We focused on interpreting possible tectonic scenarios for the generation of the plateau main morpho-tectonic features, and study possible positions and tectonic natures of the ATJ along a time span comprising the age intervals: 33 Ma to 20 Ma; 20 Ma to 10 Ma and 10 Ma to present.

For the smaller temporal scales we used multidisciplinary data with different resolution to gain insights on the dynamics of the volcano-tectonic systems in the Azores. We

approached the Terceira axis as a spreading system and we studied its behaviour with respect to GPS derived kinematics. Two configurations for the Terceira axis segmentation were tested by means of elastic half space dislocation modelling. The detailed tectonics of Terceira Island and some insights on the morpho-structure of neighbouring segments was achieved, using mainly the conjugate analysis of side scan sonar images, magnetic charts and when available detailed swath bathymetry data. Finally, we considered seismo-tectonic and geodetic data and results from a recent series of volcanic and tectonic events to constrain how magmatic accretion couples with far-field tectonic regimes interact in the Azores domain.

Our main conclusions can be summarized as follows:

IX.1 ATJ Evolution

The existence of a kinematic independent Azores domain seems to have occurred long before the interaction of the Azores plateau with the AHS, and is at least older than C13 (33.4 Ma). An estimation of the tectonic character acting through the plateau at different time intervals varies according to the kinematic model choosen but yield transtension or oblique extension as the most favourable tectonic regimes along the time span considered. This result is supported by the poor ATJ closure obtained using published kinematic poles. Considering NAM/AF finite rotation poles, the EAFZ can be approached as the structural homologue of the Pico FZ this conclusion is not corroborated by analougous EU/NAM rotations. Therefore if this structure acted as a southern plate boundary (South Azores Triple Junction - SATJ) for most of the evolution of the Azores plateau. The southern edge of stable Eurasia (here referred as the North Azores Triple Junction - NATJ), could be defined along some structures

(ETVR, S. Miguel Island) as precursors of the current continuous Terceira axis as a discrete plate boundary. We are not able to provide an age estimate for the Terceira Axis nucleation. Given the amount of extension estimated for the time span using EU-AF stage poles, probably this structure did not act as a stable plate boundary for the time span considered, and therefore it has been distributed across the Azores plateau.

Strong interaction of the SATJ with the AHS started probably at C6 times (20 Ma) according to the models referred in this study. After a period of intense melt production and topography build-up which reached a maximum at C5, rifting of the Azores plateau and onset of normal seafloor spreading begun around 7 to 4 Ma as defined in those models. BetweenC6 and C5 (ca. 15 Ma) the SATJ departed from the EAFZ (from an intra-transform context) northwestwards as suggested also by Vogt and Jung (2003).

The Linear volcanic ridges that define the internal morpho-structure of the plateau are sub-parallel to the SATJ migration path and to the current Terceira axis segmentation pattern. Three different mechanisms can be evoked to justify their growth:

1) simultaneous growth by reactivation of fracture zones as leaky transforms. 2) diachronical growth due to the AHS migration northward. 3) Diachronical growth due to SATJ migration from an intra-transform setting. A schematic representation of these three hypotheses is presented in Figure IX.1.

Reactivation of MAR fracture zones in the Azores plateau, seems a plausible explanation for the LVR in sector 1, given their orientations, but seems to be less applicable to the LVR from sector 2 as in this case, FZ traces, would correspond to a ca. 20º clockwise rotation of sector 2 domain. Evidences of such a block rotation, like development of compressional ridges, are not clearly visible across the plateau,

furthermore EU/NAM spreading directions have been fairly uniform since at least 10 Ma to the present (Luis *et al.*, 1994).

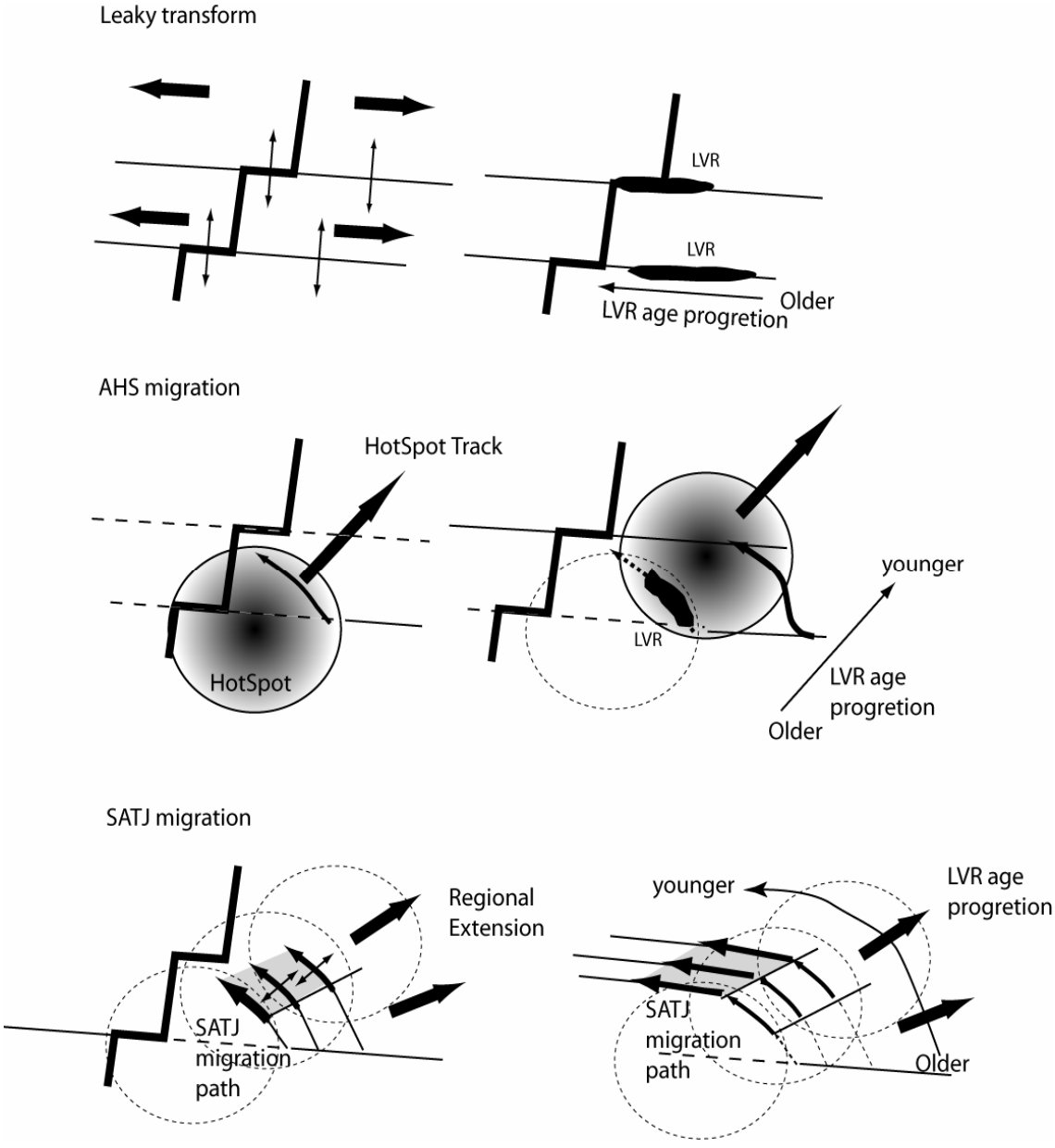

Figure IX.9 - Three possible mechanism for the generation of the LVR. Top) LVR generate in a context of bi-axial stress field as leaky transforms. Center) LVR generate as response to Azores Hot-spot north-westwards migration. Bottom) LVR generate in very recent times due to South Azores Triple Junction migration. Thick traces correspond to active LVR at a given moment. Gray polygon refers to expectable areas of distributed deformation. See text for details

The second hypothesis implies a northeastern oriented age progression of the LVR as a response to the migration in the same direction of the AHS (Vogt and Jung, 2003). These authors consider, by comparing the strikes of the LVR in both sectors that the LVR are traces of failed rifts either spreading obliquely (Sector 1) or normal (sector 2) to the main Nuvel1A conditions. Those authors propose a mechanism to justify both the migration of the plate boundary and the arcuate shape of the LVR, where thickening of the crust could have caused a zone weakening near the edge of the spreading boundary and its relocation northwards. This mechanism remains valid at a broader scale, to explain northward migration of the Triple Junction, but the age progression it implies for the LVR (progressively younger towards NE), does not fit our main observations that geological and magnetic anomaly characteristics LVR sectors are coherent internally but clearly distinct between sectors.

Finally, the third hypothesis, that we favour, links the LVR sector formation with the progressive SATJ migration northwestwards. As discussed in chapter II, considering that the ridges in each sector run parallel to the proposed SATJ migration path, we envisage that this progressive migration was underlined by areas of distributed deformation on the southern edge of the Eurasian plate. These tectonic features could be either reactivated MAR fabrics or, as it was probably the case of sector 2, newly formed. These tectonic features would dominantly control magmatism and LVR formation at each ATJ progressive migration stage. This model implies that from the EAFZ towards the Mid-Atlantic Ridge there is an age progression which seems consistent with the fact that the magnetic structure of LVR in sector 2 is more complex, and active volcanism less robust than their counterparts in sector 1. The main area of earthquake activity is currently located west of sector 1, where there are also evidences

for westward progression of these ridges. Observed active volcanism in sector 2 could be residual and feed either by Pico Central volcano and related fissural plumbing system in the case of EPVR or by analogue processes through the S. Jorge fissural system or the Terceira axis itself in the case of STVR.

As triple junction migration proceeded, older sections of the LVR are progressively abandoned as failed rifts of the distributed plate boundary. Moreover, this becomes progressively focalized along the Terceira axis and a new area of distributed deformation is created further west. This is, in our view the current status of LVR sector 1 comprising also the MAR off-axis domain between the Condor Ridge and the Graciosa parallels.

Contrary to what is referred by Vogt and Jung, we consider that the morphological transitions between LVR sectors have tectonic implications, as they correspond to discrete steps between bathymetric terraces and deepning of the Azores plateau. This sector limits as already observed, follow the strike of the expected NUVEL1A EU/AF spreading directions. Attesting to their probably recent age, they still have a reduced expression in the Azores morphology.

IX.2 ATJ Present day Structure

Inter-Island GPS observations allowed the study of the kinematic behaviour of each Island with respect to both stable Eurasia and African plates. We were able to constrain that the bulk of inter-plate deformation is focused along the Terceira axis, with the exception of its northern sector corresponding to the Central Islands Group where deformation is partitioned between Terceira-Graciosa southwards towards Condor ridge south of Faial Island. A broad segmentation pattern for the present day is proposed

based on half space elastic dislocation modelling and geodetical observables. It defines a plate boundary centered mainly on the Terceira axis up to the East Graciosa Basin longitudes and then on a southern segment defined by the Pico-Faial alignment intersection with the MAR.

This simple segmentation pattern does not fit all geological observations, and we consider therefore that the plate boundary between the western sections of the Terceira axis and the Faial-Pico volcanic ridge constitutes and area of distributed deformation. The GPS based solution, provided in Chapter IV does not accommodate fully the mechanics of the Triple Junction, the areal scatter of epicenter locations on the western LVR sector 1 nor the recent earthquake activity west of Graciosa Island documented in seismic catalogues. As the GPS solution suggests that present ongoing ATJ activity is located at the Faial Pico alignment, some tectonic transfer mechanism needs to be evoked to accommodate concomitance of this activity within this area, its concentration eastwards along the Terceira Ridge and the constrasting lack of significant seismo-tectonic activity on the deeper sections of the plateau south of this region.

Analysis of recent tectono-magmatic events and fault relations from sonar and bathymetric images, digital elevation models and ortophotomaps from Terceira Island, along with magnetic data have allowed us definition of three fault families grouped mainly in NNW-SSE, corresponding to the left lateral ruptures of 1980 in Angra do Heroismo and 1998 in Faial; WSW-ENE, also showned in recent studies based on the Faial 1998 earthquake (Dias, 2006; Fernandes, 2006) which seem conspicuous regional features in LVR sector 1 and finnaly WNW-ESE corresponding to the strike of the LVR in this sector.

The azimuth for the relative motion between Eurasia and Africa is in sector 1, N66º for the NUVEL 1A (De Mets et al, 1994) model. The azimuth for the relative motion between Eurasia to Nubia is N72º and N80º for the models DEOS2K (Fernandes *et al.,* 2003) and REVEL (Sella *et al.,* 2002), respectively. These are based solely on GPS observations and should be used as a reference for present-day motions.

The displacement vectors obtained by the elastic modelling of a set of rectangular sources, performed in chapter VII, has shown a natural agreement with the expected opening normal to the Faial fissural system. However this opening direction is oblique when compared to Eu-Af(Nub) expectable direction (between ca. 35º and 50º) and, furthermore the expectable right lateral component across this plate boundary is missing. A similar result was obtained by (Lourenço *et al.,* 1998) which showed that traction vector averages calculated from focal mechanisms parallel to the Faial graben directions, have an obliquity between ca 48 and 58º, when compared with kinematic models describing the behaviour of this plate boundary. Other LVR in this sector like S. Jorge, or the Serreta ridge seem to present a similar discrepancy given their WNW-ESE strikes.

A possible interpretation for these apparently contradictory observations is to assume a partitioning in space and time of Nuvel 1A spreading vectors and in two main components (see Figure XI.2): one of pure traction (rifting stage) and one dominated by shear (tectonic rotation stage).

Rifting events are magmatic dominated and related with dyke emplacement along LVR axis and characterized, as constrained by the Capelinhos eruption model by extension normal to the LVR axis. These spreading events trigger nearly pure dip-slip faulting in

crustal sections along dyke strike, laterally adjacent and roofing the dyke emplacement and possible fissural type eruptions on the surface. Generalizing the Capelinhos eruption geodetical observations, we can therefore consider the dyke emplacement process and the corresponding growth of the LVR as a type I magma filled crack propagation. For example, the graben in the western tip of S. Jorge Island can represent the crack tip process zone and tip depression, typical of this structures. In this regard, growth of the Islands would be intrinsically more dependent of internal magma pressure distributions and of magma migration paths across pre-existing zones of weakness during dyke emplacement process than of the external regional stress field.

Shear stages would be characterized by left lateral strike slip faulting along N150º fault planes like those which characterize the major Faial and Angra do Heroismo earthquakes, and also along the WSW-ENE faulting directions, in this case acting as probable relay zones with mixed right lateral strike slip and dip-slip displacements. Furthermore, if they are disrupted by slip along N150 faults, than opening as tension cracks or as normal faults is favoured. This might translate the mechanism and distribution of the aftershocks of the Faial 1998 earthquake.

This two modes of tectono-magmatic strain accommodation would characterize the distributed deformation nature of the interplate zone (roughly LVR sector 1) adjoining the Terceira axis and Faial-Pico axis (Figure IX.3). The stress field prevailing in this area would than be right lateral transtensional, with maximum compressive stress horizontal and sub-parallel to the LVR. This regime, and the non-coaxialiality of deformation, can induce strain partitioning as observed at times in Terceira Island field studies.

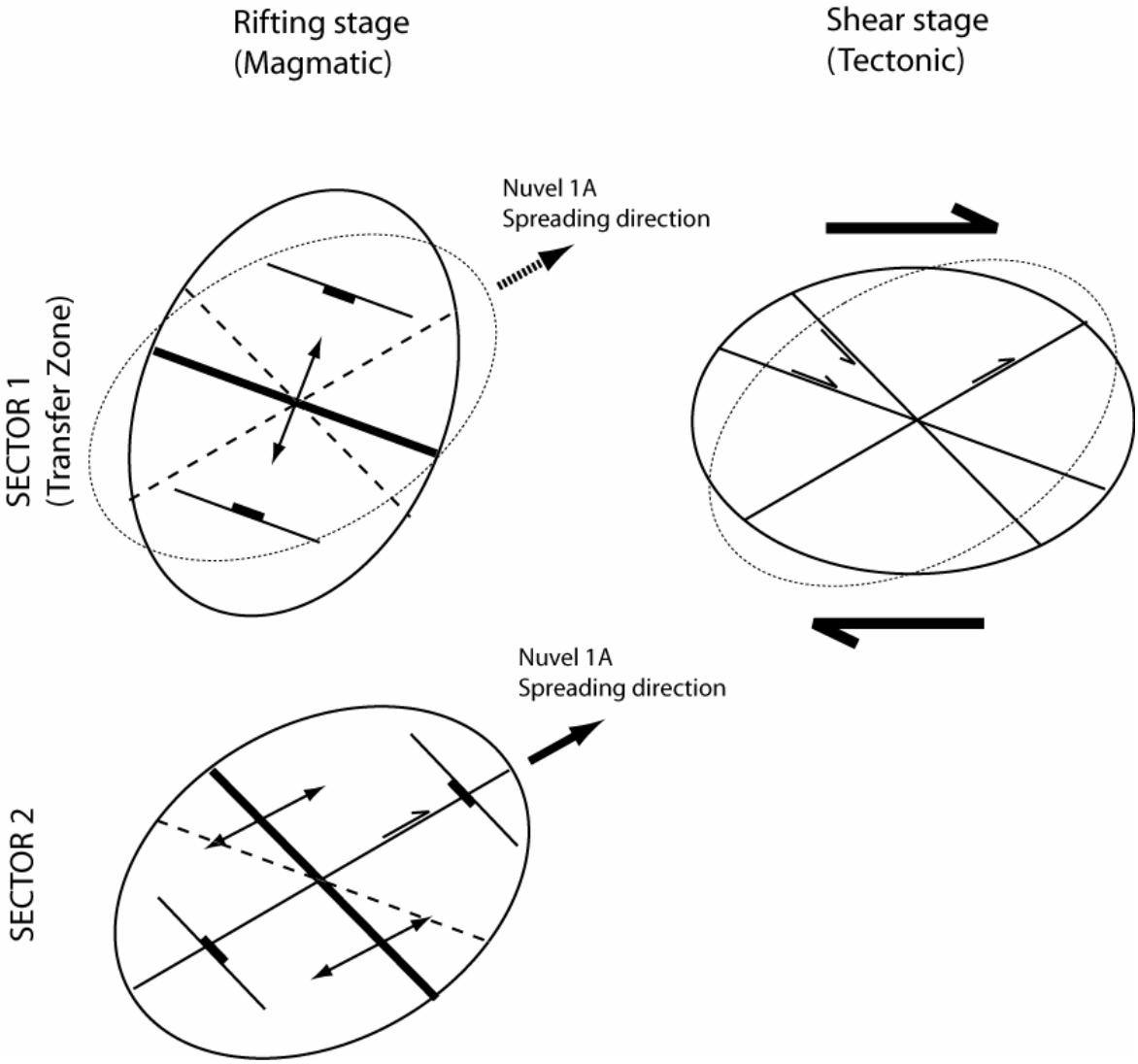

Figure IX.2 - Schematic Illustration representing the main tectono-magmatic orientations and its kinematic behavior across the studied sectors and as a function of dominant ruling processes Magmatic (left) or Tectonic (right). Active structures are presented by continuous lines. In sector 1 the tectonic regime is transtensional, whereas in sector 2 is probably that of oblique spreading.

It is not clear if this tectonic spreading regime is active in the LVR sector 2. The fault pattern configuration present in the EPVR southeastern tip, is conformal with the kinematic constraints provided by sector 1 focal mechanisms. However, lack of seismic activity is this domain implies that either these faults are dominantly aseismic or they

are becoming inactive and that LVR are being progressively abandoned as failed rifts. Consequently, in this sector, extension seems to be focalizing within the Terceira axis itself. The faulting pattern in the SETVR, despite having strike which is sub-parallel to left lateral rupture of Angra do Heroismo earthquake, is more consistent with oblique right lateral extensional regime. This imposes that the stress regime changes accordingly and is characterized by a maximum compressive stress sub-vertical and minimum compressive stress sub-horizontal and sub-parallel to the spreading directions predicted by Nuvel-1A or GPS based kinematic models (e.g. Revel and Deos2k), therefore characterized by coaxial deformation.

This focalized plate boundary domain fits between two other faulting domains defined by Ribeiro (2002) along the Terceira axis. This author suggests a relation exists between the lithosphere state of stress off axis with the response of faulting in each domain on axis (cf. Figure 4.9, pg 193 from Ribeiro *et al.,* 2002). East of the area here studied in more detail, in S. Miguel Island and its vicinities, right lateral strike slip faults are reported by this author, striking N150º, probably related with the intersection of this segment with the Gloria Fault.

The transition from distributed transtension to focalized oblique extension is defined by a set of morphological setps between LVR 1 and LVR2 sectors here interpreted as tectonic faults which are acting as tranfer zones between both domains and which strikes are parallel to Nuvel1A spreading directions (i.e WSW-ENE).

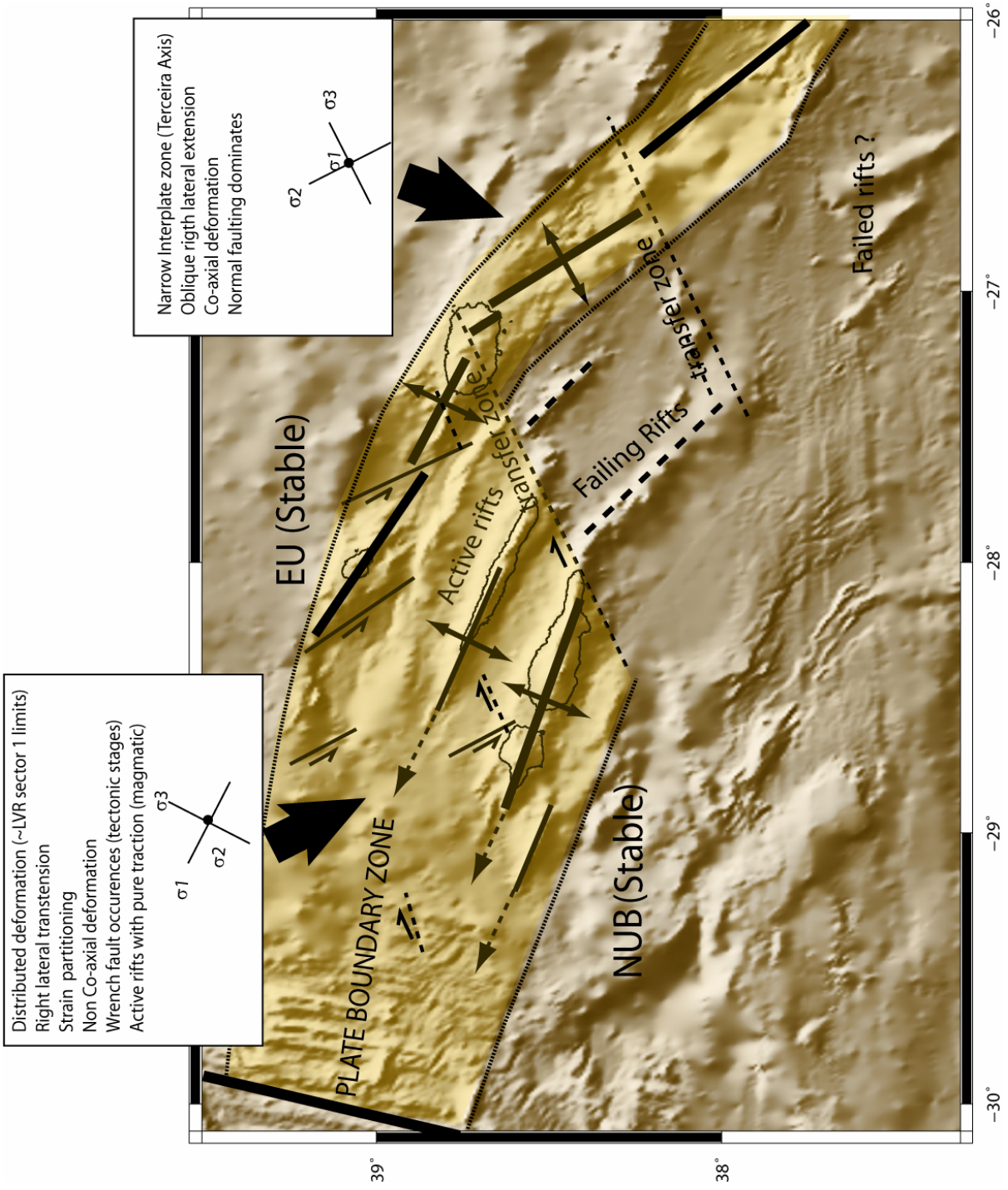

Figure IX.3 – Cartoon depicting a tectono-magmatic model for the present day in the Azores Triple Junction area a summary of all observations. White boxes synthetize each studied sector main characteristics.

IX.3 Future Research

A great deal of work needs to be performed to refine and improve the knowledge we have been gaining in the Azores domain in the past few years. The main problem in Azores interpretations is the almost absolute lack of knowledge on boundary conditions, notably, its thermal structure in depth, and the still limited data we have on the Azores plateau bathymetry itself. In my point of view future efforts in Azores research, considering each scientific domain should be :

Geodesy:

Continuing the inter-Island and intra-Island GPS observation efforts, which have been performed in the framework of TANGO and STAMINA projects, and increment intra-Island networks, would consolidate GPS interpretation by lengthening the time series in this geodynamic context and provide an additional tool to constrain how the far-field displacement vectors are partitioning within each Island complex volcano-tectonic architecture therefore constraining its crustal deformation.

Geophysics:

Our ability to perform a detailed analysis of the processes which act and shape the Azores is undermined by inexistence of a proper bathymetric basemap. A continued effort to collect swath bathymetry in this domain is crucial to allow clearer answers and as a ground to evaluate the third and fourth dimensions (i.e. depth and time).

Heat flow measurements within some of the Terceira axis basins would help clarify in what extent is the Azores truly a rift system or otherwise a fully developed spreading center. Determining the structure of the basins with reflection/refraction studies would

also provide more constraints for the gravimetric modelling as well as provide tectonic constraints on its role in Terceira axis dynamics. Refinement of the seismic catalogue, namely in what deals with azimuthal coverage, and better definition of hypocentral distribution would also favour analysis and tectonic interpretations.

Geology:

Direct seafloor observations by submersible or ROV as well as sampling of the basins walls would help define a clear crustal structure for this particular case of hyper-slow plate boundary.

Following Vogt and Jung, 2003, one of the basins within the Terceira axis, should be a target for an ODP drilling site, as an enormous amount of information could be retrieved from such an initiative. It would allow determination of the age of the basins and hence of the Terceira axis, their detailed structure, and the way hyper-slow crustal construction is achieved.

Isotopic Dating of seafloor monogenic volcanism and samples of the base of the LVR would help to constrain the Azores temporal evolution.

Analogue and Numerical Modelling:

Some insights on LVR development and the physical properties of Azores lithosphere and thermal structure could be gained by numerical modelling of the LVR growth, namely the suggestion that these structures are propagating westwards either as newly formed cracks or by reactivation of pre-existing fracture zones.

X - Cited References

Altamimi, Z., Sillard, P., Boucher, C., (2002). ITRF2000: A new release of the International Terrestrial Reference Frame for earth *Science* applications. *J. Geophys. Res.* B10, doi:10.1029/2001JB000561.

Anderson, D.L. (2001). Top-down tectonics? *Science* 293, 2016-2018.

Anderson, D.L. (2002). Plate tectonics as a far- from- equilibrium self-organized system. In: Stein S., Freymuller J. (Eds.), *AGU Monograph: Plate Boundary Zone, Geodynamics Series* 30, 411-425.

Angelier, J. and Mechler P. (1977). Sur une méthode graphique de recherche des contraintes principales également utilisable en tectonique et en séismologie: la méthode des diedres droits. *Bull.. Sóc. Geol Fr:*, 7, 6: 1309-1318.

Bastos, L., Osório, J., Barbeito, A., Hein, G. (1998). Results from geodetic measurements in the western part of the African-Eurasian plate boundary. *Tectonophysics* 294, 261-269.

Behn, M.D., Lin, J and Zuber, M. (2002). Evidence of weak oceanic transform faults. *Geophys. Res. Lett.*, v. 29, n 24, 2207, doi: 10.1029/2002GL015612

Beier, C. (2006). The magmatic evolution of oceanic plateaus: a case study from the Azores. PhD thesis, Kiel University, 175 pg.

Bird, R.T., Naar, D.F., Larson, R.L., Searle, R.C., and C.R. Scotese (1998). Plate tectonic reconstructions of the Juan Fernandez microplate: Transformation from internal shear to rigid rotation, *J. Geophys. Res.*, v. 103, no. B4, p. 7049-7067.

Bird, R.T., S.F. Tebbens, M.C. Kleinrock and D.F. Naar (1999). Episodic triple junction migration by rift propagation and microplates, *Geology 27*, 911-914.

Bonatti, E. (1990). Not so hot .hot spots. in the oceanic mantle, *Science, 250*, (4977), 107-111.

Bonnin, J. (1978). Évolution géodynamique de la ligne Acores-Gibraltar. Ph.D. Dissertation. Universite Paris VII, Paris 144pp.

Bougault, H., and Cande, S. C. (1985) Background, objectives and summary of principal results: Deep sea drilling project sites 556–564, *Initial Rep. Deep Sea Drill. Proj*., 82, 5–16.

Bourdon, B., Zindler, A., Elliott, T., Langmuir, C.H. (1996). Constraints on mantle melting at mid-ocean ridges from global 238Ur230Th disequilibria data. *Nature* 384, 231–235.

Briais A., and M. Rabinowicz (2002). Temporal variations of the segmentation of slow to intermediate spreading mid-ocean ridges, 1, Synoptic observations based on satellite altimetry data, *J. Geophys. Res.*, 107 (B5), doi:10.1029/2001JB000533.

Briole, P., De Natale, G., Gaulon, R., Pingue, F., Scarpa, R. (1986). Inversion of geodetic data and seismicity associated with the Friuli earthquake sequence (1976–1977). *Ann. Geophys.* 4, 481–492.

Buforn E., Udias A., Colombas M. (1988). "Seismicity source of the mechanisms and tectonics of the Azores-Gibraltar plate boundary". *Tectonophysics*, 152, 89-118.

Byerlee, J. D. (1990). Friction, overpressure and fault normal compression. *Geophys. Res. Lett.* 17, 2109-2112.

Calvert, A., Moore T., Richard B., McGeehin J. P., Rodrigues da Silva A. M. (2006). Volcanic history and 40Ar/39Ar and 14C geochronology of Terceira Island, Azores, Portugal. *J. Volc. Geotherm. Res.* V156, 1-2,103-115.

Cande, S.C. and Kent, D.V. (1995), Revised calibration of the geomagnetic polarity timescale for the late Cretaceous and Cenozoic. *J. Geophys. Res.,* 100, 6,093-6,095.

Cannat, M., Briais, A., Deplus, C., Escartin, J., Georgen, J., Lin, J., Mercouriev, S., Meyzen, C., Muller, M., Pouliquen, G., Rabain, A. and da Silva, P. (1999). Mid-Atlantic Ridge-Azores hotspot interactions: along-axis migration of a hotspot-derived event of enhanced magmatism 10 to 3 Ma ago. *Earth Planet. Sci. Lett.*, 173(3): 257-269.

Carbotte, S.M., Macdonald, K.C. (1994). Comparison of seafloor tectonic fabric at intermediate, fast and super fast spreading ridges: Influence of spreading rate, plate motions, and ridge segmentation on fault patterns. *J. Geophys. Res.* 99, B7, 13609-13631.

Castello-Branco, A., Zbyszewski, G., Moitinho de Almeida, F., da Veiga Ferreira, O. (1959). Rapport de la Premiere mission Geologique. Serv. Geol. Port. Mem. 4, 9–27.

Catalão, J., Miranda J. M., Lourenço N. (2006). Deformation associated with the Faial (Capelinhos) 1957-58 Eruption. Inferences from 1937-1997 geodetic measurements. *J. Volc. Geotherm. Res.* v155, Issues 3-4 , 15 July 2006, Pages 151-163.

Campan, A. (1995). Analyse cinématique de l'Atlantique équatorial: Implications sur l'évolution de l'Atlantique sud et sur la frontière des plaques Amérique du nord/Amérique du sud, thèse de doctorat, 352 pp., Univ. Pierre et Marie Curie (Paris VI), Paris.

Chapple, W.M., Tullis, T.E. (1977). Evaluation of forces that drive the plates. *J. Geophys. Res.* 82, 1967-1984.

Collette, B.J. (1974). Thermal contraction joints in a spreading floor as origin of fracture zones. *Nature* 251, 299-300.

Courtillot, V., Davaille, A., Besse, J., and Stock, J. (2003). Three distinct types of hotspots in the Earth's mantle. *Earth Planet. Sci Lett.*, 205, 295-308.

Cox, A. (1973). Introduction. In: Cox, A. (ed.), Plate tectonics and geomagnetic reversals. W. H. Freeman and Co., New York, p. 40-47.

Cox, A., Hart, R.B. (1986). Plate tectonics: how it works. Blackwell Scientific Publications, Palo Alto, 389 pp.

Cronin, V.S., (1992). Types and kinematic stability of triple junctions. *Tectonophysics* 207 (3–4), 287–301.

Dauteuil O., Bourgeois O., Mauduit T. (2002). Lithosphere strength controls oceanic transform zone structure: insights from analogue models. *Geophys. J. Int.* 150, 706-714.

Dauteuil, O., Brun, J.-P. (1993). Oblique rifting in a slow-spreading ridge. *Nature* 361, 145-148.

Davies, G.F., Richards, M. A. (1992). Mantle convection. *Journal of Geology* 100, 151-206.

DeMets, C., Gordon, R., Argus, D., Stein, S. (1994). Effect of recent revisions to the geomagnetic reversal time scale on estimates of current plate motions. *Geophys. Res. Lett.* 21, 2191-2194.

Detrick, B., Needham, H.D., Renard, V. (1995). Gravity anomalies and crustal thickness variations along the Mid-Atlantic Ridge between 10ºN and 40ºN. *J. Geophys. Res.* 100, 3767-3778.

Dias, N. A. (2006). "Estudo da sequência sísmica gerada pelo sismo do Faial de 9 de Julho de 1998: anisotropia crustal, inversão tomográfica e caracterização sismo-tectónica", *PhD thesis*, University of Lisbon.

Dosso, L., H. Bougault, C. Langmuir, C. Bollinger, O. Bonnier, and J. Etoubleau, (1999). The age and distribution of mantle heterogeneity along the Mid-Atlantic Ridge (31 –41 degrees N), *Earth Planet. Sci. Lett*., 170, 269–286.

Dziak, R. P., Bohnensteihl, D. R., Matsumoto, H., Fox, C. G., Smith, D. K., Tolstoy, M., Haxel, J., Fowler, M. (2004). P- and T-wave detection thresholds, Pn velocity estimate, and detection of lower mantle and core P-waves on Ocean Sound-Channel Hydrophones at the Mid-Atlantic Ridge. *Bull Seism Soc. Am.*

Edwards, M.H., Fornari, D.J., Malinverno, A, Ryan, B. F. (1991). The regional tectonic fabric of the East Pacific Rise from 12º50'N to 15º10'N. *J. Geophys. Res.* 96, 7995-8017.

Escartin, J., G. Hirth, and B. Evans (1997). Nondilatant brittle deformation of serpentinites: implications for the Mohr-Coulomb theory and the strength of faults. *Journal of Geophysical Research*, 102,2897-2913.

Escartin, J. M. Cannat; G. Pouliquen; A. Rabain and J. Lin. (2001). Constraints on the interaction between the Mid-Atlantic Ridge and the Azores hotspot from bathymetry and gravity (36-39N), *J. Geophys. Res.,* 106, 21719-21736.

Escartín, J., G. Hirth, and B. Evans (2001b) Strength and mode of deformation of partially serpentinized peridotites: implications for the rheology and tectonics of oceanic lithosphere, *Geology*, 29, 11, 1023-1026.

Favela, J., Anderson, D. (2000). Extensional tectonics and global volcanism. In: Boschi, E., Ekstrom, G., Morelli, A (Eds.), Problems in geophysics for the New Millennium. Editrice Compositori, Bologna, p. 463-498.

Fernandes, R.M.S., Simons, W., Ambrosius, B., Bastos, L., June (2000). Análise de diferentes metodologias no processamento de campanhas GPS. In: Actas da II Conferência Nacional de Cartografia e Geodesia. IPCC, Luso, Portugal, pp. 92-99.

Fernandes, R.M.S., Miranda, J., Catalão, J., Luis, J., Bastos, L., Ambrosius, B. (2002). Coseismic Displacements of the MW=6.1, July 9, 1998, Faial Earthquake (Azores, North Atlantic). *Geophys. Res. Lett.* 29 (16), doi:10.1029/2001GL014415.

Fernandes, R.M.S., B.A.C. Ambrosius, R. Noomen, L. Bastos, M.J.R. Wortel, W. Spakman, and R. Govers. (2003). The relative motion between Africa and Eurasia as derived from ITRF2000 and GPS data, *Geophys. Res. Lett.*, 30(16), 1828, doi:10.1029/2003GL017089.

Fernandes, R.M.S., L. Bastos, B. A. C. Ambrosius, R. Noomen, S. Matheussen, and P. Baptista, (2004). Recent geodetic results in the Azores Triple Junction region, *Pure and Applied Geophysics*, 161 (3), 683-699, doi:10.1007/s00024-003-2469-y.

Fernandes, R.M.S., L. Bastos, J.M. Miranda, N. Lourenço, B.A.C. Ambrosius, R. Noomen, W. Simons (2006). Defining the Plate Boundaries in the Azores Region. *J. Volc. Geotherm. Res.*, 156, 1-9.

Féraud, G., Kaneoka, I. and Allegre, C.J. (1980). K-Ar Ages and Stress Pattern in the Azores - Geodynamic Implications. *Earth Planet. Sci Lett.*, 46(2): 275-286.

Forsyth, D.W., Uyeda, S. (1975). On the relative importance of the driving forces of plate motion. *Geophysical Journal of the Royal Astronomical Society* 43, 163-200.

Fox, P.J., Gallo, D.G. (1984). A tectonic model for Ridge-Transform-Ridge plate boundaries: implications for the structure of oceanic lithosphere. *Tectonophysics* 104, 205–242.

Fox, P.J., Gallo, D.G. (1986). The *Geology* of North Atlantic transform plate boundaries and their aseismic extensions. In: Tucholke, B.E., Vogt, P.R. (Eds.), The Western North Atlantic Region. Geological Society of America, vol. M, pp. 157-172.

Fox, C.G., H. Matsumoto, and T.-K.A. Lau (2001): Monitoring Pacific Ocean seismicity from an autonomous hydrophone array. *J. Geophys. Res., 106*(B3), 4183–4206.

Galdeano, A., Moreau, M.G., Pozzi, J.P., Berthou, P.Y., and Malod, J.A. (1989). New paleomagnetic results from Cretaceous sediments near Lisboa (Portugal) and implications for the rotation of Iberia. *Earth Planet. Sci. Lett.*, 92:95–106.

Gaspar, J.L., Queiroz, G., Pacheco, J.M., Ferreira, T., Wallenstein, N., Almeida, M.H., Coutinho, R. (2003) - Basaltic lava balloons produced during the 1998-2001 Serreta Submarine Ridge eruption (Azores). In: Subaqueous Explosive Volcanism, White, J., Clague, D., Smellie, J. (Eds.), American Geophysical Union, Geophysical Monograph 140, 205-212.

Gente P., Dyment, J., Maia, M., Goslin, J. (2003). Interaction between the Mid-Atlantic Ridge and the Azores hot spot during the last 85 Myr: Emplacement and rifting of the hot spot-derived plateaus, *Geochemistry Geophysics Geosystystems* 4 (10), 8514 doi:10.1029/2003GC000527

Goslin, J., J.-L. Thirot, O. Noel, and J. Francheteau, (1998). Slow-ridge/hotspot interactions from global gravity, seismic tomography and 87Sr/86Sr isotope data, *Geophys. J. Int*., 135, 700–710.

Goslin, J. & the TRIATNORD Scientific Party (1999). Extent of Azores plume influence on the Mid-Atlantic Ridge north of the hotspot. *Geology*, 27, 991-994.

Goslin, J., Lourenço, N., Dziak, R., Bohnenstiehl D. R., Haxel , J. and Luis J. (2004). Long-term seismicity of the Reykjanes Ridge (North Atlantic) recorded by a regional hydrophone array. *Geophys. J. Int.* 162,2, pg 516 DOI 10.1111/j.1365-246X2005.02678.

Goslin, J. and the SIRENA Team: Bazin, S., Dziak, R.P., Fox, C.G., Fowler, M., Haxel, J., Lourenço, N., Luis, J., Martin, C., Perrot, J. & Royer, J.Y.,2004. Longterm seismicity of Northern 15°N60 °N) MidAtlantic Ridge (MAR) recorded by regional autonomous hydrophones arrays: a widespread alongridge influence of the Azores and Iceland hotspots. AGU Fall Meeting. San Francisco, 1014.

Grimison N. L., Chen W. (1986). "The Azores Gibraltar plate boundary: focal mechanisms, depths of earthquakes and their tectcmics implications". *J. Geophys, Res.*, 92, 2029-2047.

Grindlay, N. R., Fox, P.J. (1993). Lithospheric stresses associated with nontransform offsets of the Mid-Atlantic Ridge: implications from finite element analysis. *Tectonics,* 12, 982-1003.

Grindlay, N.R., Fox, P. J., Macdonald, K.C. (1991). Second-order ridge axis discontinuities in the South Atlantic: morphology, structure and evolution. *Mar. Geophys. Res.* 13, 21-49.

Gudmundsson, A. (1995). Stress fields associated with oceanic transform faults. *Earth Planet. Sci. Lett.* 136, 603-614.

Guest, J.E., J.L. Gaspar, P.D. Cole, G. Queiroz, A.M., Duncan, N. Wallenstein, T. Ferreira e J.-M. Pacheco, (1999). Volcanic *Geology* of Furnas Volcano, São Miguel, Azores. *J. Volc. Geotherm. Res.* 92 (1-2); 1-29.

Harðarson, B.S., Fitton, J.G., Ellam, R.M. and Pringle, M.S. (1997). Rift relocation - a geochemical and geochronological investigation of a paleo-rift in NW Iceland. *Earth Planet. Sci. Lett.*, 153, 181-196.

Hey, R.N., Johnson, P.D., Martinez, F., Korenaga, J., Somers, M.L., Hugget, Q.J., LeBas, T.P., Rusby, R.I., Naar, D.F. (1995). Plate boundary reorganisation at a large-offset, rapidly propagating rift. *Nature* 378, 167-170.

Hirn, A., Haessler, H., Tronc, P. H., Wittlinger, G., Victor, L. M., (1980). Aftershock sequence of the January 1, 1980, earthquake and present-day tectonics in the Azores. *Geophys. Res. Lett.* 7, 501-504.

Hirth, G., J. Escartín, and J. Lin (1998). The rheology of the lower oceanic crust: implications for lithospheric deformation at mid-ocean ridges, *in: Faulting and Magmatism at Mid-Ocean ridges, Eds. Buck et al., AGU Monograph,* 291-303.

Hossack, J.R. (1983). A cross section through the Scandinavian Caledonides constructed with the aid of branch-line maps. *Journal of Structural Gepology.* 5, 2, 103-111.

Ito, G. and J. Lin, (1995). Oceanic spreading center-hot spot interactions: Constraints from along-isochron bathymetric and gravity anomalies, *Geology*, 23, 657-660.

Ito, G., Lin, J., Graham, D. (2003). Observational and theoretical studies of the dynamics of mantle plume-Mid Ocean Ridge Interaction. *Reviews of Geophysics*, 41, 4, 1017-2003. doi:10.1029/2002RG000117.

Klitgord, K., Schouten, H. (1986). Plate kinematics of the Central Atlantic. In: Vogt, P.R., Tucholke, B.E. (Eds.), The *Geology* of North America. vol. M. The Western North Atlantic Region. *Geological Society of America*, pp. 351-378.

Krause, D. C., Watkins, N. D. (1970). North Atlantic crustal genesis in the vicinity of the Azores. *Geophys. J. R. astr. Soc.* 19, 261-283.

Ligi M and the AZORRE99 Team. (1999). Giant Volcanic Ridges Amongst the Azores Islands". *AGU Fall Metting*.

Lourenço, N., Miranda, J., Luis, J., Ribeiro, A., Mendes-Victor, L., Madeira, J., Needham, H., (1998). Morpho-tectonic analysis of the Azores Volcanic Plateau from a new bathymetric compilation of the area. *Marine Geophys. Res*. 20, 141-156.

Lourenço N., J.M. Miranda; J. Luís, I. Silva , J. Goslin And M. Ligi. (2003). High Resolution Bathymetric And Sonar Images of a Ridge Southeast of Terceira Island (Azores Plateau). *Geophysical Research Abstracts*, Vol. 5, 12602.

Luis. J. F. (2006 in press). Mirone: A multi-purpose tool for exploring grid data. Accepted for publication in *Computers & GeoSciences.*

Luis, J. F. and Neves, M. C. (2006) The isostatic compensation of the Azores Plateau: a 3D admittance and coherence analysis. *J. Volc. Geotherm Res.,* v156, Issues 1-2 , Pages 10-22.

Luis J. F., N. Lourenço, J. M. Miranda, J. L.Gaspar and G. Queiroz. (1999). A Submarine Eruption west of Terceira Island (Azores Archipelago). *Interridge News*. Vol 8: Nº1: 13-14.

Luis, J. F., Miranda, J., Galdeano, A., Patriat, P., (1998). Contraints on the structure of the Azores spreading center from gravity data. *Mar. Geophys. Res*. 20, 157-170.

Luis, J. F., Miranda, J., Galdeano, A., Patriat, P., Rossignol, J., Mendes-Victor, L. (1994). The Azores Triple Junction evolution since 10ma from an aeromagnetic survey of the Mid-Atlantic ridge. *Earth and Planet. Sci. Lett.* 125, 439-459.

Luis, J.F., (1996). Le Plateau des Açores et le Point Triple Associé: Analyse Géophysique et Evolution, Ph.D. Thesis, Paris VII, Paris.

Macdonald, K.C. (1986). The crest of the Mid-Atlantic Ridge: models for the crustal generation processes and tectonics. In: Vogt, P.R., Tucholke, B.E. (Eds.), The *Geology* of North America. The Western North Atlantic Region. *Geological Society of America*, vol. M, pp. 51-66.

Macdonald, K.C. (1988). A new view of the mid-ocean ridge from the behaviour of ridge-axis discontinuities. *Nature* 335, 217-225.

Machado, F. (1957). Caldeiras Vulcânicas dos Açores. *Atlântida*, 1(5); 275-278.

Machado, F. (1958a). Actividade Vulcânica da Ilha do Faial (Sept. To Dec. 1957). *Atlantida* 2, 225–236.

Machado, F. (1958b). Actividade Vulcânica da Ilha do Faial (Jan. to April 1957). *Atlantida* 2, 305–315.

Machado, F. (1959a). Actividade Vulcânica da Ilha do Faial (May to Aug. 1958). *Atlantida* 3, 40–55.

Machado, F. (1959b). Actividade Vulcânica da Ilha do Faial (Sept. To Oct.. 1958). *Atlantida* 3, 153–159.

Machado, F., Nascimento, J.M., Denis, A.F. (1959). Evolução Topografica do cone Vulcanico dos Capelinhos. Le Volcanisme de l' ile de Faial. *Serv. Geol. Portugal, Mem.*, vol. 4, pp. 65–71.

Machado, F., Parsons, W., Richards, A., Mulford, J.W. (1962). Capelinhos eruption of Fayal Volcano, Azores, 1957–1958. *J. Geophys. Res.* 67 (9), 3519–3529.

Madeira, J., Ribeiro, A. (1990). Geodynamic models for the Azores Triple Junction: a contribution from tectonics. *Tectonophysics* 184, 405-415.

Madureira, P, Moreira, M., Mata, J., Allegre, J. C. (2005). Primitive helium and neon isotopes in Terceira island (Azores archipelago). *Earth Planet. Sci. Lett*, 233, 429-440.

Mart, Y., Dauteuil, O. (2000). Analogue experiments of propagation of oblique rifts. *Tectonophysics* 316, 121-132.

Matias, L., Dias, N.A., Morais, I., Vales, D., Carrilho, F., Madeira, J., Gaspar, J.L., Senos, L. and Silveira, A.B., (in press, 2006). Characterization of the seismic sequence triggered by the 9th of July, 1998, earthquake near Faial (Azores). *J. Seismology*.

Mauduit, T. & Dauteuil, O. (1996a). Small-scale models of oceanic transform zones. *J. Geophys. Res.*, 101, 20195-20209.

Mauduit, T., Dauteuil O. (1996b). Fault patterns of oceanic transform zones: analog modeling. *J. Geophys. Res.* 101, B9, 20195-20209.

McKenzie, D. P. (1972). Active tectonics of the Mediterranean region. *Geophys. J. R. Astron. Soc*. 30, 109-185.

Mitchell, N. C., Scmitt, T., Isidro, E., Tempera, F., Cardigos, F., Nunes, J. C., Figueiredo, J. (1994). Multibeam sonar survey of the central Azores volcanic islands, *Interridge news*, v 13, 18-20.

Miranda J. M., J. Freire Luis, I. Abreu, L. A. Mendes Victor, A. Galdeano, J. C. Rossignol (1991). Tectonic Framework of the Açores Triple Junction, *Geophys, Res. Lett.*, v 18, n.8, p 1421-1424.

Miranda, J., Victor, L. M., Simões, J., Luis, J., Matias, L., Shimamura, H., Shiobara, H., Nemoto, H., Mochizuki, H., Hirn, A., Lépine, J. (1998). Tectonic setting of the Azores Plateau deduced from a OBS survey. *Mar. Geophys. Res*. 20, 171-182.

Mitchell, N. C., and R. A. Livermore (1998). The present configuration of the Bouvet triple junction, *Geology*, 26, 267-270.

Mittelstaedt, E., Ito, G. (2005). Plume-ridge interaction, lithospheric stresses and the origin of near-ridge volcanic lineaments. *Geoch. Geophys. Geosys*. , 6, 6, 1-20. Doi: 10.1029/2004GC000860.

Molnar, P. (1988). Continental tectonics in the aftermath of plate tectonics. *Nature*, 385, 131-137.

Montelli, R, Nolet G, Dahlen, F, Masters G, Engdahl, E and Hung, S. (2004). Finite-frequency tomography reveals a variety of mantle plumes, *Science*, Vol. 303, p. 338-343.

Moreira, M., R. Doucelande, M. D. Kurz, B. Dupré, and C. J.Allègre (1999). Helium and lead isotope geochemistry of the Azores archipelago, *Earth Planet. Sci. Lett*., 169, 189–205.

Mourgues, R., Cobbold, P. R. (2003). Some tectonic consequences of fluid pressures and seepage forces as demonstrated by sandbox modelling. *Tectonophysics*, 376, 75-97.

Müller, R.D., Roest, W.R. and Royer, J.-Y. (1998). Asymmetric seafloor spreading expresses ridge-plume interactions, *Nature*, 396, 455-459.

Naar, D.F., and R.N. Hey (1991). Tectonic evolution of the Easter microplate, *J. Geophys. Res.* 96, 7961-7993.

Navarro A, Catalao J, Miranda JM, Fernandes RM. (2003). "Estimation of the Terceira Island (Azores) main strain rates from GPS data". *Earth Planets and Space,* 55 (10): 637-642.

Nunes, J.C. (2000) Estudo geológico da depressão vulcânica de São Sebastião (Ilha Terceira, Açores) e área envolvente. *Project PPERCAS-Azores University Report*, Vol. 1/2000. Ponta Delgada, Portugal.

O'Bryan, J.W., Cohen, R., Gilliland, W.N. (1975). Experimental origin of transform faults and striated spreading-center segments. *Geological Society of America Bulletin* 86, 793-796.

Okada Y., (1985). Surface deformation due to shear and tensile faults in a half space, *Bull. Seism. Soc. Am*. 75, 1135-1154.

Oldenburg, D.W., Brune, J.N. (1972). Ridge transform fault spreading pattern in freezing wax. *Science* 178, 301-304.

Oldenburg, D.W., Brune, J.N. (1975). An explanation for the orthogonality of ocean ridges and transform faults. *J. Geophys. Res.* 80, 2575-2585.

Olivet, J.L., Bonnin, J., Beuzart, P., and Auzende, J.M., (1984). Cinématique de l'Atlantique nord et central. *Publ. Cent. Natl Exploit. Oceans, Rapp. Sci. Tech.,* 54:108–112.

Ortner, H., Reiter, F., Acs, P. (2002). Easy handling of tectonic data: the programs TectonicVB for Mac and TectonicsFP for Windows (TM). *Computers and Geosciences* 28, 1193–1200.

Parsons, T. (2002). Nearly frictionless faulting by unclamping in long-term interaction models. *Geology* 30, 1063-1066.

Rabinowicz M., and A. Briais, (2002). Temporal variations of the segmentation of slow to intermediate spreading mid-ocean ridges 2. A three-dimensional model in terms of lithosphere accretion and convection within the partially molten mantle beneath the ridge axis, *J. Geophys. Res.*, 107 (B6), doi:10.1029/2001JB000343.

Ragnarsson, R., Ford, J.L., Santangelo, C.D., Bodenschatz, E. (1996). Rifts in spreading wax layers. *Physical Review Letters* 76, 3456.

Ribeiro, A. (2002). Soft Plate and Impact Tectonics. Springer-Verlag 324 p.

Richter, F.M. (1977). On the driving mechanism of plate tectonics. *Tectonophysics* 38, 61-88.

Ritsema, J., Van Heijt, H.J. & Woodhouse, J.H. (1999). Complex shear wave velocity structure imaged beneath Africa and Iceland. *Science*, 286, 1925-1928.

Roest, W.R., and Srivastava, S.P. (1991). Kinematics of the plate boundaries between Eurasia, Iberia and Africa in the North Atlantic from the late Cretaceous to present. *Geology,* 19:613–616.

Rusby, R. and Searle, R. (1995). A history of the Easter microplate, 5.25 Ma to present. *J. Geophys. Res.* 100(B7): doi: 10.1029/94JB02779.

Schilling, J-G., (1975). Azores mantle blob: rare-earth evidence. *Earth Planet. Sci. Lett.,* 25:103-115.

Schilling, J-G., (1985). Upper mantle heterogeneities and dynamics. *Nature*, 314, 62-67.

Schilling, J.G., (1991). Fluxes and excess temperatures of mantle plumes inferred from their interaction with migrating mid-ocean ridges, *Nature*, 352, 397-403.

Scholz, C.H. (1996). Faults without friction? *Nature* 381, 556-557.

Searle, R.C. (1976). Lithospheric structure of the Azores Plateau from Rayleigh-wave dispersion. *Geophys. J. Roy. Astron. Soc.* 44; 537-546. 186.

Searle, R. (1980). Tectonics pattern of the Azores spreading centre and triple junction. *Earth and Planet. Sci. Lett.* 51, 415-434.

Self, S. (1976). The recent volcanology of Terceira, Azores: *Journal of the Geological Society of London*, v. 132, p. 645-666.

Sella, G., Dixon, T. H., Mao A., (2002). REVEL: a model for recent plate velocities from space geodesy, *J. Geophys. Res.* 107(B4), 2081, doi:10.1029/2000JB000033.

Shaw, P.R., Lin, J. 1993. Causes and consequences of variations in faulting style at the Mid-Atlantic Ridge. *J. Geophys. Res.* 98, 1839-21851.

Shemenda, A.I., Grokholsky, A.L. (1991). A formation and evolution of overlapping spreading centres (constrained on the basis of physical modeling). *Tectonophysics* 199, 389-404.

Shemenda, A.I., Grokholsky, A.L. (1994). Physical modeling of slow spreading ridges. *J. Geophys. Res.* 99, 9137-9153.

Sibson, R.H. (1994). An assessment of field evidence for 'Byerlee' friction. *Pure and Applied Geophysics* 142, 645-662.

Silveira, G., Stutzmann, E., Davaille, A., Montagner, J.-P. Mendes-Victor. L. and Sebai, A. (2006). Azores hotspot signature in the upper mantle", *J. Volc. Geotherm. Res.*, 156, 23–34.

Silveira., G. and Stutzmann, E. (2002). Anisotropic Tomography of the Atlantic Ocean. *Phys. Earth Planet. Inter.* 132, 237.

Silver, P.G., Russo, R.M., Lithgow-Bertelloni, C. (1998). Coupling of South American and African plate motion and plate deformation. *Science*, 279, 60-63.

Small, C. (1995). Observations of ridge-hotspot interactions in the Southern Ocean, *J. Geophys. Res.*, 100, 17,931–17,946.

Smith, W. H. F. & Sandwell, D. T., (1997). Global sea oor topography from satellite altimetry and ship depth soundings, Science, 277, 1956-1962.

Smith, D.K., J. Escartin, M. Cannat, M. Tolstoy, C.G. Fox, D. R. Bohnenstiehl, S. Bazin (2003). Spatial and temporal distribution of seismicity along the northern Mid-Atlantic Ridge (15-35ºN). *J. Geophys. Res.*, 108, 2167, 10.1029/2002JB001964.

Smith, D.K., Tolstoy, M., Fox, C.G., Bohnenstiehl, D.R., Matsumoto, H. and Fowler, M.J. (2002). Hydroacoustic monitoring of seismicity at the slow-spreading Mid-Atlantic Ridge. *Geophys. Res. Lett.*, 29, 13-1:13-4.

Srivastava, S.P., and Tapscott, C.R., (1986). Plate kinematics of the North Atlantic, in Tucholke, B.E., and Vogt, P.R., eds., *The Geology of North America: The Western Atlantic Region*, DNAG Series, vol. M, Geol. Soc. of America, pp. 379-404.

Srivastava, S.P., Roest, W.R., Kovacs, L.C., Oakey, G., Levesque, S., Verhoef, J., and Macnab, R., (1990a). Motion of Iberia since the Late Jurassic: results from detailed aeromagnetic measurements in the Newfoundland Basin. *Tectonophysics,* 184:229-260.

Srivastava, S.P., Schouten, H., Roest, W.R., Klitgord, K.D., Kovacs, L.C., Verhoef, J., and Macnab, R., (1990b). Iberian plate kinematics: a jumping plate boundary between Eurasia and Africa. *Nature,* 344:756–759.

Stüwe, K. (2002). Geodynamics of the lithosphere: an introduction. Springer-Verlag, 449 pp.

Tentler, T. (2003). Analogue modelling of overlapping spreading centers: insights into their propagation and coalescence. *Tectonophysics* 376, 99-115.

Thibaud, R., Gente, P. & Maia, M. (1998). A systematic analysis of the Mid-Atlantic Ridge morphology and gravity between 15°N and 40°N : constraints on the thermal structure. *J. Geophys. Res.*, 103, 24223-24243.

Turcotte, D.L. (1974). Are transform faults thermal contraction cracks? *J. Geophys. Res.* 79, 2573-2577.

Turcotte, D.L., Schubert, G. (1982). Geodynamics. John Wiley and Sons, New York. 450 p.

Verhoef, J., W.R. Roest, R. Macnab, J. Arkani-Hamed, and Members of the Project Team (1996). Magnetic anomalies of the Arctic and North Atlantic Oceans and adjacent land areas, *GSC Open file 3125*, Geological Survey of Canada, 225 pp., 300 figures.

Vogt, P.R..(1976) Plumes, sub-axial pipe flow, and topography along the mid-oceanic ridge. *Earth and Planetary Science Letters*, *29*, 309-325.

Vogt, P.R., Jung W.Y. (2003) The Terceira Rift as hyper-slow, hotspot dominated oblique spreading axis: A comparison with other slow-spreading plate boundaries, *Earth and Planet. Sci. Lett.*, 218, 77–90, doi:10.1016/S0012–821X(03)00627–7.

Wessel, P., Smith, W. (1991). Free software helps map and display data. *Eos Trans. AGU,* 72, 441.

Weston, F (1964). List of recorded volcanic eruptions in the Azores with. brief reports, Bol. Mus. Lab. Min. Geol. Fac. Ciencias de Lisboa,. 10, 3–18.

White, W. M., J. G. Schilling, and S. R. Hart (1976). Evidence for the Azores mantle plume from strontium isotopes geochemistry of the central North Atlantic, *Nature*, 263, 659–663.

Yang, T., Shen, Y., Lee, S., Solomon S.C. and Hung, S.-H. (2006). Upper mantle structure beneath the Azores hotspot from finite-frequency seismic tomography, Earth and Planetary Science Letters, Volume 250, Issues 1-2, , 15, Pages 11-26.

Zbyszewski, G., da Veiga Ferreira, O. (1959). Rapport de la Deuxième mission Géologique. Le Volcanisme de l' ile de Faial. *Serv. Geol. Portugal, Mem.*, vol. 4, pp. 29–55.

Zbyszewski, G., Candido de Medeiros, A., da Veiga Ferreira, O., e Torre de Assuncão, C. (1971). Carta geologica de Portugal na escala de 1/50,000-Ilha Terceira. *Servicos Geologicos de Portugal*, Lisboa.

Zhang, Y.-S. and T.Tanimoto (1992) Ridges, hotspots and their interpretation as observed in seismic velocity maps, *Nature*, 355, 45-49.

Zoback, M.D. (1991). State of stress and crustal deformation along weak transform faults. *Philosophical Transactions of the Royal Society of London* 337, 141-150.